TRACING MERCURY IN THE WIDER IDRIJA REGION USING STABLE ISOTOPES

Dominik Božič

Doctoral Dissertation
Jožef Stefan International Postgraduate School
Ljubljana, Slovenia

Supervisor: Prof. Dr. Milena Horvat, Jožef Stefan Institute and Jožef Stefan International Postgraduate School, Ljubljana, Slovenia
Co-Supervisor: Assist. Prof. Dr. Marko Štrok, Jožef Stefan Institute and Jožef Stefan International Postgraduate School, Ljubljana, Slovenia

Evaluation Board:
Chair: Prof. Dr. Nives Ogrinc, Jožef Stefan Institute & Jožef Stefan International Postgraduate School, Ljubljana, Slovenia
Member: Prof. Dr. David Amouroux, French National Centre for Scientific Research & Institut des Sciences Analytiques et de Physico-chimie pour l'Environnement et les Matériaux, Pau, France
Member: Prof. Dr. Sofi Jonsson, Stockholm University, Stockholm, Sweden

MEDNARODNA PODIPLOMSKA ŠOLA JOŽEFA STEFANA
JOŽEF STEFAN INTERNATIONAL POSTGRADUATE SCHOOL

Dominik Božič

TRACING MERCURY IN THE WIDER IDRIJA REGION USING STABLE ISOTOPES

Doctoral Dissertation

SLEDENJE ŽIVEGA SREBRA NA ŠIRŠEM OBMOČJU IDRIJE Z UPORABO STABILNIH IZOTOPOV

Doktorska disertacija

Supervisor: Prof. Dr. Milena Horvat
Co-Supervisor: Assist. Prof. Dr. Marko Štrok

Ljubljana, Slovenia, May 2024

Acknowledgments

First and foremost, I wish to express my gratitude to my supervisor, Prof. Dr. Milena Horvat, and my co-supervisor, Assist. Prof. Dr. Marko Štrok. I would like to emphasize that without their guidance and support, this project would not have come to fruition.

Furthermore, I extend my appreciation to the dedicated team at the Department of Environmental Sciences, with special mention to those who played an important role in my development: Dr. Igor Živković, Dr. Ermira Begu, Dr. Marta Jagodic Hudobivnik, who have taught me invaluable lessons, as well as others who assisted in various capacities, including Saeed Waqar Ali, Dr. Raghuraj Singh Chouhan, Jure Ftičar, Adna Alilović, Polona Klemenčič, Sreekanth Vijayakumaran Nair, Teodor Daniel Andron, Dr. Radojko Jaćimović, Dr. Tea Zuliani, Dr. Darja Mazej, Dr. Jan Gačnik, Dr. David Kocman, Dr. Doris Potočnik, Dr. Bor Kranjc, Dr. Nives Ogrinc, Sabina Berisha, Gyengne Francis, and Dr. Jože Kotnik. My interactions with them fostered not only productive working relationships, but also meaningful personal connections.

I would also like to thank the secretariat staff, Tina and Karolina, and other colleagues at the Jožef Stefan Institute, whose indirect contributions played an important role in the research presented here. Gratitude is also owed to the administrative and teaching staff and associates of the Jožef Stefan International Postgraduate School.

Lastly, my heartfelt appreciation goes to the staff of the Idrija Heritage Centre and the Idrija Museum, including Tatjana Dizdarevič, Martina Peljhan, Nastja Dejak, and Tomaž Bizjak, whose unwavering kindness and support have been invaluable. The same goes for the staff of the Idrija Municipal Museum.

I would also like to acknowledge the numerous friends I made during my time at the Institute, including Barbara Svetek, Rok Novak, Leja Rovan, Klara Žagar, Norbert Kavasi, and many others with whom I collaborated in the student council and on various student conference committees. Regrettably, there is not enough space to name them all.

In addition, I would like to acknowledge the primary support for my work provided by the Slovenian Research Agency, as well as additional funding from various sources, including the EU and others. Further details regarding this funding can be found in the acknowledgments chapter of the individual publications presented in this thesis.

Posebna zasluga gre moji družini ter prijateljem. Njihova podpora in ljubezen je bila neomajna. Rečem lahko le hvala iz srca.

Abstract

Mercury, a toxic element, known for its physical and chemical properties, spreads throughout the environment and is found in various ecosystems, including water, air, soil, and biological systems. The natural mercury cycle begins beneath the earth's crust, where it rises to the surface and is released into the air through volcanic activity. Mercury completes its cycle by redepositing into the geosphere, where the cycle can begin anew. Historically, mercury has been utilized as a fungicide, catalyst in various chemical processes, and in amalgamation. Human activities significantly contribute to the presence of mercury in the environment. The forms, quantities, causes, and pathways of mercury during its cycle can vary and are the subject of numerous scientific investigations.

One key characteristic of mercury is its seven stable isotopes. These isotopes can distribute differently among reactants and products during environmental conversions. Due to different reactions in various environments, individual ecosystems or subsystems can have their own isotopic signatures. This unique isotopic fingerprint allows for tracing the origins of mercury and understanding conversion processes such as photochemical induction or methylation.

The Idrija region is contaminated with mercury due to centuries-long mining activity. Elevated levels of mercury extend all the way to the Gulf of Trieste. The challenge lies in distinguishing the contributions of mining, natural sources, long-range transport, and other sources that have contributed to this pollution to varying degrees. Research on mercury isotopes in ore, soil, and lichens was conducted within the framework of this task to understand the mercury cycle in the Idrija region.

The first part of the research focused on airborne mercury content using transplanted and in-situ lichens at three locations in Slovenia: Idrija, an area historically polluted due to mercury mining; Anhovo, which contains a cement plant, another source of mercury; and Pokljuka, a natural park. The research aimed to understand the behavior of mercury using lichens as bio-monitors, with a focus on measuring stable isotopes. The results showed that the isotopic composition of mercury exhibits pronounced seasonal fluctuations, with lighter isotopes prevailing in lichens during winter and heavier isotopes during summer. Similar fluctuations to those in lichens were also observed in atmospheric particles.

The second part of the research aimed to determine the isotopic fingerprint of mercury in the Idrija mine. The results showed that the isotopic composition in the mine is very wide primarily due to mass-dependent fractionations, with weak correlations between different types of ore, ore bodies, or geological periods of origin. This indicates that the formation of mercury ore in the mine is a complex process, making its tracing challenging.

The complexity of mercury heterogeneity was also evident in soil analyses from Idrija and downstream Anhovo. Idrija soils show a wide range of values, likely associated with different ores exploited during different periods of mine operation, while this fingerprint is much more homogeneous in floodplains in Anhovo. The soils from Anhovo floodplains in contrast show a much more homogenous isotopic fingerprint.

Povzetek

Živo srebro je toksičen element, ki se zaradi svojih fizikalno-kemijskih lastnosti širi po okolju, zato ga najdemo v različnih ekosistemih, vključno z vodo, zrakom, zemljo in biološkimi sistemi. Naravni krogotok živega srebra se začne pod zemeljsko skorjo, kjer se dviga na površje in sprošča v zrak prek vulkanske aktivnosti. Svoj cikel živo srebro konča z ponovnim odlaganjem v geosfero, kjer lahko cikel ponovno začne na začetku. Zgodovinsko gledano je bilo živo srebro uporabljeno kot fungicid, kot katalizator v različnih kemičnih procesih in pri amalgamaciji. K prisotnosti živega srebra v okolju bistveno prispeva človekova dejavnosti. Oblike, količine, vzroki in poti živega srebra med krogotokom se lahko razlikujejo in so predmet številnih znanstvenih raziskav.

Ena ključna značilnost živega srebra je ta, da ima sedem stabilnih izotopov. Ti izotopi se lahko med potekom pretvorb v okolju različno porazdelijo med reaktante in produkte. Zaradi različnih reakcij v različnih okoljih imajo posamični ekosistemi ali podsistemi lahko povsem svoj izotopski podpis. Ta edinstveni izotopski prstni odtis omogoča sledenje izvorom živega srebra ter razumevanjem procesov pretvorb kot naprimer fotokemično induciranje ali metilacja.

Idrijska regija je onesnažena z živim srebrom zaradi več stoletij dolge rudarske dejavnosti. Visoke ravni živega srebra so prisotne vse do Tržaškega zaliva. Izziv je razlikovati prispevek rudarjenja, naravnih virov, transporta na dolge razdalje ter drugih virov, ki so vsak v različni meri prispevali k tej onesnaženosti. Za razumevanje kroženja živega srebra v idrijski regiji so bile v okviru te naloge izvedene raziskave njegovih izotopov v rudi, v tleh in v lišajih na širšem območju Idrije.

Prvi del raziskav se je osredotočil na vsebnost živo srebro v zraku z uporabo presajenih in in-situ lišajev na treh mestih v Sloveniji: Idriji, območju s zgodovinskim onesnaženjem zaradi rudarjenja živega srebra; Anhovu, ki vsebuje cementarno, še en vir živega srebra; in Pokljuki, naravnem parku. Raziskavaje imela za cilj razumeti vedenje živega srebra z uporabo lišajev kot biomonitorjev, pri čemer je bil poudarek predvsem na merjenju stabilnih izotopov. Rezultati so pokazali, da izotopska sestava živega srebra izkazuje izrazito sezonsko nihanje, pri čemer so v zimskem času v lišajih prevladovali lažji izotopi, poleti pa težji izotopi. Enaka nihanja kot v lišajih so bila opažena tudi v atmosferskih delcih.

Drugi del raziskave je bil usmerjen v ugotavljanje izotopskega prstnega odtisa živega rebra v idrijskem rudniku. Izsledki so pokazali, da je izotopska sestava v rudniku, predvsem glede na masno odvisne frakcionacije zelo široka, korelacije med različnimi vrstami rude, ležišči rude ali geološkimi obdobji, iz katerih izvirajo, pa so šibke. To kaže, da je tvorba rude živega srebra v rudniku kompleksen proces, sledenje le tega pa zato oteženo.

Kompleksnost heterogenosti živega srebra se je pokazala tudi v analizah tal iz Idrije in dolvodno ležečega Anhovega. Tla iz Idrije kažejo velik razpon vrednosti, kar je najbrž povezano z različnimi rudami, ki so bile izkoriščane v različnih obdobjih delovanja rudnika, medtem ko je ta odtis veliko bolj homogen na poplavnih ravnicah v Anhovem.

Contents

List of Figures

List of Tables

Abbreviations

APM	... Atmospheric Particulate Matter
CRM	... Certified Reference Material
DFSF	... Double-Focusing Sector Field
GEM	... Gaseous Elemental Mercury
GeoZS	... Geological Survey of Slovenia
GOM	... Gaseous Oxidized Mercury
ICP MS	... Inductively Coupled Plasma Mass Spectrometer
IJS	... Jožef Stefan Institute
IPS	... International Postgraduate School
LOD	... Limit Of Detection
MC ICP MS	... Multi-Collector Inductively Coupled Plasma Mass Spectrometer
MDF	... Mass Dependent Fractionation
MIF	... Mass Independent Fractionation
MS	... Mass Spectrometer
NIST	... National Institute of Standards and Technology
PBM	... Particle Bound Mercury
Q	... Quadrupole
QQQ ICP MS	... Triple-Quadrupole Inductively Coupled Plasma Mass Spectrometer

Symbols

a	...	annum
Gg	...	Giga grams
f	...	Factor used in calculating MIF from IDF
t	...	time
%	...	percent
‰	...	permille
$\alpha_{A/B}$	...	factor representing the partitioning between the isotopes A and B
$\Delta_{A\text{-}B}$	...	factor representing the fractionation between phases A and B
δ	...	Symbol for MDF
Δ	...	Symbol for MIF
Hg	...	Mercury in any form
Hg^0	...	Mercury in elemental form
Hg^{2+}	...	Oxidized Mercury
(aq)	...	Solution in water
(l)	...	liquid
CH_3Hg	...	methylated mercury (CH3Hg)
$Hg(OH)_2$	...	Mercury hydroxide
HF	...	Hydrofluoric acid
HgS	...	Cinnabar (mercury suphide)
HNO_3	...	Nitric acid
HCl	...	Hydrochloric acid
H_2O_2	...	Hydrogen peroxide
$SnCl_2$	...	Tin chloride
Mt	...	Mega tones
Ar	...	Relative atomic mass
V	...	Voltage
e	...	Base charge
B	...	Magnetic field
R	...	Radius an ion takes on its path through the magnetic field
v	...	Speed
m	...	Mass

Chapter 1

Introduction

Mercury (Hg) is one of the most toxic elements (UNEP, 2019). The history of its excavation, processing and use is related with many acute toxicological conditions (U.S. EPA, 1997). Under certain conditions, an organic form of mercury, methyl-mercury, can be formed (UNEP, 2018, 2022). This form is extremely toxic as it can penetrate cell barriers and damage the internal structure of the cell, leading to severe neurological conditions, known as Minamata disease. Due to this fact, the Minamata Convention on Mercury was signed and entered into force in 2017, with an aim to protect human health and the environment by controlling mercury supply and use, reducing emissions, managing mercury-containing waste, and safeguarding vulnerable populations (UNEP, 2019).

The legacy of mercury is particularly alive in Slovenia, where the second largest mercury mine operated for five centuries until the end of the 20th century (Kavčič, 2008). Although the mine is no longer in operation, and all mercury processing activities have ceased, continuous contamination still exists (Čar, 1996). The sources of mercury contamination are the dumps of mine waste and roasted ore scattered across the area, as well as the secondary emission sources in soils and biota that have been contaminated during centuries of pollution and are now releasing the mercury back into the environment (Baptista-Salazar & Biester, 2019; Bavec et al., 2014; Gosar, 2004a; Gosar et al., 2002; Gosar & Teršič, 2012b, 2012a; Hines et al., 2000; Kobal et al., 2017; Kocman, Vreča, et al., 2011; Kocman & Horvat, 2011; Kotnik et al., 2005; Kotnik, Horvat, Liang, et al., 2015; Miklavčič et al., 2013; Shlyapnikov et al., 2018). All these contamination sites and systems can be a potential source of mercury to the Idrijca river which transports the contamination further downstream towards the Gulf of Trieste (Covelli et al., 2006; Emili et al., 2011; Faganeli et al., 2003; Foucher et al., 2009; Gosar, 2004b; Hines et al., 2000; Horvat et al., 1999; Širca et al., 1999; Žagar et al., 2006).

New advances in analytical equipment and measurements allow the use of stable isotopes of mercury for tracing mercury in the environment and potentially determining its path through the environment (Bergquist & Blum, 2009; Buchachenko, 2013). The isotopic ratios of mercury in different environmental compartments can vary due to mass-dependent and mass-independent fractionation in the environment. This makes it possible to determine which processes have changed the isotope ratios in the sample (R. S. Smith et al., 2014; R. S. Smith, Wiederhold, & Kretzschmar, 2015). If no process has altered the isotopic ratios during the mercury cycle in the environment, the original isotopic fingerprint of the source found in specific sample could be directly linked to the source (Jiskra et al., 2015; Wiederhold, 2015).

The main objective of the dissertation is to trace mercury by using its isotopic fingerprint in the Idrija region. The structure of the thesis is as follows. In the

introduction of the thesis, a literature review is given. Section 1.1 gives a detailed overview the history of mercury in Idrija, (I) the history of the mercury mining, (II) the genesis of the ore deposit and ore body formation, and (III) the monitoring and other research activities related to mercury after the closure of the mine. Section 1.2 discusses mercury isotope chemistry, stable mercury isotopes, their fractionation, and measurement. Section 1.3 discusses mercury measurements in atmospheric samples, focusing on (I) air, (II) geogenic samples and (III) vegetation. Later, the aims and hypothesis are presented in detail in the second chapter. The third chapter consists of the three scientific publications, each focusing on a specific type of sample and addressing different hypothesis. These are answered in the final chapter, the conclusions, in a clear and organized form. Additional information and articles, co-authored that are also of relevance to this topic, are presented in the appendices.

1.1 Mercury in Idrija

The scientific literature on mercury in Idrija is divided into three parts. One is historical and has to do with ore mining, subsequent sorting, grinding and other forms of processing, and finally the retorting of the mercury in the ore into the gaseous state, which was distilled into containers and shipped all over the world (Kavčič, 2020). The second is the scientific work on the genesis of the ore-body, which was mainly carried out by the geologists who worked alongside the miners during the mine's operation. And finally, the third one is environmental research, which began with the closure of the mine in the 1990s and relates mainly to monitoring the release of mercury from the deposits and its subsequent circulation in the environment and impact on humans.

1.1.1 History of Excavation

The first discovery of mercury in Idrija believed to have occurred in 1490 or 1493 (Čar, 1988; Verbič, 1966). In the first years of mining activity, only impregnated clastic rock was mined in the 'Kurji Vrh' district of Idrija. The ratio between liquid mercury and cinnabar was 1:1 during this period of mining and the average mercury content was up to 3.5%. During this period, the mercury was washed by hand in streams and burned on heaps. It is estimated that about 100 tons of ore were burned per year (Kavčič, 2020). In 1508, on St. Ahac's Day, 22nd of June, miners discovered a significant field of black bituminous shale at a depth of 43 m below the surface. These were called the "Skonca" beds and the discovery was the main driving force for the beginning of large-scale mining in Idrija (Čar, 2013).

The next period of mining activity also saw the first use of specialized retorting equipment for mercury extraction. The annual mercury extraction increased to 80 tons per year, as these "Skonca" beds contained much more mercury (17 %) (Kavčič, 2020). The retort sites were not located near the mine, but further up in the hills around Idrija, as it was easier to transport the ore there than the wood, used for the retorting process, down in the valley (Teršič, 2010; Teršič et al., 2011). This lasted until 1652, when the first specialized retort furnace was built in the Prejnuta area in Idrija (Kavčič, 2020).

Since then, retorting has always been conducted in Idrija, but in different districts of the city and with various types of techniques. In 1751, the Spanish type of furnaces came, and later in 1787, the 'Leithner' furnaces, and then in 1886, the 'Čermak-Špirek' furnaces, and then in 1961, the rotary furnaces were set up as the last type of furnaces in Idrija. These improvements allowed the gradual increase of annual ore being burned to

up to 247 000 000 tons and the extraction of up to 577 tons of mercury from the ore with an average mercury content of 0.26% (Kavčič, 2020).

1.1.2 Ore Genesis

Research into the geology of the Idrija mine was carried out intensively during the period of mercury mining, which is reflected in the number of scientific publications during its operation under the Austro-Hungarian empire, the Italian occupation and the Socialist Federal Republic of Yugoslavia. Much of our knowledge comes from this period (cf. Berce, 1958). After the closure of the mine in the 1970s and the subsequent flooding of most of the excavation sites, access to new information on the geology of the mine is no longer possible. Most of the publications on the mine's formation had already been published by that time. The works of mining geologists (e.g., Berce, 1958; Čar, 1996, 2013; Drovenik et al., 1990; Gosar & Čar, 2006; I. Mlakar, 1974; I. Mlakar & Čar, 2009; I. Mlakar & Drovenik, 1971; Placer & Čar, 1977) form the basis of knowledge on the subject and present a comprehensive and detailed summary of the ore genesis and the mining operations development through the past centuries.

The formation history of the Idrija ore deposit began with the break-up of the Lower-Permian Triassic platform, known as the Slovenian Carbonate Slab (Stanko Buser, 1989), in the middle of the Anisian period (Čar, 1985). The resulting rifting led to hydrothermal and volcanic activity, which in turn brought mercury to the surface, as was suspected as early as the 19th century (Kossmat Franz, 1910) and proven by (I. Mlakar & Drovenik, 1971). During several phases of this activity, various types of ores, including the so-called "jeklenka", "opekovka", "jetrenka" and "koralna" ore, and "samorodno živo srebro" liquid $Hg^0_{(l)}$ (Berce, 1958) were extracted from various geological formations and ore bodies (Čar, 2013; Čebulj, 1974; Drovenik et al., 1990; Placer, 1982). Part of the ore was sin-genetic, meaning that it was deposited at the same time as the surrounding rocks, while part of the ore was epi-genetic, which impregnated the older rocks (cf. Berce, 1958). The exact depositional pathway and sequence of mercury deposition are unclear, especially for epi-genetic ores and $Hg^0_{(l)}$. It is the hypothesis of this work that isotopic composition of mercury could improve this knowledge.

1.1.3 Post-Closure Monitoring and Research

Currently, the mine and the remaining processing facilities are under the supervision of the Idrija Mercury Heritage Management Centre. Since the general increase in environmental awareness in recent decades, the focus of scientific research in Idrija has shifted from economic and geological aspects to environmental and health protection aspects.

A review of the literature shows that there are two important centers for mercury monitoring in Idrija. One is the Geological Survey of Slovenia (GeoZS) and the other is the Department of Environmental Sciences at the Jožef Stefan Institute (JSI). An overview of the ecosystems and the studies conducted can be found in Table 1.

Table 1: The overview of the major categories studied in Idrija region and some of the most notable studies about them.

Category	Research
Soil in the vicinity of Idrija	Bavec & Gosar, 2016; Bavec et al., 2015, 2018; Gosar et al., 2002, 2006; Gosar & Teršič, 2012b; Horvat et al., 2002; Horvat, Kontić, et

	al., 2003; Tomiyasu et al., 2012, 2017
Ores and geological investigations	Berce, 1958; Biester et al., 1999; Bourdineaud et al., 2020; Čar, 1996, 2013; Drovenik et al., 1990; Križman et al., 1996; Lavrič et al., 2003; Lavrič & Spangenberg, 2003; I. Mlakar, 1974; Placer, 1982; Shlyapnikov et al., 2018
Sediment transported by the river	Baptista-Salazar et al., 2017, 2018; Cerovac et al., 2018; Gosar, 2004b; Gosar, Pirc, & Bidovec, 1997; Gosar & Teršič, 2014; Gosar & Žibret, 2011; Horvat et al., 2002; Žibret & Gosar, 2006,
Water from the Idrijca river	Baptista-Salazar & Biester, 2019; Foucher et al., 2009; Hines et al., 2000; Horvat et al., 2002; Kocman, Kanduč, et al., 2011
Investigations in the Gulf of Trieste	Acquavita et al., 2012; Bratkič et al., 2013, 2017, 2018; Covelli et al., 2006; Emili et al., 2011; Faganeli et al., 2003, 2014, 2018; Hines et al., 2000, 2012; Horvat et al., 1999; Koron et al., 2011; Kotnik et al., 2017; Kotnik, Horvat, Ogrinc, et al., 2015; Ramšak et al., 2012; Širca et al., 1999
Air measurements in Idrija	Božič et al., 2022; Gosar, Pirc, Šajn, et al., 1997; Grönlund et al., 2005; Horvat et al., 2000; Horvat, Kontić, et al., 2003; Kocman, Vreča, et al., 2011; Kocman & Horvat, 2011; Kotnik et al., 2005; Lupsina et al., 1992
Living organisms from the Idrija area	Božič et al., 2022; Gnamuš, 2002; Gnamuš et al., 2000; Hines et al., 2012; Horvat, Kotnik, et al., 2003; Miklavčič et al., 2013; Žižek et al., 2007

1.2 Mercury Isotope Chemistry

Mercury (Hg), also referred to as hydrargyrum, is an element with atomic number 80 and atomic mass $Ar_{(Hg)} = 200.59$ (De Laeter et al., 2003). It occurs in three oxidation states Hg^0, Hg_2^{2+} and Hg^{2+}; elemental, mercurous, and mercuric mercury, respectively (Blum & Johnson, 2017). Mercury is found in nature in a number of phases, including solids (e.g., HgS minerals), methylated mercury (CH_3Hg), gaseous, aerosol, and liquid and in two oxidation states, namely Hg^0 and Hg^{2+} (Morel et al., 1998). This chapter discusses the forms and isotopes of mercury.

1.2.1 Mercury Isotopes

There are seven stable isotopes of mercury (De Laeter et al., 2003). Their average earths' abundance is listed in Table . In addition, there are also a large number of unstable isotopes, ranging from ^{170}Hg to ^{216}Hg (Audi et al., 2017). Their half-lives are short, up to only few minutes in most cases. They are not produced in large quantities by natural processes, this makes them unsuitable for studies of mercury cycling in the environment (De Laeter et al., 2003).

The science of mercury isotope analyses has developed relatively recently. After 2005, the introduction of new analytical techniques, such as the multi-collector equipped mass spectrometers (Krupp & Donard, 2005), enabled an accurate and widespread adoption of mercury isotope analysis for different matrices and in the concentrations found in the environment (Tsui et al., 2020). Nowadays, stable mercury isotope measurements are widely used in many settings, such as sediments (Feng et al., 2010), rivers (Donovan et al., 2016), ore (Pribil et al., 2020), oceans (Archer & Blum, 2018; Štrok et al., 2014), industrial material (Mead et al., 2013), biota (Madigan et al., 2018), and others. That the science/knowledge of mercury isotopes is an emerging field with an ever increasing numbers of publications from less than five prior to 2008 and up to 50 in 2019 (Tsui et al., 2020).

Table 2: Stable isotopic composition of Hg (De Laeter et al., 2003).

Isotope	Atomic mass/u	±	Mole fraction	±
^{196}Hg	195.965814	0.000004	0.0015	0.0001
^{198}Hg	197.966752	0.000003	0.0997	0.0002
^{199}Hg	198.968262	0.000003	0.1687	0.0022
^{200}Hg	199.968309	0.000003	0.2310	0.0019
^{20l}Hg	200.970285	0.000003	0.1318	0.0090
^{202}Hg	201.970625	0.000003	0.2986	0.0026
^{204}Hg	203.973475	0.000003	0.0687	0.0015

1.2.2 Mercury Fractionation

The reason why stable isotopes of mercury can be used as tracers to determine the source is lies in their fractionation – a partitioning between two isotopes into two phases (Manish et al., 2015). For stable isotopes, this is usually due to the difference in mass, which in turn changes the physiochemical properties and reactivity of one isotope compared to another (Wiederhold, 2015). There are two types of mercury fractionation: (I) so-called mass-dependent fractionation (MDF), which is solely influenced by mass, and (II) mass-independent fractionation (MIF), in which partitioning is forced by processes that are independent of the isotope masses (Blum et al., 2014; Blum & Johnson, 2017; Cai & Chen, 2016; Wiederhold, 2015).

MDF can be caused by one of two effects – kinetic and equilibrium ones. In the case of kinetic fractionation, the difference in the concentration of heavy and light isotopes is caused by a difference in reaction rates. In this sense, only the incomplete reaction is observed. When the reaction runs to completion, the isotope concentration in the product is the same as in the reactant. This is different from equilibrium fractionation, where the two phases are in equilibrium and react at the same rate to each other. The relative isotopic abundance is then controlled by the binding environments of the individual phase (Wiederhold, 2015). An example of kinetic fractionation would be evaporation and diffusion (Schauble, 2004), and an example of an equilibrium process would be oxidation and reduction (Schauble et al., 2009). MIF is defined as a deviation from the MDF and is controlled by several effects such as the Nuclear Volume Effect (NVE), Magnetic Isotope Effect (MIE), molecular symmetry, neutron capture, and self-shielding (Cai & Chen, 2016; Wiederhold, 2015). These reactions have some various influence on the isotope fractionation, as shown in Table (Yin et al., 2010).

Table 3: Type of reaction and the change in isotopic composition, modified after Yin et al., 2010.

	Type	phase A	phase B	$^{202}\alpha_{A/B}$	Δ_{A-B} (‰)	References
Chemical reactions	Photo reduction	$CH_3Hg^+_{(aq)}$	$Hg^0_{(g)}$	1.0013 – 1.0017	0.6	(Bergquist & Blum, 2007)
	Photo reduction	$Hg^{2+}_{(aq)}$	$Hg^0_{(g)}$	1.0006	1.5	(Bergquist & Blum, 2007)
	UV photolysis reduction	$Hg^{2+}_{(aq)}$	$Hg^0_{(g)}$	1.0006	1.34	(Yang & Sturgeon, 2009)
	Dark organically medicated reduction	$Hg^{2+}_{(aq)}$	$Hg^0_{(g)}$	1.002	1.7	(Bergquist & Blum, 2007)
	Chemical reduction ($SnCl_2$)	$Hg^{2+}_{(aq)}$	$Hg^0_{(g)}$	1.0004	1.17	(Yang & Sturgeon, 2009)
	Chemical reduction ($NaBH_4$)	$Hg^{2+}_{(aq)}$	$Hg^0_{(g)}$	1.0004	1.08	(Yang & Sturgeon, 2009)
	Chemical reduction (ethylation with NaBEt4)	$Hg^{2+}_{(aq)}$	$Hg^0_{(g)}$	1.0012	3.59	(Yang & Sturgeon, 2009)
	Volcanic emission	$Hg^0_{(p)}$	$Hg^0_{(g)}$	1.00135	1.63	(Zambardi et al., 2009)
	Absorption	$Hg^{2+}_{(aq)}$	$Hg(OH)_2$	/	0.62	(Wiederhold et al., 2010)
Biological reactions	MerA	$Hg^{2+}_{(aq)}$	$Hg^0_{(g)}$	1.0013 –1.0020	1.6	(Kritee et al., 2007, 2008)
	MerB	$CH_3Hg^+_{(aq)}$	$Hg^0_{(g)}$	1.0004	0.4	(Kritee et al., 2009)
	Methylation	$Hg^{2+}_{(aq)}$	$CH_3Hg^+_{(aq)}$	1.0026	1	(Rodŕiguez-Gonźalez et al., 2009)
Physical reactions	Evaporation	$Hg^0_{(l)}$	$Hg^0_{(g)}$	1.0067	6.5	(Estrade et al., 2009)
	Volatilization	$Hg^{2+}_{(aq)}$	$Hg^0_{(g)}$	1.0004 –1.0005	1.48	(Zheng et al., 2007)
	Evaporation	$Hg^0_{(l)}$	$Hg^0_{(g)}$	1.0009	0.8	(Estrade et al., 2009)

The partitioning of the elements in Table is described by the factors $^{202}\alpha_{A/B}$ and Δ_{A-B} which can be calculated according to Equations 1 and 2.

$$\alpha_{A/B} = {}^{R_A}/_{R_B} \tag{1}$$

$$\Delta_{A-B} = \delta_A - \delta_B \approx 10^3 ln\, \alpha_{A/B} \tag{2}$$

$^{202}\alpha_{A/B}$ stands for the partitioning of the isotope ^{202}Hg between phases A and B, R denotes the ratio of an isotope in a particular phase and Δ_{A-B} represents the fractionation between the two phases reflecting the kinetic or equilibrium partitioning. This approximation (Equation 2), where δ represents the MDF in a given phase, can be made considering that α is very close to one (Yin et al., 2010).

There are many processes that induce either MDF or MIF. Of these reactions, the effects that cause MIF are less understood than those that cause MDF. This is partly because there are fewer such processes and partly because they are more difficult to understand and more complex to detect (Wiederhold, 2015). NVE is a consequence of nonlinear volume change relative to the number of neutrons in the atom, which can sometimes be present (Wiederhold, 2015). The effects of NVE on mercury isotopes have been suggested in several studies (Jiskra et al., 2012; Wiederhold et al., 2010). MIE affects only isotopes with odd masses, nuclear spin, and magnetic moment. It has been reported in field studies and laboratory experiments, including mercury (Blum et al., 2014; Blum & Bergquist, 2007; Buchachenko, 2013). The even-MIF cannot be explained by any of these reactions. Either self-shielding or neutron capture effect is responsible for them (Cai & Chen, 2016). This variation can be up to 1.5 ‰ (Chen et al., 2012; Sun et al., 2019). Self-shielding has been observed under laboratory conditions (Mead et al., 2013) and also explained theoretically (Sommerer, 1993). As the name implies, shielding of some type is involved in this process. This is because the more abundant isotopes shield each other from photoexcitation. This would mean that less abundant isotopes such as ^{196}Hg are more easily photoexcited than ^{202}Hg. Data from experiments are broadly

consistent with this theory (Mead et al., 2013). But in the environment, such as in the atmosphere, where mercury concentrations are relatively low, the light photoexcitation has a different spectrum, and consequently it could may not be affecting mercury in a different way. Observations in nature also do not agree well with this theory (Cai & Chen, 2016; Demers et al., 2013; Gratz et al., 2010). Neutron capture is another theory that could explain the observed anomalies of even-MDF. The neutron cross section, i.e., the value expressing the likelihood of interaction between a neutron and a nucleus, varies between different isotopes (Mughabghab, 2003). In practice it is very easy for a ^{199}Hg isotope with the highest neutron cross section to grab a neutron and transform into another isotope. The only problem is that the residence time of mercury in the atmosphere is many orders of magnitude shorter than the time normally required for meaningful and significant reactions to occur (Cai & Chen, 2016).

1.2.3 Reporting of Mercury Isotope Ratios

Virtually all mercury isotope ratio studies conducted today report the ratios of mercury relative to the Certified Reference Material NIST 3133 produced by the National Institute of Standards & Technology (NIST) (National Institute of Standards & Technology, 2016). Potentially some other standard other than NIST 3133 could be used. In that case, NIST 3133 should be used as an internal standard to allow the calculation back to the same relative values, or a known standard with well-defined isotopic ratios should be used, as recommended by Blum and Bergquist (2007) and Blum et al. (2014). The relative values between the standard and analyte are reported in ‰. They are calculated using Equations 3 through 8 (Blum et al., 2014; Blum & Johnson, 2017).

$$\delta^{xxx}Hg = \left(\frac{\frac{^{xxx}Hg}{^{198}Hg}_{sample}}{\frac{^{xxx}Hg}{^{198}Hg}_{SRM3133}} - 1 \right) \times 1000 \quad (3)$$

$$\Delta^{199}Hg = \delta^{202}Hg - \delta^{xxx}Hg \times 0.2520 \quad (4)$$

$$\Delta^{199}Hg = \delta^{202}Hg - \delta^{xxx}Hg \times 0.5024 \quad (5)$$

$$\Delta^{200}Hg = \delta^{202}Hg - \delta^{xxx}Hg \times 0.7520 \quad (6)$$

$$\Delta^{201}Hg = \delta^{202}Hg - \delta^{xxx}Hg \times 0.2520 \quad (7)$$

$$\Delta^{204}Hg = \delta^{202}Hg - \delta^{xxx}Hg \times 1.4930 \quad (8)$$

The symbol xxx in the equations stands for either the isotope ^{199}Hg, ^{200}Hg, ^{201}Hg, ^{202}Hg, or ^{204}Hg. The lowercase Greek delta (δ) represents the MDF and the uppercase delta (Δ) represents the MIF. The MIF is divided into the odd and the even MIF. The odd-MIF includes the odd numbered isotopes and even-MIF includes the even numbered isotopes (Blum & Johnson, 2017; Cai & Chen, 2016). Some alternative schemes have been proposed to represent the even MIF, which are shown in Equations 9 to 12 (Cai & Chen, 2016)

$$\delta^{xxx/200}Hg = \left(\frac{\frac{^{xxx}Hg}{^{200}Hg}_{sample}}{\frac{^{xxx}Hg}{^{200}Hg}_{SRM3133}} - 1 \right) \times 1000 \quad (9)$$

$$\delta^{xxx/200}Hg = \left(\frac{\frac{^{xxx}Hg}{^{202}Hg}_{sample}}{\frac{^{xxx}Hg}{^{202}Hg}_{SRM3133}} - 1 \right) \times 1000 \quad (10)$$

$$\Delta^{198/200}Hg = \delta^{189/200}Hg + \delta^{202/200}Hg \times 1.0097 \quad (11)$$

$$\Delta^{200/202}Hg = \delta^{200/202}Hg + \delta^{198/202}Hg \times (-0.4976) \quad (12)$$

These expressions were chosen because in the traditionally used expressions (Equations 2 – 6), the $^{202}Hg/^{198}Hg$ ratio is chosen, but other isotopic combinations can also express even MIF. The next alternative would be to also use an even and an odd isotope, as shown in Equations 13 - 15 (Cai & Chen, 2016).

$$\Delta^{200/198}Hg = \delta^{200/198}Hg - \delta^{199/198}Hg \times 1.9935 \quad (13)$$

$$\Delta^{202/198}Hg = \delta^{202/198}Hg - \delta^{199/198}Hg \times 3.9679 \quad (14)$$

$$\Delta^{204/198}Hg = \delta^{204/198}Hg - \delta^{199/198}Hg \times 5.9234 \quad (15)$$

The equations δ and Δ values for are essentially derived to in the same fashion as the traditionally defined δ and Δ values with only the factors for the MIF being recalculated to account for the different isotope pairs chosen. These different methods of calculating the even-MIF enable the determination of exactly which isotope is causing this effect. This is something that the traditional approach from Equation 3 cannot do. This feature arises from the fact that there are three even mercury isotopes used to calculate $\Delta^{200}Hg$; apart from ^{200}Hg also ^{198}Hg and ^{202}Hg. Any of these isotopes can behave anomalously. It is even possible that they all contribute to the result (Cai & Chen, 2016; Chen et al., 2012).

In the majority of the literature MDF is usually presented by $\delta^{202}Hg$, odd-MIF by $\Delta^{199}Hg$, and even-MIF by $\Delta^{200}Hg$. With samples that present significant odd-MIF it can be useful to plot the $\Delta^{199}Hg/\Delta^{201}Hg$ values, as it was discovered that the majority of reactions present a slope of 1.0 but some can be as high as 1.36 (Bergquist & Blum, 2007; Ghosh et al., 2008). Plotting the slopes of mercury concentrations versus MDF or MIF values can also be useful in certain applications (e.g., Douglas & Blum, 2019; Reinfelder & Janssen, 2019).

1.2.4 Analytics of Stable Isotope Measurement

The first mass spectrometer, albeit in its most primitive form, was introduced as early as 1898 (Wien, 1898). Since then, mass spectrometers have evolved greatly. Aside from their inherent technical advantages and disadvantages, all MS instruments have the following

measurement comparison attributes: (I) mass resolution, or the ability to separate adjacent peaks, (II) abundance sensitivity, or the ability to form thin peaks that allow for better quantification, (III) mass spectral range, which determines what masses the MS can measure, and (IV) scanning speed, which determines the speed at which an instrument can acquire the measurement (Thomas, 2013).

Each MS consists of four main components. These are: (I) sample introduction, (II) ion source, (III) mass resolving body (mass analyzer) and (IV) detector (Figure 1A). The sample is in most cases introduced into the MS as a liquid, or in the case of Hg as a vapor introduced via the cold vapor generator (Bérail et al., 2017). Once ionized, atoms pass through a series of cones and electro-magnetic lenses that focus the ion beam and send it to the mass analyzer (Thomas, 2013). As with introduction and ionization, there are many methods for mass resolving. They all operate on a similar principle where changes in magnetic field or voltage affect the ions generated at the ionization source (Jakubowski et al., 2011).

In ICP-MS, the voltage (V) and magnetic field (B) can be manipulated. The deflection of a single particle is expressed as the radius (R) of the trajectory it travels. R depends on the velocity (v), mass (m), the base charge (e) and the strength of the magnetic field (B). It is calculated according to Equation 16.

$$R = \frac{vm}{Be} \tag{16}$$

Since the velocity of the particle is not known, Equation 17, which describes the relationship between the base charge, the current and the mass must be used.

$$eV = \frac{1}{2}mv^2 \tag{17}$$

If the velocity is exposed and equated, Equation 18 is obtained.

$$\frac{m}{e} = \frac{B^2R^2}{2V}. \tag{5}$$

Since e is a constant (1.60219×10^{-19} C), B and V are adjustable, and R is known due to the geometry of the ICP-MS, the mass can be calculated (Becker, 2002; Irrgeher & Prohaska, 2015; Thomas, 2013).

Mass analyzers equipped with quadrupole, operate by changing the current through four (quad) rods. This creates four electro-magnetic poles through which the ions are accelerated. The change in current affects the trajectory of the ions. The ions in this field oscillate. Heavier ions oscillate less than lighter ones. If the current is selected correctly, only the ions with the desired mass will oscillate the right amount to be led through to the detector part of the instrument (Becker, 2002, 2005). Based on it all but the select ions are deflected and do not reach the detector. The other method (DFSF) operates on the principle of combining magnetic and electric fields (dual). If only the electric current applied to the ions, the resolution would be too low. Therefore, DFSF mass analyzers change both electric current and the magnetic field. This makes them very precise. DFSF have high mass resolution and are able to separate isobaric interferences between atomic and molecular ions (Becker, 2002). Some instruments, such as the Nu Plasma II, can be equipped with both quadrupoles and DFSF and can be used to determine the natural abundances of Hg isotopes.

Choosing the right ion detector for a particular application has a major impact on the performance of the MS instrument. The most commonly used detectors are dynode

electron multipliers and Faraday cups. Faraday cups literally resemble vessels into which the ion beam is directed across the mass analyzer. When the ion hits the end of the cup, the current is generated and recorded. The operating principle behind dynode electron multiplier is the generation of secondary electrons upon an ion striking the first dynode. This process is repeated multiple times, hence the "multiple" in the name. In this way, the signal strength is increased (Vanhaecke & Degryse, 2012).

In general, the advantage of Faraday cups over other types, such as electron multipliers, is that they are easy to sequence. Faraday cups, on the other hand, have a longer lifetime (Vanhaecke & Degryse, 2012). However, they are inferior to the discrete dynode electron multipliers used in quadrupole equipped MS devices as such instruments do not produce throughputs high enough to be reliably measured by a Faraday cup (Thomas, 2013).

Most MS devices have one detector, and some have multiple – hence the name multi-collector MC. A major disadvantage of single collector devices is that they have to switch from detecting one mass to another. This transition is not instantaneous. Detectors have their own drift and some dead time, which affects the precision and accuracy of the measurements. In the cases where a wide range of linear responses and very low quantities of sample are available, such as Rb detection in fossils, discrete dynode electron multipliers perform better (Thomas, 2013). Such devices may therefore be unsuitable for extremely precise isotope ratio determinations. MC-equipped devices do away with a lot of single collector problems by measuring all of the masses of interest at the same time. In general, the multi collectors are orders of magnitude more precise (Vanhaecke & Degryse, 2012).

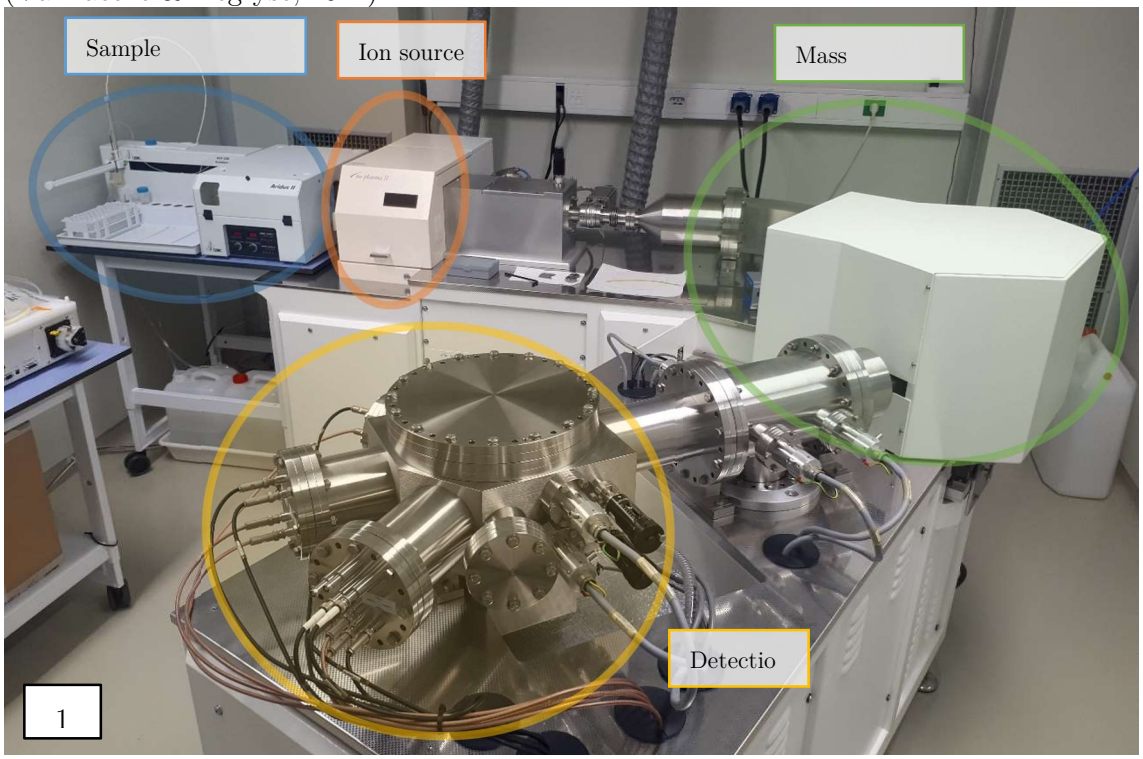

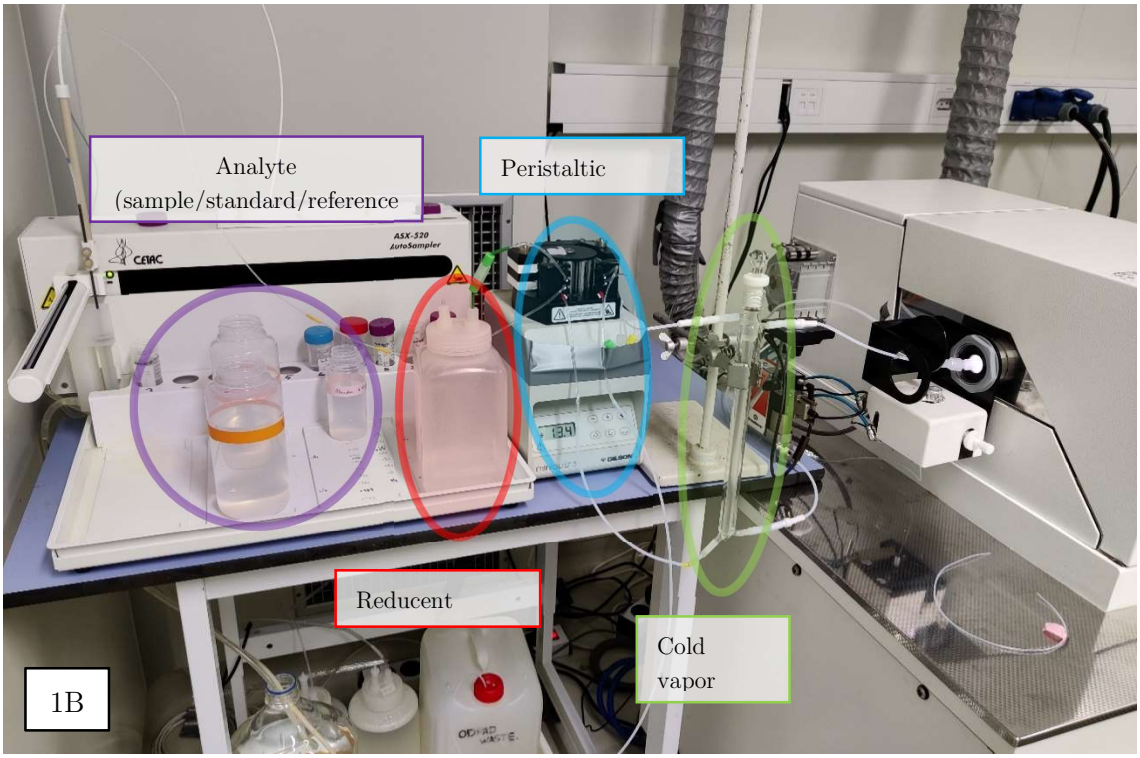

Figure 1: Above (Fig. 1A) a photograph of the Nu Plasma II MC-ICP-MS used to analyze the stable mercury isotopes from this thesis, with the main parts of an ICP-MS instrument highlighted. Below (Fig. 1B) a photograph of a sample introduction system used for mercury vapor generation.

Two of the photographs of the system used to measure the samples presented in this study are presented in Figure 1. Figure 1A presents a wider shot where a broader view of the instrumentation with various sections of an ICP-MS highlighted. This setup of the instrument has a nebulizer attached to it as a sample introduction system. On its place other devices could be used. Such nebulizer can be used for direct mercury isotope measurement but was not used in these studies at all since there were reports of its poor sensitivity (Rua-Ibarz et al., 2016) compared to the cold vapor generation method. The exact detailed photography of one of the setups used can be seen in Figure 2B. In general, all of the measurement sessions used flasks with analytes and reducing agent being pumped by a peristaltic pump that mixed the two solutions together. The mixture entered the cold vapor generator from above, while the carrier gas Ar came from bellow and transported the mercury vapors to the ion source. Prior to the introduction to the ion source, an additional line with an Ar gas was introduced. At this stage, the Tl could be added as an internal standard via the nebulizer. The waste solution was transported away from the cold vapor generator using the same peristaltic pump. For further explanation of the methodology used for each individual measurement session please refer to the methodology section of each publication (Chapter 3).

The setup as shown allowed for the relatively simple measurement of sample om sessions lasting for about one work-day or up to some 12 to 16 hours. In this time, up to 50 or 60 measurements could be made. The standard deviations of the repeated measurements for a single set of samples are presented in the article. In general, such a setup enabled the standard deviations which were close to the ones reported in most of the literature presented here, up to about ± 0.2 ‰ for δ^{202}Hg and up to about 0.1 ‰ for Δ^{199}Hg.

1.3 Mercury and its Isotopes in the Environmental Samples

The total range of mercury isotope ratios varies up to 10 ‰ for Δ^{199}Hg and up to 8 ‰ for δ^{202}Hg (Blum et al., 2014). These higher values for MIF are found in aquatic organisms. Such high values are likely caused by microbially produced MeHg that has been photochemically degraded to Hg^0, resulting in a negative MIF, but a positive one MIF in bio-accumulated MeHg (Kritee et al., 2007; Kwon et al., 2012; Tsui et al., 2013). Negative MIF is observed in samples such as some lichens (Carignan et al., 2009) and Arctic snow (Sherman et al., 2010). This MIF is most likely caused by processes of reduction of Hg^{2+} to Hg^0 and subsequent transport of odd-mass isotopes preferentially released from snow and foliage, resulting in negative values in/on these phases (Demers et al., 2013; Sherman et al., 2010). Some of the lowest MDF values have been observed in the atmospheric samples near anthropogenic emission sources (Blum et al., 2014; Sherman et al., 2012), such as coal-fired power plants, with values often averaging about -1.5 ‰ (Sun et al., 2014).

In general mercury isotopes cannot be considered as a proverbial silver bullet that can by itself solve any problem regarding the origin of mercury in the sample or the transformations it experienced. Mercury isotope analyses in the environment are best utilized where either isotopic fractionation is already suspected or one or more end members delivering mercury to the particular environmental compartment are known.

1.3.1 Mercury in the Air

There are three operationally defined forms of atmospheric mercury: gaseous elemental mercury (GEM), gaseous oxidized mercury (GOM), and atmospheric particulate matter (APM) bound mercury (PBM). GEM is present in the Hg^0 form, GOM in the Hg^{2+} form and PBM can be present in different oxidation states, sometimes noted as $Hg_{(p)}$ and either chemically or physically bound to the particulate matter (Ariya et al., 2015; Lyman et al., 2020; Si & Ariya, 2018). The residence time of mercury in the atmosphere can be very long (0.5 to 2 years) and it can be transported over long distances (Johansson & Tyler, 2001; Schroeder & Munthe, 1998). GEM and GOM can be removed from the atmosphere either, via wet deposition, dry deposition, binding to particles or deposition from gaseous phase (Douglas & Blum, 2019; Gichuki & Mason, 2014; Lodenius, 1998; Lyman et al., 2020). The mercury from the air can be deposited to the foliage and stored there for a while. Mercury is than deposited with litterfall in a process known as litterfall deposition, which deposits mercury to soil (Wang et al., 2016). The forms of mercury, their interactions and deposition pathways are presented in Figure 1.

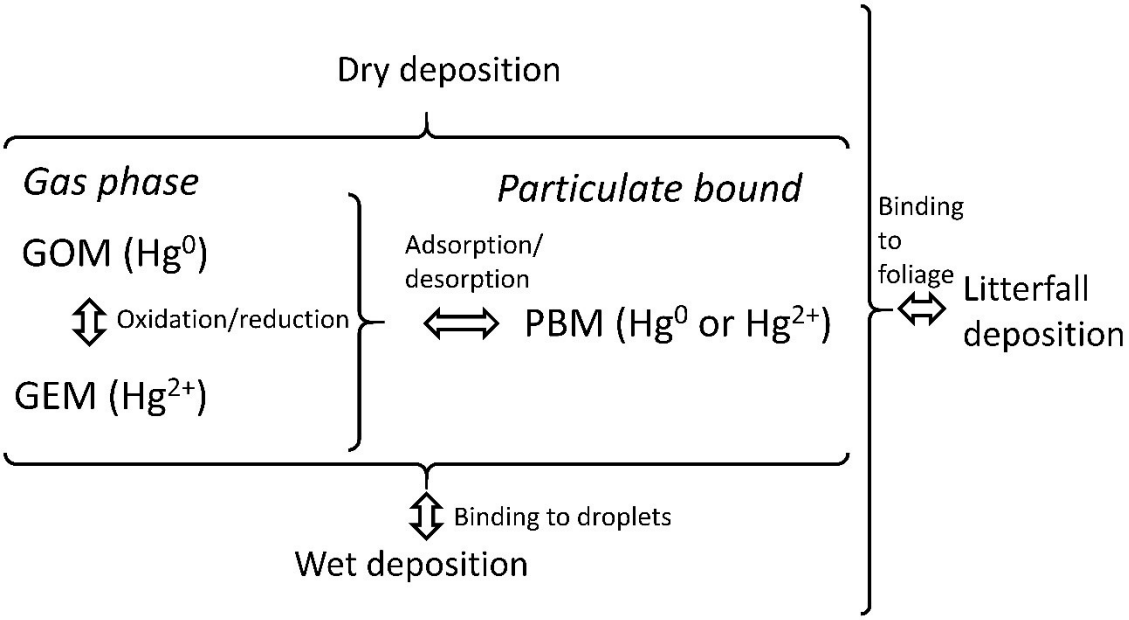

Figure 2: Forms of mercury in the atmosphere, the reactions they commonly undergo and the deposition pathways. Adapted from (Ariya et al., 2015; Si & Ariya, 2018).

Based on a review of the literature, there is no precise convention on the nomenclature based on the measurement method. In the literature concerned with atmospheric sampling, the division between active and passive methods is based on whether a pump is used to push a larger amount of air into the detector (cf. Gustin et al., 2015, 2020; McLagan et al., 2016; Naccarato et al., 2021; Szponar et al., 2020). However, in lichenology, active methods are sometimes referred to as those that require transplanting lichens to a new site and passive methods of sampling as sampling of lichens that are found in-situ (Garty, 2002). For this reason, a common nomenclature that will be used in this thesis is presented in Figure 2.

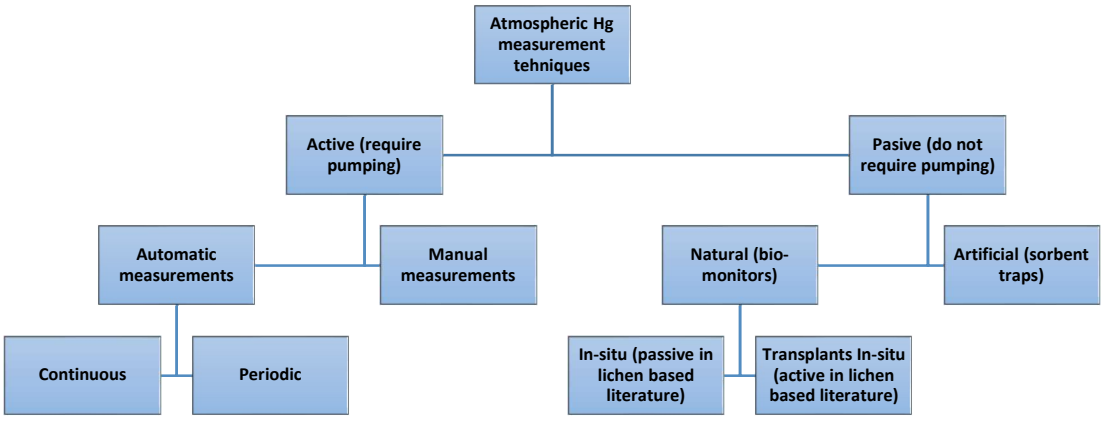

Figure 3: Types of techniques for measuring atmospheric mercury.

The first division is between active and passive devices, depends on whether pumping is required or not. Amongst the devices that require pumping, a distinction is between whether the measurements are manual or automatic. That is, if we have a simple trap to which a pump is connected and the measurements are performed in the laboratory. If the opposite is the case, there are two possibilities. Either the measurements are performed

continuously, with the sensor constantly active, or the mercury is released from the trap periodically. Devices that do not require pumping include artificial traps, which are similar to active traps but do not require pumping, and natural monitors, which are part of a larger group of bio-monitors that in case of mercury, primarily include mosses (Nickel et al., 2018; Sonke et al., 2022) and lichens (Horvat et al., 2000, Lupšina, 1992, Božič et al., 2022; T. L. Mlakar et al., 2011).

Lichens are widely used as a proxy for atmospheric composition (Lupšina et al., 1992, Conti & Cecchetti, 2001; Horvat et al., 2000; T. L. Mlakar et al., 2011; Monna et al., 2012; Szczepaniak & Biziuk, 2003). It has been shown that information on total element concentrations is not always sufficient for a meaningful identification of the source of contamination and that isotope content should be used (Barre et al., 2015, 2018). For this reason, the isotopic composition of mercury in lichens is often analyses to infer mercury sources (Barre et al., 2018; Blum et al., 2012; Carignan et al., 2009; Estrade et al., 2010; Jiménez-Moreno et al., 2016; Yamakawa et al., 2020).

1.3.2 Mercury in the Geogenic samples

Soils are an important research area of mercury science (cf. O'Connor et al., 2019; Wang et al., 2019; Zhu et al., 2018). This is because approximately 86 Gg of mercury of anthropogenic origin is stored in soil worldwide (O'Connor et al., 2019) and a total of up to 1000 Gg of mercury is stored (Obrist et al., 2018). The pathways of mercury to soil are either from atmospheric or geogenic sources. Atmospheric sources include wet and dry deposition (Jiskra et al., 2015) and can be sorted in various forms such as HgO, $HgCl_2$, HgS, or, MeHg, EtHg, or other forms of mercury (O'Connor et al., 2019) and also as Hg^0 for a shorter duration (Zhou & Obrist, 2021). These forms move differently through the soil profile and may also change from one form to another (McLagan et al., 2022). Mercury content from geogenic sources is much lower under pristine conditions (Kozin et al., 2013).

An important discovery in recent decades has been the realization of how strongly vegetation influences the storage of mercury in the soil (Wang et al., 2019). This is significant as the deposition of mercury to soil might be related to global atmospheric temperature changes (United Nations Environmental Programme, 2023). It is not exactly clear whether these changes would increase or decrease the deposition of mercury to soil (Haynes et al., 2017).

First studies on the mercury isotope ratios in soils were published in 2008, finding that the δ^{202}Hg range was up to 2.8‰ (Biswas et al., 2008). In the majority of forest soils studied, the δ^{202}Hg values ranged from -3 to -1 ‰ while the odd-MDF value ranged from 0 to -0.5 ‰ for Δ^{199}Hg and the even-MDF value was around zero (Demers et al., 2013; Jiskra et al., 2015; Zheng et al., 2016). In some soils near mercury-contaminated sites, the δ^{202}Hg value can also reach up to about 0.5 ‰ (Baptista-Salazar et al., 2018; McLagan et al., 2022). In general, the trend was that the upper, organic horizons exhibited more negative MDF values, while the lower horizons quickly changed to more positive MDF values. One such example can be found in a study by Zheng et al. (2016), in which the average shift from the upper to the lowest horizons was at least 1 ‰ at a variety of sites across North America.

Mercury ore deposits are hydrothermal in origin, but only about 0.02% of mercury is stored in such deposits, the rest is distributed in the Earth's crust (Kozin et al., 2013). Some of the ranges of mass dependently fractionating expressed in δ^{202}Hg in mines worldwide are: (I) New Idrija (USA) from -0.09‰ to 0.16‰ (Wiederhold et al., 2013), (II) McDermitt mountain (USA) -0.70‰ to -0.57‰ (Stetson et al., 2009), (III) Almadén mine (Spain) -2.25‰ to -0.96‰ (Gray et al., 2013), (IV) Monte Amiata (Italy) -2.70‰

to 1.39‰ (Pribil et al., 2020), and (V) Terlingua District (USA) -2.70‰ to 1.39‰ (Stetson et al., 2009). Specifically in Idrija, only one study was looking into the isotopic compositions of mercury. There, only two samples were measured showing the range from -0.26‰ to 0.23‰ (Foucher et al., 2009).

A large range would mean that the isotopic fingerprint may not be homogeneous and would be difficult to trace, whereas a much narrower range could be easier to trace in the environment. Isotopic analysis has been utilized to trace the likely source of mercury in different contexts. For instance, it has been employed to identify the origin of mercury from mining activities in various locations, including the Almadén mine in Spain, the New Idrija mine, the New Almadén Hg mine in the United States, and the Wanshan mining region in China (Donovan et al., 2013; Gehrke et al., 2011; Gray et al., 2013; C. N. Smith et al., 2008; R. S. Smith, Wiederhold, Jew, et al., 2015; Stetson et al., 2009; Wiederhold et al., 2013).

1.3.3 Mercury in Vegetation

Mercury in vegetation has an extremely wide-reaching effect on the environment, acting as both a sink and a source. Its role depends on whether the amount of biomass is increasing or decreasing (Zhou et al., 2021; Zhou & Obrist, 2021). This was uncovered to result in cycles of mercury concentrations fluctuations similar to the one well known for CO_2 (Jiskra et al., 2018). The importance of vegetation is not limited just to the atmosphere but also, as discussed above, to soil. Vegetation and litterfall deposition are likely the single largest sources of mercury deposition to soils (Obrist et al., 2014; Wang et al., 2019).

As the amount of biomass increases, whether in a form of a single leaf, a tree, a forest, or otherwise, some of the mercury is taken up from the atmosphere along with other compounds (Demers et al., 2013; Wang et al., 2020, 2021). The fractionation of isotopic fingerprint of both the atmosphere (Fu et al., 2019; Yu et al., 2016) and vegetation (Liu et al., 2022; Wang et al., 2021) was observed. Within one season, the isotope ratios of the leaves change from lower values at the beginning of the growing season to higher values at the end of the season (Yuan et al., 2019). In their study, Yuan et al. (2019) argue that this is due to the reductive loss of mercury from the foliage. However, there is another possible explanation, namely that mercury uptake changes during the leaf growth period. The leaves initially take up the heavier isotopes from the atmosphere, and during spring growth the pool of mercury available in the air gets scrubbed of the heavier isotopes and the isotopic composition shifts towards the lighter ones. This would explain the observed trends in the change of isotopic composition of the atmosphere detected (Fu et al., 2019; Li et al., 2020).

Such studies were thus far done in deciduous forests which marked by significant litterfall during winter, but lichens have not been specifically studied. Previous research assumed that the mercury isotope ratios of lichens are a reasonably good proxy for the isotope ratios in the atmosphere (MIF, MDF) (Carignan et al., 2009; Estrade et al., 2010). In the case of MIF, it was found that this is not the case. A first indication is that the atmospheric reservoir presents a much heavier MDF fingerprint than lichens (Demers et al., 2013; Gratz et al., 2010; Sherman et al., 2010). As discussed above, the kinetic process of photochemical reduction of Hg^{2+} in the aqueous fraction on lichens favors the odd isotopes (higher MIF), resulting in a lighter isotopic composition in lichens compared to the atmosphere (Blum et al., 2012, 2014; Demers et al., 2013).

Chapter 2

Aims and Hypothesis

2.1 Aims

The overall aim of the study is to trace mercury using its isotopic fingerprint in the Idrija region. This involves reviewing, implementing, and testing sample preparation and mercury isotope measurement procedures. The study focuses on optimizing measurement precision and accuracy using MC-ICP-MS. It initially examines lichens and atmospheric mercury concentrations in Idrija and neighboring areas to identify potential differences and specific mercury isotopic fingerprints. Subsequently, it extends the investigation to various samples from the Idrija mine, aiming to uncover correlations between excavation areas, ore types, and geological periods. Finally, the study leverages mercury isotopic composition to differentiate contamination pathways in the soils.

2.2 Hypothesis

- Hypothesis I: Mercury concentrations in transplanted and in-situ lichens are a suitable bio-marker for mercury concentrations in the atmosphere.
- Hypothesis II: There are no seasonal changes in either transplanted and in-situ lichens.
- Hypothesis III: The lichens from Idrija and Anhovo have a unique isotopic fingerprint compared to the background location at Pokljuka.
- Hypothesis IV: Atmospheric particulate matter mercury presents a similar trend in mercury concentrations and isotopic composition to the one observed in lichens.
- Hypothesis V: Ores from the Idrija mine exhibit a homogeneous and traceable isotopic fingerprint.
- Hypothesis VI: The isotopic fingerprint of ores is distinct for either the ore type, excavation site or the geological period of genesis.
- Hypothesis VII: Soils from the vicinity of ore roasting sites in Idrija present unique isotopic fingerprint.
- Hypothesis VIII: Soils in Anhovo present a distinct fingerprint closer to the Salonit cement plant, that could be traced to the pollution emanating from the plant.

Chapter 3

Scientific Publications

The dissertation consists of four publications with the candidate as the first author (three published – Section 3.1, 3.2, 3.3, one in preparation – Appendix A.3), two work reports (Appendix A.1, A.2) and a paper by a coworker (Appendix A.6) in the creation of which the candidate's work was instrumental. The publications presented here are ordered by date of publication. Supplementary material presented to the papers is presented in Appendices A.4 and A.5.

The articles presented are:

Dominik Božič, Igor Živković, Marta Jagodic Hudobivnik, Jože Kotnik, David Amouroux, Marko Štrok & Milena Horvat
Fractionation of mercury stable isotopes in lichens
Chemosphere, Volume 309, Part 1, 2022
https://doi.org/10.1016/j.chemosphere.2022.136592.

Dominik Božič, Igor Živković, Tatjana Dizdarević, Martina Peljhan, Marko Štrok & Milena Horvat
Insights into the Heterogeneity of the Mercury Isotopic Fingerprint of the Idrija Mine (Slovenia) Minerals, Volume 13, 1227
https://doi.org/10.3390/min13091227

Dominik Božič & Milena Horvat
Insights into seasonal variations in mercury isotope composition of lichens
Environmental Pollution, Volume 340, Part 1,
2024https://doi.org/10.1016/j.envpol.2023.122740

3.1 Fractionation of Mercury Stable Isotopes in Lichens

Dominik Božič, Igor Živković, Marta Jagodic Hudobivnik, Jože Kotnik, David Amouroux, Marko Štrok, Milena Horvat, Fractionation of mercury stable isotopes in lichens, Chemosphere, Volume 309, Part 1, 2022, https://doi.org/10.1016/j.chemosphere.2022.136592.

The study presented in this article monitored levels of mercury in the air using lichens that were transplanted and in-situ at three locations in Slovenia: Idrija, which is a former Hg mine with known contamination; Anhovo, a settlement with a cement production plant that is a source of Hg contamination; and Pokljuka, a national park area. The transplanted lichens were exposed to different environmental conditions and were sampled four times throughout a year. The results showed that the highest mercury concentrations were found in the Idrija area, consistent with previous research. During the summer, significant mass-dependent fractionation was observed in transplanted lichens, with a change in δ^{202}Hg from -3.0‰ in winter to -1.0‰ in summer. However, this trend was not observed in the most polluted Idrija sampling site, likely due to large amounts of Hg originating from polluted soil close to the former smelting plant. The study suggests that seasonality, particularly in summer, may affect the isotopic fractionation of Hg and should be taken into account in the sampling design and data interpretation.

The aim of this study was to provide unique information on the use of lichens as bio-monitors for the presence of Hg in the air, including stable isotope measurements, at sites with a wide range of Hg concentrations in the air. The sites included the former mercury mining area Idrija and the area around the cement production plant. These findings were particularly relevant due to the monitoring guidelines that had recently been issued for the evaluation of the effectiveness of the Minamata Convention. The guidelines outlined several monitoring possibilities, including active and passive measurements of elemental Hg, Hg speciation, and methods based on passive sampling and bio-monitoring, offering a tiered approach. Additionally, the guidelines envisaged the use of stable isotopes for source apportionment.

Chemosphere 309 (2022) 136592

Contents lists available at ScienceDirect

Chemosphere

journal homepage: www.elsevier.com/locate/chemosphere

Fractionation of mercury stable isotopes in lichens

Dominik Božič [a,b], Igor Živković [a], Marta Jagodic Hudobivnik [a], Jože Kotnik [a], David Amouroux [c], Marko Štrok [a,b], Milena Horvat [a,b,*]

[a] Department of Environmental Sciences, Jožef Stefan Institute, Jamova Street 39, Ljubljana, Slovenia
[b] Jožef Stefan International Postgraduate School, Jamova Street 39, Ljubljana, Slovenia
[c] The Institute of Analytical Sciences and Physico-Chemistry for Environment and Materials, 2 Avenue Pierre Angot, Pau Cedex 9, France

HIGHLIGHTS

- The isotopic composition of Hg in lichens changes seasonally.
- The heaviest isotopes in lichens are observed in the summer.
- At the contaminated sites, the local Hg isotopic fingerprint prevails.
- Lichens are a suitable bio-monitor in areas with elevated Hg in air.
- Natural variability of Hg in lichens prevents their use at uncontaminated sites.

GRAPHICAL ABSTRACT

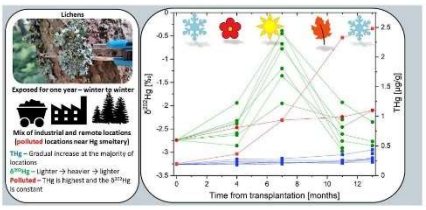

ARTICLE INFO

Handling Editor: Michael Bank

Keywords:
Mercury
Stable isotopes
Bio-monitoring
Lichens
Air

ABSTRACT

Bio-monitoring of mercury (Hg) in air using transplanted and *in-situ* lichens was conducted at three locations in Slovenia: (I) the town of Idrija in the area of the former Hg mine, where Hg contamination is well known; (II) Anhovo, a settlement with a cement production plant, which is a source of Hg contamination, and (III) Pokljuka, a part of a national park. Lichens from Pokljuka were transplanted to different sites and sampled four times—once per season, from January 2020 to February 2021. Lichens were set on tree branches, fences, and under cover, allowing them to be exposed to different environmental conditions (e.g., light and rain). The *in-situ* lichens were sampled at the beginning and the end of the sampling period. The highest concentrations were in the Idrija area, which was consistent with previous research. Significant mass-dependent fractionation has been observed in transplanted lichens during summer period. The δ^{202}Hg changed from −3.0‰ in winter to −1.0‰ in summer and dropped again to the same value in winter the following year. This trend was observed in all samples, except those from the most polluted Idrija sampling site, which was in the vicinity of the former Hg ore-smelting plant. This was likely due to large amounts of Hg originating from polluted soil close to the former smelting plant with a distinct isotopic fingerprint in this local area. The Δ^{199}Hg in transplanted lichens ranged from −0.5‰ to −0.1‰ and showed no seasonal trends. These findings imply that seasonality, particularly in summer months, may affect the isotopic fractionation of Hg and should be considered in the sampling design and data interpretation. This trend was thus described in lichens for the first time. The mechanism behind such change is not yet fully understood.

* Corresponding author. Department of Environmental Science, Jožef Stefan Institute, Jamova Street 39, Ljubljana, Slovenia.
E-mail address: milena.horvat@ijs.si (M. Horvat).

https://doi.org/10.1016/j.chemosphere.2022.136592
Received 25 May 2022; Received in revised form 2 September 2022; Accepted 21 September 2022
Available online 24 September 2022

1. Introduction

Mercury (Hg) is one of the most toxic elements. There is a global legally binding agreement regarding decreasing anthropogenic emissions and releases of Hg and its compounds—the Minamata Convention on Mercury (United Nations Environment Programme, 2019). An important aspect of the Minamata Convention is the monitoring of Hg in the atmosphere to assess the effectiveness of measures aimed at decreasing anthropogenic Hg emissions. As Hg can be transported over long distances within the atmosphere, it is often difficult to assess the contribution of local sources of Hg in the overall Hg composition of the atmosphere. This is additionally complicated by the presence of different forms of Hg in the atmosphere—gaseous elemental mercury (GEM; $Hg^0_{(g)}$), gaseous oxidised mercury (GOM; $Hg^{2+}_{(g)}$), and particulate-bound mercury (PBM; $Hg_{(p)}$)—all of which have different biogeochemical properties and cycle differently through environmental compartments (Ariya et al., 2015; Lyman et al., 2020; Si and Ariya, 2018). Therefore, it is important to improve our understanding of how to study and measure Hg in the atmosphere in order to design efficient and effective monitoring programs able to track the effectiveness of the implementation of the Minamata Convention.

There are two groups of methods for measuring Hg in the air—the so-called active and passive methods. Active methods include instruments that actively measure concentrations directly and require pumps to blow the air over Hg trap or the detector (Gustin et al., 2015). Passive methods include passive samplers (McLagan et al., 2016; Naccarato et al., 2021), pre-concentration by sorbent traps, and bio-monitoring using lichens, mosses, and other vegetation-based matrices. Correlations between such lichen use and the active methods have been reported (Mlakar et al., 2011). Bio-monitors include types of vegetation that absorb Hg from the atmosphere (Zhou and Obrist, 2021), such as mosses (Nickel et al., 2018; Szczepaniak and Biziuk, 2003) and lichens (Abas, 2021; Çobanoğlu Özyiğitoğlu, 2020). Bio-monitors are notable in the present context for the following reasons: (I) they can readily be found in nature, (II) they can provide insight into past air contamination, (III) they are less expensive and (IV) they are less likely to be vandalised than active methods (Garty, 2002).

There are two ways to apply lichens as bio-monitors—the *in-situ* method and the transplanted method. In the case of *in-situ* lichens, the lichens are collected directly where they are found, and in the case of transplanted lichens, they are collected at one spot and then exposed in another location. The transplantation method is flexible in that it allows for the exposure of lichens under a predetermined set of conditions, such as being covered to avoid rain and/or sun exposure. There are a number of studies where the concentrations of Hg in lichens (*in situ* and/or transplanted) have been measured (Berdonces et al., 2017; Horvat et al., 2000; Jeran et al., 2007; Klapstein et al., 2020; Gunnar Sillén, 1967; Mlakar et al., 2011). In some cases, the connection to pollution sources has been clearly established (Horvat et al., 2000). However, in some cases, the reality might be more difficult to interpret, especially if the relative differences in concentrations during exposure of transplanted lichens are low (Mlakar et al., 2011).

Over the last two decades, advanced analytical equipment has opened the door for researchers to determine stable isotope ratios of Hg. Isotopic analysis is an important tool used to improve our understanding of Hg cycling and behaviour in different environmental processes (Tsui et al., 2020). Hg has seven different stable isotopes, and they can fractionate during transport through and/or after deposition from the atmosphere (Blum et al., 2014). There are two types of Hg fractionation—mass dependent and mass independent. Mass-dependent fractionation (MDF) is represented as δ^{xxx}Hg, and mass-independent fractionation (MIF) as Δ^{xxx}Hg (Bergquist and Blum, 2007). There are a number of processes that affect Hg isotopic composition, including photo-reduction, evaporation, volatilization, absorption, microbial methylation, and microbial and/or chemical reduction (Yin et al., 2010). This means that Hg isotope ratios could be used to improve our understanding of the sources of Hg in the environment and assess the processes it has undergone.

Hg isotopes in lichens have already been utilised in studies attempting to discriminate pollution sources (Barre et al., 2018, 2020; Carignan et al., 2009; Estrade et al., 2010; Olson et al., 2019; Wang et al., 2020). In general, Hg isotopes in lichens have negative MDF (−2.5 to −0.5‰ for δ^{202}Hg) and MIF (−0.8 to 0.0‰ for Δ^{199}Hg) (Blum et al., 2014), while so far observed atmospheric Hg exhibits mostly positive MDF (0.0–1.5‰ for δ^{202}Hg) and negative MIF (−0.4 to 0.0‰ for Δ^{199}Hg) (Demers et al., 2013; Gratz et al., 2010; Sonke, 2011; Szponar et al., 2020; Wang et al., 2021). Various physicochemical processes can affect the Hg isotope ratios determined in lichen samples to the extent that they are not representative of the actual Hg isotopic composition in the air in which they were placed (Blum et al., 2012, 2014; Demers et al., 2013; Enrico et al., 2016).

It is presently not understood how these processes are affected by seasonal changes in temperature, sunlight exposure, or proximity to sources of Hg pollution. To the best of our knowledge, such processes have not yet been systematically studied in lichens. It should be noted that there are some MDF processes that also occur on sorbent traps and active samplers. Moreover, as described by Szponar et al. (2020), the configuration of a passive sampling device can alter the δ^{202}Hg by ≈ 1.0‰.

This study aimed to provide unique information on the use of lichens as bio-monitors for Hg presence in air, including stable isotopes measurements, at sites with a wide range of Hg concentrations in air. These sites include former mercury mining area Idrija and the second site is around the cement production plant.

These findings are especially relevant due to recently issued monitoring guidelines for the evaluation of the effectiveness of the Minamata Convention; the guidelines outline options for measuring Hg in air via a tiered approach, offering several monitoring possibilities. These include active and passive measurements of elemental Hg, Hg speciation, and methods based on passive sampling and bio-monitoring. The tiered approach of these guidelines also envisage the use of stable isotopes for source apportionment (UNEP, 2022).

2. Sampling locations

The sampling locations are presented in Fig. 1.

Idrija is a town with a wealthy history of Hg mining. The metasomatic Hg–rich ore in the dolomite is associated with Triassic igneous activity (Drovenik et al., 1990). It has been mined for about 500 years. The mine and a nearby smeltery have not operated since the 1990s; however, even decades after the closure, the concentrations of Hg in the air remain high, up to 5000 ng/m^3 (Grönlund et al., 2005; Kocman et al., 2011; Kocman and Horvat, 2011; Kotnik et al., 2005). For this study, the *in-situ* lichens were collected, and transplanted lichens were exposed at the following three locations: (I) Spodnja Idrija, a settlement located about 3 km downstream the Idrijca river from the town of Idrija, (II) Idrija, a town located above the mine shafts in the town, and (III) the Idrija smeltery, located at the site of former smelting plant. At the same sites, *in-situ* lichens were also collected. The average temperature at the Idrija meteorological station was 10.1 °C in 2020, the temperatures were below freezing for 8% of the year and above 15 °C for 31% of the year. The average winter humidity was 81% while the average summer humidity was 86%. The humidity was below 50% for 5% of the year (Slovenian Environmental Agency, 2022).

Anhovo is a settlement in western Slovenia, located in the middle of the Soča Valley. It is the site of the Salonit–Anhovo cement production plant. The annual average output of Hg from the plant has been estimated at 10 kg, with two-thirds comprised of GOM, one-third of GEM, and less than one percent of PBM (Mlakar et al., 2010). Transplanted lichens were exposed at the following four sites around the plant: (I) Anhovo and (II) Vodarna, which are both to the south of the Salonit–Anhovo cement plant, (III) Morsko, which is just north of the plant,

and (IV) Ročinj, which is about 3 km up the river. At the same sites, *in-situ* lichens were also collected. The prevailing wind direction is from the north-east to the south-west along the Soča river valley (Mlakar et al., 2011). There is no meteorological station in Anhovo, but the average temperature in 2020 in nearby Tolmin was 9.6 °C. The temperatures were below 0 °C for 6% of the year and above 15 °C for 24% of the year. The average winter humidity was 74% while the average summer humidity was 76%. The humidity was below 50% for 18% of the year (Slovenian Environmental Agency, 2022).

Pokljuka is a plateau with an average height of around 1200 m_{asl}. It is part of the Triglav National Park. It can be considered a clean or reference location with no known local Hg sources. Lichens were collected at five spots, spread 1 km apart in the spruce woods covering Pokljuka. The average temperature in 2020 was 8.6 °C, the temperatures were below freezing for 10% of the year, and above 15 °C for 23% of the year. The average winter humidity was 78% while the average summer humidity was 80%. The humidity was below 50% for 8% of the year (Slovenian Environmental Agency, 2022).

3. Methodology

3.1. Sampling of lichens and sample preparation

The epiphytic *Hypogymnia physodes* lichens were chosen, as they can be found at all of the study locations. This enables a direct comparison between the concentrations of Hg (Bergamaschi et al., 2007). The collection and transplantation processes were in line with the recommendations for sampling from Garty (2002). The *in-situ* lichens were collected at the beginning and end of the study period, January 2020 to February 2021. At first sampling, enough lichens were collected at Pokljuka to transplant them to all of the sampling sites. For each site, four bags of lichens were prepared for exposure. Bags were made from polyester mesh and each contained some 50 g of lichen attached to the bark. One bag per season was collected; the first at the beginning of the collection period (0 M) and the subsequent ones after four months (4 M), seven months (7 M), eleven months (11 M) and thirteen months (13 M), as indicated in Supplementary material S1. The *in-situ* lichens were collected at the same site or close to where the transplants were exposed. In the case of two sites—the towns of Anhovo and Idrija—additional bags with lichens were set under a roof cover (abbreviated further by C) but were still unsheltered from the sides. This was done to prevent direct exposure to rain and kept the lichens shaded, protected from direct sun exposure.

In the laboratory, lichens were moistened with deionised water, but not washed, in order to ease their removal from pieces of bark. Care was taken to minimise the removal of the PBM physically trapped in and/or bound to the cell wall. Lichen thalli were separated from the bark using polytetrafluoroethylene tweezers. The samples were lyophilised, and after immersion in liquid nitrogen, they were crushed in a zirconium mortar and ground with a vibration micro-pulveriser. The pulverised lichens were then homogenised. The dry weights of the samples were determined by weighing ≈0.1 g of the sample and heating it at 105 °C for 24 h in a drying oven.

Lichens were digested using a microwave digestion system (UltraWave, Milestone, Italy). About 0.3 g of each sample was weighed in precleaned polytetrafluoroethylene tubes. Then, 3 mL of 65% HNO_3 and 0.4 mL of 30% HCl (both suprapure grade) were added. The samples were subjected to closed-vessel microwave digestion at a max power of 1500 W and max pressure of 100 bar. The solution was filtered (0.45 µm), quantitatively transferred into 10-mL polyethylene graduated tubes, and diluted with Milli-Q water to 10 mL. Before measurements, 2 mL of the samples was again diluted to 10 mL with 5% HNO_3.

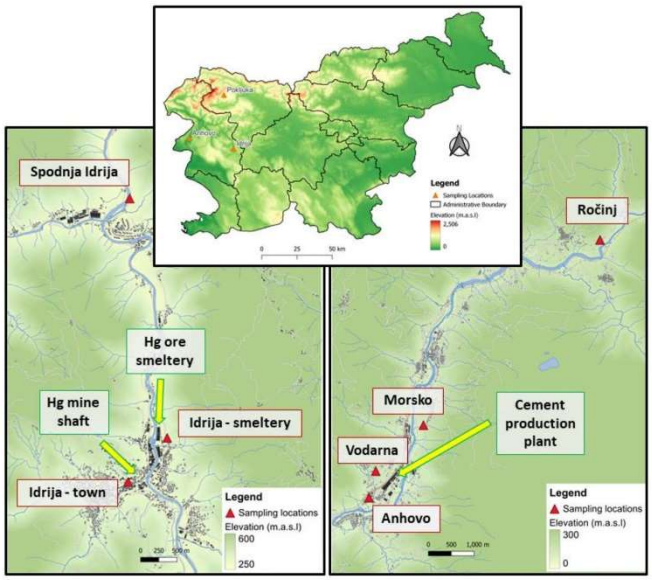

Fig. 1. Sampling locations are marked by orange triangles, and individual sampling sites are marked by red triangles in the zoomed-in view. Data from the Surveying and Mapping Authority of the Republic of Slovenia (2022). (For interpretation of the references to colour in this figure legend, the reader is referred to the Web version of this article.)

3.2. Direct measurements of Hg in air

The sampling of atmospheric Hg was performed at the same sites from July to December 2020 (Fig. 1). The sampling and measurements were performed using a LUMEX Hg Analyzer RA 915 M (Lumex Scientific, Russia). It measures only GEM using cold-vapor atomic absorption spectrometry with the applied Zeeman background correction. At each location, the detector was active for 30 min. Background correction was done every 10 min. The detection time was set at 1-s intervals. The obtained data was recorded by a computer using the Lumex software Rapid. The variability of the individual measurements was calculated as the standard deviation among all the measurements at a given time. The natural variability is presented as the standard deviation among all the measurements. The manufacturer specifies the limit of detection (LOD) for the instrument as 0.1 ng/m^3 for air and limit of quantification (LOQ) is 10 times that at 1 ng/m^3. During our long term experiments the precision was 22% (n = 600, k = 1, at 6 ng/m^3).

3.3. Determination of Hg concentration and isotopic ratios in lichens

Hg concnetrationswere measured with the Agilent 8800 (Agilent, USA) Triple-Quadrupole Inductively Coupled Plasma Mass Spectrometer (QQQ-ICP-MS). Instrumental operating conditions are provided in the supplementary material, Table S2. The measuring curve was derived from the NIST 3133 Standard Reference Material (Hg Standard Solution by National Institute of Standards and Technology).

Quality assurance and control were assessed using two matrix-matched reference materials (RMs)—IAEA 336 (Lichen) and BCR 482 (Lichen)—which were analysed in each batch of samples. The number of measured IAEA 336 replicates was 28. The reference value of 0.200 μg/g (0.160–0.240; 95% confidence interval) was matched by the average of our measurements of 0.201 ± 0.014 μg/g. The number of measured BCR 482 replicates was 12. The reference value of 0.480 μg/g (0.460–0.500; 95% confidence interval) was matched by the average of our measurements of 0.510 ± 0.020 μg/g. The LOD was determined by tripling the standard deviation of the procedural blanks and was 0.014 μg/g, representing less than 10% of the lowest Hg concentration in a lichen sample.

The samples were measured in duplicates. The differences were less than 3% in the majority of cases. However, in some cases in samples from the Idrija smeltery, the differences were as high as 16%, details in the supplementary material (Supplementary material S5). This marks the inhomogeneity of the sampled material. The reported results are the average of the two measurements. To evaluate the natural variability in the transplants, the standard deviation among the five lichens taken at Pokljuka at 0 M was calculated. The average concentration was 0.23 ± 0.05 μg/g, and the range from the lowest to highest was 0.18–0.3 μg/g.

Natural variability had to be applied to all the lichens subsequently transplanted from Pokljuka. Variability due to inhomogeneity and natural variability have been combined into a one overall variability, used here according to Equation (1).

$$overall\ variability = \sqrt[2]{inhomogeneity^2 + natural\ variability^2} \quad (1)$$

Isotopic ratios of Hg in the lichens were analysed with a Nu Plasma II (Nu instruments Ltd., Ametek, UK) Multi-Collector Inductively Coupled Plasma Mass Spectrometer (MC-ICP-MS) at the Jožef Stefan Institute (JSI). The instrument and the preparation lab are kept under clean conditions. Its operating conditions are provided in the Supplementary material S3. The *in-situ* lichens were analysed at the Institut des Sciences Analytiques et de Physicochimie pour l'Environnement et les Matériaux (IPREM). The procedure was the same as described in Yamakawa et al. (2021).

An auto-sampler ASX-520 (Teledyne Cetac, NE, USA) was used for sample introduction. The sample solution was pumped via a peristaltic pump to a 'T split' where it was mixed with $SnCl_2$ in a solution (3% w/v in 10% v/v HCl) to reduce Hg. The mix of solutions was transported to the phase separator. The recovery was as high as 99.6%. It was estimated using the concentration of Hg in the waste solution pumped out from the separation cell. From the phase separator, the elemental Hg vapor was carried over to the instrument by Ar sweep gas flow. The measurements were performed at Hg concentrations of 1 ng/mL. Intensities at m/z of 202 have been between 0.5 and 1.2 V. Outlier rejection of an individual measurement inside the cycle was done for the values above the relative three standard deviations (SD).

All measurements were done according to the sample–standard–sample bracketing technique (Peel et al., 2008). The results were reported using δ and Δ notations as shown in Equations (2) and (3) (Blum et al., 2014; Blum and Johnson, 2017), where f represents the correction factor, which was 0.2520 for Δ^{199}Hg, 0.5024 for Δ^{200}Hg, 0.7520 for Δ^{201}Hg, and 1.4930 for Δ^{204}Hg, and ^{xxx} represents the atomic mass of an isotope.

$$\delta^{xxx}Hg = \left(\frac{\frac{^{xxx}Hg}{^{198}Hg_{sample}}}{\frac{^{xxx}Hg}{^{198}Hg_{SRM3133}}} - 1 \right) \times 1000 \quad (2)$$

$$\Delta^{xxx}Hg = \delta^{202}Hg - \delta^{xxx}Hg \times f \quad (3)$$

At IJS and IPREM, the long term uncertainty of the measurements were evaluated using the NIST 8610 (UM-Almaden) (National Institute of Standards and Technology, 2017), while accuracy was reported as the standard deviation of the repeated NIST 8610 measurements (Table 1). All the uncertainties of the Hg isotope data in this paper are expressed at k = 2.

4. Results and discussion

4.1. Lichen and air Hg concentrations

The highest Hg concentration in *in-situ* lichens was found in the Idrija area—in order from highest to lowest were the Idrija smeltery, the town of Idrija, and Spodnja Idrija. This was in agreement with previously published data for Idrija (Horvat et al., 2000; Kocman et al., 2011; Kotnik et al., 2005). In the lichens from Anhovo and Vodarna (downwind from the cement plant), the Hg concentrations were higher than in the lichens upwind, as was previously observed by Mlakar et al. (2011).

There was some observable variability in the Hg concentrations between the first and second *in-situ* samplings (0 M and 13 M); details in supplementary material S5. Relative difference was up to four times, as was the case with the Idrija smeltery (1.4 ± 0.15 to 6.0 ± 0.26 μg/g). This could be a consequence of the so-called 'nugget effect,' where a single unit of PBM or a droplet of elemental Hg present on a single lichen thalli might significantly increase the Hg concentration; this has been observed by Kocman et al. (2011).

The Hg concentrations in transplanted lichens increased in the Idrija area but remained largely the same at both Pokljuka and Anhovo. The highest increase was observed at the Idrija smeltery, while the increase was lower at the other two sampling locations in Idrija. There is a slight dip in concentrations of Hg in spring (4 M) lichens of majority of the sampling sites. These include all of the Anhovo area sites, Spodnja Idrija and some decrease in the upward trend of increase at Idrija – town. Such dip is also evident at Pokljuka for which only three measurements were available. This observation rules out the possibility that this decrease is a consequence of exposure of lichen at a new location. Such a decrease would than likely reflect the overall change in the concentration of Hg in the forest air. Such a trend has already been observed. Jiskra et al. (2018) observed a cyclical trend of increases and decreases of atmospheric Hg concentration in a forest system which they attributed to uptake of Hg by the leaves of the trees in the spring and summer. When the leaves fall from the trees, they decay and Hg may be reemitted back

Table 1
Values of stable isotopes from the NIST 8610 [‰] certificate with the U in parentheses, as well as the ones measured in this study with the standard deviation of the samples in parentheses.

Organisation	n		δ199Hg	δ200Hg	δ201Hg	δ202Hg	δ204Hg	Δ199Hg	Δ200Hg	Δ201Hg	Δ204Hg
NIST	n/a	‰	−0.17	−0.27	−0.46	−0.56	−0.82	−0.03	0.00	−0.04	0.00
		U (k = 2)	(0.01)	(0.01)	(0.02)	(0.03)	(0.07)	(0.02)	(0.01)	(0.01)	(0.02)
IJS	19	‰	−0.17	−0.25	−0.44	−0.49	−0.74	−0.05	0.00	−0.06	−0.02
		2 * S.D.	(0.15)	(0.12)	(0.17)	(0.20)	(0.18)	(0.11)	(0.07)	(0.09)	(0.25)
IPREM	20	‰	−0.15	−0.24	−0.40	−0.51	−0.77	−0.02	0.01	−0.02	0.02
		2 * S.D.	(0.12)	(0.10)	(0.16)	(0.16)	(0.19)	(0.09)	(0.06)	(0.09)	(0.12)

into the air. Therefore, the lichen Hg concentrations might reflect, at least in part, the ones in the air.

Lichens shielded from direct sunlight and dry or wet deposition gained Hg more slowly than the openly exposed lichens in the town of Idrija (Fig. 2). In Idrija – town this meant 0.46 ± 0.05 μg/g for openly exposed lichens compared to 0.31 ± 0.05 μg/g for covered lichens. In Anhovo the difference is much less significant. The differences between the shielded and open-air exposed lichens were likely the consequence of the cover preventing some of the direct Hg deposition.

The concentrations of Hg in air showed the same trend as the one observed in lichens, with the highest average concentrations of Hg at the Idrija smeltery and the lowest in Anhovo and Pokljuka. Similar findings were already described by Mlakar et al. (2011). A relationship between the average Hg concentrations in air and lichens can therefore be estimated. This relationship gets established relatively soon after transplantation, already at four months. At locations with lower concentrations of Hg (Anhovo), correlation was not clearly evident (Fig. 3).

The Hg concentrations in air fluctuated significantly over time. At the Idrija – smeltery, the concentrations ranged from 5.10 to 78.2 ng/m^3. This could be the consequence of the changes in wind direction and speed between different measurements. At other locations, the Hg concentration was relatively stable. Unfortunately, the sampling device used (Lumex RA 915 M) is not very suitable for reliable determinations of Hg at concentrations around 1 ng/m^3. The data for all of the sampling site apart of the Idrija – smeltery and Idrija – town barely above the LOQ (Supplementary material S4). To gain better knowledge a more sophisticated equipment or method and longer measurement times should be used.

4.2. Hg isotope ratios

Fig. 4 represents the temporally sorted values for the mass-dependent and independent fractionation presented by δ^{202}Hg and Δ^{199}Hg, respectively, for *in-situ* and transplanted lichens. The data is presented in the Supplementary material S6.

The δ^{202}Hg in lichens ranged from −3.0 to −0.5‰, and the Δ^{199}Hg from −0.5 to −0.0‰. This was in line with the previously published data

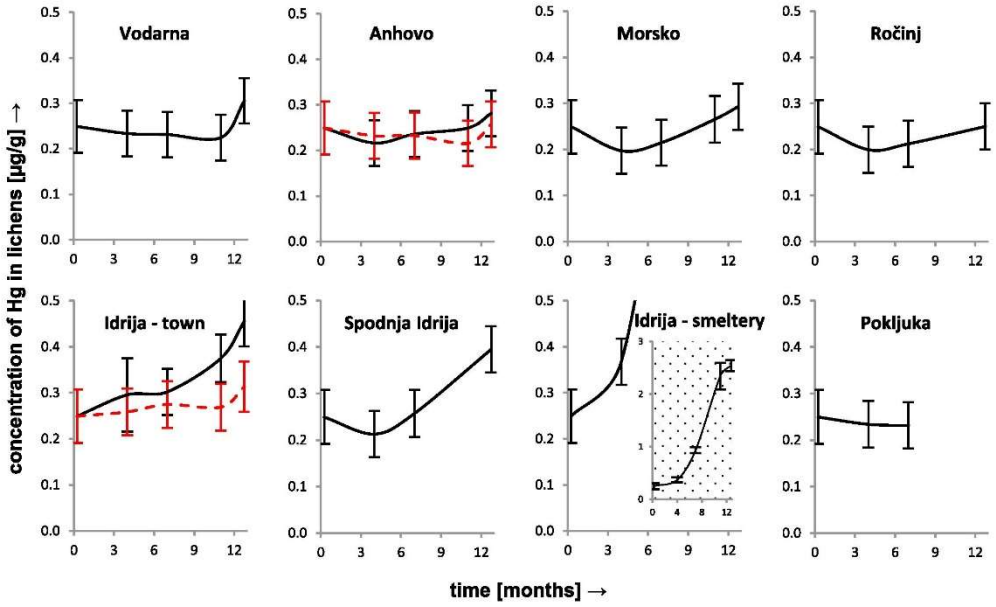

Fig. 2. Graphs representing changes in Hg concentration in the transplanted lichens (normally exposed indicated in black and covered indicated by dashed red lines). To cover the whole concentration range, additional zoomed out graph is present at Idrija smeltery region. (For interpretation of the references to colour in this figure legend, the reader is referred to the Web version of this article.)

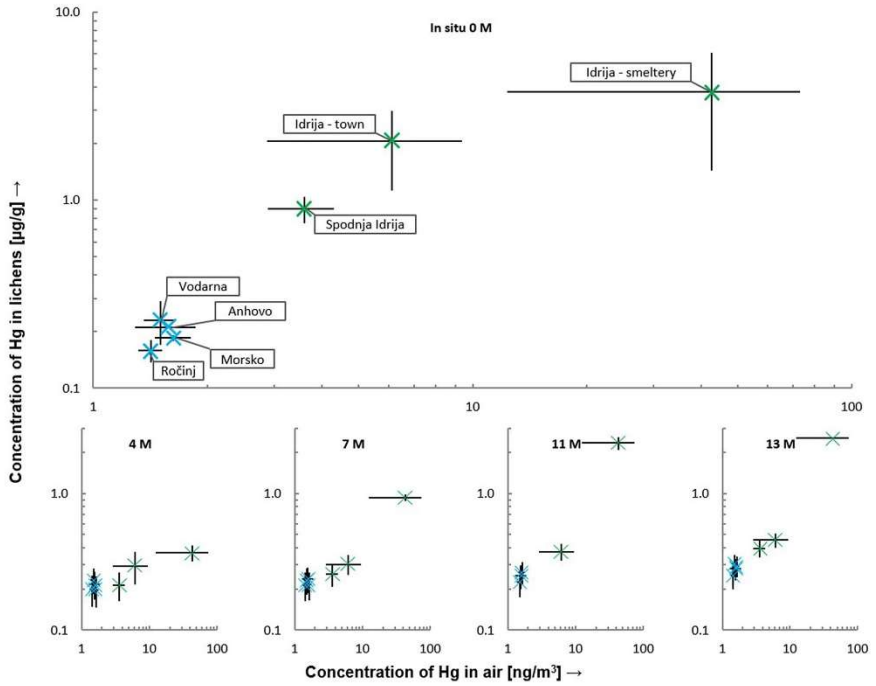

Fig. 3. Relationship between the in *in-situ* (0 M) and transplanted lichens (4 M, 7 M, 11 M, 13 M) and air concentration of Hg. Idrija sites in green and Anhovo ones in blue. X and Y axis in log scale. (For interpretation of the references to colour in this figure legend, the reader is referred to the Web version of this article.)

(Barre et al., 2020; Blum et al., 2012; Carignan et al., 2009). The *in-situ* δ^{202}Hg was the lowest in Pokljuka, with −3.1 ± 0.6‰ among the five samples measured there. In general, the Idrija samples had lower δ^{202}Hg values than those from the Anhovo area (−2.0 ± 0.3 vs. −1.6 ± 0.6‰).

To evaluate the natural variability, the isotopic composition of the five lichens from Pokljuka was analysed. The standard deviation among them for δ^{202}Hg was 0.3‰, and for Δ^{199}Hg, it was 0.1‰. The variations among the locations that were relatively close to one another were also high. For example, in Anhovo and Vodarna, which are only a few hundred meters away from each other, the difference was 0.6‰. The highest δ^{202}Hg for Anhovo was −2.0 ± 0.2‰, while at Vodarna, which is only a few hundred meters away; the highest δ^{202}Hg was −1.4 ± 0.2‰.

There was a major change in δ^{202}Hg of the transplanted lichens during the time of their exposure. In winter, at the beginning and end of the exposure period, the δ^{202}Hg values were the lowest, while in the summer, the highest values were observed. The average difference between summer and winter values for δ^{202}Hg was 1.7‰. The δ^{202}Hg values returned close to the starting values of the Pokljuka *in-situ* values and not to those found in the *in-situ* lichens at an individual site. This trend was observed at all sampling sites except the Idrija smeltery.

In a similar study of mosses by Enrico et al. (2016), the shift in δ^{202}Hg was observed between the samples collected during the spring–summer and fall–winter seasons. There was no discrimination among individual seasons, spring and summer values are presented together and the fall and winter ones together. The spring–summer isotopes showed an average increase of 0.4‰ compared to those in the fall–winter ones.

Covered lichens from the location in the town of Idrija showed a lesser response of δ^{202}Hg than those that were exposed to open air (by 0.3‰). Similar finding was observed by Enrico et al. (2016) where the mosses that were left covered showed a lesser response of δ^{202}Hg by up to 0.7‰ compared to the covered mosses.

An outlier from these trends was the Idrija - smeltery. There, the isotopic composition only continued to increase slightly throughout the whole year, ending close to the *in-situ* value.

This could be explained through the new Hg rapidly accumulating, as seen in the Hg concentration data. This was due to the proximity to the former smeltery, which is a source of Hg reemission (Kocman et al., 2011).

The similarity of the Hg isotopic composition of both the shielded and open air–exposed lichens indicated that the shade provided by the cover did not significantly influence the isotopic composition. It is therefore likely, that the majority of Hg comes in the form of Hg^0 and is deposited with dry deposition.

Some correlations can be made between the lichen δ^{202}Hg and other environmental factors. The most obvious one is the temperature, which followed the same trend of lowest in the winter and highest in the summer. It was observed that the δ^{202}Hg in lichen was the lowest where the temperatures were the lowest. So the Pokljuka which had the lowest temperatures, most days below 0 °C, also had lowest δ^{202}Hg values. On the other hand, there was little difference between the average humidity during winter or summer months at all of the locations. The other correlation is with leaf cover. The leaves in Slovenia start growing in spring and fall off in autumn. As previously discussed, another correlation is with the concentrations of Hg in the forest air. The forest δ^{202}Hg in air fluctuates in the exact same way as in the lichens (Fu et al., 2019). However, no explanation of the mechanism was provided in the study,

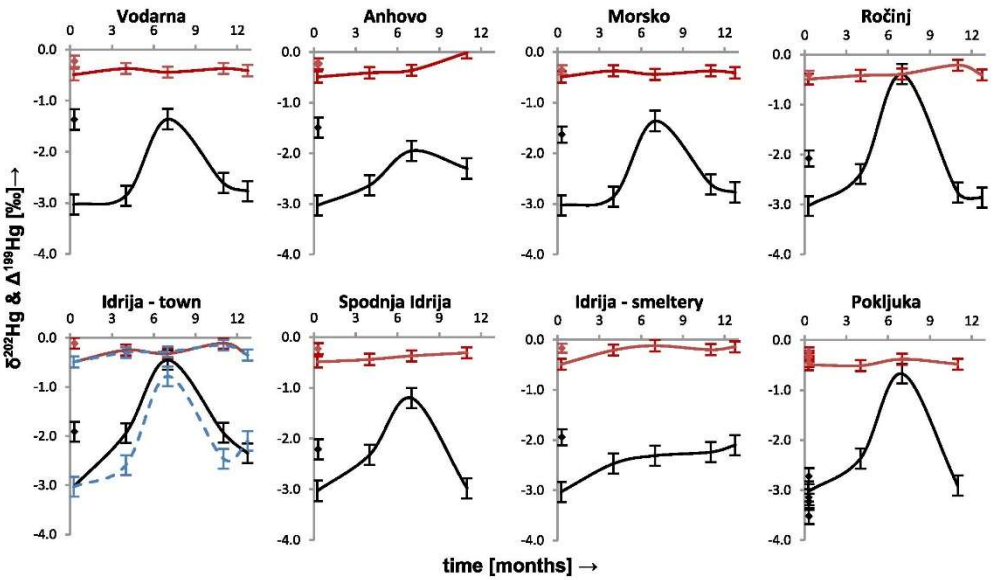

Fig. 4. Graphs representing the δ^{202}Hg (black) and Δ^{199}Hg (red) in transplanted lichens over time. The dashed blue lines represent the isotopic composition of the covered sample. The ◆ marks represent the *in-situ* lichens collected at the beginning of the sampling period (0 M). Error bars represent the long-term uncertainty (k = 2) of the standard reference material. (For interpretation of the references to colour in this figure legend, the reader is referred to the Web version of this article.)

apart from the speculation that higher vegetation activity likely induces higher δ^{202}Hg. It must be considered that the range of change of δ^{202}Hg in forest air described by Fu et al. (2019) is similar to that in lichens observed here, albeit from ≈0 to ≈ 2‰. The temperature might affect also the evasion of Hg from soils (Obrist et al., 2014; Zhou et al., 2021) which would be cyclical and connected to temperature. Lichens have been observed as the most metabolically active at temperatures above freezing (Kappen et al., 1996). This would mean that any process that might include both Hg and lichen metabolism might be impacted by the temperature.

There are a few potential mechanisms that could affect the isotopic ratios of the lichens. They would likely be a complex mix of these mechanisms and potentially others.

Kinetic fractionation during the uptake is one such mechanism, as suggested first by Demers et al. (2013). There such a mechanism was suggested to explain the difference between lighter isotopes found in leaves and heavier in the air in forest ecosystem. When the Hg passes from air to leaves, the heavier isotopes preferably stay in the air and lighter ones are more easily incorporated. The same might be true for lichens as speculated by Blum et al. (2014).

Evaporation of Hg^0 is another mechanism that supports some of these observations. The increased evaporation of lighter isotopes from the lichen thalli during the hotter summer months of the year, leaving the heavier behind and thereby increasing the δ^{202}Hg. During evaporation experiments, a positive MDF shift of ≈1.2‰ for δ^{202}Hg has been observed (Ghosh et al., 2013). Though this is not an analogous experiment it is more likely that the remaining Hg becomes depleted in lighter isotopes making its signature more positive.

Reduction of Hg^{2+} could cause some changes in its isotopic ratios. The Hg^{2+} already bound to a lichen get photo-reduced to Hg^0 and then escape from it. These changes would make the δ^{202}Hg more positive (Enrico et al., 2016; Sun et al., 2019; Zheng et al., 2019; Zheng and Hintelmann, 2010). But this is likley a minor factor as the the chenge of δ^{202}Hg in lichens showed little correlation regardles of the expousure to light.

Equilibration to new isotopic signature in the air is another mechanism that could explain the findings. As stated above, the concentration of Hg and the δ^{202}Hg in the air changes. The heaviest isotopes can be found during the summer which get incorporated into the lichen at the time. While during the winter, more lighter isotopes get incorporated.

Concentration effect might be another factor effecting the previous three. With lower forest canopy gaseous Hg concentrations in the spring and summer due to plant uptake, there should be less fractionation of Hg^0 by lichens during uptake since at lower concentrations there is less chance for Hg loss by volatilization before subsequent oxidation in leaves. At higher concentrations of atmospheric Hg in winter, isotope discrimination during lichen uptake could be more fully expressed since there is a greater chance for Hg volatilization before oxidation in leaves.

There was a slight trend of increase in Δ^{199}Hg in the transplanted lichens in all locations (from −0.5 to −0.0‰), but there were no discernible seasonal trends. The trend of slight increase in Δ^{199}Hg could be explained by the fact that the lichens in Pokljuka received higher amounts of light before they were collected and transplanted. After transplantation, some of the lichens in the bags had less exposure to light and therefore were not as subject to photo-reduction or inducing MIF and began to reflect Δ^{199}Hg closer to 0.0‰.

5. Conclusions

It was shown that lichens can be effectively used for Hg monitoring, using concentrations or isotopes, in areas above background concentrations such as around the former Hg mine and smeltery. It was observed that transplanted or *in-situ* lichens bio-monitoring provides similar results in terms of Hg concentration.

A trend in the change of δ^{202}Hg throughout the four seasons has been observed. The exact drivers behind the increase and decrease of δ^{202}Hg are not known but are correlated with temperature and deciduous plant leaf growth. The potential mechanisms could be linked to fractionation upon the uptake of Hg, the evaporation of Hg^0, photoreduction and subsequent loss of Hg^{2+} in the leaves or the change in the isotopic ratios of local air. These effects might be influenced by the concentration of air Hg as well. The exact mechanisms affecting the Hg isotopic composition of the lichens might be a complex mixture of all of these factors.

This, in turn, means that lichens cannot be viewed as a one-time probe into atmospheric Hg but rather as part of a larger system that includes natural and anthropogenic sources that change through time and interact with one another. In the case of heavily contaminated sites, these trends are overridden due to the high Hg concentrations with a determined isotopic composition.

This study affirmed the idea that bio-monitoring using lichens can be successfully applied in regional and global monitoring as it offers cost effective approach, but overall, the protocols should be precisely defined or even better standardized.

Author roles

Dominik Božič: Methodology, Investigation, Data curation, Writing – original draft, Visualization. **Igor Živković:** Methodology, Investigation. **Marta Jagodic Hudobivnik:** Investigation, **Jože Kotnik:** Investigation, **David Amouroux:** Investigation. **Marko Štrok:** Methodology, Supervision, Writing – Review. **Milena Horvat:** Conceptualization, Writing – Review, Supervision, Project administration, Funding acquisition.

Declaration of competing interest

The authors declare that they have no known competing financial interests or personal relationships that could have appeared to influence the work reported in this paper.

Data availability

Data will be made available on request.

Acknowledgements

This study has been supported financially by (I) the MercOx project (project no. 16ENV01), which has received funding from the EMPIR program co-financed by the Participating States, and the European Union's Horizon 2020 research and innovation program IGOSP (Integrated Global Observation System for Persistent Pollutions; project no. 689443) founded by the European Commission in the framework of program 'the European network for observing our changing planet (ERA-405 PLANET); (II) the GMOS-Train (project no. 860497), which has received funding from the European Unions' Horizon 2020 research and innovation program under the Maria Sklodowska-Curie fund; and (III) the Slovenian Research Agency (ARRS; grants no. P1-0143, PR-54685 and IsoCont J1-3033).

The authors would like to thank Mr. Francis Maaire Gyengne and Mrs. Sabina Berisha for their help with sample collection and preparation, Dr. Emmanuel Tessier with isotopic analysis and Mr. Saeed Waqar Ali for help with figure curation.

Appendix A. Supplementary data

Supplementary data to this article can be found online at https://doi.org/10.1016/j.chemosphere.2022.136592.

References

Abas, A., 2021. A systematic review on biomonitoring using lichen as the biological indicator: a decade of practices, progress and challenges. Ecol. Indicat. 121, 107197 https://doi.org/10.1016/j.ecolind.2020.107197.

Ariya, P.A., Amyot, M., Dastoor, A., Deeds, D., Feinberg, A., Kos, G., Poulain, A., Ryjkov, A., Semeniuk, K., Subir, M., Toyota, K., 2015. Mercury physicochemical and biogeochemical transformation in the atmosphere and at atmospheric interfaces: a review and future directions. Chem. Rev. 115 (10), 3760–3802. https://doi.org/10.1021/cr500667e.

Barre, J.P.G., Deletraz, G., Sola-Larrañaga, C., Santamaria, J.M., Bérail, S., Donard, O.F. X., Amouroux, D., 2018. Multi-element isotopic signature (C, N, Pb, Hg) in epiphytic lichens to discriminate atmospheric contamination as a function of land-use characteristics (Pyrénées-Atlantiques, SW France). Environ. Pollut. 243, 961–971. https://doi.org/10.1016/j.envpol.2018.09.003.

Barre, J.P.G., Queipo-Abad, S., Sola-Larrañaga, C., Deletraz, G., Bérail, S., Tessier, E., Elustondo Valencia, D., Santamaría, J.M., de Diego, A., Amouroux, D., 2020. Comparison of the isotopic composition of Hg and Pb in two atmospheric bioaccumulators in a pyrenean beech forest (iraty forest, western pyrenees, France/Spain). Frontiers in Environmental Chemistry 1 (November), 1–16. https://doi.org/10.3389/fenvc.2020.582001.

Berdonces, M.A.L., Higueras, P.L., Fern, M., Borreguero, A.M., Carmona, M., 2017. The role of native lichens in the biomonitoring of gaseous mercury at contaminated sites. J. Environ. Manag. 186, 207–213. https://doi.org/10.1016/j.jenvman.2016.04.047.

Bergamaschi, L., Rizzio, E., Giaveri, G., Loppi, S., Gallorini, M., 2007. Comparison between the accumulation capacity of four lichen species transplanted to a urban site. Environ. Pollut. 148 (2), 468–476. https://doi.org/10.1016/j.envpol.2006.12.003.

Bergquist, B.A., Blum, J.D., 2007. Mass-dependent and -independent fractionation of Hg isotopes by photoreduction in aquatic systems. Science 318 (5849), 417–420. https://doi.org/10.1126/science.1148050.

Blum, J.D., Johnson, M.W., 2017. Recent developments in mercury stable isotope analysis. Rev. Mineral. Geochem. 82, 733–757. https://doi.org/10.2138/rmg.2017.82.17. July 2013.

Blum, J.D., Johnson, M.W., Gleason, J.D., Demers, J.D., Landis, M.S., Krupa, S., 2012. Mercury concentration and isotopic composition of epiphytic tree lichens in the athabasca oil sands region. In: Developments in Environmental Science, first ed., vol. 11. Elsevier Ltd, pp. 373–390. https://doi.org/10.1016/B978-0-08-097760-7.00016-0.

Blum, J.D., Sherman, L.S., Johnson, M.W., 2014. Mercury isotopes in earth and environmental sciences. Annu. Rev. Earth Planet Sci. 42 (February), 249–269. https://doi.org/10.1146/annurev-earth-050212-124107.

Carignan, J., Estrade, N., Sonke, J.E., Donard, O.F.X., 2009. Odd isotope deficits in atmospheric Hg measured in lichens. Environ. Sci. Technol. 43 (15), 5660–5664. https://doi.org/10.1021/es900578v.

Çobanoğlu Özyiğitoğlu, G., 2020. Use of lichens in biological monitoring of air quality. In: Environmental Concerns and Sustainable Development. https://doi.org/10.1007/978-981-13-5889-0_3.

Demers, J.D., Blum, J.D., Zak, D.R., 2013. Mercury isotopes in a forested ecosystem: implications for air-surface exchange dynamics and the global mercury cycle. Global Biogeochem. Cycles 27 (1), 222–238. https://doi.org/10.1002/gbc.20021.

Drovenik, M., Dolenec, T., Režun, B., Pezdič, J., 1990. On the mercury ore from the Grübler orebody, Idrija. Geologija 33 (1), 397–446. https://doi.org/10.5474/geologija.1990.010.

Enrico, M., Roux, G. Le, Marusczak, N., Heimbürger, L.E., Claustres, A., Fu, X., Sun, R., Sonke, J.E., 2016. Atmospheric mercury transfer to peat bogs dominated by gaseous elemental mercury dry deposition. Environ. Sci. Technol. 50 (5), 2405–2412. https://doi.org/10.1021/acs.est.5b06058.

Estrade, N., Carignan, J., Donard, O.F.X., 2010. Isotope tracing of atmospheric mercury sources in an urban area of Northeastern France. Environ. Sci. Technol. 44 (16), 6062–6067. https://doi.org/10.1021/es100674a.

Fu, X., Zhang, H., Liu, C., Zhang, H., Lin, C.J., Feng, X., 2019. Significant seasonal variations in isotopic composition of atmospheric total gaseous mercury at forest sites in China caused by vegetation and mercury sources. Environ. Sci. Technol. 53 (23), 13748–13756. https://doi.org/10.1021/acs.est.9b05016.

Garty, J., 2002. Biomonitoring heavy metal pollution with lichens. In: Protocols in Lichenology. https://doi.org/10.1007/978-3-642-56359-1_27, 458–482.

Ghosh, S., Schauble, E.A., Lacrampe Couloume, G., Blum, J.D., Bergquist, B.A., 2013. Estimation of nuclear volume dependent fractionation of mercury isotopes in equilibrium liquid-vapor evaporation experiments. Chem. Geol. 336, 5–12. https://doi.org/10.1016/j.chemgeo.2012.01.008.

Gratz, L.E., Keeler, G.J., Blum, J.D., Sherman, L.S., 2010. Isotopic composition and fractionation of mercury in Great Lakes precipitation and ambient air. Environ. Sci. Technol. 44 (20), 7764–7770. https://doi.org/10.1021/es100383w.

Grönlund, R., Edner, H., Svanberg, S., Kotnik, J., Horvat, M., 2005. Mercury emissions from the Idrija mercury mine measured by differential absorption lidar techniques and a point monitoring absorption spectrometer. Atmos. Environ. 39 (22), 4067–4074. https://doi.org/10.1016/j.atmosenv.2005.03.027.

Gunnar Sillén, Lars, 1967. The ocean as a chemical system. Science 156 (June), 1189–1197.

Gustin, M.S., Amos, H.M., Huang, J., Miller, M.B., Heidecorn, K., 2015. Measuring and modeling mercury in the atmosphere: a critical review. Atmos. Chem. Phys. 15 (10), 5697–5713. https://doi.org/10.5194/acp-15-5697-2015.

Horvat, M., Jeran, Z., Spiric, Z., Jacimovic, R., Miklavcic, V., 2000. Mercury and other elements in lichens near the INA Naftaplin gas treatment plant, Molve, Croatia. J. Environ. Monit. 2 (2), 139–144. https://doi.org/10.1039/a906973i.

Jeran, Z., Mrak, T., Jaćimović, R., Batič, F., Kastelec, D., Mavsar, R., Simončič, P., 2007. Epiphytic lichens as biomonitors of atmospheric pollution in Slovenian forests. Environ. Pollut. 146 (2), 324–331. https://doi.org/10.1016/j.envpol.2006.03.032.

Jiskra, M., Sonke, J.E., Obrist, D., Bieser, J., Ebinghaus, R., Myhre, C.L., Pfaffhuber, K.A., Wängber, I., Kyllönen, K., Wirthy, D., Martin, L.G., Labuschagne, C., Mkololo, T., Ramonet, M., Magand, O., Dommergue, A., 2018. A vegetation control on seasonal variations in global atmospheric mercury concentrations. Nat. Geosci. 11 (4), 244–250. https://doi.org/10.1038/s41561-018-0078-8. In this issue.

Kappen, L., Schroeter, B., Scheidegger, C., Sommerkorn, M., Hestmark, G., 1996. Cold resistance and metabolic activity of lichens below 0°C. Adv. Space Res. 18 (12), 119–128. https://doi.org/10.1016/0273-1177(96)00007-5.

Klapstein, S.J., Walker, A.K., Saunders, C.H., Cameron, R.P., Murimboh, J.D., O'Driscoll, N.J., 2020. Spatial distribution of mercury and other potentially toxic elements using epiphytic lichens in Nova Scotia. Chemosphere 241, 125064. https://doi.org/10.1016/j.chemosphere.2019.125064.

Kocman, D., Horvat, M., 2011. Non-point source mercury emission from the Idrija Hg-mine region: GIS mercury emission model. J. Environ. Manag. 92 (8), 2038–2046. https://doi.org/10.1016/j.jenvman.2011.03.034.

Kocman, D., Vreča, P., Fajon, V., Horvat, M., 2011. Atmospheric distribution and deposition of mercury in the Idrija Hg mine region, Slovenia. Environ. Res. 111 (1), 1–9. https://doi.org/10.1016/j.envres.2010.10.012.

Kotnik, J., Horvat, M., Dizdarević, T., 2005. Current and past mercury distribution in air over the Idrija Hg mine region, Slovenia. Atmos. Environ. 39, 7570–7579. https://doi.org/10.1016/j.atmosenv.2005.06.061, 39 SPEC. ISS.

Lyman, S.N., Cheng, I., Gratz, L.E., Weiss-Penzias, P., Zhang, L., 2020. An updated review of atmospheric mercury. Sci. Total Environ. 707, 135575 https://doi.org/10.1016/j.scitotenv.2019.135575.

McLagan, D.S., Mitchell, C.P.J., Huang, H., Lei, Y.D., Cole, A.S., Steffen, A., Hung, H., Wania, F., 2016. A high-precision passive air sampler for gaseous mercury. Environ. Sci. Technol. Lett. 3 (1), 24–29. https://doi.org/10.1021/acs.estlett.5b00319.

Mlakar, T.L., Horvat, M., Vuk, T., Stergaršek, A., Kotnik, J., Tratnik, J., Fajon, V., 2010. Mercury species, mass flows and processes in a cement plant. Fuel 89 (8), 1936–1945. https://doi.org/10.1016/j.fuel.2010.01.009.

Mlakar, T.L., Horvat, M., Kotnik, J., Jeran, Z., Vuk, T., Mrak, T., Fajon, V., 2011. Biomonitoring with epiphytic lichens as a complementary method for the study of mercury contamination near a cement plant. Environ. Monit. Assess. 181 (1–4), 225–241. https://doi.org/10.1007/s10661-010-1825-5.

Naccarato, A., Tassone, A., Martino, M., Moretti, S., MacAgnano, A., Zampetti, E., Papa, P., Avossa, J., Pirrone, N., Nerentorp, M., Munthe, J., Wängberg, I., Stupple, G. W., Mitchell, C.P.J., Martin, A.R., Steffen, A., Babi, D., Prestbo, E.M., Sprovieri, F., Wania, F., 2021. A field intercomparison of three passive air samplers for gaseous mercury in ambient air. Atmos. Meas. Tech. 14 (5), 3657–3672. https://doi.org/10.5194/amt-14-3657-2021.

National Institute of Standards & Technology, 2017. Report of Investigation Reference Material 8610 Isotopes in UM-Almaden Mono-Elemental Secondary Standard. Department of Commerce - USA.

Nickel, S., Schröder, W., Schmalfuss, R., Saathoff, M., Harmens, H., Mills, G., Frontasyeva, M.V., Barandovski, L., Blum, O., Carballeira, A., de Temmerman, L., Dunaev, A.M., Ene, A., Fagerli, H., Godzik, B., Ilyin, I., Jonkers, S., Jeran, Z., Lazo, P., et al., 2018. Modelling spatial patterns of correlations between concentrations of heavy metals in mosses and atmospheric deposition in 2010 across Europe. Environ. Sci. Eur. 30 (1), 1–17. https://doi.org/10.1186/s12302-018-0183-8.

Obrist, D., Pokharel, A.K., Moore, C., 2014. Vertical profile measurements of soil air suggest immobilization of gaseous elemental mercury in mineral soil. Environ. Sci. Technol. 48 (4), 2242–2252. https://doi.org/10.1021/es4048297.

Olson, C.L., Jiskra, M., Sonke, J.E., Obrist, D., 2019. Mercury in tundra vegetation of Alaska: spatial and temporal dynamics and stable isotope patterns. Sci. Total Environ. 660, 1502–1512. https://doi.org/10.1016/j.scitotenv.2019.01.058.

Peel, K., Weiss, D., Chapman, J., Arnold, T., Coles, B., 2008. A simple combined sample-standard bracketing and inter-element correction procedure for accurate mass bias correction and precise Zn and Cu isotope ratio measurements. J. Anal. At. Spectrom. 23 (1), 103–110. https://doi.org/10.1039/b710977f.

Si, L., Ariya, P.A., 2018. Recent advances in atmospheric chemistry of mercury. Atmosphere 9 (2), 1–18. https://doi.org/10.3390/atmos9020076.

Slovenian Environmental Agency, 2022. Daily weather reports. https://meteo.arso.gov.si/met/en/.

Sonke, J.E., 2011. A global model of mass independent mercury stable isotope fractionation. Geochem. Cosmochim. Acta 75 (16), 4577–4590. https://doi.org/10.1016/j.gca.2011.05.027.

Sun, R., Jiskra, M., Amos, H.M., Zhang, Y., Sunderland, E.M., Sonke, J.E., 2019. Modelling the mercury stable isotope distribution of Earth surface reservoirs: implications for global Hg cycling. Geochem. Cosmochim. Acta 246, 156–173. https://doi.org/10.1016/j.gca.2018.11.036.

Surveying and Mapping Authority of the Republic of Slovenia, 2022. No Title. https://egp.gu.gov.si/egp/?lang=en.

Szczepaniak, K., Biziuk, M., 2003. Aspects of the biomonitoring studies using mosses and lichens as indicators of metal pollution. Environ. Res. 93 (3), 221–230. https://doi.org/10.1016/S0013-9351(03)00141-5.

Szponar, N., McLagan, D.S., Kaplan, R.J., Mitchell, C.P.J., Wania, F., Steffen, A., Stupple, G.W., Monaci, F., Bergquist, B.A., 2020. Isotopic characterization of atmospheric gaseous elemental mercury by passive air sampling. Environ. Sci. Technol. 54 (17), 10533–10543. https://doi.org/10.1021/acs.est.0c02251.

Tsui, M.T.K., Blum, J.D., Kwon, S.Y., 2020. Review of stable mercury isotopes in ecology and biogeochemistry. Sci. Total Environ. 716, 135386 https://doi.org/10.1016/j.scitotenv.2019.135386.

UNEP, 2022. United nations. https://www.mercuryconvention.org/sites/default/files/documents/information_document/4_INF12_MonitoringGuidance.English.pdf.

United Nations Environment Programme, 2019. Minamata Convention on Mercury, United Nations.

Wang, X., Yuan, W., Lin, C.J., Luo, J., Wang, F., Feng, X., Fu, X., Liu, C., 2020. Underestimated sink of atmospheric mercury in a deglaciated forest chronosequence. Environ. Sci. Technol. 54 (13), 8083–8093. https://doi.org/10.1021/acs.est.0c01667.

Wang, X., Yuan, W., Lin, C.J., Feng, X., 2021. Mercury cycling and isotopic fractionation in global forests. Crit. Rev. Environ. Sci. Technol. 1–24. https://doi.org/10.1080/10643389.2021.1961505, 0(0).

Yamakawa, A., Amouroux, D., Tessier, E., Bérail, S., Fettig, I., Barre, J.P.G., Koschorreck, J., Rüdel, H., Donard, O.F.X., 2021. Hg isotopic composition of one-year-old spruce shoots: application to long-term Hg atmospheric monitoring in Germany. Chemosphere 279. https://doi.org/10.1016/j.chemosphere.2021.130631.

Yin, R., Feng, X., Shi, W., 2010. Application of the stable-isotope system to the study of sources and fate of Hg in the environment: a review. Appl. Geochem. 25 (10), 1467–1477. https://doi.org/10.1016/j.apgeochem.2010.07.007.

Zheng, W., Hintelmann, H., 2010. Nuclear field shift effect in isotope fractionation of mercury during abiotic reduction in the absence of light. J. Phys. Chem. A 114 (12), 4238–4245. https://doi.org/10.1021/jp910353y.

Zheng, W., Demers, J.D., Lu, X., Bergquist, B.A., Anbar, A.D., Blum, J.D., Gu, B., 2019. Mercury stable isotope fractionation during abiotic dark oxidation in the presence of thiols and natural organic matter [Research-article]. Environ. Sci. Technol. 53 (4), 1853–1862. https://doi.org/10.1021/acs.est.8b05047.

Zhou, J., Obrist, D., 2021. Global Mercury Assimilation by Vegetation. Environmental Science & Technology. https://doi.org/10.1021/acs.est.1c03530.

Zhou, J., Wang, Z., Zhang, X., Driscoll, C.T., 2021. Measurement of the vertical distribution of gaseous elemental mercury concentration in soil pore air of subtropical and temperate forests. Environ. Sci. Technol. 55 (3), 2132–2142. https://doi.org/10.1021/acs.est.0c05204.

3.2 Mercury Source Apportionment in Contaminated Soils Using Isotope Fingerprinting

Dominik Božič, Igor Živković, Tatjana Dizdarević, Martina Peljhan, Marko Štrok & Milena Horvat Insights into the Heterogeneity of the Mercury Isotopic Fingerprint of the Idrija Mine (Slovenia), Minerals, Volume 13, 1227, 2023, https://doi.org/10.3390/min13091227

In the study presented here, we aimed to define the isotopic composition range of mercury (Hg) originating from the Idrija mine. We conducted comprehensive analyses on samples obtained from the mine itself and from the Mercury Heritage Management Centre's geological collection, representing diverse geological periods, genesis types, ore categories, formations, excavation sites, and levels. Our analyses encompassed both Hg concentration and isotopic composition, yielding a range of δ202Hg from -1.35‰ to 0.46‰ and Δ199Hg from -0.18‰ to 0.16‰.

While a relatively consistent ore fingerprint was observed in one excavation field, the overall isotopic composition of the Idrija mine appeared heterogeneous. This study provides the first statistically robust constraints on Hg's isotopic composition from the Idrija mine, offering potential insights for future research on similar ore deposits and the tracing of Hg from the mine to its surrounding environment.

Despite our efforts to pinpoint the isotopic characteristics of different periods of Hg deposition, we were able to draw several conclusions concerning various sample types and excavation sites:

-The Idrija mine exhibits a relatively wide isotopic fingerprint compared to most other findings, with a δ202Hg range of -1.35‰ to 0.46‰.

-The ranges of Mass-Independent Fractionation (MIF) observed are similar to those of other mines, with Δ199Hg ranging from -0.16‰ to 0.18‰.

-We identified one instance of a relatively uniform fingerprint in the Kropač excavation field.

-The isotopic fingerprints of cinnabar and Hg(l) from the same excavation site cannot be statistically differentiated.

This study contributes valuable insights by describing a wide range of Hg isotopic fingerprints found within the mine. This information may prove beneficial to other researchers studying complex Hg deposits worldwide or those specifically investigating the Idrija deposit.

minerals

MDPI

Article

Insights into the Heterogeneity of the Mercury Isotopic Fingerprint of the Idrija Mine (Slovenia)

Dominik Božič [1,2], Igor Živković [1,2], Tatjana Dizdarević [3], Martina Peljhan [3], Marko Štrok [1,2] and Milena Horvat [1,2,*]

[1] Department of Environmental Science, Jožef Stefan Institute, 1000 Ljubljana, Slovenia; dominik.bozic@ijs.si (D.B.)
[2] Jožef Stefan International Postgraduate School, 1000 Ljubljana, Slovenia
[3] Idrija Mercury Heritage Management Centre, 5280 Idrija, Slovenia
* Correspondence: milena.horvat@ijs.si

Abstract: To determine the range of the isotopic composition of mercury (Hg) from the Idrija mine, samples from the mine itself and from the Mercury Heritage Management Centre geological collection were analyzed. Samples from various geological periods, genesis types, ore types, formations, and excavation fields and levels were analyzed. Both Hg concentration and isotopic composition were measured. The δ^{202}Hg ranged from −1.35‰ to 0.46‰, and the Δ^{199}Hg ranged from −0.18‰ to 0.16‰. A relatively homogenous ore fingerprint was obtained from one of the excavation fields; otherwise, the isotopic fingerprint of the Idrija mine seems to be heterogenous. This study presents the first statistically robust constraints on the isotopic composition of Hg from the Idrija mine, which may help in further studies of the isotopic composition of similar ore bodies or the potential tracing of Hg from the mine to the environment in the vicinity or downstream of the mine.

Keywords: mercury; isotope; ore; mine

Citation: Božič, D.; Živković, I.; Dizdarević, T.; Peljhan, M.; Štrok, M.; Horvat, M. Insights into the Heterogeneity of the Mercury Isotopic Fingerprint of the Idrija Mine (Slovenia). *Minerals* **2023**, *13*, 1227. https://doi.org/10.3390/min13091227

Academic Editors: Kejun Hou and Yanhe Li

Received: 29 August 2023
Revised: 11 September 2023
Accepted: 12 September 2023
Published: 18 September 2023

1. Introduction

Tracking the pathways of mercury (Hg), a toxic trace element monitored by the United Nations Environmental Program, is of great importance [1–4]. Part of the terrestrial cycle of Hg [5,6] is represented by legacy mining sites. One such site is located in Idrija, Slovenia, where Hg ore has been mined and processed over the last five centuries. In the last century, the Idrija Hg mine was the subject of intensive research by geologists [7–12]. Extensive research has shown that the elevated Hg content in this area is due to: (I) outcrops of Hg-bearing geological formations [7,13], (II) mining and processing activities [14,15], (III) the re-emission of mine tailings and ore deposits [15,16], and (IV) the re-emission from soils and biota contaminated by sources I–III [15,17,18].

The ore genesis is likely best summarized by Berce [7]. The first Hg impregnation of rock formations occurred during rifting in the Triassic period and was accompanied by the impregnation of rocks with barite, fluor, copper, manganese, strontium, and zinc. The Hg-bearing chlorine vapors came from deep beneath the crust. On their way to the surface, they likely dissolved the pyrite present in the carbonates, which introduced sulphur (S). The vapors also experienced a drop in pressure and temperature. These conditions were favorable for the precipitation of cinnabar (HgS). The impregnation process took a relatively long time and occurred under various conditions, depending on which forms of HgS were formed.

In the so-called Jeklenka ore, with its black steel-like hew, the cinnabar crystals are relatively small, and concentrations of Hg reach up to 78% in some sources [19]. In the more reddish-colored Opekovka ore, the crystals are larger, but the Hg concentrations are lower. In some cases, the ore was deposited syngenetically with sedimentary layers, forming banded ore, Opekovka, Jeklenka, and Coral ores, while in others, it was deposited

epigenetically, directly into the already-formed rock formation, creating impregnations or substitutions [7,12]. Liquid Hg ($Hg0_{(l)}$) is also present and thought to have originated from two sources: (I) the primary direct deposition of Hg during primary impregnation due to a lack of sulfur ions that would bind it to HgS or (II) subsequent remobilization of the primary HgS due to leaching by the pore water, which resulted from the tectonic fracturing in the area [7,11,12].

The emergence of new analytical technologies that enable the determination of the ratios between the stable isotopes of Hg has allowed new possibilities for isotopic fingerprinting and provenience determination [20]. This is because Hg isotopes fractionate in both mass-dependent and mass-independent ways. Mass-dependent fractionation (MDF) is mostly the result of reactions such as evaporation, thiol-ligand binding, microbial methylation and reduction, and iron oxide sorption, while mass-independent fractionation (MIF) is mostly the result of photochemical reactions [21,22]. MDF is expressed as a ratio between a chosen isotope pair, while MIF is quantified by comparing the measured MDF with the one predicted using the measured MDF value and the kinetic MDF law established through transition state theory. When the variations are minor, typically less than about 10‰, these values can be approximated [21]. There are also two types of MIF that are observed. One is the odd-MIF, affecting the odd isotopes of Hg, and the other is even-MIF, affecting the even isotopes of Hg. Odd-MIF stems from the magnetic isotope effect, which takes place in photochemical radical pair reactions, while even-MIF is more cryptic and believed to stem from the nuclear self-shielding effect [21]. Ores exhibit a wide range of MDF, sometimes with some odd-MIF and no even-MIF [21,23–25].

The isotopic fingerprinting of Hg likely originating from mining areas has been employed in various settings. For example, the origin of Hg from mines and production facilities has been determined in the Almadén mine in Spain; the New Idrija mine; the New Almadén Hg mine in the US [23,24,26–30], and the Wanshan mining region in China [31,32]. In the Idrija region, few articles have been published on mercury isotopes [18,33], and only two samples of Hg ore have been measured thus far [34]. To our knowledge, no study has attempted to significantly constrain the isotopic fingerprint of an excavation field, an ore type, a formation, or a geological period. This information could aid in the further determination of the isotopic fingerprint of Hg excavated during different periods of operation at the Idrija mine. For this purpose, a sampling of the ores from the Idrija mine was carried out. It was expected that potential correlations might be uncovered which would aid in the Hg ore deposition description and the characterization of the isotopic fingerprint of the ores mined at a certain period of the mine's operation.

2. Materials and Methods

2.1. Sampling

Samples were collected in the summer of 2022 from the still-accessible levels of the former Hg mine in Idrija. Samples were excavated using a hammer and collected in zip-lock bags. The $Hg_{(l)}$, which was in small puddles on the rocks, was scooped from the rocks using a plastic Pasteur pipette. Today, only three of the mine's 15 upper levels are accessible; therefore, most of the samples were taken from the geological collection of the Idrija Mercury Heritage Management Centre. As these were museum exponates, only small pieces could be broken off or sawed off with a circular saw, as was attempted with the more compact pieces. In total, about 5 g of each single sample was collected. The types of samples are given in Table 1. These samples include ore types and formations. The names of the samples were preserved as they are found in the geological collection and are the same as those commonly used in the previous literature about Idrija ore deposits and by the miners during the period of the active Hg excavation.

Table 1. Types of samples and descriptions.

Type of Sample	Description
Carbone shale	Carbone shales are the oldest rocks of the Idrija ore deposit. They are composed of mud, clays, silt, and silicate sand with occasional inclusions of conglomerates, which are interchanged rapidly. Afterwards, the tectonic processes shape the shales into various bodies with the common name of Carbone shales. These rocks are gray to dark gray in color and very soft, which makes them difficult to excavate. Carbone shales include $Hg_{(l)}$ and cinnabar, with the ratio between the two commonly being 1:1. The Hg content reached up to 10% of Hg, but in most cases, it was around 0.3%.
Impregnated cinnabar	Impregnated cinnabar is represented by pyrite (FeS_2) and cinnabar (HgS) concretions in mudstone that were impregnated with $Hg_{(l)}$. The concretion is composed of pyrite, with mostly idiomorphic cryosections substituted with HgS. A detailed description is given by Mlakar and Drovenik [11].
Opekovka ore	Opekovka, or brick, ore was named by the miners. Opekovka ore is relatively common in the mine but is usually found in rather small deposits.
Jeklenka ore	Jeklenka, or steel, ore is a gaelic cinnabar type of ore composed of a cinnabar rich in organic matter. It has a fluidic structure and a metallic gray hue.
Impregnated dolomite	Dolomite $CaMg(CO_3)_2$ impregnated with Hg, mostly as cinnabar, which fills in the pores in dolomite and, in some cases, substitutes for the original rock.
Skonca beds	A geological formation containing both cinnabar and $Hg_{(l)}$. A detailed description is offered by Čar [19]
$Hg_{(l)}$	Elemental Hg^0 in liquid form.
Tufa	Tufa is composed of particles of silicate (SiO_2), claystone, and plankton radiolites and some other particles. The matrix is mostly chalcedony (SiO_2, trigonal) and pyrite. In the polished thin sections, a gradual granularity can be observed. The color ranges from green, in Tufa that is poorer in Hg, to the red, in Tufa that is richer in Hg.
Banded ore	Banded ore presents an interchanging sequence of layers of mudstone with cinnabar-impregnated chalcedony. Many infield fractures with cinnabar are observed. The chalcedony impregnated with cinnabar has the distinct color of Opekovka ore.
Jetrenka ore	Jetrenka, or liver, ore is syngenetically formed Hg in bituminous shale or, in some cases, a bituminous radiolarite. Jetrenka ores are found next to slip-faults where the organic matter mixed with cinnabar got smeared over the fault and produced a distinct liver-like color.
Conglomerate ore	Conglomerate ore consists of unsorted, differently sized rounded clasts in a sand-sized dolomite matrix. It contains veins and impregnations of cinnabar, which primarily substitutes for the matrix.
Coral ore	Coral ore is a syngenetic ore represented by black bituminous silicate sandstone that is rich in brachiopod shales. Miners mistook the brachiopod shells for corals, giving this ore its name. It is a part of the Skonca beds.
Karoli ore	Karoli ores are among the most unique ores of the deposit, as they are only found in the deepest part of the mine of the same name. The genesis of this type of ore has not been sufficiently studied. It is, however, known that it is an epigenetic ore with strong pyrite mineralization, which was later crushed and substituted with cinnabar.

2.2. Sample Preparation

The samples were crushed in an agate mortar. Rock samples were digested using the Ethos microwave digestion system (Milestone, Sorisole, Italy). Approximately 0.2 g of the sample was weighed into pre-cleaned polytetrafluoroethylene tubes. For digestion, 5 mL of 65% HNO_3 (nitric acid), 2 mL of 40% HF (hydrofluoric acid), 1 mL of 30% HCl (hydrochloric acid), and 1 mL of 30% H_2O_2 (hydrogen peroxide), all supra-pure grade, were used. The digestion process included 30 min for ramping up to the maximum temperature of 150 °C at a maximum power of 1200 W. This temperature was maintained for an additional 30 min, and cooling to room temperature took 1.5 h. The digestate was quantitatively transferred into 30-mL polyethylene tubes by rinsing them with 10 mL of Milli-Q water. Here, 10 mL of 5% H_2BO_3 (boric acid) were added to neutralize the HF. The digestion products of the ore samples were then diluted 100-fold. The digestion of the $Hg_{(l)}$ samples was performed

using with the same reagent mix but without microwave assistance. It was subsequently diluted 1000-fold. In both cases, the dilutions were carried out with 5% HNO_3.

2.3. Analysis

The Hg concentration was determined using a Model Hg-201 semiautomated mercury analyzer and cold vapor atomic absorption spectroscopy (CV-AAS: Sanso Seisakusho Co., Tokyo, Japan). Quality assurance and control were evaluated using a standard reference material, NIST 2711 Montana Soil II (the closest available analogue to the geological material) [35]. The average recovery for Hg was 101.2%, with relative standard deviation of ±5.6% (number of samples (N) was 6).

The isotopic ratios of Hg were analyzed using a Nu Plasma II (Nu Instruments, Wrexham, UK) Multicollector Inductively Coupled Plasma Mass Spectrometer (MC-ICP-MS). The details of the operating conditions are given in Table 2.

Table 2. Operating conditions of Nu Plasma II MC-ICP-MS.

Parameter	Setting
Sampler cone	Ni, FB9
Skimmer cone	Ni, HS1-7
RF power	1300 W
Ar cooling gas	13.0 L/min
Ar auxiliary gas	0.8 L/min
Ar sweep gas flow	20 mL/min
Ar mix gas flow	70 mL/min
$SnCl_2$ and sample uptake rate	0.9–1.1 mL/min
Mass separation	1
Blocks	1
Measurements per block	30
Magnet delay time [s]	2
Transfer time [s]	50
Wash time—5% HNO_3	10 s
Analytical concentration	1–1.5 ng/mL
Sensitivity	1–5 V
Total analysis time	11 min

Briefly, the sample solution was pumped via a peristaltic pump into a T split, where it was mixed with $SnCl_2$ in solution (3% w/v) to reduce the Hg^{2+} in the solution to Hg^0 in the gaseous phase. The mix of solutions was transported to the phase separator, where Ar gas carried the produced Hg^0 to the MC-ICP-MS. The measurements were then performed at Hg concentrations between 1 and 1.5 ng/mL. The signal intensities at an m/z of 202 were between 1 and 5 V, depending on the measurement session. Blank measurements were constantly monitored and presented no more than 1% to 3% of the signal for an individual sample measurement.

Measurements were performed according to the sample-standard-sample bracketing method [35], using the NIST 3133 standard [36]. The deviation between the sample and the standard voltage was always less than 10%. The results for isotopic composition were denoted by δ for MDF and Δ for MIF (Equations (1) and (2)), where f represents the

correction factor (0.2520 for Δ^{199}Hg, 0.5024 for Δ^{200}Hg, 0.7520 for Δ^{201}Hg, and 1.4930 for Δ^{204}Hg) and ^{xxx}Hg represents the mass number of a particular mercury isotope [21,37].

$$\delta^{xxx}Hg = \left(\frac{\frac{^{xxx}Hg}{^{198}Hg}_{sample}}{\frac{^{xxx}Hg}{^{198}Hg}_{NIST\ 3133}} - 1 \right) \times 1000 \quad (1)$$

$$\Delta^{xxx}Hg = \delta^{xxx}Hg - \delta^{202}Hg \times f \quad (2)$$

Accuracy is reported as the standard deviation of repeated NIST 8610 (UM-Almadén) measurements (Table 3) [38]. The standard deviations for the isotope values are given with the expanded factor (k = 2). Additionally, NIST 2711a (Montana soil) standard reference material was used, as it represented the closest match to the samples used here [39].

Table 3. The repetitive measurements of NIST 8610 and NIST 2711a. Standard deviation is abbreviated by SD and where not number was given it is noted by n.a. for not given.

Sample				δ^{199}Hg (‰)	δ^{200}Hg (‰)	δ^{201}Hg (‰)	δ^{202}Hg (‰)	δ^{204}Hg (‰)	Δ^{199}Hg (‰)	Δ^{200}Hg (‰)	Δ^{201}Hg (‰)	Δ^{204}Hg (‰)
NIST 8610	This study	N = 16	Avg.	−0.15	−0.27	−0.45	−0.54	−0.82	−0.01	0.01	−0.04	−0.01
			2SD	(0.04)	(0.05)	(0.08)	(0.10)	(0.17)	(0.04)	(0.03)	(0.03)	(0.04)
	[38]	n.a.	Avg.	−0.17	−0.27	−0.46	−0.56	−0.82	−0.03	−0,00	−0.04	0.00
			2SD	(0.01)	(0.01)	(0.02)	(0.03)	(0.07)	(0.02)	(0.01)	(0.01)	(0.02)
NIST 2711a	This study	N = 6	Avg.	−0.20	−0.07	−0.22	−0.14	−0.19	−0.16	0.00	−0.11	0.02
			2SD	(0.04)	(0.07)	(0.09)	(0.12)	(0.17)	(0.03)	(0.02)	(0.02)	(0.05)
	[39]	N = 6	Avg.	−0.26	−0.11	−0.34	−0.24	n.a.	−0.20	0.01	−0.16	n.a.
			2SD	(0.22)	(0.24)	(0.27)	(0.37)	n.a.	(0.17)	(0.15)	(0.10)	n.a.

3. Results and Discussion

In the mine samples, a range of almost 2‰ was observed for δ^{202}Hg (from −1.35‰ to 0.53‰), while Δ^{199}Hg ranged by about 0.4‰ (from −0.16‰ to 0.18‰). The average δ^{202}Hg was −0.46‰ (±1.10‰ 2SD), the average Δ^{199}Hg was 0.01 (±0.17‰ 2SD), and the average Hg content (c(Hg)) was 23.9%. No statistically significant even-MIF was observed in these samples, as expected for geological material [21]. The sample type, with the collection identification number, when applicable; the individual periods from which particular samples were obtained; the excavation field and level; the isotopic composition and Hg content, are presented in Table 4.

The range of MDF in ore samples (a single Opekovka sample and a single Jeklenka sample) previously reported for Idrija is much more constrained, at 0.49‰ for δ^{202}Hg (−0.26‰ to 0.23‰) [34]. The range of δ^{202}Hg in some other mines was 0.25‰ (−0.09‰ to 0.16‰) for the New Idrija mine (USA) [26], 0.13‰ (−0.57‰ to −0.70‰) for McDermitt cinnabar [23], 1.07‰ (−0.92‰ to 0.15‰) for the Almadén mine (Spain) [24], 1.29‰ (−2.25‰ to −0.96‰) for Monte Amiata (Italy) [25], and 4.09‰ (−2.70‰ to 1.39‰) for the Terlingua District (USA) [23]. These high values in the Terlingua District are reportedly due to the fact that various hydrothermally deposited Hg-bearing minerals (montroydrite, kleinite, terlinguaite, metacinnabar, and calomel) were measured. It has been suggested that fractionation in the Terlingua District was caused either by isotopic fractionation during mineral formation due to different formation temperatures, paragenesis or variable redox states or bond strengths between the different minerals [23,40], and, in the case of $Hg_{(l)}$-containing minerals, by the different proportions between the mineral-bound and liquid phases [23]. Similarly, the Δ^{199}Hg ranges of the Terlingua District are more restricted as compared to δ^{202}Hg and reach 0.46‰ [24]. The results presented here bring the isotopic composition of Idrija close to that of the other well-documented hydrothermal Hg deposits. This indicates that the isotopic composition of Idrija ores cannot be considered homogenous.

Table 4. Type of sample, with the museum identification, when applicable; the geologic period from which the sample originates; its Hg isotopic fingerprint, and the Hg content. N.a. stands for not available and was used for any samples for which we had no data in that category. The samples from the museum have the museum identification number written next to them.

Type of Sample and Museum Identification	Geologic Period [Ma]	Excavation Field and Level	δ^{199}Hg (‰)	δ^{200}Hg (‰)	δ^{201}Hg (‰)	δ^{202}Hg (‰)	δ^{204}Hg (‰)	Δ^{199}Hg (‰)	Δ^{200}Hg (‰)	Δ^{201}Hg (‰)	Δ^{204}Hg (‰)	cHg (‰)
Carbone shale	Carboniferous (358.9–298.9)	Kropač (I/20)	−0.36	−0.67	−1.06	−1.35	−2.03	−0.02	0.01	−0.04	−0.01	0.608
Impregnated cinnabar (499)		Karbon (III/4)	0.03	0.21	0.26	0.46	0.63	−0.08	−0.02	−0.09	−0.05	0.021
Impregnated cinnabar (508)		Karbon (III/4)	−0.15	−0.42	−0.61	−0.91	−1.37	0.08	0.04	0.07	−0.02	0.767
Opekovka ore (513)	Middle Permian (272.9–259.1)	Kreda (VI)	−0.04	0.24	0.32	0.53	0.87	−0.18	−0.03	−0.09	0.07	85.5
Jeklenka ore (525)		n./a.	−0.07	−0.05	−0.12	−0.08	−0.13	−0.05	−0.01	−0.06	−0.02	69.5
Impregnated dolomite (542)	Lower Triassic (251.9–247.2)	Grübler (XIII/8)	0.02	0.19	0.22	0.35	0.53	−0.06	0.02	−0.04	0.01	0.006
Impregnated dolomite (559)		Kreda (VII)	−0.22	−0.61	−0.90	−1.25	−1.89	0.10	0.02	0.04	−0.03	54.4
Impregnated dolomite (964)		Rop Koželj (n.a.)	−0.16	−0.27	−0.43	−0.59	−0.88	−0.01	0.02	0.01	0.00	0.095
Impregnated dolomite (806)	Anisian (247.2–242.0)	Leithner (III)	−0.12	−0.19	−0.33	−0.38	−0.56	−0.03	0.00	−0.05	0.01	0.020
Impregnated dolomite (807)		Leithner (III)	−0.13	−0.18	−0.33	−0.36	−0.54	−0.04	0.00	−0.06	0.00	9.75
Skonca beds	Ladinian (242–237)	Kropač (I/20)	−0.24	−0.51	−0.80	−1.14	−1.71	0.05	0.06	0.05	−0.01	4.66
Skonca beds		Kropač (I/20)	−0.04	−0.35	−0.50	−0.78	−1.19	0.16	0.04	0.09	−0.03	10.3
Skonca beds		Kropač (I/17)	−0.23	−0.62	−0.88	−1.28	−1.92	0.09	0.02	0.08	−0.01	10.0
$Hg_{(l)}$		Kropač (I/20)	−0.05	−0.24	−0.33	−0.56	−0.88	0.10	0.04	0.09	−0.04	100
$Hg_{(l)}$		Kropač (I/20)	−0.08	−0.41	−0.59	−0.89	−1.33	0.14	0.04	0.08	−0.01	100
$Hg_{(l)}$		Kropač (I/20)	0.00	−0.16	−0.27	−0.44	−0.64	0.11	0.06	0.06	0.02	100
Tufa		Kropač (I/20)	−0.11	−0.46	−0.63	−0.99	−1.50	0.14	0.04	0.12	−0.03	0.324
Banded ore (404)		Ziljska (I/15)	−0.18	−0.27	−0.44	−0.55	−0.87	−0.04	0.01	−0.03	−0.05	6.07
Banded ore (414)		Ziljska I/16)	−0.07	0.01	−0.08	−0.01	0.06	−0.07	0.01	−0.08	0.07	0.003
Jeklenka ore (433)		Ziljska (I/14)	−0.14	−0.16	−0.29	−0.33	−0.50	−0.05	0.00	−0.04	−0.01	10.57
Jeklenka ore (435)		n.a.	−0.13	−0.32	−0.50	−0.66	−1.01	0.04	0.02	0.00	−0.02	9.10
Conglomerate Ore (580)		Urban (IV)	−0.02	0.08	0.05	0.14	0.21	−0.06	0.00	−0.06	0.00	30.1
Conglomerate Ore (581)		Urban (IV)	0.02	0.13	0.11	0.25	0.36	−0.05	0.00	−0.07	−0.01	13.0
Jetrenka ore (944)		Turniš (I/4)	−0.15	−0.38	−0.60	−0.78	−1.22	0.05	0.01	−0.01	−0.06	0.929
Conglomerate Ore	n.a.	n.a.	−0.04	0.07	0.02	0.10	0.15	−0.07	0.01	−0.06	−0.01	2.65
Coral ore (999)		n.a.	−0.20	−0.45	−0.67	−0.91	−1.39	0.03	0.01	0.01	−0.03	14.9
Karoli ore		n.a.	−0.06	−0.04	−0.13	−0.10	−0.16	−0.03	0.01	−0.06	−0.01	15.2

Plots of $\delta^{202}Hg/\Delta^{199}Hg$ and $\Delta^{199}Hg/\Delta^{201}Hg$ are shown in Figure 1. They can be used both in comparison of different trends in data or potential groupings. In general, a trend towards more negative values was observed in $\Delta^{199}Hg$ with increasing $\delta^{202}Hg$ (Figure 1A).

This is the opposite of the trend for the minerals from the Terlingua District and Almadén, which show more positive values in both δ^{202}Hg and Δ^{199}Hg [23,24]. However, the data from Mt. Amiata show a similar trend. The trend at Mt. Amiata was statistically weak and was not discussed further by the authors [25]. In addition, results derived from roasted calcines and sediment near the New Idrija mine [29], the Yuba River below the New Idrija mine [27], and contaminated pore waters from Tennessee [41] also show a similar trend to that revealed in this study. Some MIF could be caused by the interactions with the surface [40], which might potentially shift the fingerprint differently in different cases. At this stage, there are not enough analogous results to draw a conclusion.

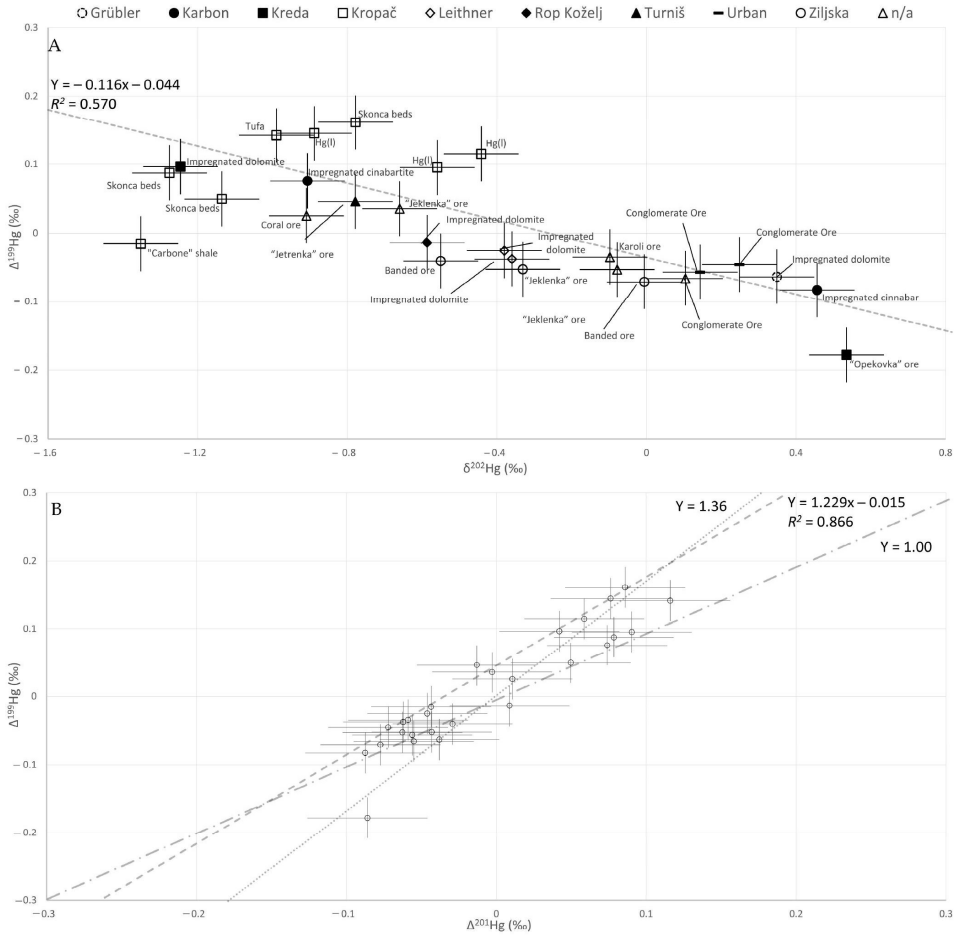

Figure 1. The plot of δ^{202}Hg versus Δ^{199}Hg with a table of different types of excavation, as well as the labels of different types of ore (**A**) and Δ^{199}Hg versus Δ^{201}Hg (**B**). The regression lines for both observed data and the slope of 1 and 1.36 as observed for photoreduction of MeHg [22] for odd-MIF (**B**).

$\Delta^{199}Hg/\Delta^{201}Hg$ slopes can be a useful tool in Hg isotope studies, as they clearly present any deviation between the two odd-MIF values, which can be present. The slope of the $\Delta^{199}Hg/\Delta^{201}Hg$ presents a regression line of 1.23 (Figure 1B), which is between the slopes of the Terlingua District minerals, with a slope of 1.66 [23], and Mt. Amiata, with a slope of 0.68 and an R^2 of 0.13. It is known from laboratory experiments that the photochemical reduction of Hg^{2+} yields residual Hg^{2+}, with a $\Delta^{199}Hg/\Delta^{201}Hg$ ratio of 1.00, and the photodegradation of methyl-mercury (MeHg) yields residual MeHg, with a $\Delta^{199}Hg/\Delta^{201}Hg$ ratio of 1.36 [22].

The plots of $cHg/\delta^{202}Hg$ (Figure 2A) and $cHg/\Delta^{199}Hg$ (Figure 2B) show that higher concentrations (above 0.1%) show no relationship with the isotopic fingerprint. However, below 0.1%, the isotopic fingerprint shows relatively more positive $\delta^{202}Hg$ and more negative $\Delta^{199}Hg$ values. It was assumed that there could be a potential correlation between either MDF or MIF with cHg.

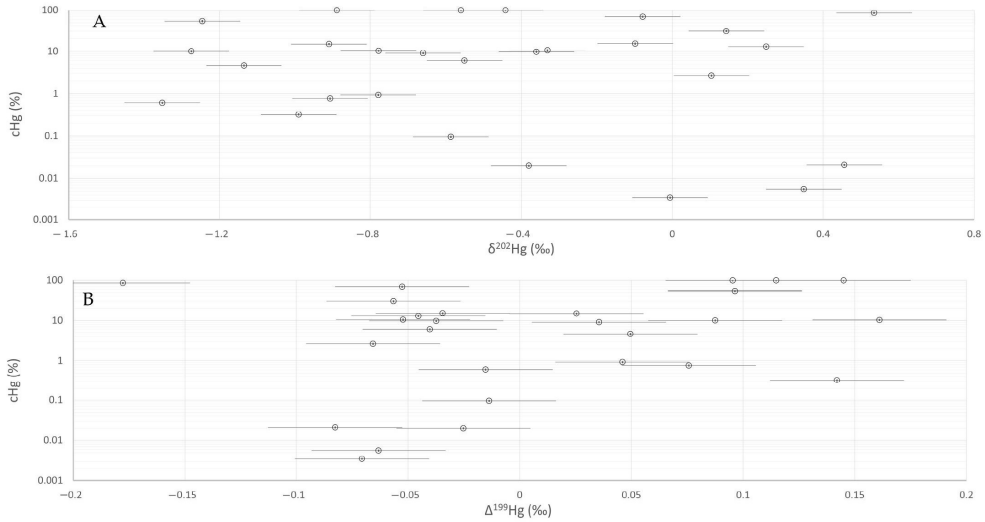

Figure 2. The plots of $\delta^{202}Hg$ versus cHg (**A**) and $\Delta^{199}Hg$ versus cHg (**B**). Note that vertical error bars are much narrower in comparison to the horizontal ones due to the logarithmic scale.

There are no distinct groups formed when we take into account the time periods of the samples. This could be because most of the samples are from the Ladinian period. However, if we group the samples according to type and excavation site, some trends can be identified. The samples of $Hg_{(l)}$, Skonca beds, and Tufa, all of which are derived from the same excavation site (Kropač), are grouped together on the $\delta^{202}Hg/\Delta^{199}Hg$ plot (Figure 1A). These samples were taken close to one another (in a single shaft, about 10 m apart). The similarity between the Skonca beds and Tufa with the $Hg_{(l)}$ fingerprint indicates that either there is no major fractionation occurring when $Hg_{(l)}$ is leached or that the original pool of Hg from which both groups are derived had a uniform Hg fingerprint. The pool size, which is unknown in this case, might play an important role as a proportionally small but severely fractionated leachate and would not change the overall fingerprint.

At the other excavation sites, fewer samples were measured, and therefore, they cannot be considered significant, or they had a very broad fingerprint. These include, for example, impregnated cinnabar from the Karbon excavation site, with a range greater than 1‰ ($\delta^{202}Hg$), and impregnated dolomite and carbonate shale from the Kreda excavation site, with a range of 2‰ ($\delta^{202}Hg$; Figure 1A).

Overall, it appears that the isotopic fingerprint of a single excavation site may be homogenous, but this is by no means true for all excavation sites. The results presented here suggest not only that the isotopic fingerprint of the entire mine cannot be constrained below a few permilles but also that an individual excavation site can have a wide range of isotopic fingerprints. It appears that the constraints placed on the isotopic fingerprint by sample type and period are also very broad or statistically weak.

4. Conclusions

Although attempts to constrain the isotopic fingerprint of different periods of Hg deposition have not been informative beyond the mere range of end members, some conclusions with respect to the different sample types or excavation sites can be drawn:

1. The isotopic fingerprint of the Idrija mine is generally relatively broad as comparable to most other findings, with the MDF fingerprint (δ^{202}Hg) ranging from −1.35‰ to 0.46‰.
2. The MIF ranges are similar to those of other mines, with Δ^{199}Hg ranging from −0.16‰ to 0.18‰.
3. Only one example of a relatively homogenous fingerprint was observed at the Kropač excavation field.
4. The isotopic fingerprints of cinnabar and $Hg_{(l)}$ from the same excavation site are statistically indistinguishable.

This study's most valuable aspect seems not to be the tracing of Hg in the environment or to the Gulf of Trieste, but the description of a wide variety of samples in the isotopic fingerprint of Hg found in the mine. This could be useful for other researchers, either in designing studies of complex Hg deposits elsewhere around the world or for those specifically looking into the Idrija deposit.

Author Contributions: Conceptualization, D.B., T.D. and M.H.; methodology, D.B., I.Ž., M.P., T.D. and M.Š.; formal analysis, I.Ž.; investigation, D.B.; data curation, D.B. and M.H.; writing—original draft preparation, D.B.; writing—review and editing, I.Ž., M.P., T.D., M.Š. and M.H.; visualization, D.B.; supervision, M.Š. and M.H.; project administration, M.H.; funding acquisition, T.D. and M.H. All authors have read and agreed to the published version of the manuscript.

Funding: This study has been supported financially by the Slovenian Research Agency (ARRS; grants P1-0143, PR-54685, J1-3033).

Data Availability Statement: Data will be made available upon request.

Conflicts of Interest: The authors declare no conflict of interest.

References

1. UNEP. *Guidance on Monitoring of Mercury and Mercury Compounds to Support Evaluation of the Effectiveness of the Minamata Convention*; UNEP: Geneva, Switzerland, 2022.
2. UNEP. *Global Mercury Assessment 2018*; UNEP: Geneva, Switzerland, 2019.
3. Kwon, S.Y.; Blum, J.D.; Yin, R.; Tsui, M.T.-K.; Yang, Y.H.; Choi, J.W. Mercury stable isotopes for monitoring the effectiveness of the Minamata Convention on Mercury. *Earth Sci. Rev.* **2020**, *203*, 103111. [CrossRef]
4. United Nations Environment Programme. *Minamata Convention on Mercury*; United Nations: New York, NY, USA, 2019.
5. Gustin, M.S.; Bank, M.S.; Bishop, K.; Branfireun, B.; Chételat, J.; Eckley, C.S.; Hammerschmidt, C.R.; Lamborg, C.; Lyman, S.; Zhang, T.; et al. Science of the Total Environment Mercury biogeochemical cycling: A synthesis of recent scientific advances. *Sci. Total Environ.* **2020**, *737*, 139619. [CrossRef] [PubMed]
6. Bishop, K.; Shanley, J.B.; Riscassi, A.; de Wit, H.A.; Eklöf, K.; Meng, B.; Mitchell, C.; Osterwalder, S.; Schuster, P.F.; Webster, J.; et al. Recent advances in understanding and measurement of mercury in the environment: Terrestrial Hg cycling. *Sci. Total Environ.* **2020**, *721*, 137647. [CrossRef]
7. Berce, B. Geologija živosrebrnega rudišča Idrija. *Geol. Trans. Rep.* **1958**, *4*, 1–61.
8. Placer, L. Rekonstrukcija krovne zgradbe idrijsko Žirovskega ozemlja. *Geologija* **1973**, *16*, 317–334.
9. Placer, L. Tektonski Razvoj Idrijskega Rudišča [Structural History of the Idrija Mercury Deposit]. Ph.D. Thesis, University of Ljubljana, Ljubljana, Slovenia, 1982; Volume 94.

10. Drovenik, M.; Dolenec, T.; Režun, B.; Pezdič, J. On the mercury ore from the Grübler orebody, Idrija. *Geologija* **1990**, *33*, 397–446. [CrossRef]
11. Mlakar, I.; Drovenik, M. Strukturne in generske posebnosti idrijskega rudišča. *Geologija* **1971**, *14*, 67–126.
12. Mlakar, I. Geological structure and mineralization of the Idrija ore deposit. *Geologija* **1972**, *15*, 47–62.
13. Placer, L.; Čar, J. Srednjetriadna zgradba idrijskega ozemlja. *Geologija* **1977**, *20*, 141–166.
14. Mlakar, I. Osnovni parametri proizvodnje rudnika Idrija skozi stoletja do danes. *Irdijski Razgledi* **1974**, *21*, 1–40.
15. Kotnik, J.; Horvat, M.; Dizdarevič, T. Current and past mercury distribution in air over the Idrija Hg mine region, Slovenia. *Atmos Environ.* **2005**, *39*, 7570–7579. [CrossRef]
16. Čar, J. Mineralized rocks and ore residues in the Idrija region. In Proceedings of the Meeting of Researchers o Idrija as a Natural and Anthoropogenic Laboratory—Mercury as a Major Pollutant, Idrija, Slovenija, 24–25 May 1996; pp. 10–15.
17. Kocman, D.; Horvat, M. Non-point source mercury emission from the Idrija Hg-mine region: GIS mercury emission model. *J. Environ. Manag.* **2011**, *92*, 2038–2046. [CrossRef]
18. Božič, D.; Živković, I.; Hudobivnik, M.J.; Kotnik, J.; Amouroux, D.; Štrok, M.; Horvat, M. Fractionation of mercury stable isotopes in lichens. *Chemosphere* **2022**, *309*, 136592. [CrossRef]
19. Čar, J. Ladinian skonca beds of the Idrija Ore Deposit (W Slovenia). *Geologija* **2013**, *56*, 151–174.
20. Tsui, M.T.K.; Blum, J.D.; Kwon, S.Y. Review of stable mercury isotopes in ecology and biogeochemistry. *Sci. Total Environ.* **2020**, *716*, 135386. [CrossRef] [PubMed]
21. Blum, J.D.; Sherman, L.S.; Johnson, M.W. Mercury isotopes in earth and environmental sciences. *Annu. Rev. Earth Planet Sci.* **2014**, *42*, 249–269. [CrossRef]
22. Bergquist, B.A.; Blum, J.D. Mass-dependent and -independent fractionation of Hg isotopes by photoreduction in aquatic systems. *Science* **2007**, *318*, 417–420. [CrossRef]
23. Stetson, S.J.; Gray, J.E.; Wanty, R.B.; Macalady, D.L. Isotopic variability of mercury in ore, mine-waste calcine, and leachates of mine-waste calcine from areas mined for mercury. *Environ. Sci. Technol.* **2009**, *43*, 7331–7336. [CrossRef]
24. Gray, J.E.; Pribil, M.J.; Higueras, P.L. Mercury isotope fractionation during ore retorting in the Almadén mining district, Spain. *Chem. Geol.* **2013**, *357*, 150–157. [CrossRef]
25. Pribil, M.J.; Rimondi, V.; Costagliola, P.; Lattanzi, P.; Rutherford, D.L. Assessing mercury distribution using isotopic fractionation of mercury processes and sources adjacent and downstream of a legacy mine district in Tuscany, Italy. *Appl. Geochem.* **2020**, *117*, 104600. [CrossRef]
26. Wiederhold, J.G.; Smith, R.S.; Siebner, H.; Jew, A.D.; Brown, G.E.; Bourdon, B.; Kretzschmar, R. Mercury isotope signatures as tracers for Hg cycling at the new idria Hg mine. *Environ. Sci. Technol.* **2013**, *47*, 6137–6145. [CrossRef]
27. Donovan, P.M.; Blum, J.D.; Yee, D.; Gehrke, G.E.; Singer, M.B. An isotopic record of mercury in San Francisco Bay sediment. *Chem. Geol.* **2013**, *349–350*, 87–98. [CrossRef]
28. Gehrke, G.E.; Blum, J.D.; Marvin-DiPasquale, M. Sources of mercury to San Francisco Bay surface sediment as revealed by mercury stable isotopes. *Geochim. Cosmochim. Acta* **2011**, *75*, 691–705. [CrossRef]
29. Smith, R.S.; Wiederhold, J.G.; Jew, A.D.; Brown, G.E.; Bourdon, B.; Kretzschmar, R. Stable Hg isotope signatures in creek sediments impacted by a former Hg mine. *Environ. Sci. Technol.* **2015**, *49*, 767–776. [CrossRef]
30. Smith, C.N.; Kesler, S.E.; Blum, J.D.; Rytuba, J.J. Isotope geochemistry of mercury in source rocks, mineral deposits and spring deposits of the California Coast Ranges, USA. *Earth Planet. Sci. Lett.* **2008**, *269*, 399–407. [CrossRef]
31. Yin, R.; Feng, X.; Meng, B. Stable mercury isotope variation in rice plants (*Oryza sativa* L.) from the Wanshan mercury Mining District, SW China. *Environ. Sci. Technol.* **2013**, *47*, 2238–2245. [CrossRef] [PubMed]
32. Yin, R.; Feng, X.; Wang, J.; Li, P.; Liu, J.; Zhang, Y.; Chen, J.; Zheng, L.; Hu, T. Mercury speciation and mercury isotope fractionation during ore roasting process and their implication to source identification of downstream sediment in the Wanshan mercury mining area, SW China. *Chem. Geol.* **2013**, *336*, 72–79. [CrossRef]
33. Baptista-Salazar, C.; Hintelmann, H.; Biester, H. Distribution of mercury species and mercury isotope ratios in soils and river suspended matter of a mercury mining area. *Environ. Sci. Process. Impacts* **2018**, *20*, 621–631. [CrossRef]
34. Foucher, D.; Ogrinc, N.; Hintelmann, H. Tracing mercury contamination from the Idrija mining region (Slovenia) to the gulf of Trieste using Hg isotope ratio measurements. *Environ. Sci. Technol.* **2009**, *43*, 33–39. [CrossRef] [PubMed]
35. Peel, K.; Weiss, D.; Chapman, J.; Arnold, T.; Coles, B. A simple combined sample-standard bracketing and inter-element correction procedure for accurate mass bias correction and precise Zn and Cu isotope ratio measurements. *J. Anal. At. Spectrom.* **2008**, *23*, 103–110. [CrossRef]
36. National Institute of Standards & Technology. *Certificate of Analysis Standard Reference Material 3133 Mercury (Hg) Standard Solution*; Department of Commerce, National Institute of Standards & Technology: Gaithersburg, MD, USA, 2016.
37. Blum, J.D.; Johnson, M.W. Recent developments in mercury stable isotope analysis. *Rev. Miner. Geochem.* **2017**, *82*, 733–757. [CrossRef]
38. National Institute of Standards & Technology. *Report of Investigation Reference Material 8610 Isotopes in UM-Almaden Mono-Elemental Secondary Standard This Mercury*; National Institute of Standards & Technology: Gaithersburg, MD, USA, 2017.
39. Estrade, N.; Carignan, J.; Sonke, J.E.; Donard, O.F. Measuring hg isotopes in bio-geo-environmental reference materials. *Geostand Geoanal Res.* **2009**, *34*, 79–93. [CrossRef]

40. Sherman, L.S.; Blum, J.D.; Nordstrom, D.K.; McCleskey, R.; Barkay, T.; Vetriani, C. Mercury isotopic composition of hydrothermal systems in the Yellowstone Plateau volcanic field and Guaymas Basin sea-floor rift. *Earth Planet Sci. Lett.* **2009**, *279*, 86–96. [CrossRef]
41. Demers, J.D.; Blum, J.D.; Brooks, S.C.; Donovan, P.M.; Riscassi, A.L.; Miller, C.L.; Zheng, W.; Gu, B. Hg isotopes reveal in-stream processing and legacy inputs in East Fork Poplar Creek, Oak Ridge, Tennessee, USA. *Environ. Sci. Process. Impacts* **2018**, *20*, 686–707. [CrossRef] [PubMed]

3.3 Insights into Seasonal Variations in Mercury Isotope Composition of Lichens

Dominik Božič & Milena Horvat Insights into seasonal variations in mercury isotope composition of lichens Environmental Pollution, Volume 340, Part 1, 2024 https://doi.org/10.1016/j.envpol.2023.122740

In this study, the authors investigated the use of lichens for assessing mercury (Hg) concentrations in the atmosphere, emphasizing their cost-effectiveness. They addressed uncertainties regarding data consistency across seasons, diverse sampling methods (transplantation or in-situ collection), and various locations. The research involved high-frequency sampling of in-situ and transplanted lichens and atmospheric particulate matter (APM) across pristine to Hg-contaminated sites.

Isotopic analysis revealed that Hg isotopic composition in lichens experienced mass-dependent fractionation and seasonal variations, with the heaviest isotopes in summer and the lightest in winter. These patterns held across polluted and unpolluted environments, in both lichen types, and APM. The results suggested a correlation between Hg concentration and isotopic composition changes in lichens and environmental factors, indicating a potential causal relationship.

Environmental factors, particularly summer temperatures, appeared to have influenced the heavier isotopic signature in lichens during that season. Similarities with APM-bound Hg implied a shared underlying mechanism. This study underscored the importance of considering temporal trends and sampling methods when interpreting findings.

In summary, this investigation into Hg isotope composition in lichens, across diverse environments and sampling techniques, offered insights into seasonal dynamics and influencing factors. It confirmed the consistency previous research and highlighted a common set of mechanisms governing Hg isotopic changes. The resemblance between APM and lichen isotopic data suggested an intriguing interconnection, deepening our understanding of mercury bio-monitoring using lichens.

These findings enhanced our understanding of mercury behavior in lichens and its interaction with environmental factors. However, caution was needed when using lichens as atmospheric Hg proxies across various locations. Future studies should explore specific mechanisms underlying isotopic composition changes and their implications for mercury pollution monitoring, considering natural variations and acclimation time for transplanted lichens.

Environmental Pollution 340 (2024) 122740

Contents lists available at ScienceDirect

Environmental Pollution

journal homepage: www.elsevier.com/locate/envpol

Insights into seasonal variations in mercury isotope composition of lichens☆

Dominik Božič [a,b], Milena Horvat [a,b,*]

[a] Department of Environmental Science, Jožef Stefan Institute, Jamova Street 39, Ljubljana, Slovenia
[b] Jožef Stefan International Postgraduate School, Jamova Street 39, Ljubljana, Slovenia

ARTICLE INFO

Keywords:
Mercury
Isotopes
Lichens
Seasonal cycling
Atmospheric particulate matter

ABSTRACT

Lichens are commonly used to assess mercury (Hg) concentrations in air because of their cost-effectiveness. However, recent research has revealed temporal variations in the isotopic composition of Hg. Previous work on this topic leaves open questions about the repeatability of data over multiple seasons, different types of sampling (transplantation or in-situ collection), and diverse locations. This study aims to address these issues by conducting a high-frequency sampling campaign of in-situ and transplanted lichens and atmospheric particulate matter (APM). Sampling sites included a range of areas, from pristine to Hg-contaminated sites. Isotopic analysis showed that the isotopic composition of Hg in lichens undergoes mass-dependent fractionation and changes with time. The heaviest isotopic composition was observed in summer and the lightest in winter. These trends were consistent across polluted and unpolluted environments, as well as in both in-situ and transplanted lichens and in APM. The results further indicated towards a correlation between changes in Hg concentrations and isotopic composition in lichens and environmental factors. All of these variables seem to be changing at the same frequency and may have not just correlation but also causation relationship. Environmental factors seem to be influencing the Hg concentrations and isotopic composition. The summer high temperatures might be influencing the heavier isotopic fingerprint observed in lichens during the same season. Similarities with APM-bound Hg suggest a common underlying mechanism. This study highlights the importance of considering temporal and seasonal trends, as well as the method of lichen sampling, when interpreting results. Researchers using lichens as proxies for atmospheric Hg concentrations or isotope ratios should consider these findings when designing their studies.

1. Introduction

Mercury (Hg) is a recognized environmental pollutant of considerable concern due to its toxicity. Addressing the imperative need for comprehending the cycling of Hg in the environment, a global initiative, outlined in guidelines for Hg measurement in the atmosphere, adopts a multi-tiered approach encompassing diverse monitoring methods, including bio-monitoring (UNEP, 2022). Passive bio-monitoring, employing lichens as indicators, holds significant promise owing to their exclusive reliance on atmospheric nutrients, and this approach is extensively utilized for assessing various pollutants (Abas, 2021; Berdonces et al., 2017; Garty, 2002; Szczepaniak & Biziuk, 2003), including Hg (Barre et al., 2015, 2018, 2020; Mlakar et al., 2011). The use of lichens in bio-monitoring offers distinct advantages over alternative methods. Lichens can be retrospectively sampled post-pollution events in their natural habitats, obviating the need for electricity, and are less susceptible to vandalism, maintaining a minimal ecological footprint (Garty, 2002). This makes lichens a compelling alternative to some other passive or active methods, which exhibit up to 12% variations in Hg concentrations across different brands (Naccarato et al., 2021) and differences exceeding a permille in mass-dependent fractionating isotope fingerprints (Szponar et al., 2020).

However, the suitability of lichens as proxies for atmospheric isotopic composition raises certain concerns. Lichens may be differentially impacted by various types of Hg deposition, contingent on whether it is wet or dry (Graydon et al., 2008), as well as the chemical forms of atmospheric Hg species, including Hg bound to particles, oxidized, or elemental Hg (Lyman et al., 2020; Si & Ariya, 2018). Lichens have the potential to fractionate Hg isotopes, potentially deviating from the true atmospheric fingerprint. Initial indications of this phenomenon were observed by Demers et al. (2013), who proposed that foliage may fractionate Hg towards lighter isotopes during the uptake process. Yuan

☆ This paper has been recommended for acceptance by Michael Bank.

* Corresponding author. Department of Environmental Science, Jožef Stefan Institute, Jamova Street 39, Ljubljana, Slovenia.
E mail address: milena.horvat@ijs.si (M. Horvat).

https://doi.org/10.1016/j.envpol.2023.122740
Received 3 July 2023; Received in revised form 24 September 2023; Accepted 12 October 2023
Available online 19 October 2023

et al. (2019) documented the gradual accumulation of Hg in leaves over the growing season, while Fu et al. (2019) noted concurrent shifts towards heavier isotopes in the atmosphere and lighter ones in foliage during the summer months. Moreover, global fluctuations in Hg concentrations attributed to global Hg uptake during summer, akin to CO2, have been observed (Jiskra et al., 2018). These observations have contributed to the evolving understanding of the Hg cycle in forests and foliage (Liu et al., 2022; Wang et al., 2021; Zhou et al., 2021). Changes in atmospheric Hg have been noted not only in foliage but also in atmospheric particulate matter (APM), influenced by a combination of global and local factors (Guo et al., 2021; Li et al., 2020; Xu et al., 2019). This raises questions about the reflection of these trends in lichens and whether their utility as bio-monitors and proxies might be compromised. The key questions revolve around whether the isotopic composition of lichens varies seasonally and, if so, whether it mirrors changes observed in other foliage, atmospheric gaseous Hg, or APM. In essence, do lichens enrich in lighter isotopes during the growing season like the rest of the foliage, or do they exhibit enrichment in heavier isotopes in alignment with the atmospheric trends?

To our knowledge, the first significant study to observe substantial shifts in isotopic composition in lichens during the season was conducted by Božič et al. (2022). In that work, the primary focus was on correlating atmospheric Hg concentrations using active and passive methods on transplanted lichens, transplanted to various locations to elucidate micro-local variations. Since the observation of isotopic composition changes was serendipitous and not the primary focus, certain limitations in the study design required addressing in the present study: (I) Increased sampling frequency from once per season to monthly or more frequent intervals to better delineate differences between periods with heavier and lighter isotopic compositions. (II) An investigation of the natural variability of lichens was undertaken to enhance the overall robustness of observations. (III) A parallel examination of in-situ and transplanted lichens was performed. (IV) Environmental factors such as temperature and precipitation were thoroughly examined. (V) The Hg isotopic composition of APM was compared to lichen Hg levels. To ensure the continuity of measurements, some of the same sites utilized in the 2020–2021 sampling campaign (Božič et al., 2022) were revisited in the subsequent 2021–2022 sampling campaign.

The objective of this study was to expand our comprehension of lichens as atmospheric proxies under diverse conditions, employing both transplantation and in-situ sampling methodologies. The resulting data provides insights into the limitations of lichen-based bio-monitoring. The findings further our understanding of trends in Hg uptake by lichens and the potential seasonal variations in atmospheric Hg concentrations and isotope ratios.

2. Sampling sites

Pokljuka is a plateau in the Julian Alps in Slovenia (Supplementary material A, Fig. S1). It is a forested area that stretches in both north-south and east-west directions for about 10 km. The plateau lies at an altitude between 1000 and 1400 m above sea level and is part of the Triglav National Park, which ensures that it remains as untouched as possible. In addition, the plateau is not surrounded by major industrial facilities that emit Hg, so the local environmental impact of human activities in this area is negligible and largely caused by long-distance Hg transport. During the winter, Pokljuka is the only one among the sampling sites that is constantly covered with snow for many months (Supplementary Material B).

Idrija is a small town in the Dinaric hills of western Slovenia, nestled in a deep valley (Supplementary material A, Fig. S1). The area is characterized by lush forests. The town has a few thousand residents and is today a regional industrial hub. Idrija gained recognition since the end of 15th century due to the discovery of one of the major Hg ore deposits. This has caused significant environmental problems due to the release of Hg into the surrounding area. This is especially concerning as Idrija's location at the bottom of a deep valley creates conditions favourable for the capturing emissions through temperature inversion. Several studies have been conducted to understand the extent of the impact on local ecosystems (Biester et al., 1999; Gnamuš et al., 2000; Gosar & Teršič, 2012; Hines et al., 2000; Horvat et al., 2002, 2003; Kocman, Kanduč, et al., 2011; Kocman, Vreča, et al., 2011; Kocman & Horvat, 2011; Kotnik et al., 2005; Miklavčič et al., 2013; Tomiyasu et al., 2012, 2017; Žagar et al., 2006; Žižek et al., 2007).

The Reactor Centre Podgorica (RCP) is located in the Ljubljana basin, a lowland area in central Slovenia (Supplementary material A, Fig. S1). In winter, this region often experiences temperature inversion start lead to the formation of smog and dense fog. The RCP is located on the so-called Savsko polje, which surrounds the Sava River, about 800 m south of the site. The surrounding area is mainly used for agriculture, with a small forest located about 1 km to the west. There are no forests in the immediate vicinity, the nearest forested area is over 4 km away. The city of Ljubljana is located 3 km to the southwest, and a major highway is located 500 m northwest of the RCP. In the northern vicinity, is a municipal water treatment plant (WWTP) that is also responsible for the treatment of water from the Novartis pharmaceutical factory. The factory used to manufacture Hg-containing pesticides. Limited evidence suggests that Hg concentrations in the air can reach levels as high as 20 ng/m^3 at certain times, compared to the average Hg concnetration of 1–2 ng/m^3. Since these levels are associated with winds blowing from the direction of the WWTP, this increase in Hg concentration appears to be related to the WWTP.

3. Experimental

3.1. Sample collection

Lichen specimens were gathered under two distinct conditions. Firstly, there were the in-situ lichens, which were collected from the various trees surrounding the research location. Secondly, there were the transplanted lichens, which were essentially the in-situ lichens transferred to a new environment at the start of the sampling period. The transplantation (collection and placement) and the collection of the fists in-situ lichens all occurred in a one-week time window (14th to 21st of November 2021). The transplanted lichens were collected at Pokljuka, where approximately 5 kg of material was mixed by shaking the collection box. To facilitate transplantation, small plastic mesh bags measuring 10 by 30 cm were created. Each bag was divided into three compartments, each measuring 10 by 10 cm. These bags had a depth of less than 0.5 cm when fully loaded, just enough to accommodate a piece of bark with the attached lichen. The bags were interwoven with wire to provide structure and ensure that the lichens faced outward toward the elements while the bark, their substrate, faced inward towards the surfaces they were placed on. Sampling of both in-situ and transplanted lichens occurred approximately once a month (see Supplementary A, Table 1), resulting in around 10 samplings per site over the course of a year-long campaign. Sampling commenced in the beginning of fall 2021 and concluded in the beginning of fall 2022. The sampling sites for Pokljuka and Idrija were consistent with those in (Božič et al., 2022), with the addition of one site at RCP. One of the bags was intentionally designed to be larger to accommodate a greater number of lichens. This larger bag was transplanted to Pokljuka to evaluate the variability in measured concentrations and isotope ratios within the bag. The variability between bags was assessed by preparing four additional bags that were measured at the end of the sampling period. For a detailed description of the sampling procedure, please refer to Supplementary Material A, Fig. S2, and Fig. S3.

APM-collecting filters were conditioned in a room maintained at a constant temperature of 20 °C and a humidity level of 45% before sampling. An APM sampling device (LVS6-RV by Sven Leckel, Berlin) equipped with a filter holder according to CEN EN 12341 standards was utilized. Fourteen sampling events were conducted at RCP, and two

were conducted at Idrija. A 2 μm PTFE filter with a 46.2 mm diameter (Whatman, UK) was employed for sampling. Air was filtered until the filters became clogged and the pump could no longer maintain the specified air flow rate, which was set at 3 m3/h.

Weather data were obtained from the Slovenian Environmental Agency (Slovenian Environmental Agency, 2022) and are presented in Supplementary Material A, Fig. 2, and Supplementary Material B. Temperature data were recorded simultaneously from the PM-2.5 sampling unit.

3.2. Sample preparation

Lichen sample preparation began with removal of the lichens from the bark using polytetrafluoroethylene forceps. These were then placed in plastic containers and immersed in liquid nitrogen to de-vitalize and store them. This step might have removed some of the particulates, but lichens were not thoroughly washed. Prior to digestion, the lichens were lyophilised at −40 °C with a vacuum of 0.27 mbar for 24 h in a Martin Christ Liophilizer (Martin Christ Gefriertrocknungsanlagen, Germany). A microwave digestion system (UltraWave, Milestone, Italy) was used for digestion. A total of 0.3 g of each lichen sample was weighed into pre-cleaned polytetrafluoroethylene tubes, and 3 ml of 65% HNO_3 and 0.5 ml of 30% HCl (both supra-pure grade) were added. The samples were then subjected to closed-vessel microwave digestion at a maximum power of 1500 W and a maximum pressure of 100 bar. The resulting solution was filtered through a 0.45 μm filter, quantitatively transferred into 10 ml polyethylene graduated tubes, and diluted with Milli-Q water.

APM filters were cut in half with pre-cleaned scissors to better fit the digestion chamber. A combination of 1.5 ml HNO3, 0.5 ml HCl, and 0.1 ml HF (per analysis purity) was used for digestion. Samples were digested using the same procedure as for the lichens described above. These samples were then analysed for their Hg concentrations. Since some of the Hg concentrations in the solution were too low for isotopic measurements (a minimum of at least 1 ng/ml of Hg is required for isotopic measurements), some of the samples had to be pooled together into one vial and preconcentrated to be used for isotope determination (Supplementary material A). All APM samples were subsequently filtered and transferred into glass impingers in which HF was neutralised with 10 ml of 5% (w/w) H_3BO_3. The impingers were used for Hg preconcentration using the procedure described by Ali et al. (2023). Briefly, N_2 gas was used to purge the impingers filled with $SnCl_2$ solution, reducing and converting the Hg to gaseous form. This Hg was then trapped into an oxidising solution of concentrated HNO_3, which was diluted to the appropriate concentration for further measurements.

3.3. Analyses

Hg concentrations in the solution were quantified using a Model Hg-201 semiautomated Hg analyser employing cold vapor atomic absorption spectroscopy (CV-AAS, Sanso Seisakusho Co., Japan). Between 0.5 and 1 ml of the sample was transferred into the reduction chamber. A reducing agent consisting of SnCl2 in a 10% w/w mixture of 10% v/v HCl (supra-pure) to Mili-Q water was utilized.

Quality assurance and quality control (QA/QC) procedures were implemented by analyzing every tenth sample in duplicate. For calibration, a 1 ng/ml NIST 3133 standard Hg solution was prepared, and the volume transferred was adjusted until the signals matched within 50% of the signal from 1 ng/ml of the NIST 3133 solution. Prior to usage, pipettes were calibrated, and a reagent blank value of 4% was subtracted from all measurements. Procedural blank values were subtracted separately for each batch of lichen and APM samples. For lichen samples, a matrix-matched reference material, BCR 482, was utilized, yielding a recovery of 92.6% (RSD 8.8%, N = 8). As no direct reference material was available for APM, NIST 1648a (urban particulate matter) was used, resulting in a recovery of 98.5% (RSD 13.4%, N = 6). The concentration values' uncertainty was assessed using the ISO GUM approach and amounted to 4.1% (k = 2).

Isotopic ratios of Hg were determined using a multi-collector inductively coupled plasma mass spectrometer (MC-ICP-MS) provided by Nu Plasma II (Nu Instruments, UK). All measurements followed the sample–standard–sample bracketing technique (Peel et al., 2008). The measurements are denoted with δ and Δ symbols, as detailed in Equations (1) and (2) (Blum et al., 2014; Blum & Johnson, 2017). The correction factor "f" was applied, with values of 0.2520 for Δ^{199}Hg, 0.5024 for Δ^{200}Hg, 0.7520 for Δ^{201}Hg, and 1.4930 for Δ^{204}Hg. The atomic mass of an isotope was represented by "xxx."

$$\delta^{xxx}Hg = \left(\frac{\frac{^{xxx}Hg}{^{198}Hg_{sample}}}{\frac{^{xxx}Hg}{^{198}Hg_{NIST3133}}} - 1 \right) \times 1000 \quad (1)$$

$$\Delta^{xxx}Hg = \delta^{202}Hg - \delta^{xxx}Hg \times f \quad (2)$$

Operating conditions of the instrument can be found in Supplementary Material A, Table S1. The long-term uncertainty of the measurements was determined using NIST 8610 (UM-Almadén, (National Institute of Standards & Technology, 2017), with accuracy reported as the standard deviation of repeated NIST 8610 measurements. All ranges for isotopic values are presented with an expanded factor (k = 2). Detailed results of the isotopic analysis of NIST 8610 and BCR 482 (lichen) matrix-matched reference material are provided in Supplementary Material A, Table S2. For instance, for the commonly used isotope pair for Mass-Dependent Fractionation (MDF), δ^{202}Hg, the difference between our repeated (N = 32) measurements of NIST 8610 and the NIST-reported value was less than 0.00‰, with an expended standard deviation between measurements (k = 2) at 0.14‰. Similarly, for the most commonly used isotope pair for Mass-Independent Fractionation (MIF), Δ^{199}Hg, the difference was 0.03‰, with an expended standard deviation between measurements (k = 2) at 0.03‰. Unfortunately, we have found no published NIST 1648a findings, but our data for its isotopic composition is provided for potential further comparison by peers in Supplementary Material A, Table S2.

APM Hg concentrations were calculated by determining the volume of air drawn through the sampling device based on time and pump flow rate, and then dividing the Hg concentration by these values. The concentration of APM in the air was determined by dividing the weight of APM on the filters by the volume of air pumped. Weights of the APM were calculated by subtracting the weight of clean filters from the weight of dirty filters. All weighing procedures were conducted in environmentally controlled clean room conditions. Normalized Hg values were computed by dividing the Hg concentrations in APM by the concentrations of APM in the air.

4. Results and discussion

4.1. Comparison of sampling variabilities

Multiple sources of variability must be taken into account for both in-situ and transplantation sampling techniques. In the case of in-situ lichens, natural variability at the collection site was assessed in the study conducted by Božič et al. (2022). This assessment revealed a relative standard deviation of 21.8% for Hg concentrations and standard deviations (k = 2) of 0.58‰ for δ^{202}Hg and 0.18 for Δ^{199}Hg (N = 5). In the present study, we examined two sources of variability: (I) among different bags within 1 m of each other, and (II) within a single bag. The between-bag variability was calculated at 8.9% for Hg concentration, and 0.34‰ and 0.06‰ for δ^{202}Hg and Δ^{199}Hg, respectively (N = 4). Within-bag variability for Hg concentrations was slightly lower at 8.7%, while isotopic ratio variability exhibited a lower figure for δ^{202}Hg at 0.14‰ and a slightly higher value for Δ^{199}Hg at 0.09‰ (N = 4).

A comparison of the within-bag and between-bag variabilities with instrumental variabilities indicates that their standard deviations are roughly similar (as discussed in Section 3.3 and Supplementary Material A, Table S2). However, it's noteworthy that in-situ variabilities tend to be higher, suggesting that transplanted lichens offer greater precision compared to in-situ lichen samples. These findings imply that the utilization of transplanted lichens could potentially lead to more dependable and consistent measurements. Furthermore, these variability values offer qualitative evidence regarding the significance of observed trends and offer insight into the reliability and robustness of the presented data.

4.2. Lichen Hg concentrations

The lichens transplanted to Idrija showed a similar response to the lichens in the 2020–2021 sampling campaign. In both cases, it took approximately one year for Hg concentrations to reach those of the in-situ lichens (Fig. 1 A). The highest concentrations in the in-situ lichens were observed in winter. The reason for the highest Hg concentrations in Idrija lichens could be the biomass burning during the coldest months of the year. Since the local biomass is contaminated with Hg (Kotnik et al., 2015), Hg concentrations in the air are potentially elevated in winter. This effect was exacerbated by the local temperature inversion in the Idrija valley, which is typical for winter.

An opposite trend in Hg concentrations was observed at RCP and Pokljuka in both transplanted and in-situ lichens. At these sites, the lowest Hg concentrations were observed in winter. The difference between winter and summer Hg concentrations was also smaller than in Idrija, ranging from 0.1 to 0.2 μg/g. Such large variations in Hg concentrations were not detected in previous sampling campaign at any of the locations (Božič et al., 2022), possibly due to the lower temporal resolution. The reason for this decrease in concentration during the winter months is not known. Lichen activity is dependent on moisture, temperature, and solar radiation, with lichens being most active at temperatures above freezing (Honegger, 2007). Therefore, they may take up less Hg during the winter months. Some of the potentially relevant environmental factors, such as precipitation and temperature, are shown in Supplementary Material A Fig. S4 and Supplementary Material B.

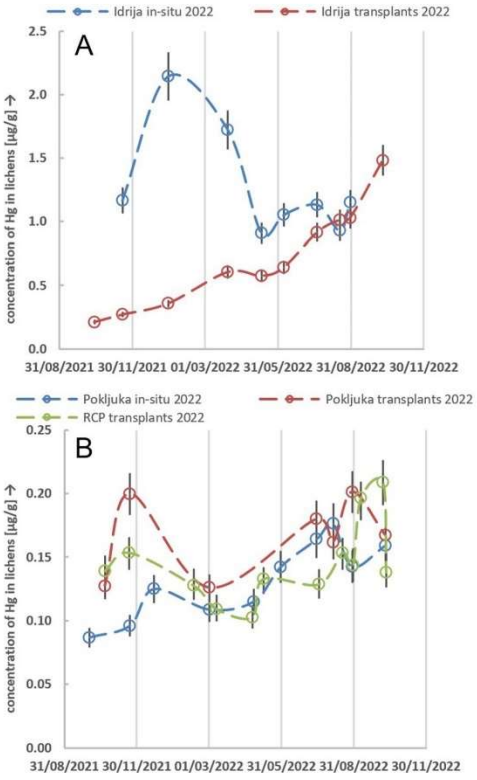

Fig. 1. The concentrations of Hg in the lichens.

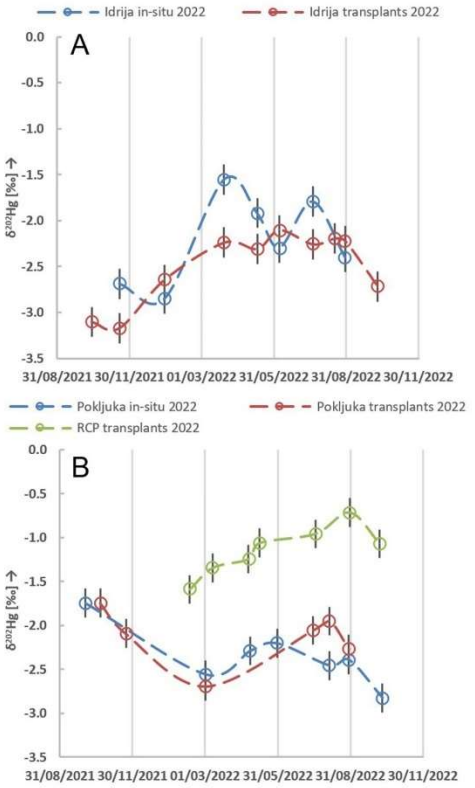

Fig. 2. Mass dependant mercury stable isotope ratios, as δ^{202}Hg values, in lichens. Top: Idrija in-situ and transplants. Bottom: Pokljuka transplants and in-situ and RCP transplants.

4.3. Hg isotopes in lichen

During the sampling campaigns conducted between 2020 and 2021, a conspicuous trend in isotopic composition emerged, characterized by a skewing of values towards heavier isotopes during the summer months, resulting in a range of approximately 3‰ for δ^{202}Hg (Božič et al., 2022).

In the subsequent campaign spanning 2021–2022, the maximum range between the heaviest and lightest isotopic compositions narrowed to about 1.5‰ for δ^{202}Hg, as observed at the Idrija site (in-situ) and illustrated in Fig. 2A. Nevertheless, all sampling sites exhibited a consistent seasonal pattern, with lighter isotopic compositions prevailing during the winter months, akin to the findings reported by Božič et al. (2022), where a more comprehensive exploration of potential mechanisms underlying these changes can be found. Notably, the data presented herein unveil an additional observation, namely, that certain sites exhibit significantly distinct Hg isotope fingerprints despite similar Hg concentrations. For instance, the disparity between the RCP and Idrija sites compared to the Pokljuka site is approximately 1.5‰.

No discernible seasonal trends were detected in Δ^{199}Hg, mirroring the observations made in lichen samples from the 2020–2021 sampling campaign (Božič et al., 2022). However, Idrija exhibited significantly elevated Δ^{199}Hg values in comparison to other sites, averaging −0.12 ± 0.07‰ and −0.08 ± 0.11‰ for transplanted and in-situ lichens, respectively. Conversely, Pokljuka displayed values of −0.30 ± 0.11‰ and −0.26 ± 0.15‰ for transplanted and in-situ lichens, respectively. Moreover, Δ^{199}Hg values in RCP lichens closely approximated those at Pokljuka, with Δ^{199}Hg measuring −0.24 ± 0.11‰ (Supplementary Material A, Table S6). Similar outcomes had been previously observed but had not yet been subjected to interpretation in the study conducted by Božič et al. (2022). The elevated Δ^{199}Hg values in Idrija are likely attributed to the presence of Hg originating from geogenic sources, with the Δ^{199}Hg in ores, as reported by Foucher et al. (2009), approaching zero.

In instances where both transplanted and in-situ lichens were subjected to analysis (Idrija, Pokljuka), the distinctions between isotopes that fractionate mass-dependently and independently within the two groups were minimal (Fig. 2). The average difference for δ^{202}Hg in Idrija was 0.06 ± 1.07‰, and for Δ^{199}Hg, it was 0.04 ± 0.11‰. At Pokljuka, the difference for δ^{202}Hg was 0.28 ± 0.54‰, and for Δ^{199}Hg, it was 0.04 ± 0.21‰. This implies that the observed isotopic composition remains consistent whether lichens are transplanted or naturally situated, even within a relatively short timeframe compared to changes in Hg concentrations. This observation aligns with the proposition by Božič et al. (2022) that lichens adapt their isotopic composition to their environment at a rapid pace.

The δ^{202}Hg and Δ^{199}Hg values discerned in lichens may signify a distinct isotopic fingerprint in different geographic regions, the influence of divergent mechanisms shaping the isotopic fingerprint, or a combination thereof. It is probable that variations in the atmospheric Hg isotopic fingerprint between sites contribute significantly to the observed discrepancies, given that all lichens were exposed to similar atmospheric conditions. Evidently, lichens exhibit alterations in their isotopic composition over time, irrespective of the sampling site, and display varying δ^{202}Hg and Δ^{199}Hg values across different locations.

4.4. Atmospheric particulate matter

At RCP, concentrations of Hg bound to atmospheric particulate matter (APM) exhibited a pronounced seasonal disparity, with Hg levels in winter (58.6 pg/m3) surpassing those in summer (ranging from 2.57 to 5.22 pg/m3) (Fig. 3A). Considering that APM concentrations in this investigation were also elevated during winter (Fig. 3B), it becomes imperative to factor in the proportional presence of Hg within these APM samples. Normalization of the Hg values revealed that the relative concentrations were notably higher in winter, reaching up to 15 μg/g in contrast to 2 μg/g observed in summer (Supplementary Material A, Fig. S4, Table S3). Comparable fluctuations in APM Hg concentrations were observed near a coal-fired power plant in China, spanning a three-year period, where concentrations ranged from approximately ~200 pg/m3 during summer to ~20 pg/m3 during winter (Sun et al., 2021). In urban settings like Beijing, Hg concentrations within APM can reach several hundred pg/m3 during winter (Huang et al., 2020). The

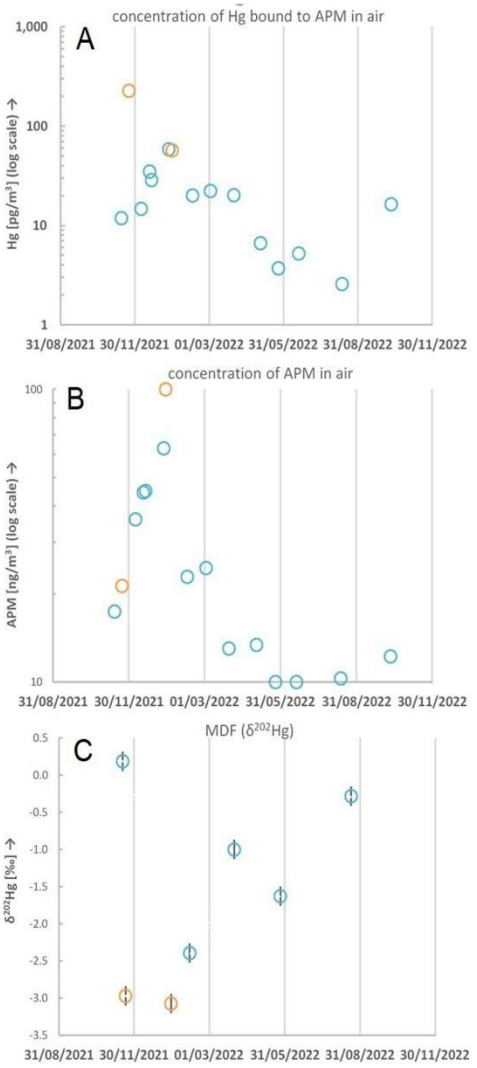

Fig. 3. Mercury and particle mass concentrations, and mercury stable isotope ratios in Idrija (orange) and RCP (blue) APM filters. Top: the concentration of Hg bound to APM in air; middle: the concentration of APM in air; and bottom: the mass-dependent fractionation (δ^{202}Hg) in APM. (For interpretation of the references to colour in this figure legend, the reader is referred to the Web version of this article.)

underlying causes for these Hg concentration variations in APM are likely akin to the factors contributing to higher Hg concentrations in lichens in Idrija, chiefly attributed to biomass burning and fossil fuel combustion. Additionally, the operation of wastewater treatment plants (WWTP) could be a contributing factor, although data regarding Hg

releases into the water treatment system is currently unavailable. In Idrija, Hg concentrations in the APM reached up to 0.01% of the APM mass (Supplementary Material A, Fig. S4), possibly stemming from the nugget effect (Kocman, Vreča, et al., 2011), where larger HgS particles or 'nuggets' are present in atmospheric particles.

However, the Hg isotopic composition of APM at RCP exhibited a parallel seasonal trend to that of lichens, featuring a lighter isotopic composition during winter and a heavier one during summer (Fig. 3C). Moreover, similarities in the isotopic signatures indicated that the isotopic composition between Idrija and RCP deviated by approximately ~0.5–1‰ for δ^{202}Hg during the corresponding time frames in both cases. These similarities suggest that both entities may be influenced by a common underlying mechanism. Notably, at RCP, a significant surge in Δ^{199}Hg was detected during the spring and summer months, specifically from May to July, with a Δ^{199}Hg value of 0.60 ± 0.03‰, exceeding the annual average of 0.10‰ observed at other sampling points. Furthermore, a slight decline in δ^{202}Hg was noted in the same sample collected in May (Fig. 3C). These findings align with the observations made by Huang et al. (2021), who reported an increase in Δ^{199}Hg and a decrease in δ^{202}Hg for aerosols exposed to light, attributed to photoreduction. This time period also coincided with the lowest precipitation levels (Supplementary Material A, Fig. S2A) and relatively low cloud cover, coupled with maximum sunshine duration (Supplementary Material B).

5. Conclusion

In summary, this investigation into Hg isotope composition in lichens, encompassing both contaminated and pristine environments and employing transplanting and in-situ collection techniques, has yielded valuable insights into seasonal dynamics and influencing factors on Hg isotope composition and Hg concentrations. These findings, consistently corroborated by prior research (Božič et al., 2022), highlight the similarity of the observed seasonal alterations in Hg isotopic composition through multiple years across diverse environmental conditions and sampling methods. They also suggest that while diverse mechanisms may govern Hg concentrations at various sites, a common set of mechanisms drives changes in isotopic composition. Moreover, the resemblance between APM isotopic data and lichen isotopic fingerprints implies an intriguing interconnectedness between lichens and APM in terms of their Hg isotopic signatures, expanding our understanding of the broader environmental implications and deepening our appreciation of the complexity of Hg bio-monitoring using lichens.

These findings significantly enhance our comprehension of Hg behaviour in lichens and its interaction with environmental factors, fostering a deeper understanding of the intricacies of Hg bio-monitoring using lichens across diverse sites and climates. As this study, conducted under specific geographic conditions, may not be universally applicable to all environments and locations, caution should be exercised when using lichens as proxies for assessing Hg concentrations or isotope ratios in the atmosphere until further investigations are carried out. Future research can build upon these findings to delve into the specific mechanisms underpinning the observed isotopic composition changes and their implications for Hg pollution monitoring. It is advisable to conduct comprehensive studies that consider factors such as natural and seasonal variations in lichen samples and potential local pollution sources. Additionally, extended sampling periods for lichen collections can yield a broader range of variations in Hg concentrations and isotope ratios at a given site. When utilizing transplanted lichens for a particular location, allowing sufficient time for lichens to acclimate to their new surroundings likely important at least in case of the transplantation to a polluted site.

Credit author roles

Dominik Božič:: Conceptualisation, Methodology, Investigation, Data curation, Writing – original draft, Visualisation. Milena Horvat: writing – review, Supervision, Funding acquisition.

Declaration of competing interest

The authors declare that they have no known competing financial interests or personal relationships that could have appeared to influence the work reported in this paper.

Data availability

Data will be made available on request.

Acknowledgements

This study has been supported financially by the Slovenian Research And Innovation Agency (ARIS); grants no. P1-0143, PR- 54685, and J1-3033.

Appendix A. Supplementary data

Supplementary data to this article can be found online at https://doi.org/10.1016/j.envpol.2023.122740.

References

Abas, A., 2021. A systematic review on biomonitoring using lichen as the biological indicator: a decade of practices, progress and challenges. Ecol. Indicat. 121, 107197 https://doi.org/10.1016/j.ecolind.2020.107197.

Ali, W.S., Božič, D., Nair, V.S., Živković, I., Gačnik, J., Audron, D.T., Hudobivnik, J.M., Kocman, D., Horvat, 2023. Optimization of a preconcentration method for the analysis of mercury isotopes in low-concentration biological samples. Under review.

Barre, J.P.G., Deletraz, G., Frayret, J., Pinaly, H., Donard, O.F.X., Amouroux, D., 2015. Approach to spatialize local to long range atmospheric metal input (Cd, Cu, Hg, Pb) in epiphytic lichens over a meso-scale area (Pyrénées Atlantiques, southwestern France). Environ. Sci. Pollut. Control Ser. 22 (11), 8536–8548. https://doi.org/10.1007/s11356-014-3990-5.

Barre, J.P.G., Deletraz, G., Sola-Larrañaga, C., Santamaria, J.M., Bérail, S., Donard, O.F. X., Amouroux, D., 2018. Multi-element isotopic signature (C, N, Pb, Hg) in epiphytic lichens to discriminate atmospheric contamination as a function of land-use characteristics (Pyrénées Atlantiques, SW France). Environ. Pollut. 243, 961–971. https://doi.org/10.1016/j.envpol.2018.09.003.

Barre, J.P.G., Queipo-Abad, S., Sola-Larrañaga, C., Deletraz, G., Bérail, S., Tessier, E., Elustondo Valencia, D., Santamaría, J.M., de Diego, A., Amouroux, D., 2020. Comparison of the isotopic composition of Hg and Pb in two atmospheric bioaccumulators in a Pyrenean beech forest (Iraty Forest, Western Pyrenees, France/Spain). Frontiers in Environmental Chemistry 1 (November), 1–16. https://doi.org/10.3389/fenvc.2020.582001.

Berdonces, M.A.I., Higueras, P.L., Fern, M., Borreguero, A.M., Carmona, M., 2017. The role of native lichens in the biomonitoring of gaseous mercury at contaminated sites. J. Environ. Manag. 186, 207–213. https://doi.org/10.1016/j.jenvman.2016.04.047.

Biester, H., Gosar, M., Müller, G., 1999. Mercury speciation in tailings of the Idrija mercury mine. J. Geochem. Explor. 65 (3), 195–204. https://doi.org/10.1016/S0375-6742(99)00027-8.

Blum, J.D., Johnson, M.W., 2017. Recent developments in mercury stable isotope analysis. Rev. Mineral. Geochem. 82 (2013), 733–757. https://doi.org/10.2138/rmg.2017.82.17.

Blum, J.D., Sherman, L.S., Johnson, M.W., 2014. Mercury isotopes in earth and environmental sciences. Annu. Rev. Earth Planet Sci. 42 (February), 249–269. https://doi.org/10.1146/annurev-earth-050212-124107.

Božič, D., Živković, I., Hudobivnik, M.J., Kotnik, J., Amouroux, D., Štrok, M., Horvat, M., 2022. Fractionation of mercury stable isotopes in lichens. Chemosphere 309 (September), 136592. https://doi.org/10.1016/j.chemosphere.2022.136592.

Demers, J.D., Blum, J.D., Zak, D.R., 2013. Mercury isotopes in a forested ecosystem: implications for air-surface exchange dynamics and the global mercury cycle. Global Biogeochem. Cycles 27 (1), 222–238. https://doi.org/10.1002/gbc.20021.

Fu, X., Zhang, H., Liu, C., Zhang, H., Lin, C.J., Feng, X., 2019. Significant seasonal variations in isotopic composition of atmospheric total gaseous mercury at forest sites in China caused by vegetation and mercury sources. Environ. Sci. Technol. 53 (23), 13748–13756. https://doi.org/10.1021/acs.est.9b05016.

Garty, J., 2002. Biomonitoring heavy metal pollution with lichens. In: Protocols in Lichenology, pp. 458–482. https://doi.org/10.1007/978-3-642-56359-1_27.

Gnamuš, A., Byrne, A.R., Horvat, M., 2000. Mercury in the soil plant deer predator food chain of a temperate forest in Slovenia. Environ. Sci. Technol. 34 (16), 3337–3345. https://doi.org/10.1021/es991419w.

Gosar, M., Teršič, T., 2012. Environmental geochemistry studies in the area of the Idrija mercury mine, Slovenia. Environ. Geochem. Health 34, 27–41. https://doi.org/10.1007/s10653-011-9410-6.

Graydon, J.A., Louis, St, V, L., Hintelmann, H., Lindberg, S.E., Sandilands, K.A., Rudd, J. W.M., Kelly, C.A., Hall, B.D., Mowat, L.D., 2008. Long-term wet and dry deposition of total and methyl mercury in the remote boreal ecoregion of Canada. Environ. Sci. Technol. 42 (22), 8345–8351. https://doi.org/10.1021/es801056j.

Guo, J., Sharma, C.M., Tripathee, L., Kang, S., Fu, X., Huang, J., Shrestha, K.L., Chen, P., 2021. Source identification of atmospheric particle-bound mercury in the Himalayan foothills through non-isotopic and isotope analyses. Environ. Pollut. 286 https://doi.org/10.1016/j.envpol.2021.117317.

Hines, M.E., Horvat, M., Faganeli, J., Bonzongo, J.C.J., Barkay, T., Major, E.B., Scott, K. J., Bailey, E.A., Warwick, J.J., Lyons, W.B., 2000. Mercury biogeochemistry in the Idrija River, Slovenia, from above the mine into the Gulf of Trieste. Environ. Res. 83 (2), 129–139. https://doi.org/10.1006/enrs.2000.4052.

Honegger, R., 2007. Water relations in lichens. In: Fungi in the Environment. Cambridge University Press, pp. 185–200. https://doi.org/10.1017/CBO9780511541797.010.

Horvat, M., Jereb, V., Fajon, V., Logar, M., Kotnik, J., Faganeli, J., Hines, M.E., Bonzongo, J.-C., 2002. Mercury distribution in water, sediment and soil in the Idrijca and Soča river systems. In: Environment, Analysis, vol. 2.

Horvat, M., Kontić, B., Kotnik, J., Ogrinc, N., Jereb, V., Fajon, V., Logar, M., Faganeli, J., Rajar, R., Sirca, A., Petkovšek, G., Zagar, D., Dizdavevič, T., 2003. Remediation of mercury polluted sites due to mining activities. Crit. Rev. Anal. Chem. 33 (4), 291–296. https://doi.org/10.1080/714037679.

Huang, Q., He, X., Huang, W., Reinfelder, J.R., 2021. Mass-independent fractionation of mercury isotopes during photoreduction of soot particle bound Hg(II). Environ. Sci. Technol. 55 (20), 13783–13791. https://doi.org/10.1021/acs.est.1c02679.

Huang, Q., Reinfelder, J.R., Fu, P., Huang, W., 2020. Variation in the mercury concentration and stable isotope composition of atmospheric total suspended particles in Beijing, China. J. Hazard Mater. 383 https://doi.org/10.1016/j.jhazmat.2019.121131.

Jiskra, M., Sonke, J.E., Obrist, D., Bieser, J., Ebinghaus, R., Myhre, C.L., Pfaffhuber, K.A., Wängberg, I., Kyllönen, K., Worthy, D., Martin, L.G., Labuschagne, C., Mkololo, T., Ramonet, M., Magand, O., Dommergue, A., 2018. A vegetation control on seasonal variations in global atmospheric mercury concentrations. Nat. Geosci. 11 (4), 244–250. https://doi.org/10.1038/s41561-018-0078-8.

Kocman, D., Horvat, M., 2011. Non-point source mercury emission from the Idrija Hg-mine region: GIS mercury emission model. J. Environ. Manag. 92 (8), 2038–2046. https://doi.org/10.1016/j.jenvman.2011.03.034.

Kocman, D., Kanduč, T., Ogrinc, N., Horvat, M., 2011a. Distribution and partitioning of mercury in a river catchment impacted by former mercury mining activity. Biogeochemistry 104 (1–3), 183–201. https://doi.org/10.1007/s10533-010-9495-5.

Kocman, D., Vreča, P., Fajon, V., Horvat, M., 2011b. Atmospheric distribution and deposition of mercury in the Idrija Hg mine region, Slovenia. Environ. Res. 111 (1), 1–9. https://doi.org/10.1016/j.envres.2010.10.012.

Kotnik, J., Horvat, M., Dizdarevič, T., 2005. Current and past mercury distribution in air over the Idrija Hg mine region, Slovenia. Atmos. Environ. 39 (39), 7570–7579. https://doi.org/10.1016/j.atmosenv.2005.06.061.

Kotnik, J., Horvat, M., Liang, L., Levanič, T., 2015. Mercury in tree rings from Idrija Hg mine area. International Conference on Mercury as a Global Pollutant, Korea.

Li, C., Chen, J., Angot, H., Zheng, W., Shi, G., Ding, M., Du, Z., Zhang, Q., Ma, X., Kang, S., Xiao, C., Ren, J., Qin, D., 2020. Seasonal variation of mercury and its isotopes in atmospheric particles at the coastal Zhongshan Station, Eastern Antarctica. Environ. Sci. Technol. 54 (18), 11344–11355. https://doi.org/10.1021/acs.est.0c04462.

Liu, Y., Liu, G., Wang, Z., Guo, Y., Yin, Y., Zhang, X., Cai, Y., Jiang, G., 2022. Understanding foliar accumulation of atmospheric Hg in terrestrial vegetation: progress and challenges. Crit. Rev. Environ. Sci. Technol. 52 (24), 4331–4352. https://doi.org/10.1080/10643389.2021.1989235.

Lyman, S.N., Cheng, I., Gratz, L.E., Weiss Penzias, P., Zhang, L., 2020. An updated review of atmospheric mercury. Sci. Total Environ. 707 (November), 135575 https://doi.org/10.1016/j.scitotenv.2019.135575.

Miklavčič, A., Mazej, D., Jačimović, R., Dizdarevič, T., Horvat, M., 2013. Mercury in food items from the Idrija mercury mine area. Environ. Res. 125, 61–68. https://doi.org/10.1016/j.envres.2013.02.008.

Mlakar, T.L., Horvat, M., Kotnik, J., Jeran, Z., Vuk, T., Mrak, T., Fajon, V., 2011. Biomonitoring with epiphytic lichens as a complementary method for the study of mercury contamination near a cement plant. Environ. Monit. Assess. 181 (1–4), 225–241. https://doi.org/10.1007/s10661-010-1825-5.

Naccarato, A., Tassone, A., Martino, M., Moretti, S., MacAgnano, A., Zampetti, E., Papa, P., Avossa, J., Pirrone, N., Nerentorp, M., Munthe, J., Wängberg, I., Stupple, G. W., Mitchell, C.P.J., Martin, A.R., Steffen, A., Babi, D., Prestbo, E.M., Sprovieri, F., Wania, F., 2021. A field intercomparison of three passive air samplers for gaseous mercury in ambient air. Atmos. Meas. Tech. 14 (5), 3657–3672. https://doi.org/10.5194/amt-14-3657-2021.

National Institute of Standards & Technology, 2017. Report of Investigation Reference Material 8610 Isotopes in UM-Almaden Mono-Elemental Secondary Standard This Mercury. Department of Commerce, USA.

Peel, K., Weiss, D., Chapman, J., Arnold, T., Coles, B., 2008. A simple combined sample-standard bracketing and inter-element correction procedure for accurate mass bias correction and precise Zn and Cu isotope ratio measurements. J. Anal. Atomic Spectrom. 23 (1), 103–110. https://doi.org/10.1039/b710977f.

Si, L., Ariya, P.A., 2018. Recent advances in atmospheric chemistry of mercury. Atmosphere 9 (2), 1–18. https://doi.org/10.3390/atmos9020076.

Slovenian Environmental Agency, 2022. Daily weather reports. https://meteo.arso.gov.si/met/en/.

Sun, L., Zhang, X., Zheng, J., Zheng, Y., Yuan, D., Chen, W., 2021. Mercury Concentration and Isotopic Composition on Different Atmospheric Particles (PM10 and PM2.5) in the Subtropical Coastal Suburb of Xiamen Bay, Southern China, vol. 261. Atmospheric Environment. https://doi.org/10.1016/j.atmosenv.2021.118604.

Szczepaniak, K., Biziuk, M., 2003. Aspects of the biomonitoring studies using mosses and lichens as indicators of metal pollution. Environ. Res. 93 (3), 221–230. https://doi.org/10.1016/S0013-9351(03)00141-5.

Szponar, N., McLagan, D.S., Kaplan, R.J., Mitchell, C.P.J., Wania, F., Steffen, A., Stupple, G.W., Monaci, F., Bergquist, B.A., 2020. Isotopic characterization of atmospheric gaseous elemental mercury by passive air sampling. Environ. Sci. Technol. 54 (17), 10533–10543. https://doi.org/10.1021/acs.est.0c02251.

Tomiyasu, T., Kodamatani, H., Imura, R., Matsuyama, A., Miyamoto, J., Akagi, H., Kocman, D., Kotnik, J., Fajon, V., Horvat, M., 2017. The dynamics of mercury near Idrija mercury mine, Slovenia: Horizontal and vertical distributions of total, methyl, and ethyl mercury concentrations in soils. Chemosphere 184, 244–252. https://doi.org/10.1016/j.chemosphere.2017.05.123.

Tomiyasu, T., Matsuyama, A., Imura, R., Kodamatani, H., Miyamoto, J., Kono, Y., Kocman, D., Kotnik, J., Fajon, V., Horvat, M., 2012. The distribution of total and methylmercury concentrations in soils near the Idrija mercury mine, Slovenia, and the dependence of the mercury concentrations on the chemical composition and organic carbon levels of the soil. Environ. Earth Sci. 65 (4), 1309–1322. https://doi.org/10.1007/s12665-011-1379-z.

UNEP, 2022. Guidance on Monitoring of Mercury and Mercury Compounds to Support Evaluation of the Effectiveness of the Minamata Convention.

Wang, X., Yuan, W., Lin, C.J., Feng, X., 2021. Mercury cycling and isotopic fractionation in global forests. Crit. Rev. Environ. Sci. Technol. 1–24. https://doi.org/10.1080/10643389.2021.1961505.

Xu, H.M., Sun, R.Y., Cao, J.J., Huang, R.J., Guinot, B., Shen, Z.X., Jiskra, M., Li, C.X., Du, B.Y., He, C., Liu, S.X., Zhang, T., Sonke, J.E., 2019. Mercury stable isotope compositions of Chinese urban fine particulates in winter haze days: implications for Hg sources and transformations. Chem. Geol. 504, 267–275. https://doi.org/10.1016/j.chemgeo.2018.11.018.

Yuan, W., Sommar, J., Lin, C.J., Wang, X., Li, K., Liu, Y., Zhang, H., Lu, Z., Wu, C., Feng, X., 2019. Stable isotope evidence shows re-emission of elemental mercury vapor occurring after reductive loss from foliage. Environ. Sci. Technol. 53 (2), 651–660. https://doi.org/10.1021/acs.est.8b04865.

Zhou, J., Obrist, D., Dastoor, A., Jiskra, M., Ryjkov, A., 2021. Vegetation uptake of mercury and impacts on global cycling. Nat. Rev. Earth Environ. 2 (4), 269–284. https://doi.org/10.1038/s43017-021-00146-y.

Žagar, D., Knap, A., Warwick, J.J., Rajar, R., Horvat, M., Četina, M., 2006. Modelling of mercury transport and transformation processes in the Idrijca and Soča river system. Sci. Total Environ. 368 (1), 149–163. https://doi.org/10.1016/j.scitotenv.2005.09.068.

Žižek, S., Horvat, M., Gibičar, D., Fajon, V., Toman, M.J., 2007. Bioaccumulation of mercury in benthic communities of a river ecosystem affected by mercury mining. Sci. Total Environ. 377 (2–3), 407–415. https://doi.org/10.1016/j.scitotenv.2007.02.010.

Chapter 4

Conclusions

4.1 Comment on the analytical procedure used.

The procedures employed, developed and/or optimized were suitable for performing the analysis of mercury isotopic ratios in various environmental samples. The first requirement for such work was the testing out procedures for sample digestion. Various methods were tried, including different reagents (HNO_3, HCl, HF, H_3BO_3 and H_2O_2) and different types of digestion systems (Appendix A.1 and A.2). The best procedure chosen was then implemented in studies (presented in publications in Section 3.1, 3.2, 3.3). After the digestion phase, the analysis phase also needed to be set up and properly tested. For this purpose, different configurations of mercury introduction and calibration were tested. The main variations were the different separation cells and inclusion or omission of Tl as an internal standard. The best solution was the Tekran© derived separation cell, which achieved recoveries of 99.6% and no use of Tl (Section 3.1 and Appendix A1).

In some cases where the concentrations were too low, a preconcentration was required. This method was co-developed with a co-worker who took the lead in writing the paper on the method (Appendix A.6). However, the first mention and practical application was performed in the frame of this dissertation and is presented here (Section 3.3).

4.2 Use of lichens as bio-monitors for mercury concentrations and isotopic ratios in the atmosphere the Idrija polluted area as well as in the pristine environment.

This topic was discussed in the papers titled: Fractionation of Mercury Stable Isotopes in Lichens (Božič et al., 2022, Section 3.1) and Insights into Seasonal Variations in Mercury Isotope Composition of Lichens (Božič & Horvat, 2024, Section 3.3) and it corresponded to the first hypothesis.

The relationship between the concentrations of mercury in the atmosphere, measured via traditional active sampling methods, and transplanted lichens has been established (Section 3.1). For example, where atmospheric mercury concentrations were high (up to ~100 ng/m^3), the concentrations of mercury in lichens were also high, whereas where they were low (~1 - 2 ng/m^3), the lichen concentrations were correspondingly low. However, this relationship was found not to be linear and was accompanied by significant uncertainties, raising questions about the reliability of lichens as exact proxies. Furthermore, concentrations above a few ng/m^3 in air are seldom exceeded in most

environments, except for contaminated areas such as Idrija. Lichens transplanted from the pristine Pokljuka location to Idrija showed a response to the new environment within one month. After one year, mercury concentrations in the transplanted lichens exceeded some concentrations of the in-situ lichens (in-situ concentrations ranging from ∼1.0 to ∼6.0 µg/g, while transplants after one year ranged from ∼1.5 to ∼2.5 µg/g). Thus, a one-year time period appears sufficient for lichens to fully respond to a new environment in heavily polluted areas. However, due to the relatively broad concentration ranges, determining the exact point at which an individual lichen becomes acclimated to the new environment is not feasible. For example, in the Anhovo area, lichens exhibited similar mercury concentrations to those in Pokljuka, suggesting that, at least in terms of mercury, Anhovo lichens are not polluted. The concentrations of mercury in in-situ lichens were initially thought to be relatively static (Section 3.1). However, a more detailed study (Section 3.2), involving higher sampling frequency, repeated measurements of in-situ lichens, and enhanced accuracy, revealed that they also exhibit variability. Although the exact cause of this variability is unknown, it has provided new insights into the reasons for changes in isotopic fingerprint. Higher concentrations of mercury in Idrija may result from biomass combustion, which itself is contaminated with mercury. In central Slovenia and Pokljuka, concentrations did not vary as significantly. Consequently, lichens either transplanted or in-situ can serve as bio-markers of highly contaminated environments but not as precise measurement methods in all settings and time frames, rejecting the hypothesis I.

It was observed that the mercury isotopic composition changes from relatively light to relatively heavy at several sites during the summer. These observations were first made during the January 2020 to January 2021 (Section 3.1) season and were subsequently repeated during the September 2021 to September 2022 season (Section 3.3), ensuring better data robustness. These observations rejected the hypothesis II, but allowed for the formulation of the potential explanations for such occurrences: (I) Kinetic fractionation, suggesting that when mercury passes from air into lichens, heavier isotopes preferentially remain in the air while lighter ones are more readily absorbed by lichens, (II) evaporation of Hg^0, implying enhanced evaporation of lighter isotopes from lichen thalli during hotter summer months, (III) reduction of Hg^{2+} already bound to lichen, implying that mercury is photo-reduced to Hg^0 and then more easily escapes from the lichen, skewing the isotopic composition toward heavier isotopes, and (IV) equilibration to a new isotopic signature, suggesting that lichens simply adapt to any isotopic fingerprint of the atmosphere.

Only one location from the initial study (Section 3.1), situated directly atop the former roasting site, appeared to exhibit a distinct and unique trend towards a single isotopic ratio value. However, subsequent more detailed studies (Section 3.3) revealed that isotopic ratios, even at such heavily polluted sites, vary, and the initial study may have considered too few time points to effectively discern the trend, a problem that was later addressed. This means that the hypothesis III is rejected.

Concurrently, a study of mercury concentration and isotopic composition in APM was conducted finding similar results to the ones in lichens (Section 3.3), Confirming the hypothesis IV. It is likely that similar factors as for lichens likely play a role for APM as well due to the similarities for both mercury concentrations and isotopic ratios.

4.3 Heterogeneity of the mercury isotopic fingerprint in Idrija mine ores.

This topic was discussed in the paper titled : Mercury Source Apportionment in Contaminated Soils Using Isotope Fingerprinting (Božič et al., 2023, Section 3.2). The Mercury MDF ranged approximately ∼2‰ (δ^{202}Hg), which is a relatively vast range. Conversely, the Mass-Independent Fractionation (MIF) exhibited a relatively consistent fingerprint between -0.08 to 0.16‰ (Δ^{199}Hg), with a tendency toward higher values at lighter isotopic values. For even-MIF, the samples demonstrated homogeneity with values close to zero. These findings reject the hypothesis V.

It was discovered that in the case of mercury mining in Idrija, there appears to be no discernible connection between the characteristics of the sample, including its geological period of formation, type, or excavation site. In such types of mercury ore deposits, heterogeneity emerges as a significant factor that warrants consideration. Only some samples from the Kropač ore body showcased a relatively consistent fingerprint, no correlation could be established for other samples from distinct geological periods, ore types, and excavation sites. Thus, it is more plausible that the case of Kropač represents an exception rather than the norm. This implies that the isotopic composition of ores processed and roasted in Idrija is heterogeneous. The hypothesis VI must therefore be rejected.

This suggests that ore from Idrija can be viewed as relatively uniform regarding MIF. Environmental samples from the region displaying MIF values other than zero likely underwent significant processes altering their fingerprint (e.g., methylation) or originated from alternative sources. Samples exhibiting mercury MDF ranges from ∼1.5‰ to 0.5‰ (δ^{202}Hg) could potentially be directly linked to the mine. In the context of other samples, the mercury isotopic fingerprint can assist in narrowing down potential mercury sources. Given that the Idrija mine serves as a significant pollution source in the area, most mercury contamination there can be directly attributed to the mine. However, in areas further away, such as downstream of the Idrijca river where dilution begins to take effect and other sources may be present, the isotopic fingerprint may not offer a distinct and unequivocal trace.

4.4 Isotopic fingerprint in soils from the Idrija area.

This topic was discussed in the paper in preparation titled: Elucidating Origin of Mercury in Soils in the Vicinity of Emission Sources with the Help of Mercury Isotope Ratios (Božič et al., 2024, Appendix A.3) where significant differences in isotopic fingerprints have been observed across various locations. For instance, soils near one of the oldest roasting sites at Pšenk exhibit relatively heavy ratios compared to soils from younger sites like Prejnuta and Brusovše. Sites in closer proximity to the roasting sites also display heavier isotopic fingerprints than those farther away, suggesting the presence of another source in the soils or potential fractionation during transportation, resulting in lighter isotopes being carried further. This in turn confirms the hypothesis VII.

The heterogeneity of mercury in ores may also contribute to the variability of mercury in soils, along with the mixing of mercury originating primarily from processed ores or via different atmospheric deposition pathways. Samples collected within a hundred meters of each other exhibit distinct isotopic fingerprints, underscoring the need for meticulous sampling to account for all potential factors and ensure adequate spatial density.

An intriguing observation is that soils from the Anhovo floodplains display relatively homogeneous isotopic fingerprints. This uniformity could possibly result from homogenization by the river itself. The fingerprint in the Anhovo flood plains appears distinct enough to differentiate it from other lighter ones found further up the valley slope. But since the elevation above the river plays the major role in the distribution of different isoropic fingerprins and not the distance from the Salonit cement plant, hypothesis VIII is rejected.

Appendix A: Other publications and supplementary material

A.1 Work Report: Evaluation of Select Procedures for Analysis; Multi-Elemental and Isotopic Composition of Hg in Lichens

Institut "Jožef Stefan", Ljubljana, Slovenija

Department of Environmental Sciences,
Jamova 39, P.O. Box 3000, 1001 Ljubljana, Slovenia

IJS 'Delovno Poročilo' Work Report
IJS-DP-number. 13492

EVALUATION OF SELECT PROCEDURES FOR ANALYSIS; MULTI-ELEMENTAL AND ISOTOPIC COMPOSITION OF HG IN LICHENS

Dominik Božič, Igor Živković, Marta Jagodic Hudobivnik, Darja Mazej, Marko Štrok, Milena Horvat

Ljubljana, March 2021

Contents

1 Introduction

The present report summarizes the procedures tested and used for the preparation of lichen samples for total mercury concentration (THg), the multi-elemental analysis and determination of the isotopic composition of stable Hg isotopes.

We aim to give a reader an insight into the decision of choosing the best method for lichen preparation. There were two general methods chosen, the first using hydrofluoric acid (HF), nitric acid (HNO_3) and hydrochloric (HCl) with heating on a hot plate (hereafter referred to as a method A) and the other using only nitric acid (HNO_3, method B1) or a mixture of nitric and hydrochloric (HCl) acids (method B2) but with the digestion performed in a microwave oven. Method A was chosen as it allowed the easiest implementation of HF into the digestion process. HF was assumed to enhance the digestion efficiency of the lichens if inorganic silica-containing material was present. But this method requires an evaporation step to remove HF which is damaging to the instruments. Another way to achieve similarly efficient digestion result could be achieved by increasing the temperature and pressure during microwave digestion. For this, the methods B1 and B2 were devised. In this way the step of open evaporation is not necessary. The microwave setup used does not allow for large scale HF digestion (more than a couple of samples in a lifecycle of thermal probe, but a special upgrade can be purchased for such purpose); therefore, a microwave digestion with HF was not possible. But in any case this would still necessitate the evaporation, which is why this combination was not tested.

To find out how each method influences the THg, multi-elemental, and isotopic analysis, a series of experiments were conducted by analyzing two, reference materials. The results were then compared.

An important aspect of this study was also to see what method is the best in the domain of time economics. That is a partial reason why THg was analyzed with two different instruments.

Additionally, the multi-elemental analysis allowed the determination of plethora of elements. The ones that had no reference values are reported as an orientation value.

2 Experimental

2.1 Standards and reference materials

Two reference and two standard materials were used in this study. These were IAEA 336 (Trace and minor elements in lichen) [1], BCR 482 (lichen certified reference material) [2]; and NIST 3133 (Mercury (Hg) Standard Solution) [3] and NIST 8610 (Mercury Isotopes in UM-Almaden Mono-Elemental Secondary Standard) [4]. For multi-elemental analysis an additional standard, Periodic table mix 1 for ICP (TraceCERT®) [5], was used.

2.2 Laboratory material and reagents

-HNO_3 (65%, Suprapur, low in Hg, Merck)
-HCl (30% Suprapur, Merck)
-HF (48%, analytical grade ISO, Merck)
-$Mg(ClO_4)_2$ (analytical grade, Perkin-Elmer Corporation)
-$AgNO_3$ (analytical grade)
-$SnCl_2$ (Emsure – for analysis, max 0.000001% Hg, Superlco)

-Boric acid crystals, H_3BO_3 (analytical grade ISO, Merck)
-Milli-Q deionised water (< 18 MΩ, Millipore).
-Teflon vials (25 ml, Savillex)
-Hot plate (e.g. Ceran 500, 22SR) and aluminum block.
-Precision balance (e.g. Sartorius, MC-21 OS)
-Micro soaps (Micro-90® concentrated cleaning solution, International Products Corporation)
-microwave digestion system (ULTRAWAVE, Single Reaction Chamber Ultrawave Digestion System, MILESTONE, Italy)
-45 µm filters.

2.3 Cleaning of vials

In the case of the Teflon vials used for method A, the vessels were soaked for 12 h in a plastic container filled with a soap solution (Micro solution 2% in tap water). They were rinsed thoroughly first with tap water and then with Milli-Q water. Afterwards they were put in the vessels in 50% (v/v) concentrated HNO_3 solution and heated at 100°C for 48 h. Afterwards they were transferred to the solution of 10% (v/v) concentrated HCl for 24 h. Then they were again rinsed thoroughly (4 times) with Milli-Q water. For storage, the vessels are kept in polyethylene plastic bags and filled with 1% HCl.
The Teflon vials used for methods B1 and B2 were cleaned by adding the same reagents and using the same procedure as for the digestion. If the samples were measured after some samples with vastly different matrices and elemental composition, such cleaning was performed twice.

2.4 Method A digestion

0.1 g to 0.3 g of dry sample was weighed in the Teflon vials. 5 mL of mixture of concentrated HNO_3/HF (2:1) and 1 mL of concentrated HCl was added. Vials were closed and heated for 24 h at 110 °C. For THg measurement only, the solution was diluted to the mark (25 mL) with boric acid 5% (w/v), which converted HF to BF_4^-. For multi-elemental measurement and isotopic analysis, the HCl and HF needed to be removed. This was performed by evaporating the solution until only cca. 1 mL was left. This took about 5 h at 100 °C. Then the Milli-Q water was added to the mark in order to dilute the sample. In order to check whether any HF or HCl was left, $Mg(ClO_2)_4$ and $AgNO_3$ were added to two separate blank digested samples. On average this type of digestion with all the associated preparations took some 12 man-hours over 4 days for around 60 samples.

2.5 Methods B1 and B2 digestion

For the first batch of measurements, about 0.3 g sample was weighed into pre-cleaned Teflon tubes. 3 mL of 65 % HNO_3 was added and samples were subjected to closed vessel microwave digestion at max power 1500 W and max pressure 100 bar: ramp to 240 °C 20 min and hold 15 min. Then the samples were allowed to equilibrate at room temperature. The solution was further quantitatively transferred into 10 mL polyethylene graduated tubes and diluted to 10 mL with Milli-Q water. The same procedure was applied for blank sample and certified reference material. Before measurements, additional dilutions (1/5) with 5% HNO_3 were done for measurements. The method B2 differed only by addition of 0.4 mL of 30% HCl to digestion in the microwave. The samples were filtered (0.45 µm) before the

measurement on ICP-QQQ. On average this type of digestion with all the associated preparations took some 10 man-hours over 2 days for around 60 samples.

3 Measurement of total mercury and multi-elemental analysis

Hg was measured by two methods. First was Cold Vapor Atomic Absorption Spectroscopy (CV-AAS) and the second was the Triple-Quad Inductively Coupled Plasma Mass Spectrometer (ICP-QQQ).

3.1 Cold vapor atomic absorption spectroscopy

An aliquot (0.1 – 1 mL) of sample was transferred to the reaction vessel, reduced with $SnCl_2$ and aerated with outside air until equilibrium of mercury vapors is reached. During this circulation, acid gasses leaving the sample solution are removed by acid gas trap containing 10% NaOH solution. After that, the mercury vapor is introduced to the absorption cell by turning the four-way valve and measured by CV-AAS (Automatic Mercury Analyzer Model Hg-201, Sanso Seisakusho Co., LTD). The measurements were performed on 12.1.2021. On average this type of analysis with all the associated preparations took some 5 man-hours for up to 60 samples.

3.2 ICP-QQQ

For the determination of total element concentrations in prepared samples, Agilent 8800 (Agilent Technologies, CA, USA) ICP-QQQ was used. General parameters are described in Table 1. For the elimination of interferences, collision/reaction cell was used with He, H_2 or O_2 gas. The concentrations were determined based on external calibration of Periodic table mix 1 for ICP for selected elements (Na, Mg, Al, P, S, Cl, K, Ca, Ti, V, Cr, Fe, Co, Cu, Zn, As, Se, Br, Sr, Rb, Mo, Cd, Sn, Sb, Te, Cs, Ba, Pt, Au, Hg, Tl, Pb and U) and NIST 3133 for Hg. On average this type of analysis with all the associated preparations took some 3 man-hours for up to 60 samples.

Table 1: Operating conditions of Aglient 8800 ICP-QQQ

General parameters	
Nebulizer	MicroMist
Spray chamber	Scott double-pass
RF Power [W]	1550
Plasma gas flow [L/min]	15
Carrier gas [L/min]	0.95
Makeup gas [L/min]	0.10
Sampling depth [mm]	8.0
Sample uptake rate [rps]	0.1
Sampling and skimmer cones	Nickel
Isotopes of internal standards	^{45}Sc, ^{89}Y, ^{103}Rh, ^{157}Gd
Masses of the elements and the way in which they were sampled with reaction gas used in square brackets	
Na	23 -> 23 Na [He]
Mg	24 -> 24 Mg [He]
Al	27 -> 27 Al [He]
P	31 -> 47 PO [O_2]
S	34 -> 50 SO [O2]
K	39 -> 39 K [He]
Ca	44 -> 60 CaO [O2]
Ti	47 -> 63 TiO [O2]

V	51 -> 67 VO [O2]
Cr	52 -> 52 Cr [O_2]
Mn	55 -> 55 Mn [He]
Fe	56 -> 56 Fe [H_2]
Co	59 -> 59 Co [He]
Ni	60 -> 60 Ni [He]
Cu	65 -> 65 Cu [He]
Zn	66 -> 66 Zn [He]
As	75 -> 91 AsO [O2]
Se	78 -> 78 Se [H_2]
Br	79 -> 79 Br [He]
Rb	85 -> 85 Rb [He]
Sr	88 -> 88 Sr [He]
Cd	114 -> 114 Cd [He]
Sb	123 -> 123 Sb [He]
Te	130 -> 130 Te [He]
Cs	133 -> 133 Cs [He]
Ba	137 -> 137 Ba [He]
Hg	202 -> 202 Hg [He]
Tl	205 -> 205 Tl [He]
Pb	208 -> 208 Pb [He]
U	238 -> 238 U [He]

The measurement of the method A samples was performed on 13.1.2021, the measurement of method B1 samples was performed 2.3.2021 and of the method B2 samples it was preformed 5.3.2021.
Since only the Na, Al, P, Cr, Mn, Fe, Co, Ni, Cu, Zn, As, Se, Rb, Sr, Cd, Cs, Ba, Hg, Pb were given a certified value in the reports for either IAEA 336 or BCR 482, only these are reported with recoveries.

3.3 Isotopic analysis

For the isotopic analysis the multi-collector type mass spectrometer (MC-ICP-MS) was used. The Hg isotope measurements of the samples were performed with the Nu plasma II MC-ICP-MS (Nu instruments Ltd, Ametek, UK). It is kept under the clean room conditions. Its operating conditions are given in Table 2.

Table 2: Operating conditions of Nu Plasma II MC-ICP-MS

Plasma conditions	
RF power [W]	1300
Ar cooling gas [L/min]	13.0
Ar auxiliary gas [L/min]	0.8
Nebulizer gas pressure [Psi]	36 – 37
Tl standard introduction (Aridus II™)	
MicroMist AR-35-FMO2LE & ARG-1-UM02 [mL/min]	0.2
Ar sweep gas [mL/h]	10
Sample uptake rate [mL/min]	0.9 – 1.1
Spray chamber [°C]/membrane [°C]	110/160
Hg vapor generation	
Ar sweep gas flow [L/min]	20 – 25

SnCl2 uptake rate [mL/min]	0.9 – 1.1
Sample uptake rate	0.9 – 1.1
Method settings	
Mass separation	1
Cup configuration	^{196}Hg(L4) ^{198}Hg(L2) ^{199}Hg(L1) ^{200}Hg(Ax) ^{201}Hg(H1) ^{202}Hg(H2) ^{203}Tl(H3) ^{204}Hg, ^{204}Pb (H4) ^{205}Hg(H5) ^{208}Pb(H8)
Blocks	1 block
Measurements per block	30
Magnet delay time [s]	2
Transfer time [s]	310
Wash time – 5% HNO_3 & 3% HCl [s]	200
Analytical concentration [ng/mL]	1
Sensitivity [V]	0.5 – 1.2
Total analysis time [min]	21

An auto-sampler ASX-520 (Teledyne Cetac, NE, USA) was used to set the syringe into appropriate sample. The solution was pumped via a peristaltic pump to a T section where it was joint by a $SnCl_2$ in a solution (3% w/v in 10% v/v HCl) to reduce the Hg. The mix of solutions was carried over to the phase separator where the elemental Hg vapor was carried over to the instrument by Ar sweep gas flow.
The measurements were performed at Hg concentrations of 1 ng/mL. This gave the intensities between 0.5 and 1.2 V at the m/z of 202, depending on the measurement session. Outlier rejection of an individual measurement inside the cycle was done using the NICE (Nu Instruments Calculation Editor) for the values above three standard deviations (S.D.). All measurements were done according to the sample-standard-sample bracketing technique (Equation 1) [6]

$$\frac{^{xxx}Hg}{^{yyy}Hg}_{SSB} = \left(\frac{\frac{^{xxx}Hg}{^{yyy}Hg}_{NIST\ 3133\ before} + \frac{^{xxx}Hg}{^{yyy}Hg}_{NIST\ 3133\ aftef}}{2} \right) \quad (1)$$

where the value between two Hg isotopes XXX and YYY is used as a correction and the rest of δ and Δ are calculated as is exampled in [7].
The HF digested samples were measured on 30.10.2020. The measurements of the microwaved samples were performed in March 2021.

4 Results

4.1 Performance of acid tests

Since there was no observable precipitate that would form after the addition of either $Mg(ClO_2)_4$ or $AgNO_3$ to the solution after the evaporation of the solution containing the HF, HCl and HNO_3 it is clear that F and Cl were mostly removed. This meant that such a solution can be diluted and used for further analyses.

4.2 Comparison of CV-AAS and ICP-QQQ for THg determination

The comparison between the two methods can be seen from Table 3. In both cases the solution was prepared via the method A in January 2021. The reference for Hg in IAEA 336 is 0.20 ± 0.04 (k = 2) µg/g, in BCR 482 it is 0.48 ± 0.04 (k = 2) µg/g while the NIST 3133 was pipetted such as to be 1 ± 0.01 (k = 2) µg/mL in the solution after the dilution (Table 3).

Table 3: Comparison between THg values obtained by CV-AAS and ICP-QQQ

	CV-AAS	ICP-QQQ
	µg/g ± S.D	µg/g ± S.D.
Sample 1	0.19 ± 0.01	0.19 ± 0.02
Sample 2	0.22 ± 0.01	0.22 ± 0.03
Sample 3	0.17 ± 0.01	0.17 ± 0.02
Sample 4	0.21 ± 0.01	0.22 ± 0.01
Sample 5	0.18 ± 0.01	0.20 ± 0.00
Sample 6	0.20 ± 0.01	0.24 ± 0.00
Sample 7	0.28 ± 0.05	0.30 ± 0.04
Sample 8	0.21 ± 0.01	0.22 ± 0.00
Sample 9	1.73 ± 0.06	1.85 ± 0.18
Sample 10	0.14 ± 0.01	0.15 ± 0.01
IAEA 336	0.18 ± 0.02	0.17 ± 0.01
BCR 482	0.43 ± 0.04	0.44 ± 0.03
NIST 3133	0.95 ± 0.01	0.96 ± 0.01

Table 4 represents the recoveries of the best case results. These were calculated from the longer term averages and do not correspond to the values from the tables 3, 5 & 6, all the samples and reference materials were prepared via the method A.

Table 4: Comparison between recoveries obtained by CV-AAS and ICP-QQQ.

	CV-AAS	ICP-QQQ
	% ± S.D	% ± S.D
R - IAEA 336	84 ± 11	89 ± 11
R - BCR 482	90 ± 8	92 ± 9
R - NIST 3133	95 ± 3	96 ± 3

If we plot the values against each other a slope of 0.946 and R^2 of 0.998 is obtained. The paired t test is used to compare the methods. Since the difference the p value is 0.056 which is higher than the significance level $\alpha = 0.05$, meaning that we accept the null hypothesis, making the results statistically the same.

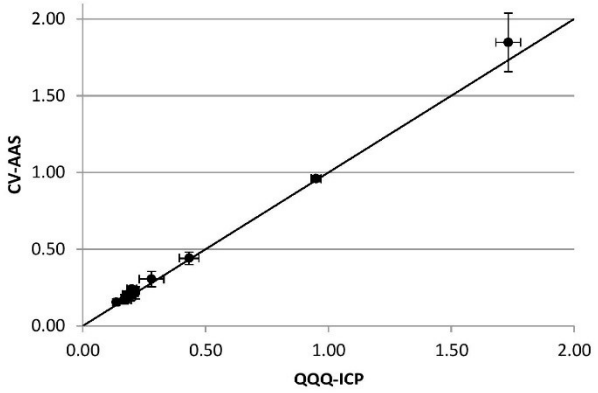

Figure 1: Drawn is the line for the slope of 1. X axis represents the THg values measured by QQQ-ICP and Y axis represents those done by CV-AAS.

4.3 Comparison of preparation procedures for multi elemental measurement

The multi-elemental results of the comparison of different preparation methods are presented in the Table 5. The concentrations of the elements in the samples and the certified values with the uncertainties and relative standard deviations are given in Table 6.

Table 5: Recoveries (%) of multi-elemental analysis of standards prepared with different methods. The uncertainties are a combined uncertainty of the reference material and from the measurement.

Sample	IAEA 336	IAEA 336	IAEA 336	BCR 482	BCR 482
Method	A	B1	B2	B1	B2
Repetitions	N = 4	N = 8	N = 8	N = 8	N = 8
Na	100 ± 7	117 ± 13	91 ± 7	/	/
Al*	115 ± 10	112 ± 11	98 ± 9	99 ± 10	86 ± 6
P*	100 ± 13	102 ± 10	94 ± 10	/	/
K	93 ± 6	99 ± 11	97 ± 7	/	/
V	89 ± 11	115 ± 8	110 ± 8	/	/
Cr*	88 ± 5	114 ± 4	109 ± 4	103 ± 8	97 ± 11
Mn	98 ± 6	117 ± 7	115 ± 6	/	/
Fe	99 ± 8	111 ± 7	117 ± 5	/	/
Co	87 ± 11	100 ± 10	98 ± 9	/	/
Ni	/	/	/	104 ± 8	119 ± 8
Cu	93 ± 9	103 ± 21	104 ± 8	98 ± 7	107 ± 6
Zn	113 ± 8	106 ± 15	116 ± 6	98 ± 7	120 ± 4
As	105 ± 10	117 ± 15	96 ± 7	91 ± 11	104 ± 6
Se	137 ± 12	115 ± 11	115 ± 10	/	/
Br	67 ± 8	/	/	/	/
Rb*	90 ± 6	88 ± 9	88 ± 7	/	/
Sr	97 ± 6	103 ± 8	102 ± 6	/	/

Cd*	99 ± 7	101 ± 12	97 ± 7	94 ± 21	100 ± 4
Sb	67 ± 7	181 ± 12	66 ± 8	/	/
Cs	89 ± 6	101 ± 5	91 ± 6	/	/
Ba	93 ± 9	106 ± 5	104 ± 9	/	/
Hg	84 ± 13	85 ± 10	92 ± 12	87 ± 5	92 ± 6
Pb*	84 ± 9	97 ± 7	92 ± 7	95 ± 11	101 ± 6

Table 6: Concentrations of standards, as reported by BCR and IAEA, as well as their uncertainties and the measured concentrations with the relative uncertainties. C – Concentration [µg/g], rsd – relative standard deviation (%) and U – 95% confidence interval.

	IAEA 336		IAEA 336		IAEA 336		IAEA 336		BCR 482		BCR 482		BCR 482	
	A		B1		B2		Reference values		B1		B2		Reference values	
	C	rsd	C	rsd	C	rsd	C	U	C	rsd	C	rsd	C	U
Na	321	4	375	11	296	4	320	40	81	8	60	5	/	/
Mg	617	4	791	10	585	4	/	/	677	7	498	5	/	/
Al	781	5	762	8	681	4	680	110	1094	10	947	6	1103	24
P	610	8	623	3	589	2	610	120	689	9	684	4	/	/
S	576	7	670	2	717	2	/	/	2128	6	2011	5	/	/
K	1708	3	1820	10	1783	4	1840	200	3699	13	3569	3	/	/
Ca	2312	5	2918	5	2811	2	/	/	2426	6	2480	4	/	/
Ti	85.6	9	20	5	33.3	3	/	/	29.8	7	49.4	6	/	/
V	1.31	8	1.69	1	1.61	2	1.47	0.22	4.35	8	4.37	5	/	/
Cr	0.93	4	1.2	2	1.18	2	1.06	0.07	4.26	8	4.02	11	4.12	0.15
Mn	61.4	4	73.6	5	73.8	4	63	6	31.5	13	32.5	6	/	/
Fe	425	6	478	4	513	2	430	50	851	6	900	4	/	/
Co	0.25	6	0.29	4	0.29	3	0.29	0.05	0.31	3	0.31	5	/	/
Ni	0.9	8	1	5	1.1	5	/	/	2.6	8	2.9	8	2.47	0.07
Cu	3.34	6	3.7	20	3.82	3	3.6	0.5	6.92	7	7.54	6	7.03	0.19
Zn	34.4	5	31.7	14	35.7	3	30.4	3.4	99.1	7	120.5	4	100.6	2.2
As	0.8	8	0.74	14	0.82	3	0.63	0.08	0.77	10	0.88	5	0.85	0.07
Se	0.3	8	0.26	7	0.28	3	0.22	0.04	0.41	3	0.42	5	/	/
Br	8.7	5	2	66	1.6	9	12.9	1.7	4	44	4.9	8	/	/
Rb	1.59	1	1.55	7	1.59	2	1.76	0.22	7.56	20	8.12	5	/	/
Sr	9.1	1	9.6	5	9.7	2	9.3	1.1	10	12	10.2	5	/	/
Mo	0.05	2	0.06	12	0.05	6	/	/	0.38	38	0.36	6	/	/
Cd	0.12	3	0.12	11	0.12	3	0.12	0.014	0.53	21	0.56	4	0.56	0.02
Sb	0.049	2	0.033	10	0.048	5	0.073	0.01	0.132	8	0.24	6	/	/
Te	0.12	4	0.12	9	0.12	7	/	/	0.22	11	0.23	8	/	/
Cs	0.098	2	0.111	5	0.103	2	0.11	0.013	0.225	12	0.211	6	/	/
Ba	6	1	6.8	5	6.8	3	6.4	1.1	12.7	10	13	6	/	/
Hg	0.17	8	0.17	3	0.19	6	0.2	0.04	0.42	4	0.44	6	0.48	0.02
Tl	0.01	3	0.01	8	0.01	9	/	/	0.04	14	0.04	6	0.48	0.02
Pb	4.13	6	4.76	4	4.63	3	4.9	0.6	38.81	11	41.37	6	40.9	1.4
U	0.04	3	0.04	10	0.04	3			0.04	4	0.04	7		

4.4 Comparison of preparation procedures for isotopic analysis

The isotopic results of the comparison of different preparation methods are presented in the Table 7. There was only one measurement per sample, due to the constraints with analysis time and problems with instrument stability. So, to validate the standard deviations the ones calculated for NIST 8610 and NIST 3133 are given in the Table 8.

Table 7: Comparison of the delta Hg values for the BCR 482 lichen obtained on MC-ICP-MS for different methods versus values found in the literature [8], [9].

Dgestion	$\delta^{199}Hg$	$\delta^{200}Hg$	$\delta^{201}Hg$	$\delta^{20}2Hg$	$\delta^{204}Hg$	$\Delta^{199}Hg$	$\Delta^{200}Hg$	$\Delta^{201}Hg$	$\Delta^{204}Hg$
Method A	-1.01	-0.80	-1.70	-1.51	-2.33	-0.63	-0.04	-0.57	-0.08
Method B1	-0.95	-0.98	-2.64	-2.29	-4.52	-0.37	0.17	-0.92	-1.12
Method B2	-1.16	-0.88	-2.12	-1.89	-2.60	-0.68	0.07	-0.70	0.22
Berail (2017)	-1.07	-0.81	-2.00	-1.68	-2.46	-0.64	0.04	-0.73	0.38
Estrade (2009)	-0.99	-0.68	-1.71	-1.48	n/a	-0.62	0.06	-0.60	n/a

Table 8: The delta values for NIST 8610 and NIST 3133 reference materials that were measured with the samples for each method.

			$\delta^{199}Hg$	$\delta^{200}Hg$	$\delta^{201}Hg$	$\delta^{202}Hg$	$\delta^{204}Hg$	$\Delta^{199}Hg$	$\Delta^{200}Hg$	$\Delta^{201}Hg$	$\Delta^{204}Hg$
Methods		n	‰ ± 2 S.D.	‰ ± 2 S.D.	‰ ± 2 S.D.	‰ ± 2 S.D.	‰ ± 2 S.D.	‰ ± 2 S.D.	‰ ± 2 S.D.	‰ ± 2 S.D.	‰ ± 2 S.D.
A	NIST 8610	4	-0.18 ±0.15	-0.27 ±0.14	-0.49 ±0.17	-0.53 ±0.13	-0.77 ±0.07	-0.04 ±0.12	0.00 ±0.06	-0.09 ±0.08	0.02 ±0.20
B (1 & 2)	NIST 8610	6	-0.17 ±0.12	-0.25 ±0.11	-0.51 ±0.38	-0.55 ±0.24	-0.66 ±0.50	-0.03 ±0.13	0.03 ±0.10	-0.10 ±0.25	-0.15 ±0.45
B (1 & 2)	NIST 3133	4	-0.06 ±0.32	0.00 ±0.29	0.02 ±0.63	-0.01 ±0.51	0.21 ±0.40	-0.06 ±0.19	0.01 ±0.06	0.02 ±0.27	0.22 ±0.49
reference	NIST 8610	/	-0.17 ±0.01	-0.27 ±0.01	-0.46 ±0.02	-0.56 ±0.03	-0.82 ±0.07	-0.03 ±0.02	0.00 ±0.01	-0.04 ±0.01	0.00 ±0.02

5 Discussion and conclusion

All the methods presented are fit for multi-elemental and isotopic studies in terms of instrument protection.

It can be concluded that both ICP-QQQ and CV-AAS methods give comparable results for THg measurement.

Some 5 % of lost mercury might be attributed to evaporation step of the method A. Recoveries for Method A range from 84 to 92 % while recoveries for methods B1 and B2 range from 85 to 92 %.

With this setup we can measure the presented elemental concentrations at the presented uncertainties.

The digestion method A is somewhat more time consuming than the method B. Overall the best value method and analytical technique is method B, more specifically B2 with ICP-QQQ as it gives us the best ratio between time used and information gathered.

The measured elemental concentrations for BCR-482 and IAEA-336 are presented and can be used as an orientation value in any similar study.

The standard deviations for the measurements of isotopic composition conducted at the time of method A digested samples are comparable to the ones found in the literature (Table 6). Therefore even the theoretically worst method for sample digestion still returns sufficiently good results. When the methods with and without digestion with HCl are compared it can be seen that method B2 outperforms the method B1 in all but one case (δ^{199}Hg). To properly evaluate all the uncertainties, this should to be evaluated in a larger scale and more rigorous way.

6 References

[1] IAEA, "Reference sheet - Reference Material IAEA-366 - Trace and minor elements in lichen," no. October 1994. IAEA, Vienna, p. 4, 1999, [Online]. Available: https://nucleus.iaea.org/rpst/Documents/rs_iaea-336.pdf.

[2] Institute for Reference Materials and Measurements, "CERTIFIED REFERENCE MATERIAL BCR® – 482 CERTIFICATE OF ANALYSIS," no. 1. European Commision, pp. 1–2, 2006.

[3] National Institute of Standards & Technology, "Certificate of Analysis Certificate of Analysis Standard Reference Material 3133 Mercury (Hg) Standard Solution." Department of Commerce - USA, 2016.

[4] National Institute of Standards & Technology, "Report of Investigation Reference Material 8610 sotopes in UM-Almaden Mono-Elemental Secondary Standard This Mercury." Department of Commerce - USA, 2017.

[5] Trace CERT, "Periodic table mix 1 for ICP," *Sigma Aldritch*. pp. 1–4, 2015, [Online]. Available: http://www.sigmaaldrich.com/catalog/product/sial/92091.

[6] K. Peel, D. Weiss, J. Chapman, T. Arnold, and B. Coles, "A simple combined sample-standard bracketing and inter-element correction procedure for accurate mass bias correction and precise Zn and Cu isotope ratio measurements," *J. Anal. At. Spectrom.*, vol. 23, no. 1, pp. 103–110, 2008, doi: 10.1039/b710977f.

[7] J. D. Blum and M. W. Johnson, "Recent developments in mercury stable isotope analysis," *Rev. Mineral. Geochemistry*, vol. 82, no. July 2013, pp. 733–757, 2017, doi: 10.2138/rmg.2017.82.17.

[8] J. Carignan, N. Estrade, J. E. Sonke, and O. F. X. Donard, "Odd isotope deficits in atmospheric Hg measured in lichens," *Environ. Sci. Technol.*, vol. 43, no. 15, pp. 5660–5664, 2009, doi: 10.1021/es900578v.

[9] S. Bérail *et al.*, "Determination of total Hg isotopic composition at ultra-trace levels by on line cold vapor generation and dual gold-amalgamation coupled to MC-ICP-MS," *J. Anal. At. Spectrom.*, vol. 32, no. 2, pp. 373–384, 2017, doi: 10.1039/c6ja00375c.

A.2 Work Report: Comparison Between Hot-Plate and Microwave Digestion Recoveries of Soil Samples

Institut "Jožef Stefan", Ljubljana, Slovenija

Department of Environmental Sciences,
Jamova 39, P.O. Box 3000, 1001 Ljubljana, Slovenia

IJS 'Delovno Poročilo' - Work Report
IJS-DP-number 13685

COMPARISON BETWEEN HOT-PLATE AND MICROWAVE DIGESTION RECOVERIES OF SOIL SAMPLES

Dominik Božič, Marta Jagodic Hudobivnik, Darja Mazej, Milena Horvat

Ljubljana, December 2021

Contents

1 Introduction

If there is a need for an environmental sample to be digested, the analyst can choose between many ways to do so. Different mixture of reagents as well as different equipment can be used. HF acid is well suited for digestion of silicates while it cannot be present in the solution used for measurement on instruments using glass parts. The amount of HCl acid should also not exceed 0.5 % in the solution as it negatively effects the measurements. On the other hand it has been observed that HCl mobilized mercury better than the nitric acid [1]. To neutralize the HF, boric acid can be used, which might contain some impurities, which could contaminate the sample. So a preferential method might be to evaporate the solution leaving little to no HF in it. To perform the digestion itself two methods are widely used. One is to heat the vials on a hot block in an open fume hood 'hot plate digestion' and another in a closed microwave heating machine 'microwave'.
Here two methods of digestion are presented. Both of them are slight modifications of the standard operating procedures for digestion of sediments and soils used at the 'Jožef Stefan' Institute - Department of Environmental Sciences. Similar study has been already performed for lichens [1]. There it has been found out that closed digestion with no HF addition gives better performance. But the focus of this study will be on the soils which necessitates the addition of HF. Two procedures were tested. The open procedure included open digestion and evaporation while the closed procedure included closed digestion and neutralization with H_3BO_3.

2 Experimental

2.1 Standards and reference materials

There were three standard reference soil materials used for this study:

- ERM-CC141a (Loam Soil),
- IAEA-SOIL-7 (Trace Elements in Soil),
- NIST 2711 (Montana Soil II).

For multi-elemental analysis the Periodic table mix 1 for ICP (TraceCERT®) [2], was used for Hg the NIST 3133 reference material was used [3]

2.2 Reagents

- Ultrapure water (Milli-Q water 18.2 MΩ cm, Millipore)
- HNO_3 (65%, Suprapur, Merck)
- H_2O_2 (30%, analytical grade, Applichem)
- H_3BO_3 (analytical grade, Merck)
- HF (48%, analytical grade ISO, Merck)
- HCl (30%, s.p., Merck)

2.3 Hot plate digestion

0.25 g to 0.35 g of dry sample was weighted into the Teflon vials. 2 mL of concentrated HF, 3 mL of concentrated HNO_3 and 1 mL of concentrated HCl was slowly added to the vial. The vials were covered ad heated on a hot-plate for 72 h at 140 °C. After which 2 mL of H_2O_2 was added and the heating was repeated for 24 h at 140 °C. Then 2 mL of ultrapure water was added and the solution was again heated for 24 h at 110 °C.
The evaporation was performed at 105 °C on a hot-plate using an aluminum block. This took some 7 h. The evaporation was left to go on until about 0.5 – 1 mL of solution was left. In all of the samples, some specks of undigested material were

observed. The solution was then diluted with 9 mL of ultrapure water. The Teflon vials were weighted than the solution was filtered (0.45 µm, Agilent) and transferred to 10 mL plastic vials. For multi-elemental analysis the samples were diluted five times with ultrapure water.
In total such procedure took one week to complete. At one time up to 30 samples can easily be digested in this way. An important drawback of this method is that it is hard to precisely quantify when there is only one mL of solution left in the vials. If there is too much, there is a risk of some HF still being present in the solution, but if everything evaporates new matrix may form in the precipitate which must be digested again. Another problem with such method is that during the evaporation there are more chances for droplets from one vial to enter another during opening/closing of the vials or handling procedure.

2.4 Microwave digestion

0.25 g of dry sample was weighted in the Teflon reactor vessels. 5 mL of HNO_3, 1 mL of HCl, 2 mL of HF and 1 mL of H_2O_2 were added. The vessels were subjected to the microwave digestion using Ethos 1 (Milestone Srl., Italy) system. The max power was set to 1200 W and the max T at 210 °C. The ramp up to this temperature was set at 30 min and the system was set to hold this temperature for one hour. After the digestion, the vessels were left to cool and were then filled with 12 mL of 5% H_3BO_3. After this step, the same heating procedure was executed again, only this time with only 30 min set for holding the temperature.
After the digestion, the samples were quantitatively transferred to the 30 mL vials. The vessels were rinsed twice with ultrapure water and the vials were quantitatively filled to close to the 30 mL mark. The dilution was made by quantitative transfer of 0.5 mL of the digested solution to a 10 mL vial and dilution with ultrapure water to 6 mL.
With microwave the highest throughput possible is 8 samples plus a standard reference material and a blank sample a day. There is a lot less chances for contamination during the digestion in comparison to the hot-plate digestion.

3 Multi-elemental analysis

For the determination of total element concentrations in prepared samples, Agilent 8800 (Agilent Technologies, CA, USA) Triple-Quad Inductively Coupled Plasma Mass Spectrometer QQQ-ICP-MS was used. The mode of operation is the same as in Božič et al. [4].

4 Results

4.1 Visual inspection

At the visual inspection of the samples digested using open digestion there were some specs of material observed in all of the soil and particulate mattes samples. In the case of closed digestion, the solution was transparent or close to transparent with no visual specs of any kind left to be seen by naked eye.

4.2 Hot plate digestion

In Table 2 the recoveries of the elements in ERM-CC141a and IAEA-SOIL-7 for which the concentrations are reported in the certificates are given.

Table 2: The concentrations (c), standard deviations (S.D.), (k = 2) and recoveries (R) in the ERM-CC141a and IAEA-SOIL-7 are given. n denotes the number of measurements. Recoveries are in % while the concentrations are in µg/g.

		ERM-CC141a (n = 1)		IAEA-SOIL-7 (n = 4)	
		measured	certified	measured	certified
Al	c [µg/g]	/	/	15598	47000*
	S.D.	/	/	1643	3000
	R [%]			**33**	
Ti	c [µg/g]	/	/	1901	3000*
	S.D.	/	/	104	400
	R [%]			**63**	
Cr	c [µg/g]	32	86	34.8	60.0
	S.D.	/	8	7.4	11.0
	R [%]	**37**		**58**	
Mn	c [µg/g]	231	464	396	631
	S.D.	/	18	62	27
	R [%]			**63**	
Fe	c [µg/g]	/	/	15684	25700*
	S.D.	/	/	918	500
	R [%]			**61**	
Co	c [µg/g]	4	8.5	4.80	8.90
	S.D.	/	0.5	0.59	0.50
	R [%]	**51**		**54**	
Ni	Average	20	26.4	10.0	26.0
	Deviation	/	2.4	0.7	5.0
	Recovery	**75**		**39**	
Cu	c [µg/g]	11	14.4	3.77	11.00
	S.D.	/	1.4	0.28	2.00
	R [%]	**76**		**34**	
Zn	c [µg/g]	49	57	39.7	104.0
	S.D.	/	4	5.0	3.0
	R [%]	**86**		**38**	
As	c [µg/g]	9.84	9.9	7.4	13.4
	S.D.	/	1.5	0.4	0.9
	R [%]	**89**		**55**	
Cd	c [µg/g]	0.333	0.350	1.45	1.90*
	S.D.	/	0.050	0.09	0.80
	R [%]	**95**		**76**	
Sr	c [µg/g]	/	/	40.4	108.0
	S.D.	/	/	2.0	5.0
	R [%]			**37**	
Mo	c [µg/g]	/	/	0.90	2.50*
	S.D.	/	/	0.49	1.60
	R [%]			**36**	

***denotes the values reported as reference values.**

4.3 Closed digestion

In Table 3 the recoveries of the elements in ERM-CC141a, IAEA-SOIL-7 and NIST 2711 are presented for which the concentrations are reported in the certificates are given.

Table 3: The concentrations (c), standard deviations (S.D.), (k = 2) and recoveries (R) in the ERM-CC141a, IAEA-SOIL-7 and NIST 2711 are given. n denotes the number of measurements. Recoveries are in % while the concentrations are in µg/g.

		ERM-CC141a (n = 4)		IAEA-SOIL-7 (n = 4)		NIST 2711 (n = 8)	
		measured	certified	measured	certified	measured	certified
Na	c [µg/g]	/	/	2062	2400*	10714	12000
	S.D.	/	/	399	100	1729	3170
	R [%]			**86**		**89**	
Mg	c [µg/g]	/	/	10309	11300*	8063	10700
	S.D.	/	/	1488	300	2255	600
	R [%]			**91**		**75**	
Al	c [µg/g]	/	/	35523	47000*	51684	67200
	S.D.	/	/	6654	3000	10156	600
	R [%]			**76**		**77**	
K	c [µg/g]	/	/	11071	12100*	21340	25300
	S.D.	/	/	1384	12100	2158	1000
	R [%]			**91**		**84**	
Ca	c [µg/g]	/	/	133202	163000*	24420	24200
	S.D.	/	/	7725	6000	2746	600
	R [%]			**82**		**101**	
Ti	c [µg/g]	/	/	2403	3000*	/	/
	S.D.	/	/	457	400	/	/
	R [%]			**80**			
V	c [µg/g]	/	/	/	/	75.8	80.7
	S.D.	/	/	/	/	18.2	5.7
	R [%]					**94**	
Cr	c [µg/g]	81.9	86.0	58.6	60.0	40.2	52.3
	S.D.	19.8	8.0	12.2	11.0	9.0	2.9
	R [%]	**95**		**98**		**77**	
Mn	c [µg/g]	449	464	594	631	/	/
	S.D.	74	18	98	27	/	/
	R [%]	**97**		**94**			
Fe	c [µg/g]	/	/	23055	25700*	26456	28200
	S.D.	/	/	3619	500	5050	400
	R [%]			**90**		**94**	
Co	c [µg/g]	7.81	8.5	7.82	8.90	8.84	9.89
	S.D.	1.78	0.5	1.56	0.50	1.97	0.18
	R [%]	**92**		**88**		**89**	
Ni	c [µg/g]	23.0	26.4	21.7	26.0	17.1	21.7
	S.D.	5.6	2.4	4.6	5.0	4.6	0.7
	R [%]	**87**		**83**		**79**	
Cu	c [µg/g]	13.4	14.4	9.1	11.0	/	/

	S.D.	3.3	1.4	2.1	2.0	/	/
	R [%]	**93**		**83**			
Zn	c [µg/g]	56.1	57	130.5	104.0	329.8	414
	S.D.	12.2	4	94.7	3.0	65.2	11
	R [%]	**98**		**125**		**80**	
As	c [µg/g]	9.28	9.90	13.19	13.40	100.8	107
	S.D.	2.25	1.50	2.99	0.90	20.4	5
	R [%]	**94**		**98**		**94**	
Sr	c [µg/g]	/	/	103	108	218	242
	S.D.	/	/	16	5	28	10
	R [%]			**95**		**90**	
Hg	c [µg/g]	/	/	/	/	6.01	7.42
	S.D.	/	/	/	/	1.60	0.18
	R [%]					**81**	
Pb	c [µg/g]	41.7	41	59.4	60.0	1095	1400
	S.D.	12.6	4	16.0	5.0	209	10
	R [%]	**102**		**99**		**78**	

***denotes the values reported as reference values.**

5 Discussion and conclusion

The average recovery using open digestion was 58 % while the average recovery using closed digestion was 90 %. It is clear that microwave is the preferred method for digestion of soil samples. Also in terms of ease of use, the microwave digestion is the preferred choice as it enables a higher throughput of samples and there are fewer opportunities for a chance user error to occur while setting up the digestion.

6 References

[1] D. Božič, I. Živković, M. J. Hudobivnik, D. Mazej, M. Štrok, and M. Horvat, "EVALUATION OF SELECT PROCEDURES FOR ANALYSIS ; MULTI-ELEMENTAL AND ISOTOPIC COMPOSITION OF HG IN LICHENS," Ljubljana, 2021.

[2] Trace CERT, "Periodic table mix 1 for ICP," *Sigma Aldritch*. pp. 1–4, 2015, [Online]. Available: http://www.sigmaaldrich.com/catalog/product/sial/92091.

[3] National Institute of Standards & Technology, "Certificate of Analysis Standard Reference Material 3133 Mercury (Hg) Standard Solution," Department of Commerce - USA, 2016.

[4] D. Božič *et al.*, "RESULTS OF MULTI-ELEMENTAL AND ISOTOPIC COMPOSITION OF WESTEREN SLOVENIA LICHENS," Ljubljana, 2021.

A.3 Article in Preparation: Elucidating Origin of Mercury in Soils in the Vicinity of Emission Sources with the Help of Mercury Isotope Ratios

Dominik Božič, Igor Živković, Takashi Tomiyasu, Jože Kotnik, Gregor Puhar, & Milena Horvat, unpublished, in preparation

In this research, we carried out an analysis of surface soils from two specific areas in western Slovenia: Idrija and Anhovo. Idrija is renowned for housing one of the world's largest mercury mines, while Anhovo is located downstream of Idrija and is home to a cement production facility known to be a source of mercury contamination. Samples were collected from both sites, and we assessed their total mercury levels and isotopic composition.

At both the Idrija and Anhovo locations, the spectrum of isotopic fingerprints, which exhibit variations in mass-dependent fractionation, is remarkably broad. This highlights the intricate nature of the underlying factors shaping our findings. In Idrija, the isotopic fingerprints tend to shift towards lighter values (more negative $\delta 202$Hg values) as you move farther from the roasting and ore processing areas. While the exact sources and mechanisms behind mercury presence are not completely clear, it is possible that the heavier isotopic signature is linked to mercury originating from the mine, whereas the lighter one is associated with mercury deposited from the atmosphere onto the soil.

In the case of Anhovo, mercury concentrations are notably lower compared to Idrija. However, due to its position downstream of Idrija, the influence of mercury contamination from the mining area is still noticeable. The floodplain areas show a heavier isotopic fingerprint, while locations higher up in the valley sides exhibit a more uniform and lighter isotopic composition.

Determining whether the mercury in Idrija is of anthropogenic or natural origin presents a significant challenge. Nonetheless, the observed transition from heavier to lighter isotopes could be a valuable tool for identifying the most contaminated areas, not only in these two specific sites but also in similar locations elsewhere.

Elucidating origin of mercury in soils in the vicinity of emission sources with the help of mercury isotope ratios

Authors: Dominik Božič[1,2], Igor Živković[1], Takashi Tomiyasu[3], Jože Kotnik[1,2], Gregor Puhar[1,4], xxxx xxxx[5], and Milena Horvat[1,2]

- [1]Department of Environmental Science, Jožef Stefan Institute, Jamova Street 39, Ljubljana, Slovenia
- [2]Jožef Stefan International Postgraduate School, Jamova Street 39, Ljubljana, Slovenia
- [3]Graduate School of Science and Engineering, Kagoshima University, Korimoto, Kagoshima 890-0065, Japan
- [4]University of Ljubljana, Faculty of Chemistry and Chemical Technology, Večna pot 113, 1000 Ljubljana, Slovenia
- [5]University of Ljubljana, Biotechnical Faculty, Jamnikarjeva 101, 1000 Ljubljana

Corresponding author: Milena Horvat – milena.horvat@ijs.si, Brinje 40, 1262 - Dol pri Ljubljani, Slovenia

Keywords: mercury, isotopic fractionation, soil

Abstract

In this study, we conducted an examination of topsoils from two sites in western Slovenia: Idrija and Anhovo. Idrija is known as a location of one of the world's largest mercury (Hg) mines, while Anhovo is situated downstream of Idrija, housing a cement production plant known to be a source of Hg contamination. Samples were collected from both locations, and we measured their total mercury concentrations as well as their isotopic composition.

At both Idrija and Anhovo sites, the range of mass-dependent fractionating isotope fingerprints is notably wide, highlighting the complexity of the mechanisms underlying our findings. In Idrija, the isotopic fingerprint progressively skews towards lighter ones (more negative δ^{202}Hg values) with increasing distance from the roasting and ore processing sites. Although the precise mechanisms and sources of mercury remain uncertain, it is plausible that the heavier isotopic fingerprint is associated with mercury originating from the mine, while the lighter one is attributed to atmospheric mercury deposition on the soil.

In the case of Anhovo, Hg concentrations are generally orders of magnitude lower compared to Idrija. However, due to its location downstream of Idrija, the effects of Hg contamination from the mining area are still evident. The floodplains exhibit a heavier isotopic fingerprint, whereas areas situated higher up the valley sides display a relatively uniform and lighter isotopic composition.

It is challenging to pinpoint the exact origin of mercury in Idrija as being either anthropogenic or natural. Nevertheless, the observed shift from heavier to lighter isotopes could prove valuable in identifying the most contaminated areas, not only within these two locations but also at similar sites elsewhere.

1 Introduction

Tracing the pathways of mercury (Hg), a toxic trace element, into soils is of interest, as soils constitute one of the largest reservoirs of Hg on Earth (UNEP, 2019, 2022). Within terrestrial ecosystems, Hg has become a major area of scientific investigation (Bishop et al., 2020; Gustin et al., 2020; Kwon et al., 2020; O'Connor et al., 2019).

One such ecosystem under scrutiny is located in Idrija, Slovenia, which has a historical legacy of Hg ore mining and processing spanning five centuries, leading to significant pollution in the region (Bavec, 2015; Bavec et al., 2015; Gosar & Teršič, 2014; Kobal et al., 2017; Kotnik et al., 2005; Miklavčič et al., 2013). Throughout its history, various locations in the Idrija area have been involved in Hg ore processing (Gosar & Čar, 2006). These include Hg ore roasting activities at Pšenk, a hilltop a few kilometers southwest of Idrija, during the 16th and 17th centuries. Later in the 18th century, roasting operations shifted to the north part of Idrija at Prejunta, situated on the left bank of the Idrijca River. These activities ceased in 1842 when processing moved to the right bank of the river at the Brusovše location, where modernized furnaces were utilized. Hg ore grinding and roasting continued at this site until 1995 (Kavčič, 2008, 2020). These historical activities have introduced substantial amounts of Hg into the soils (Bavec et al., 2018; Gosar et al., 2002, 2006; Tomiyasu et al., 2012, 2017).

In a study conducted by Tomiyasu et al. (2017), a comprehensive examination of Hg speciation in soil profiles on both banks of the Idrijca River was undertaken. This study measured concentrations of methylmercury (MeHg), ethylmercury (EtHg), major oxides, and carbon forms, such as total organic carbon (TOC) and total nitrogen (N). The study observed correlations between N, TOC, MeHg, and EtHg and documented variations in Hg concentration and distribution profiles on the left and right banks of the Idrijca River. The authors speculated about different pathways for Hg delivery into the soils, based on their distinct chemical compositions. They proposed a theory involving atmospheric deposition of Hg with litterfall for the right bank soils, although they could not definitively identify the source on the left bank (Tomiyasu et al., 2017). Both banks are forested, which may account for some differences, with the left bank primarily composed of silicate rocks and the right bank largely consisting of carbonates; however, no ore-bearing outcrops are present at either sampling site (I. Mlakar & Čar, 2009). Up to this point, the exact origin of Hg, particularly on the left bank, has remained elusive.

Another system potentially influenced in a similar manner is Anhovo. Anhovo was once home to an asbestos production plant but now exclusively produces cement (T. L. Mlakar et al., 2010). Nevertheless, the site continues to impact the environment through the combustion and emission of various compounds, including approximately 11 kg of Hg annually (T. L. Mlakar et al., 2011). It is well-established that Hg is dispersed throughout the valley (Vijayakumaran Nair et al., 2022), yet, to our knowledge, no isotopic study of Hg in soils has been conducted in this region. Hg is brought down with the Idrijca River to the Soča river bringing the Hg to the area as well (Gosar, 2004; Gosar et al., 1997; Horvat et al., 2002; Žagar et al., 2006; Žibret & Gosar, 2006).

The advent of new analytical technologies enabling the determination of stable Hg isotope ratios has opened up new avenues for isotope fingerprinting and provenance determination (Tsui et al., 2020). Mercury isotope determination offers a potent tool for tracing the origin of Hg or understanding the transformations it undergoes during transport and deposition (Douglas & Blum, 2019; Ghosh et al., 2008; Jiskra et al., 2021; C. Liu et al., 2022). This capability arises from the fact that

Hg isotopes fractionate both in a mass-dependent (MDF) and mass-independent (MIF) manner. Typically, the Hg isotopic fingerprint consists of the MDF signature, expressed as δ^{202}Hg, along with odd-MIF (Δ^{199}Hg) and even-MIF (Δ^{200}Hg) (Bergquist & Blum, 2007; Blum et al., 2014).

In soil, the isotopic fingerprint can vary considerably, encompassing both MDF and odd-MIF. In two studies scrutinizing Hg isotopes in soil, the MDF ranged from approximately -2.0‰ to -1.0‰, and the odd-MIF ranged from -0.5‰ to -0.0‰ (Jiskra et al., 2015; Zheng et al., 2016). Jiskra et al. (2015) contended that roughly 90% of the Hg deposited in forest ecosystems arrives via litter deposition. In Zheng et al.'s (2016) examination of various forest soil profiles, it was observed that the top organic horizons exhibited high Hg concentrations, which sharply decreased after the horizons of decomposed leaves. Additionally, the isotopic MDF signature in the top organic horizons was lighter, transitioning to a heavier signature after the horizon of heavily decomposed leaves. This shift in isotopic composition with depth was attributed to decomposing litter capturing additional Hg from the air, thereby enriching the soil with heavier Hg isotopes. Subsequently, this Hg was mobilized and transported to lower horizons of the soil. Given that leaves exhibit a slightly negative odd-MIF fingerprint (Zhou et al., 2021), this is also reflected in the soils (Demers et al., 2013). There is to our knowledge no study conducted in the forest environment close to the known pollution source that would investigate such specific conditions.

Characterizing Hg isotopes from the Idrija mine revealed an MDF that is heavier than that found in vegetation, with a minimum δ^{202}Hg value of -1.35% (Božič et al., 2023). Studies on sediments from the Idrijca and Soča rivers, into which the Idrijca flows, have shown a relatively heavier MDF fingerprint (Baptista-Salazar et al., 2018; Foucher et al., 2009). This implies that there should be a point where the isotopic composition is heaviest near the pollution source and another point, much farther away, where pollution is no longer detectable. The objective of this study is to delineate this transition. It remains uncertain whether the shift from a polluted to a pristine environment is abrupt or gradual and how extensive its reach may be.

2 Samples

Sampling was carried out using shovels. Initially, any observed plants and foliage were removed, followed by the collection of a layer approximately five centimeters thick, primarily consisting of the organic horizon, commonly referred to as 'topsoil.' Prior to analysis, the soils were ground down using an agate mortar and then sieved through a 0.2 mm sieve.

2.1 Idrija

In Idrija, soil samples were collected during the sampling campaigns in May 2012 and June 2014. These samples were intentionally collected from the vicinity of three roasting sites in Idrija, each active during different periods of ore excavation. These sites include the Pšenk roasting site from the 16th century, the Prejnuta district of Idrija where the smeltery was situated in the 17th and 19th centuries, and the Brusovše district of Idrija, where roasting and ore grinding took place until the mine's closure at the end of the previous century (Gosar & Čar, 2006; Kavčič, 2008, 2020; Teršič et al., 2011).

The sampling sites were renamed based on the work of Tomiyasu et al. (2012, 2017), to have a consistent nomenclature across this article (Table 1). An orthophoto map of the area is presented in Figure 1. Figure 2 depicts a cross-section of the Idrija valley and the locations where the samples were collected, along with the locations

of some of the Hg ore roasting sites that were in proximity to these sampling locations.

Table 1: The table scheme for conversion of the naming scheme of this paper to the ones from (Tomiyasu et al., 2012, 2017)**.**

Sample names in this study	Sample names from Tomiyasu et al. (2012, 2017)	Coordinates (WGS 84) North	East
Idrija-01	Psenk 1	45.98448	14.00732
Idrija-02	Chimmney 8	46.00997	14.03291
Idrija-03	Chimmney 6	46.00989	14.03571
Idrija-04	Chimmney 7-1	46.00907	14.03446
Idrija-05	Chimmney 7-2	46.00907	14.03446
Idrija-06	Chimmney 9	46.00792	14.03122
Idrija-07	Station 2*	46.00952	14.02883
Idrija-08	Station 2-4	46.00915	14.02659
Idrija-09	Station 2-3	46.00912	14.02681
Idrija-10	Psenk 2	45.98469	14.00756

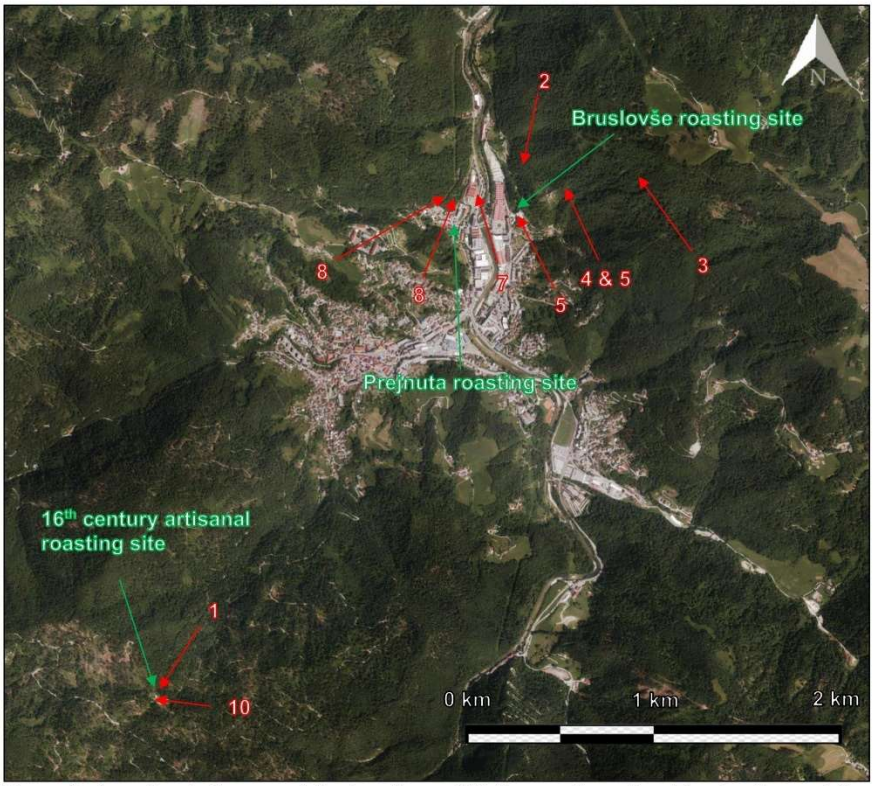

Figure 1: An orthophoto map of the locations of Idrija sampling sites. The locations of the nearby roasting sites are marked. Orthophoto from the Slovene environmental agency (Slovenian Environment Agency, 2023).

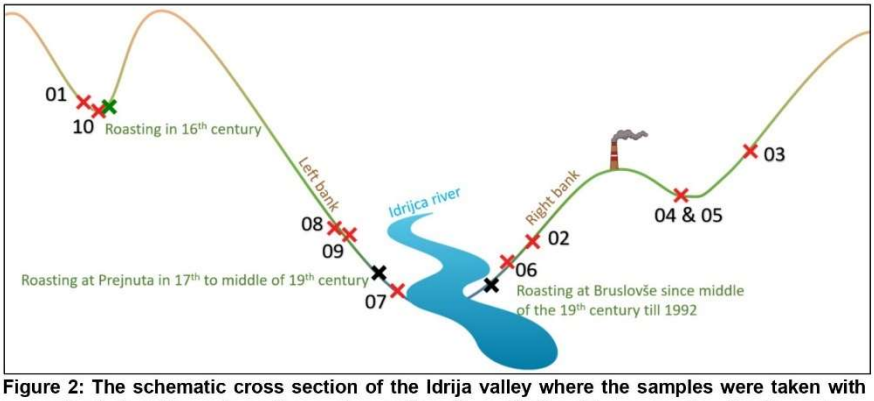

Figure 2: The schematic cross section of the Idrija valley where the samples were taken with approximate locations of roasting and sampling sites with the chimney venting the fumes from Bruslovše site as well.

2.2 Anhovo

Anhovo is situated approximately 30 km west of Idrija and 50 km downstream along the Idrijca River, which eventually merges into the Soča (Italian: Isonzo) River. The primary anthropogenic source of Hg emission in Anhovo is the chimney of the Anhovo Cement Production Plant (ACPP) (T. L. Mlakar et al., 2010, 2011). ACPP is situated at the base of a deep valley, where relatively constant winds disperse pollution throughout the valley (Vijayakumaran Nair et al., 2022). This necessitates a somewhat different approach to sampling and data interpretation compared to Idrija. While a substantial amount is known about the locations of the roasting sites in Idrija, and numerous studies have addressed this issue, relatively little is known about Hg in Anhovo. Therefore, instead of a targeted approach aimed at a specific pollution source, we conducted a blanket sampling of the entire part of the valley.

Soil samples in Anhovo were collected by the staff of the Biotechnical Faculty at the University of Ljubljana in the first half of 2023. A map depicting the sampling locations can be found in Figure 3, and Table 3 provides information regarding the distances from each sampling point to the ACPP chimney and the respective altitude above sea level (asl).

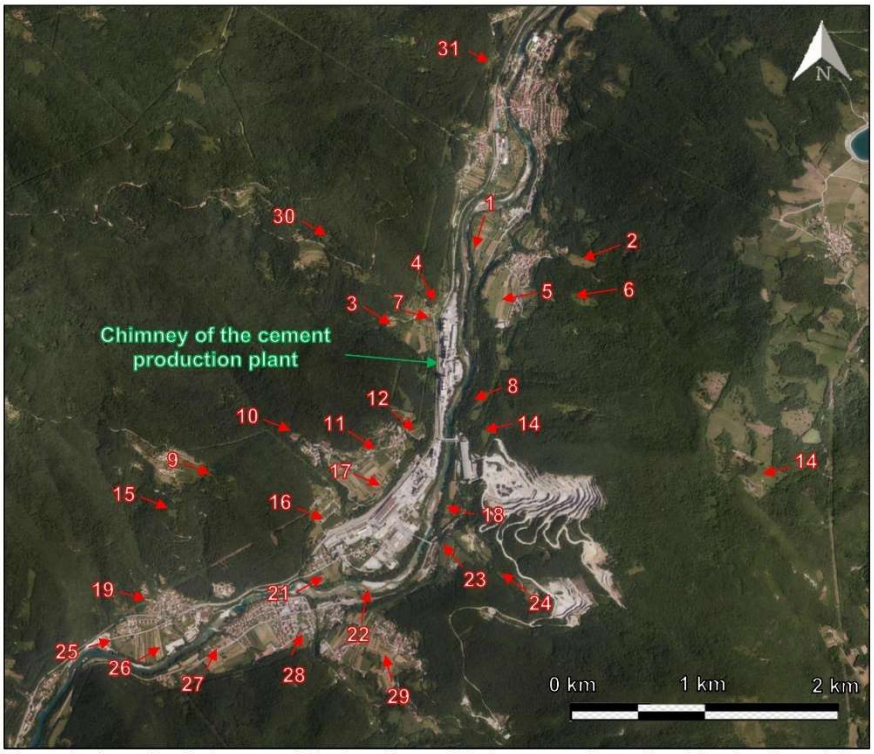

Figure 3: An orthophoto map of the locations of Anhovo sampling sites. The location of the chimney of the cement production plant is marked. Orthophoto from the Slovene environmental agency (2023).

Table 3: Table with the information about the distance between the chimney of the ACPP and the individual sampling point and its altitude$_{asl}$. The coordinates are also given.

Sample name	Ground distance to Anhovo chimney [m]	Altitude above the sea level [m]	Coordinates (WGS 84)	
			North	East
Anhovo-01	920	103	46.07646	13.63091
Anhovo-02	1225	212	46.07566	13.64058
Anhovo-03	401	154	46.07158	13.62289
Anhovo-04	343	110	46.07266	13.62659
Anhovo-05	575	143	46.07327	13.63253
Anhovo-06	1065	279	46.07367	13.63934
Anhovo-07	153	116	46.07085	13.62658
Anhovo-08	1210	130	46.06689	13.63106
Anhovo-09	1774	375	46.06155	13.60667
Anhovo-10	1074	169	46.06452	13.61379
Anhovo-11	664	141	46.06346	13.62146
Anhovo-12	425	139	46.06480	13.62530
Anhovo-13	555	157	46.06432	13.63157
Anhovo-14	2450	643	46.06325	13.65706
Anhovo-15	2135	293	46.05952	13.60303
Anhovo-16	1351	110	46.05879	13.61663
Anhovo-17	903	134	46.06073	13.62143
Anhovo-18	938	94	46.05984	13.62824

Anhovo-19	2600	118	46.05347	13.60055
Anhovo-21	1660	91	46.05540	13.61681
Anhovo-22	1623	88	46.05439	13.62052
Anhovo-23	1188	127	46.05763	13.62842
Anhovo-24	1464	175	46.05581	13.63296
Anhovo-25	2971	86	46.05114	13.59825
Anhovo-26	2755	87	46.05068	13.60239
Anhovo-27	2500	92	46.05035	13.60748
Anhovo-28	2075	100	46.05165	13.61533
Anhovo-29	2025	153	46.05060	13.62274
Anhovo-30	1308	420	46.07660	13.61607
Anhovo-31	2220	135	46.08873	13.63183

3 Analytical

3.1 Mercury concentrations

To determine the total mercury content (THg) in soil samples, Zeeman atomic absorption spectrometry with high-frequency modulation of light polarization (ZAAS-HFM) (RA 915+, Lumex, Russia), in conjunction with an added pyrolysis unit (PYRO 915, Lumex, Russia) was utilized. This combination of the pyrolysis unit and the ZAAS detector enables the determination of Hg in complex matrices without the need for prior sample preparation and dissolution. After preliminary drying, homogenization, and weighing of approximately 0.2 g of the sample, the sample was incinerated in the pyrolysis unit at 800 °C. This process causes bound Hg in the sample to vaporize, forming elemental Hg vapors. The concentration of these vapors was measured through absorption signals in the detector, which were recorded using the corresponding Rapid software. The method was calibrated using various concentrations of SI-traceable NIST 3133 Hg standard. The accuracy of the measurements was confirmed by analyzing a certified reference material, ERM-CC141 (loam soil). The method's detection limit is 0.5 ng/g, in accordance with US EPA 7473 and ASTM D7622 methods.

3.2 Preparation for the isotopic analysis

Soils were digested using the Ethos microwave digestion system (Milestone, Italy). Approximately 0.2 g of the sample was weighed into precleaned polytetrafluoroethylene tubes. For digestion, we used 5 mL of 65% HNO_3 (nitric acid), 2 mL of 40% HF (hydrofluoric acid), 1 mL of 30% HCl (hydrochloric acid), and 1 mL of 30% H_2O_2 (hydrogen peroxide). The digestion protocol consisted of a 30-minute ramp to achieve a peak temperature of 150°C at a maximum power of 1200 W. This temperature was maintained for an additional 30 minutes, followed by a cooling period of 1.5 hours to reach room temperature. Digestate was quantitatively transferred into 30 mL polyethylene tubes by rinsing them with 10 mL of Milli-Q water. Additionally, 10 mL of 5% H_3BO_3 (boric acid) was added to neutralize HF. The soil digestions were diluted 20 times using 5% HNO_3.

Soils were digested using the Ethos microwave digestion system (Milestone, Italy). About 0.2 g of the sample was weighed into precleaned polytetrafluoroethylene tubes. For digestion, 5 mL of 65% HNO_3 (nitric acid), 2 mL of 40% HF (hydro fluoric acid), 1 mL of 30% HCl (hydro chloric acid), and 1 ml of 30% H_2O_2 (hydrogen peroxide) were used. The process for digestion included 30 min for ramping up to the maximum temperature of 150°C and at a maximum power of 1200 W. This temperature was sustained for another 30 min, and cooling down to room temperature took 1.5 h. The digestate was quantitatively transferred into 30 mL

polyethylene tubes by rinsing them with 10 ml Milli-Q water. Here, 10 ml of 5 % H_2BO_3 (boric acid) was added to neutralize HF. The soil digestions were diluted 20 times. Dilutions were performed with 5% HNO_3.

To ensure that the Hg concentrations of Hg in the sample for the isotopic analysis were set at 1 ng/ml, the Hg concentrations of the diluted solution were measured. This was done using a Model Hg-201 semiautomated mercury analyzer using cold vapor atomic absorption spectroscopy (CV-AAS: Sanso Seisakusho Co., Tokyo, Japan), An aliquot (0.1 – 1 mL) of sample was transferred to the reaction vessel, reduced with $SnCl_2$ and aerated with outside air until equilibrium of mercury vapor is reached. During this circulation, acid gasses leaving the sample solution are removed by acid gas trap containing 10% NaOH (sodium hydroxide) solution. After that, the mercury vapor is introduced to the absorption cell by turning the four-way valve and measured by CV-AAS. The samples were then diluted to the necessary concentration with 5% HNO_3.

3.3 Mercury isotopic composition

The mercury isotopic composition was measured on the Nu Plasma II (Nu instruments, Wrexham, Uk) Multi-Collector Inductively Coupled Plasma Mass Spectrometer (MC-ICP-MS) according to the procedure outlined in (Božič et al., 2023). Briefly, the sample solution was pumped via a peristaltic pump into a "T split," where it was mixed with $SnCl_2$ in a solution to reduce Hg. The mix of solutions was transported to the phase separator, and the produced Hg^0 in gaseous and was subsequently carried by Ar gas to the MC-ICP-MS. The measurements were then performed at Hg concentrations of 1ng/mL. The intensities at m/z of 202 were at around 1 V.

The results were reported using δ and Δ notations (Equations 1 and 2), where *f* represents the correction factor (0.2520 for Δ^{199}Hg, 0.5024 for Δ^{200}Hg, 0.7520 for Δ^{201}Hg, and 1.4930 for Δ^{204}Hg) and ^{xxx}Hg represents the mass number of a specific mercury isotope (Blum et al., 2014; Blum & Johnson, 2017).

$$\delta^{xxx}Hg = \left(\frac{\frac{^{xxx}Hg}{^{198}Hg_{sample}}}{\frac{^{xxx}Hg}{^{198}Hg_{SRM3133}}} - 1 \right) \times 1000 \quad (1)$$

$$\Delta^{xxx}Hg = \delta^{xxx}Hg - \delta^{202}Hg \times f \quad (2)$$

The results of the repeated measurements of the reference material (NIST 8610) and the matrix-matched standard (NIST 2711A) are outlined in Table 3. The similarity observed indicates the trueness of the measurements. The results were comparable to the reported or reference values. The expanded deviation by the factor of two is used in this study to present the uncertainties of the measurements in the graphs.

Table 3: The comparison between the literature reported values versus the values measured for the reference materials. The reported values for the NIST 2711A were by (Estrade et al., 2009) **and for NIST 8610 from the certificate provided by the National Institute for Standards and Technology** (National Institute of Standards & Technology, 2017).

Sample Name	δ^{199}Hg [‰]	δ^{200}Hg [‰]	δ^{201}Hg [‰]	δ^{202}Hg [‰]	δ^{204}Hg [‰]	Δ^{199}Hg [‰]	Δ^{200}Hg [‰]	Δ^{201}Hg [‰]	δ^{204}Hg [‰]

NIST 2711A	-0.26	-0.11	-0.34	-0.24	/	-0.20	0.01	-0.16	/
Reported values	(0.22)	(0.24)	(0.27)	(0.37)	/	(0.17)	(0.15)	(0.10)	/
NIST 2711A (N = 14)	-0.25	-0.10	-0.31	-0.16	-0.23	-0.21	-0.02	-0.19	0.01
Measured values	(0.09)	(0.08)	(0.16)	(0.13)	(0.22)	(0.07)	(0.06)	(0.17)	0.32
NIST 8610	-0.17	-0.27	-0.46	-0.56	-0.82	-0.03	0.00	-0.04	0.00
Reported values	(0.01)	(0.01)	(0.02)	(0.03)	(0.07)	(0.02)	(0.01)	(0.01)	(0.02)
NIST 8610 (N = 45)	-0.15	-0.27	-0.45	-0.54	-0.86	-0.02	0.00	-0.05	-0.06
Measured values	(0.09)	(0.10)	(0.17)	(0.15)	(0.29)	(0.07)	(0.08)	(0.17)	(0.30)

4 Results

The THg values and the Hg isotope ratios of all of the samples measured are presented in Table 4.

Table 4: The concentrations of Hg as well as the isotope ratios in samples.

Sample Name	cHg [µg/g]	± 2*SD	δ^{199}Hg [‰]	δ^{200}Hg [‰]	δ^{201}Hg [‰]	δ^{202}Hg [‰]	δ^{204}Hg [‰]	Δ^{199}Hg [‰]	Δ^{200}Hg [‰]	Δ^{201}Hg [‰]	δ^{204}Hg [‰]
Idrija-01	7.74	0.93	-0.49	-0.77	-1.23	-1.55	-2.34	-0.10	0.00	-0.07	-0.04
Idrija-02	16.7	2.0	-0.28	-0.54	-0.86	-1.10	-1.70	-0.01	0.01	-0.04	-0.06
Idrija-03	87.0	10.4	-0.26	-0.50	-0.76	-1.08	-1.41	0.01	0.04	0.05	0.19
Idrija-04	254	30	-0.27	-0.47	-0.78	-0.99	-1.46	-0.02	0.03	-0.03	0.02
Idrija-05	255	30	-0.30	-0.48	-0.80	-0.99	-1.48	-0.05	0.02	-0.06	-0.01
Idrija-06	1650	197	-0.13	-0.17	-0.26	-0.37	-0.56	-0.03	0.02	0.01	-0.01
Idrija-07	688	82	-0.07	-0.07	-0.21	-0.16	-0.27	-0.03	0.02	-0.08	-0.02
Idrija-08	267	32	-0.11	0.18	0.19	0.28	0.37	-0.18	0.04	-0.02	-0.05
Idrija-09	235	28	-0.05	0.14	0.10	0.32	0.50	-0.13	-0.02	-0.14	0.02
Idrija-10	20.6	2.5	0.02	0.25	0.31	0.60	0.80	-0.13	-0.05	-0.14	-0.09
Anhovo-01	0.624	0.016	-0.24	-0.46	-0.77	-0.96	-1.44	0.00	0.02	-0.05	-0.01
Anhovo-02	0.234	0.028	-0.38	-0.68	-1.06	-1.32	-1.94	-0.05	-0.02	-0.07	0.02
Anhovo-03	0.282	0.022	-0.40	-0.81	-1.35	-1.74	-2.56	0.04	0.06	-0.04	0.04
Anhovo-04	0.816	0.003	-0.51	-1.10	-1.52	-2.04	-3.01	0.00	-0.08	0.01	0.04
Anhovo-05	0.304	0.018	-0.41	-0.67	-0.99	-1.31	-1.86	-0.08	-0.01	0.00	0.10
Anhovo-06	0.364	0.013	-0.37	-0.72	-1.23	-1.64	-2.57	0.05	0.11	0.00	-0.11
Anhovo-07	0.288	0.021	-0.45	-0.85	-1.25	-1.73	-2.80	-0.02	0.02	0.05	-0.21
Anhovo-08*	0.264	0.010	/	/	/	/	/	/	/	/	/
Anhovo-09*	0.291	0.014	/	/	/	/	/	/	/	/	/
Anhovo-10*	0.139	0.004	/	/	/	/	/	/	/	/	/
Anhovo-11	0.336	0.006	-0.27	-0.33	-0.54	-0.66	-1.03	-0.10	0.00	-0.04	-0.04
Anhovo-12*	0.299	0.010	/	/	/	/	/	/	/	/	/
Anhovo-13*	0.305	0.023	/	/	/	/	/	/	/	/	/
Anhovo-14*	0.143	0.000	/	/	/	/	/	/	/	/	/
Anhovo-15	0.206	0.000	-0.33	-0.61	-0.97	-1.26	-1.82	-0.01	0.03	-0.02	0.07
Anhovo-16*	0.366	0.002	/	/	/	/	/	/	/	/	/
Anhovo-17	0.466	0.040	-0.30	-0.64	-1.03	-1.37	-1.98	0.05	0.05	0.00	0.06
Anhovo-18	0.780	0.042	-0.21	-0.33	-0.52	-0.67	-0.95	-0.04	0.00	-0.01	0.05
Anhovo-19*	0.278	0.002	/	/	/	/	/	/	/	/	/
Anhovo-21	1.68	0.01	-0.27	-0.46	-0.55	-0.68	-1.02	-0.10	-0.12	-0.04	0.00
Anhovo-22	4.62	0.89	-0.11	-0.22	-0.32	-0.52	-0.79	0.02	0.05	0.07	-0.01
Anhovo-23*	0.274	0.029	/	/	/	/	/	/	/	/	/
Anhovo-24	0.338	0.009	-0.18	-0.37	-0.26	-0.73	-1.01	0.01	0.00	0.29	0.08
Anhovo-25	3.17	0.15	-0.28	-0.53	-0.82	-1.13	-1.72	0.01	0.04	0.04	-0.03
Anhovo-26	5.37	0.19	-0.14	-0.20	-0.38	-0.37	-0.57	-0.04	-0.01	-0.10	-0.01
Anhovo-27	0.192	0.006	-0.38	-0.62	-0.91	-1.22	-1.85	-0.08	-0.01	0.00	-0.03
Anhovo-28	0.393	0.011	-0.47	-0.95	-1.39	-1.95	-2.88	0.02	0.03	0.08	0.04
Anhovo-29*	0.438	0.012	/	/	/	/	/	/	/	/	/
Anhovo-30	0.188	0.011	-0.35	-0.74	-1.13	-1.46	-2.21	0.02	-0.01	-0.03	-0.04
Anhovo-31	1.11	0.04	-0.33	-0.77	-1.18	-1.57	-2.39	0.07	0.02	0.01	-0.04

**Isotope ratios not measured.*

5 Findings

5.1 Idrija

The data for Idrija samples presented in Table 4 are graphically shown in Figure 4A for the relationship between the MDF and MIF and in Figure 4B for the THg and MDF.

At Pšenk roasting site from 16th century the THg value was 7.47 µg/g, and at Idrija-10, the THg value was higher, at 20.6 µg/g. This makes sense as the Idrija-01 was further away from the location of ore roasting by some 50 m, while Idrija-10 was right on top of the site itself. The relative isotopic composition is even more telling with the MDF signatures being extremely wide apart with Idrija-01 exhibiting δ^{202}Hg of -1.55‰ while Idrija-10 exhibiting δ^{202}Hg of 0.60‰. Both sources exhibit a similar MIF (Δ^{199}Hg) at -0.10 for Idrija-01 and -0.13 for Idrija-10.

Idrija-01, a sampling point in a forest ecosystem, most commonly receives Hg in the soil through litterfall deposition (Jiskra et al., 2015; Y. Liu et al., 2022; Zhou et al., 2021), with an average δ^{202}Hg below ≈ -2.0‰ and Δ^{199}Hg between -0.5‰ and 0.0‰ (Wang et al., 2021; Zheng et al., 2016). Apart from this, elemental gaseous Hg can be directly fixed into soil (Obrist et al., 2014), but it does not represent an important part of Hg fixing from the atmosphere (Zhou & Obrist, 2021). Therefore, the light isotopic composition of Idrija-01 might be the background isotopic composition of litterfall from the trees nearby.

However, Idrija-10 sample was excavated on a forest clearing and was covered by a comparatively thinner (0.5 cm) layer of fallen leaves. The relatively heavy isotopic composition of Idrija-10 likely represented the isotopic composition of the mix of roasted and not-yet-roasted ores of the Pšenk retorting site with the additional input from the litterfall deposition. This can be assumed based on the location of the sampling and the higher THg found at the site. From the data on Hg isotopic composition of Idrija mine Hg it is known that the MDF isotopic composition can reach up to 0.53‰ for δ^{202}Hg (Božič et al., 2023). Similar results were obtained by Baptista-Salazar et al. (2018) in soil samples from a nearby artisanal roasting site, with an isotopic composition of 0.06‰ for δ^{202}Hg.

In previous study on these specific soil samples, it was discovered that Idrija-01 contains about five times the levels of MeHg than Idrija-10 (Tomiyasu et al., 2017). And since it is well known that methylation of Hg makes its isotopic fingerprint lighter (Blum et al., 2014), this could be also the case here. But we would argue against that since firstly the levels of MeHg are three orders of magnitude lower (20.9 ng/g in Idrija-01 and 4.90 ng/g in Idrija 2) (Tomiyasu et al., 2017) than the levels THg. One more consideration supporting the theory that Hg in Idrija-01 came from the mine and that the one from Idrija-10 did not is the fact that while the Hg from the Idrija mine does exhibit a wide range of MDF, it does present a fairly specific range of MIF, with the lightest isotopic fingerprint presenting samples also having a positive MIF. The samples at about -1.2‰ (δ^{202}Hg) exhibit a MIF fingerprint of around 0.1‰ to 0.2‰, far higher than the one detected at Idrija-01 (-0.10 for Δ^{199}Hg).

The soils near the Prejnuta roasting site exhibit far higher THg compared to the ones near Pšenk roasting site. The THg reach from 688 µg/g near the riverside (Idrija-07) down to 267 (Idrija-08) and 235 (Idrija-09) up the hill. This makes sense as the roasting and other mining related activities were in the area present for much longer. The MDF isotopic fingerprint is relatively narrow compared to the samples from Pšenk roasting site from -0.16‰ (Idrija-07) to 0.28‰ and 0.32‰ (for Idrija-08 and Idrija-09 respectively). This might be the consequence that all of the area is so

heavily polluted with the Hg from the mine that it trumps over all other sources (Bavec et al., 2014; Čar, 1996) with cinnabar and that cinnabar representing more than half of the Hg found in soils in the area (Bavec & Gosar, 2016). The notion that the Hg in area is directly connected to the mine is also supported by the fact that the same trajectory of MIF fractionation is observed here as in the mine with the lighter isotopic MDF fingerprint presenting a relatively higher MIF (Δ^{199}Hg) fingerprint (-0.03‰ for Idrija-07 and -0.18‰ and -0.13‰ for Idrija-08 and Idrija-09 respectfully).

The samples near the Brusovše roasting site exhibit the highest THg levels amongst all of the sites. Idrija-06 which was excavated closest to the site exhibits the THg of 1650 µg/g. Idrija-04 and Idrija-05 which were some distance up the hill above the roasting site, but close to the chimney from which the gases from the roasting site were routed to underground, exhibited the THg of 254 and 255 µg/g and Idrija-03 which was the highest up exhibiting the THg of 87.0 µg/g. Idrija-04 site which was a bit further away on the next slope downstream on the same side of the river exhibited the THg of 16.7 µg/g. Similarly, to the decreasing THg further away from the roasting site, the isotopic composition gets lighter (for δ^{202}Hg Idrija-06: -0.37‰, Idrija-05 and Idrija-04: -0.99‰, Idrija-03: -1.08‰. and Idrija-02: -1.10‰). This trend is similar to the one observed near Bruslovše roasting site and could likely be explained by the same way by the Hg being a mix of the one from the mining activity and naturally occurring deposition common for forest ecosystems. Only that the part of the Hg from the former is skewed higher near the roasting site and the part of the Hg form the latter is skewed higher further away. There were some investigations into the connections between MeHg and other organic forms (Tomiyasu et al., 2017), but we would consider that again the concentrations of organic Hg forms are orders of magnitude lower and would likely not influence the isotopic fingerprint in a significant way. It has to be noted that the Hg in the topsoil in the area is likely less than hundred years old as we can observe from the historic photographs and postcards from the area that have been preserved that the area around the Brusovše roasting site was barren less than a hundred years ago (Idrija Municipal Museum, 2023). Nowadays the area is covered with a thick vegetation. This means that the soils studied present the record of the last century of Hg deposition.

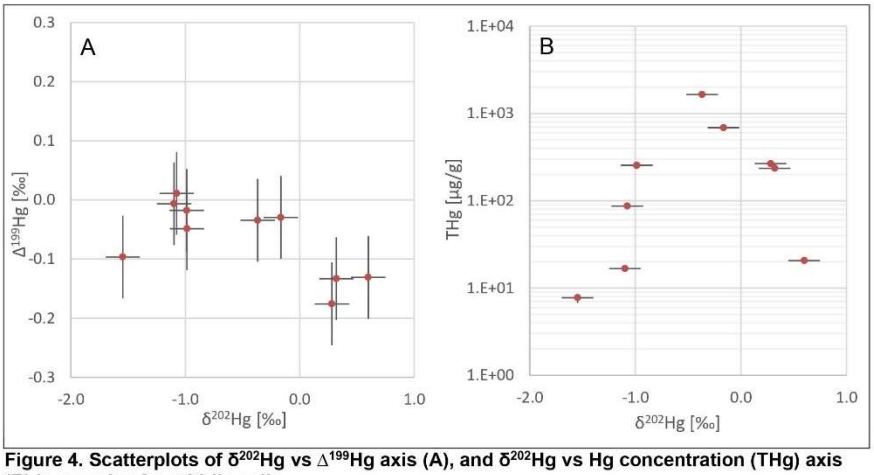

Figure 4. Scatterplots of δ^{202}Hg vs Δ^{199}Hg axis (A), and δ^{202}Hg vs Hg concentration (THg) axis (B) in samples from Idrija soils.

5.2 Anhovo

Anhovo soils present the THg range, which is orders of magnitude lower than that of Idrija, with the majority of the concentrations below one µg/g while the isotopic fingerprint is similar in range for both MIF and MDF (Table 4, Figure 5). Both of the measured values can be compared either one against another and either to the ground distance (the distance that takes into account the topography of the terrain) to the ACPP or the altitude. These relationships are shown in Figure 5.

A trend of higher THg is observed further away from the cement production plant at Anhovo-21, -22, -25, and -26 (Figure 5A). These points all lay close to the Soča river which mean that they might be influenced by Hg brought downstream from the Idrija mining area (Baptista-Salazar & Biester, 2019; Cerovac et al., 2018; Foucher et al., 2009; Hines et al., 2000). The highest point still located on a floodplain is Anhovo-01 at 103 m_{asl}. Points below this altitude (excluding Anhovo-28, excluded as it is already too downstream) all lay on the potential historic floodplains. If these points are excluded, the distribution of Hg across the investigated area is more uniform. The influence of the river is affirmed by examination of the chart of the THg versus the $altitude_{asl}$ (Figure 5B). The highest THg values can be observed at the lowest altitudes. Generally, a slight decreasing trend of THg with altitude can be observed. Therefore, it can be assumed that the Hg at lower attitudes is influenced by the Hg brought by the Soča river, while the Hg at higher altitudes bears the influence from either natural sources or the ACPP.

The isotopic fingerprint augments these findings. The chart of δ^{202}Hg vs. the ground distance (Figure 5C) seems not to carry as much information as the one of δ^{202}Hg vs. the $altitude_{asl}$ (Figure 5D). The range of MDF isotopic fingerprint found in the soils on floodplains is from -1.22 ‰ to 0.37 ‰ (δ^{202}Hg). This isotopic range is similar to the one observed in the previous isotopic studies of Idrija sediments. Foucher et al. (2009) observed the MDF isotopic fingerprint from around -0.5 to 0.0 ‰ while Baptista-Salazar et al. (2018) observed a range from -0.96 ‰ to 0.12 ‰ and as mentioned above the Idrija-07 exhibited the fingerprint of -0.16 ‰. Therefore, it seems the most likely that Hg from the floodplains of Anhovo and its surroundings came from Idrija mining area.

Other Anhovo samples present a lighter isotopic fingerprint ranging from -1.26 ‰ to -2.04 ‰ (δ^{202}Hg), with two outliers at Anhovo-11 and Anhovo-24. As with THg, here also there no trend in the MDF fingerprint above the level of floodplains to the altitudes few hundred meters above them. This means that either the Hg load from the ACPP is uniform thorough the entire Anhovo area or more likely that the influence of ACPP is minimal and is not detectable. The isotopic fingerprint of Anhovo above the floodplains also has a similar range to the one seen in the soils from Idrija which were collected further away from the roasting sites (Idrija-01, -02). Therefore, it seems that this could be the range Hg found naturally in forest ecosystems in western Slovenia. In any case, this study is unable to find a direct connection between the Hg from the cement production plant and soils. On the contrary, it shows that the highest concentrations in the soil are likely resulting from the the Hg input from Idrijca/Soča river system, which is draining area heavily contaminated with Hg from Idrija mine.

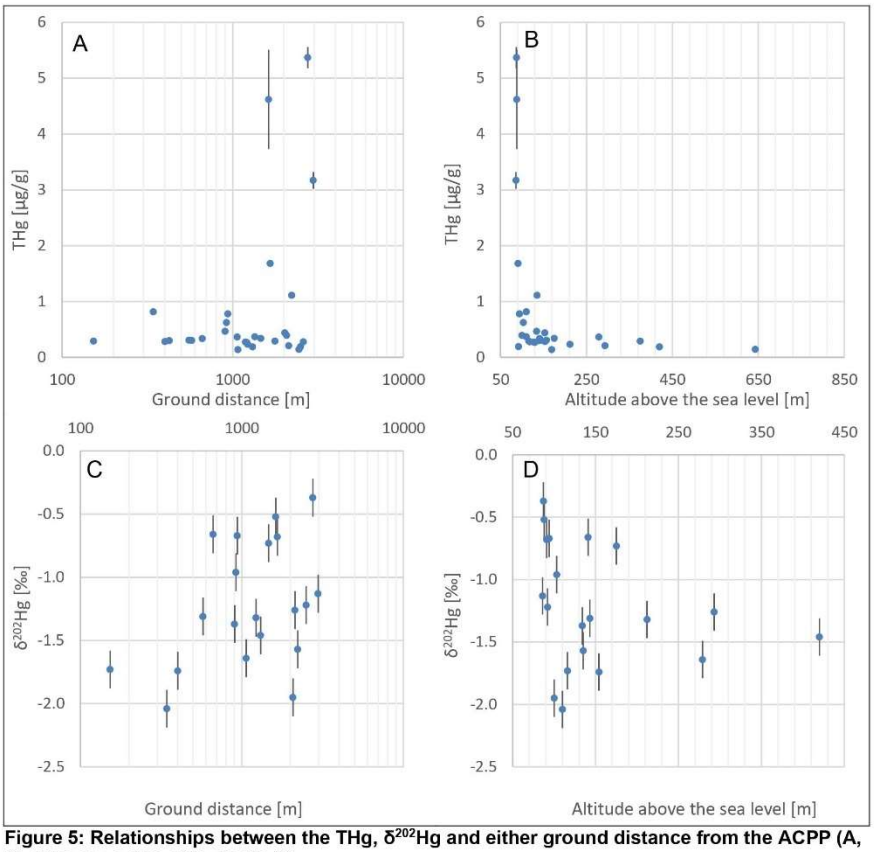

Figure 5: Relationships between the THg, δ^{202}Hg and either ground distance from the ACPP (A, C) chimney or the altitude (B, D).

6 Conclusion

As it is often the case with natural sciences the answer to the question how the transition from the contaminated to pristine Hg isotopic fingerprint looks is not straight forward as expected. Firstly, it is unclear whether the points further away from the pollution source are already represent the naturally occurring forest Hg fingerprint. Secondly, different geographical features might mean that this transition could be different from place to place, like for example in Anhovo where the occurrence of the floodplains is the major predictor of heavier isotopic fingerprint. Thirdly, there are different sources of pollution as again in Anhovo there is the combination of Hg emitted from the ACPP and brought down with the Soča river. Fourthly, the time from when the source of pollution plays the role as the Pšenk roasting site samples show a relatively extremely rapid change of the isotopic composition on a distance of only some hundred meters. Finally, there are also some potential outliers which cannot be easily explained.

What can be said in general that the influence of Hg pollution in soil of the Idrija region diminishes after a kilometer from the respectable roasting site. In

Anhovo the influence of ACPP might either affect the entire valley up to elevations of few hundred meters or is negligible. The pollution coming with Soča river is only limited to the flood plains of the valley.

Author roles

Dominik Božič: methodology, investigation, data curation, writing – original draft, visualization. **Igor Živković:** methodology, writing – review & editing. **Takashi Tomiyasu:** writing – review & editing. **Jože Kotnik:** investigation. **Gregor Puhar:** investigation. **Milena Horvat:** conceptualization, writing – review & editing, supervision, funding acquisition.

Declaration of interests

The authors declare that they have no known competing financial interests or personal relationships that could have influenced the work reported in this paper.

Data availability

Data will be made available upon request.

Acknowledgments

This study has been supported financially by (I) the GMOS-Train (project # 860497), which has received funding from the European Unions' Horizon 2020 research and innovation program under the Maria Skłodowska–Curie fund, (II) the Slovenian Research Agency (ARRS; grants P1-0143, PR-54685, J1-3033) and (III) Support from the Japan Society for the Promotion of Science (JSPS) Grants-in-Aid #22404002 and #25257302.

References

Baptista-Salazar, C., & Biester, H. (2019). The role of hydrological conditions for riverine Hg species transport in the Idrija mining area. *Environmental Pollution*, *247*, 716–724. https://doi.org/10.1016/j.envpol.2019.01.109

Baptista-Salazar, C., Hintelmann, H., & Biester, H. (2018). Distribution of mercury species and mercury isotope ratios in soils and river suspended matter of a mercury mining area. *Environmental Science: Processes and Impacts*, *20*(4), 621–631. https://doi.org/10.1039/c7em00443e

Bavec, & Gosar, M. (2016). Speciation, mobility and bioaccessibility of Hg in the polluted urban soil of Idrija (Slovenia). *Geoderma*, *273*, 115–130. https://doi.org/10.1016/j.geoderma.2016.03.015

Bavec, Š. (2015). Geochemical investigations of potentially toxic trace elements in urban sediments of idrija. *Geologija*, *58*(2), 111–120. https://doi.org/10.5474/geologija.2015.009

Bavec, Š., Biester, H., & Gosar, M. (2014). Urban sediment contamination in a former Hg mining district, Idrija, Slovenia. *Environmental Geochemistry and Health*, *36*(3), 427–439. https://doi.org/10.1007/s10653-013-9571-6

Bavec, Š., Biester, H., & Gosar, M. (2018). A risk assessment of human exposure to mercury-contaminated soil and household dust in the town of Idrija (Slovenia). *Journal of Geochemical Exploration*, *187*, 131–140. https://doi.org/10.1016/j.gexplo.2017.05.005

Bavec, Š., Gosar, M., Biester, H., & Grčman, H. (2015). Geochemical investigation of mercury and other elements in urban soil of Idrija (Slovenia). *Journal of*

Geochemical Exploration, *154*, 213–223. https://doi.org/10.1016/j.gexplo.2014.10.011

Bergquist, B. A., & Blum, J. D. (2007). Mass-dependent and -independent fractionation of Hg isotopes by photoreduction in aquatic systems. *Science*, *318*(5849), 417–420. https://doi.org/10.1126/science.1148050

Bishop, K., Shanley, J. B., Riscassi, A., de Wit, H. A., Eklöf, K., Meng, B., Mitchell, C., Osterwalder, S., Schuster, P. F., Webster, J., & Zhu, W. (2020). Recent advances in understanding and measurement of mercury in the environment: Terrestrial Hg cycling. *Science of the Total Environment*, *721*. https://doi.org/10.1016/j.scitotenv.2020.137647

Blum, J. D., & Johnson, M. W. (2017). Recent developments in mercury stable isotope analysis. *Reviews in Mineralogy and Geochemistry*, *82*(July 2013), 733–757. https://doi.org/10.2138/rmg.2017.82.17

Blum, J. D., Sherman, L. S., & Johnson, M. W. (2014). Mercury isotopes in earth and environmental sciences. *Annual Review of Earth and Planetary Sciences*, *42*(February), 249–269. https://doi.org/10.1146/annurev-earth-050212-124107

Božič, D., Živković, I., Dizdarević, T., Peljhan, M., Štrok, M., & Horvat, M. (2023). Insights into the Heterogeneity of the Mercury Isotopic Fingerprint of the Idrija Mine (Slovenia). *Minerals*, *13*(9), 1227. https://doi.org/10.3390/min13091227

Čar, J. (1996). Mineralized rocks and ore residues in the Idrija region. *Meeting of Researchers o Idrija as a Natural and Anthoropogenic Laboratory - Mercury as a Major Pollutant*, 10–15.

Cerovac, A., Covelli, S., Emili, A., Pavoni, E., Petranich, E., Gregorič, A., Urbanc, J., Zavagno, E., & Zini, L. (2018). Mercury in the unconfined aquifer of the Isonzo/SoČa River alluvial plain downstream from the Idrija mining area. *Chemosphere*, *195*, 749–761. https://doi.org/10.1016/j.chemosphere.2017.12.105

Demers, J. D., Blum, J. D., & Zak, D. R. (2013). Mercury isotopes in a forested ecosystem: Implications for air-surface exchange dynamics and the global mercury cycle. *Global Biogeochemical Cycles*, *27*(1), 222–238. https://doi.org/10.1002/gbc.20021

Douglas, T. A., & Blum, J. D. (2019). Mercury Isotopes Reveal Atmospheric Gaseous Mercury Deposition Directly to the Arctic Coastal Snowpack. *Environmental Science and Technology Letters*, *6*(4), 235–242. https://doi.org/10.1021/acs.estlett.9b00131

Estrade, N., Carignan, J., Sonke, J. E., & Donard, O. F. X. (2009). Measuring hg isotopes in bio-geo-environmental reference materials. *Geostandards and Geoanalytical Research*, *34*(1), 79–93. https://doi.org/10.1111/j.1751-908X.2009.00040.x

Foucher, D., Ogrinc, N., & Hintelmann, H. (2009). Tracing mercury contamination from the idrija mining region (slovenia) to the gulf of trieste using Hg isotope ratio measurements. *Environmental Science and Technology*, *43*(1), 33–39. https://doi.org/10.1021/es801772b

Ghosh, S., Xu, Y., Humayun, M., & Odom, L. (2008). Mass-independent fractionation of mercury isotopes in the environment. *Geochemistry, Geophysics, Geosystems*, *9*(3), 1–10. https://doi.org/10.1029/2007GC001827

Gosar, M. (2004). Soil-plant mercury concentrations in the Idrijca river terraces (Slovenia). *Geologija*, *47*(2), 259–271. https://doi.org/10.5474/geologija.2004.021

Gosar, M., & Čar, J. (2006). Influence of mercury ore roasting sites from 16th and 17th century on the mercury dispersion in surroundings of Idrija. *Geologija*, *49*(1), 91–101. https://doi.org/10.5474/geologija.2006.007

Gosar, M., Pirc, S., & Bidovec, M. (1997). Mercury in the Idrijca River sediments as a reflection of mining and smelting activities of the Idrija mercury mine. *Journal of Geochemical Exploration*, *58*(2–3), 125–131. https://doi.org/10.1016/S0375-6742(96)00064-7

Gosar, M., Šajn, R., & Biester, H. (2002). Mercury speciation in soils and attic dust in the Idrija area. *Geologija*, *45*(2), 373–378. https://doi.org/10.5474/geologija.2002.035

Gosar, M., Šajn, R., & Biester, H. (2006). Binding of mercury in soils and attic dust in the Idrija mercury mine area (Slovenia). *Science of the Total Environment*, *369*(1–3), 150–162. https://doi.org/10.1016/j.scitotenv.2006.05.006

Gosar, M., & Teršič, T. (2014). Contaminated sediment loads from ancient mercury ore roasting sites, Idrija area, Slovenia. *Journal of Geochemical Exploration*, *149*, 97–105. https://doi.org/10.1016/j.gexplo.2014.11.012

Gustin, M. S., Bank, M. S., Bishop, K., Bowman, K., Bran, B., Chételat, J., Eckley, C. S., Hammerschmidt, C. R., Lamborg, C., Lyman, S., Martínez-cortizas, A., Sommar, J., Tsui, M. T., & Zhang, T. (2020). Science of the Total Environment Mercury biogeochemical cycling : A synthesis of recent scientific advances. *Science of the Total Environment*, *737*. https://doi.org/10.1016/j.scitotenv.2020.139619

Hines, M. E., Horvat, M., Faganeli, J., Bonzongo, J. C. J., Barkay, T., Major, E. B., Scott, K. J., Bailey, E. A., Warwick, J. J., & Lyons, W. B. (2000). Mercury biogeochemistry in the Idrija River, Slovenia, from above the mine into the Gulf of Trieste. *Environmental Research*, *83*(2), 129–139. https://doi.org/10.1006/enrs.2000.4052

Horvat, M., Jereb, V., Fajon, V., Logar, M., Kotnik, J., Faganeli, J., Hines, M. E., & Bonzongo, J.-C. (2002). Mercury distribution in water, sediment and soil in the Idrijca and Soča river systems. In *Environment, Analysis* (Vol. 2).

Idrija Municipal Museum. (2023). *Photography and post card collection at the museum.* www.muzej-idrija-cerkno.si

Jiskra, M., Heimbürger-Boavida, L. E., Desgranges, M. M., Petrova, M. V., Dufour, A., Ferreira-Araujo, B., Masbou, J., Chmeleff, J., Thyssen, M., Point, D., & Sonke, J. E. (2021). Mercury stable isotopes constrain atmospheric sources to the ocean. *Nature*, *597*(7878), 678–682. https://doi.org/10.1038/s41586-021-03859-8

Jiskra, M., Wiederhold, J. G., Skyllberg, U., Kronberg, R. M., Hajdas, I., & Kretzschmar, R. (2015). Mercury Deposition and Re-emission Pathways in Boreal Forest Soils Investigated with Hg Isotope Signatures. *Environmental Science and Technology*, *49*(12), 7188–7196. https://doi.org/10.1021/acs.est.5b00742

Kavčič, I. (2008). *Živo srebro: Zgodovina idrijskega žgalništva* (1st ed.).

Kavčič, I. (2020). *Reflections of a Silver Era*. Idrija Mercury Mine.

Kobal, A. B., Snoj Tratnik, J., Mazej, D., Fajon, V., Gibičar, D., Miklavčič, A., Kocman, D., Kotnik, J., Sešek Briški, A., Osredkar, J., Krsnik, M., Prezelj, M., Knap, Križaj, B., Liang, L., & Horvat, M. (2017). Exposure to mercury in susceptible population groups living in the former mercury mining town of Idrija, Slovenia. *Environmental Research*, *152*, 434–445. https://doi.org/10.1016/j.envres.2016.06.037

Kotnik, J., Horvat, M., & Dizdarevič, T. (2005). Current and past mercury distribution in air over the Idrija Hg mine region, Slovenia. *Atmospheric Environment*, *39*(39 SPEC. ISS.), 7570–7579. https://doi.org/10.1016/j.atmosenv.2005.06.061

Kwon, S. Y., Blum, J. D., Yin, R., Tsui, M. T. K., Yang, Y. H., & Choi, J. W. (2020). Mercury stable isotopes for monitoring the effectiveness of the Minamata Convention on Mercury. *Earth-Science Reviews*, *203*(January), 103111. https://doi.org/10.1016/j.earscirev.2020.103111

Liu, C., Fu, X., Xu, Y., Zhang, H., Wu, X., Sommar, J., Zhang, L., Wang, X., & Feng, X. (2022). Sources and Transformation Mechanisms of Atmospheric Particulate Bound Mercury Revealed by Mercury Stable Isotopes. *Environmental Science and Technology*, *56*(8), 5224–5233. https://doi.org/10.1021/acs.est.1c08065

Liu, Y., Liu, G., Wang, Z., Guo, Y., Yin, Y., Zhang, X., Cai, Y., & Jiang, G. (2022). Understanding foliar accumulation of atmospheric Hg in terrestrial vegetation: Progress and challenges. *Critical Reviews in Environmental Science and Technology*, *52*(24), 4331–4352. https://doi.org/10.1080/10643389.2021.1989235

Miklavčič, A., Mazej, D., Jaćimović, R., Dizdarevič, T., & Horvat, M. (2013). Mercury in food items from the Idrija Mercury Mine area. *Environmental Research*, *125*, 61–68. https://doi.org/10.1016/j.envres.2013.02.008

Mlakar, I., & Čar, J. (2009). *Geološka karta idrijsko - cerkljanskega hribovja med stopnikom in rovtami 1:25.000*. Geological Survey of Slovenija.

Mlakar, T. L., Horvat, M., Kotnik, J., Jeran, Z., Vuk, T., Mrak, T., & Fajon, V. (2011). Biomonitoring with epiphytic lichens as a complementary method for the study of mercury contamination near a cement plant. *Environmental Monitoring and Assessment*, *181*(1–4), 225–241. https://doi.org/10.1007/s10661-010-1825-5

Mlakar, T. L., Horvat, M., Vuk, T., Stergaršek, A., Kotnik, J., Tratnik, J., & Fajon, V. (2010). Mercury species, mass flows and processes in a cement plant. *Fuel*, *89*(8), 1936–1945. https://doi.org/10.1016/j.fuel.2010.01.009

National Institute of Standards & Technology. (2017). *Report of Investigation Reference Material 8610 sotopes in UM-Almaden Mono-Elemental Secondary Standard This Mercury*. Department of Commerce - USA.

Obrist, D., Pokharel, A. K., & Moore, C. (2014). Vertical profile measurements of soil air suggest immobilization of gaseous elemental mercury in mineral soil. *Environmental Science and Technology*, *48*(4), 2242–2252. https://doi.org/10.1021/es4048297

O'Connor, D., Hou, D., Ok, Y. S., Mulder, J., Duan, L., Wu, Q., Wang, S., Tack, F. M. G., & Rinklebe, J. (2019). Mercury speciation, transformation, and transportation in soils, atmospheric flux, and implications for risk management: A critical review. *Environment International*, *126*(March), 747–761. https://doi.org/10.1016/j.envint.2019.03.019

Slovenian Environment Agency. (2023, October). *Geoportal ARSO*. Http://Gis.Arso.Gov.Si/Geoportal/Catalog/Main/Home.Page#.

Teršič, T., Gosar, M., & Biester, H. (2011). Environmental impact of ancient small-scale mercury ore processing at Pšenk on soil (Idrija area, Slovenia). *Applied Geochemistry*, *26*(11), 1867–1876. https://doi.org/10.1016/j.apgeochem.2011.06.010

Tomiyasu, T., Kodamatani, H., Imura, R., Matsuyama, A., Miyamoto, J., Akagi, H., Kocman, D., Kotnik, J., Fajon, V., & Horvat, M. (2017). The dynamics of mercury near Idrija mercury mine, Slovenia: Horizontal and vertical distributions of total,

methyl, and ethyl mercury concentrations in soils. *Chemosphere*, *184*, 244–252. https://doi.org/10.1016/j.chemosphere.2017.05.123

Tomiyasu, T., Matsuyama, A., Imura, R., Kodamatani, H., Miyamoto, J., Kono, Y., Kocman, D., Kotnik, J., Fajon, V., & Horvat, M. (2012). The distribution of total and methylmercury concentrations in soils near the Idrija mercury mine, Slovenia, and the dependence of the mercury concentrations on the chemical composition and organic carbon levels of the soil. *Environmental Earth Sciences*, *65*(4), 1309–1322. https://doi.org/10.1007/s12665-011-1379-z

Tsui, M. T. K., Blum, J. D., & Kwon, S. Y. (2020). Review of stable mercury isotopes in ecology and biogeochemistry. *Science of the Total Environment*, *716*, 135386. https://doi.org/10.1016/j.scitotenv.2019.135386

UNEP. (2019). *Global Mercury assessment 2018*.

UNEP. (2022). *Guidance on monitoring of mercury and mercury compounds to support evaluation of the effectiveness of the Minamata Convention*.

Vijayakumaran Nair, S., Kotnik, J., Gačnik, J., Živković, I., Koenig, A. M., Mlakar, T. L., & Horvat, M. (2022). Dispersion of airborne mercury species emitted from the cement plant. *Environmental Pollution*, *312*. https://doi.org/10.1016/j.envpol.2022.120057

Wang, X., Yuan, W., Lin, C. J., & Feng, X. (2021). Mercury cycling and isotopic fractionation in global forests. *Critical Reviews in Environmental Science and Technology*, *0*(0), 1–24. https://doi.org/10.1080/10643389.2021.1961505

Žagar, D., Knap, A., Warwick, J. J., Rajar, R., Horvat, M., & Četina, M. (2006). Modelling of mercury transport and transformation processes in the Idrijca and Soča river system. *Science of the Total Environment*, *368*(1), 149–163. https://doi.org/10.1016/j.scitotenv.2005.09.068

Zheng, W., Obrist, D., Weis, D., & Bergquist, B. A. (2016). Mercury isotope compositions across North American forests. *Global Biogeochemical Cycles*, 1475–1492. https://doi.org/10.1111/1462-2920.13280

Zhou, J., & Obrist, D. (2021). Global Mercury Assimilation by Vegetation. *Environmental Science & Technology*. https://doi.org/10.1021/acs.est.1c03530

Zhou, J., Obrist, D., Dastoor, A., Jiskra, M., & Ryjkov, A. (2021). Vegetation uptake of mercury and impacts on global cycling. *Nature Reviews Earth and Environment*, *2*(4), 269–284. https://doi.org/10.1038/s43017-021-00146-y

Žibret, G., & Gosar, M. (2006). Calculation of the mercury accumulation in the Idrijca River alluvial plain sediments. *Science of the Total Environment*, *368*(1), 291–297. https://doi.org/10.1016/j.scitotenv.2005.09.086

A.4 Supplementary Material to the Article: Fractionation of Mercury Stable Isotopes in Lichens

Supplementary material

Table S1: The sampling sites marked whether the covered lichens were exposed at the spot and the remarks about the site. The dates for lichen collection and air measurements are presented.

Sampling sites		
Site	Covered	Remarks
Vodarna	/	SW, of the plant
Anhovo	Yes	SW, of the plant
Morsko	/	NE, of the plant
Ročinj	/	NE, 3 km up the river Soča
Spodnja Idrija	/	2 km down the river Idrijca
Idrija – town	Yes	In vicinity of the mine shafts
Idrija – smeltery	/	In vicinity of the former smeltery
Pokljuka	/	5 sampling sites 2 km apart

Lichen collection and air measurements	
Sample	Date [yyyy/mm/dd]
1st *in-situ* (0 M)	2020/01/16 – 2020/01/21
1st transplants (4 M)	2020/05/06 – 2020/06/09
1st air	2020/07/16
2nd air	2020/08/14
2nd transplants (7 M)	2020/08/14 – 2020/08/019
3rd air	2020/10/16
4th air	2020/10/29
5th air	2020/11/06
6th air	2020/11/11
7th air	2020/12/01
3rd transplants (11 M)	2020/12/01 – 2020/12/14
8th air (Pokljuka only)	2020/12/15
4th transplants & *in-situ* 13 M	2021/02/15 – 2021/02/23

Table S2: Operating conditions of Aglient 8800 QQQ-ICP-MS and the measurement curve parameters.

Nebulizer	MicroMist
Spray chamber	Scott double-pass
RF Power [W]	1550
Plasma gas flow [L/min]	15
Carrier gas [L/min]	0.95
Makeup gas [L/min]	0.10
Sampling depth [mm]	8.0
Sample uptake rate [rps]	0.1
Sampling and skimmer cones	Nickel
Isotopes for internal standards	^{45}Sc, ^{89}Y, ^{103}Rh, ^{157}Gd
Isotope	202
Analysis gas	He
R^2 of the calibration curve	0.999
Conc. range of the calibration curve [ng/g]	0.01 – 250
Sample solution range [ng/g]	1 – 34

Table S3: Operating conditions of Nu Plasma II MC-ICP-MS.

Plasma conditions	
RF power [W]	1300
Ar cooling gas [L/min]	13.0
Ar auxiliary gas [L/min]	0.8
Hg vapor generation	
Ar sweep gas flow [L/min]	40 – 60
$SnCl_2$ and sample uptake rate [mL/min]	0.9 – 1.1
Method settings	
Mass separation	1
Cup configuration	^{196}Hg(L4), ^{198}Hg(L2), ^{199}Hg(L1), ^{200}Hg(Ax), ^{201}Hg(H1), ^{202}Hg(H2), ^{204}Hg, ^{204}Pb (H4), ^{208}Pb(H8)
Blocks	1
Measurements per block	30
Magnet delay time [s]	2
Transfer time [s]	50
Wash time – 5% HNO_3 & 3% HCl [s]	280
Analytical concentration [ng/mL]	1
Sensitivity [V]	0.5 – 1.2
Total analysis time [min]	11

Table S4. Arithmetic mean of Hg concentrations in air [ng/m^3] measured by Lumex RA915M detector ± S.D., calculated from the measurements at 1 s interval.

		2020/07/16	2020/08/14	2020/10/16	2020/10/29	2020/11/06	2020/11/11	2020/12/01	2020/12/15
Vodarna	Mean	1.49	1.71	1.35	1.61	1.29	1.58	1.50	
	S.D.	(1.07)	(1.00)	(1.18)	(1.38)	(1.05)	(0.93)	(1.03)	
Anhovo	Mean	1.65	1.66	2.00	1.24	1.23	1.44	1.80	
	S.D.	(1.12)	(1.08)	(1.21)	(1.12)	(1.01)	(1.16)	(1.02)	
Morsko	Mean	1.55	1.80	1.89	1.41	1.62	1.45	1.67	
	S.D.	(1.05)	(1.15)	(1.16)	(1.14)	(1.12)	(1.19)	(1.02)	
Ročinj	Mean	1.43	1.33	1.31	1.37	1.53	1.37	1.58	
	S.D.	(1.04)	(1.05)	(1.09)	(1.14)	(1.03)	(1.14)	(1.01)	
Spodnja Idriaja	Mean	3.21	4.85	2.92	3.11	3.16	4.28	3.65	
	S.D.	(1.34)	(1.46)	(1.58)	(1.54)	(1.30)	(2.10)	(1.41)	
Idrija – town	Mean	4.68	5.82	13.00	2.83	4.34	5.91	6.34	
	S.D.	(4.83)	(4.64)	(27.10)	(5.07)	(2.61)	(3.76)	(5.52)	
Idrija - smeltery	Mean	78.20	55.80	64.20	5.10	67.40	13.90	14.60	
	S.D.	(110.0)	(76.80)	(155.0)	(6.12)	(129.0)	(12.90)	(10.70)	
Pokljuka	Mean								1.16
	S.D.								(1.02)

Table S5: The concentrations of Hg (c) in the in situ samples and the transplants. The results are in [µg/g].

Sampling site		in situ 0 M	4 M	7 M	11 M	13 M	in situ 13 M
Vodarna	c	0.290	0.225	0.231	0.225	0.300	0.170
	U	(0.066)	(0.050)	(0.050)	(0.050)	(0.050)	(0.069)
Anhovo	c	0.211	0.216	0.236	0.249	0.281	0.212
	U	(0.050)	(0.050)	(0.050)	(0.050)	(0.050)	(0.051)
Anhovo (C)	c		0.232	0.233	0.215	0.257	
	U		(0.005)	(0.050)	(0.050)	(0.050)	
Morsko	c	0.178	0.197	0.215	0.265	0.293	0.191
	U	(0.050)	(0.050)	(0.050)	(0.050)	(0.006)	(0.050)
Ročinj	c	0.179	0.199	0.212	*	0.250	0.137
	U	(0.050)	(0.050)	(0.050)		(0.050)	(0.050)
Idrija – town	c	2.806	0.229	0.295	0.375	0.455	1.131
	U	(0.121)	(0.080)	(0.050)	(0.052)	(0.054)	(0.050)
Idrija – town (C)	c		0.259	0.275	0.269	0.313	
	U		(0.050)	(0.051)	(0.051)	(0.055)	
Spodnja Idrija	c	1.036	0.213	0.257	*	0.395	0.756
	U	(0.413)	(0.050)	(0.050)		(0.050)	(0.083)
Idrija – smelter	c	6.070	0.368	0.932	2.341	2.542	1.437
	U	(0.260)	(0.050)	(0.055)	(0.252)	(0.107)	(0.155)
Pokljuka a	c	0.249	0.261	0.232	*	*	
	U	(0.058)	(0.050)	(0.050)			
Pokljuka b	c	0.221					
	U	(0.051)					
Pokljuka c	c	0.313					
	U	(0.050)					
Pokljuka d	c	0.201					
	U	(0.051)					
Pokljuka e	c	0.183					
	U	(0.050)					

*** not enough sample for the analysis.**

Table S6: The isotopic ratios of Hg in in-situ and transplanted lichens. Values in ‰. The standard deviation of the repeated NIST 8610 standard reference material for the samples measured at IJS and the ones at IPREM are given in the brackets.

Location	Time of sampling	$\delta^{199}Hg$	$\delta^{200}Hg$	$\delta^{201}Hg$	$\delta^{202}Hg$	$\delta^{204}Hg$	$\Delta^{199}Hg$	$\Delta^{200}Hg$	$\Delta^{201}Hg$	$\Delta^{204}Hg$
NIST 8610 2*S.D.	IJS	(0.15)	(0.12)	(0.17)	(0.20)	(0.18)	(0.11)	(0.07)	(0.09)	(0.25)
	IPREM	(0.12)	(0.10)	(0.16)	(0.16)	(0.19)	(0.09)	(0.06)	(0.09)	(0.12)
Pokljuka a	0 M	-1.19	-1.52	-2.69	-3.03	-4.41	-0.43	0.00	-0.41	0.11
Vodarna	In situ 0 M	-0.57	-0.64	-1.29	-1.37	-2.13	-0.23	0.05	-0.26	-0.09
	4 M	-1.09	-1.46	-2.56	-2.86	-4.22	-0.37	-0.02	-0.41	0.06
	7 M	-0.78	-0.70	-1.32	-1.36	-2.16	-0.44	-0.02	-0.30	-0.13
	11 M	-1.03	-1.26	-2.29	-2.61	-3.65	-0.37	0.06	-0.33	0.25
	13 M	-1.11	-1.43	-2.53	-2.77	-3.97	-0.41	-0.03	-0.45	0.17
Anhovo	In situ 0 M	-0.61	-0.74	-1.38	-1.49	-2.18	-0.23	0.01	-0.26	0.05
	4 M	-1.08	-1.34	-2.36	-2.63	-3.74	-0.41	-0.02	-0.39	0.19
	7 M	-0.85	-1.01	-1.79	-1.95	-2.79	-0.36	-0.03	-0.32	-0.5
	11 M	-0.59	-0.99	-1.91	-2.30	-3.40	-0.01	0.17	-0.18	0.03
Ročinj	In situ 0 M	-0.94	-1.02	-1.96	-2.08	-3.12	-0.41	0.03	-0.40	-0.01
	4 M	-1.03	-1.24	-2.20	-2.39	-3.39	-0.42	-0.04	-0.40	0.18
	7 M	-0.49	-0.12	-0.51	-0.39	-0.55	-0.39	0.08	-0.22	0.02
	11 M	-0.90	-1.33	-2.62	-2.76	-4.10	-0.21	0.05	-0.55	0.01
	13 M	-1.13	-1.43	-2.61	-2.86	-4.25	-0.41	0.01	-0.46	0.02
Morsko	In situ 0 M	-0.76	-0.80	-1.57	-1.63	-2.44	-0.35	0.02	-0.34	0.00
	4 M	-1.09	-1.46	-2.56	-2.86	-4.22	-0.37	-0.02	-0.41	0.06
	7 M	-0.78	-0.70	-1.32	-1.36	-2.16	-0.44	-0.02	-0.30	-0.13
	11 M	-1.03	-1.26	-2.29	-2.61	-3.65	-0.37	0.06	-0.33	0.25
	13 M	-1.11	-1.43	-2.53	-2.77	-3.97	-0.41	-0.03	-0.45	0.17
Idrija - town	In situ 0 M	-0.59	-0.94	-1.75	-1.91	-2.87	-0.11	0.02	-0.31	-0.02
	4 M	-0.74	-0.98	-1.61	-1.94	-2.78	-0.25	0.00	-0.15	0.12
	7 M	-0.43	-0.20	-0.63	-0.45	-0.68	-0.32	0.02	-0.29	-0.01
	11 M	-0.60	-0.95	-1.68	-1.93	-3.05	-0.11	0.02	-0.23	-0.17
	13 M	-0.94	-1.21	-2.11	-2.35	-3.36	-0.35	-0.03	-0.34	0.14
Idrija – town covered	4 M	-0.96	-1.25	-2.31	-2.59	-3.99	-0.30	0.05	-0.36	-0.12
	7 M	-0.48	-0.36	-0.76	-0.78	-1.43	-0.28	0.03	-0.17	-0.26
	11 M	-0.77	-1.22	-2.10	-2.46	-3.61	-0.15	0.01	-0.25	0.05
	13 M	-0.88	-1.11	-1.94	-2.10	-3.11	-0.35	-0.06	-0.36	0.02
Spodnja Idrija	In situ 0 M	-0.79	-1.09	-1.88	-2.21	-3.33	-0.23	0.01	-0.22	-0.04
	4 M	-1.02	-1.23	-2.13	-2.32	-3.23	-0.44	-0.06	-0.38	0.24
	7 M	-0.68	-0.57	-1.12	-1.20	-1.86	-0.37	0.03	-0.22	-0.06
	11 M	-1.06	-1.47	-2.46	-2.98	-4.38	-0.31	0.02	-0.22	0.06
Idrija - smelter	In situ 0 M	-0.66	-0.98	-1.62	-1.94	-2.89	-0.17	0.00	-0.17	0.00
	4 M	-0.84	-1.23	-2.17	-2.47	-3.77	-0.21	0.02	-0.31	-0.08
	7 M	-0.70	-1.12	-1.91	-2.31	-3.50	-0.12	0.04	-0.17	-0.05
	11 M	-0.76	-1.19	-1.80	-2.24	-3.18	-0.20	-0.06	-0.11	0.17
	13 M	-0.67	-1.09	-1.68	-2.10	-3.18	-0.14	-0.04	-0.10	-0.05
Pokljuka	In situ (0 M) a	-1.19	-1.52	-2.69	-3.03	-4.41	-0.43	0.00	-0.41	0.11
	In situ (0 M) b	-1.26	-1.67	-2.90	-3.23	-4.62	-0.45	-0.05	-0.47	0.20
	In situ (0 M) c	-1.12	-1.78	-2.83	-3.52	-5.12	-0.23	-0.01	-0.18	0.13
	In situ (0 M) d	-1.04	-1.34	-2.35	-2.72	-4.14	-0.35	0.03	-0.30	-0.07
	In situ (0 M) e	-1.10	-1.57	-2.59	-3.14	-4.69	-0.31	0.01	-0.23	0.00
	4 M	-1.11	-1.28	-2.20	-2.37	-3.26	-0.51	-0.09	-0.42	0.29
	7 M	-0.55	-0.30	-0.69	-0.67	-1.11	-0.38	0.04	-0.19	-0.11
	11 M	-1.21	-1.52	-2.51	-2.91	-3.96	-0.48	-0.05	-0.32	0.37

A.5 Supplementary Material to the Article: Insights into Seasonal Variations in Mercury Isotope Composition of Lichens

Supplementary material

Lichen samples were systematically collected from three distinct sites at semi-regular intervals, typically once per month. These sites included Idrija, Pokljuka, and RCP, each with precise geographic coordinates referenced on the WGS 84 ellipsoid as follows: Idrija (46.007389N, 14.03099E), Pokljuka (46.34956N, 13.94178E), and RCP (46.09372N, 14.59464E) (Figure S1).

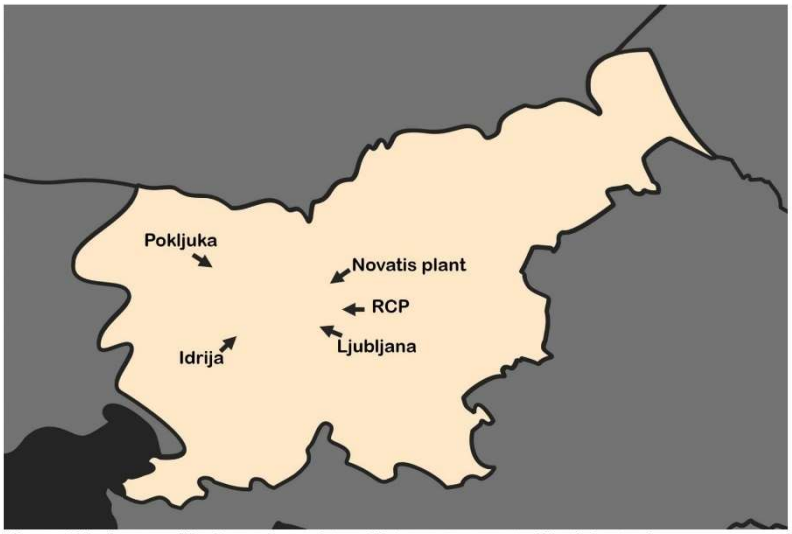

Figure S1: A map with the main points of interest presented in this study.

Figure S2 illustrates the spatial distribution of the collected samples across the three sites. It is worth noting that not all samples were collected during each individual sampling trip due to specific challenges encountered during the sampling process. Firstly, at the Idrija site, all in-situ lichens had been collected by midsummer, rendering further collection unfeasible. Secondly, adverse weather conditions during certain sampling instances, characterized by rain, led to the lichens deteriorating and developing mold by the time they reached the laboratory. Consequently, these lichens exhibited Hg concentrations up to twice as high as the others, rendering some of them unsuitable for Hg isotopic analysis. These factors account for some of the disparities between the data depicted in Figure S1 and that presented in Figures 1 and 3 in the main text.

Figure S2: The sampling trips to various locations are noted on a time scale. The top row is Pokljuka (triangles), the middle row is Idrija (squares), and the bottom row is RCP (circles).

Regarding atmospheric particulate matter (APM) sampling, it was conducted at intervals delineated in Figure S3. Given the low Hg concentrations encountered in APM, it became necessary to aggregate and preconcentrate certain samples. Additionally, due to the reduced availability of APM during the summer months, an extended operational duration of the pump was necessary. In the case of Idrija, only two

Table S3: Concentrations of Hg bound to APM, AMP concentrations in air, and the normalised Hg concentrations.

	Sample		Hg bound to APM		APM concentration in air	Normalised Hg concentration
			[pg/m³]	±	[ng/m³]	[µg/g]
Idrija	18/11/2021	22/11/2021	227.7	29.6	21.3	106.82
	14/01/2022	14/01/2022	57.2	7.4	106.7	5.72
RCP	13/10/2021	15/10/2021	14.8	1.9	10.9	13.56
	12/11/2021	13/11/2021	11.9	1.5	17.4	6.81
	08/12/2021	09/12/2021	14.8	1.9	36.0	4.11
	18/12/2021	19/12/2021	35.0	4.6	44.5	7.87
	21/12/2021	22/12/2021	28.6	3.7	45.0	6.36
	10/01/2022	12/01/2022	58.6	7.6	63.0	9.31
	04/02/2022	10/02/2022	20.0	2.6	22.9	8.75
	01/03/2022	04/03/2022	22.2	2.9	24.5	9.07
	28/03/2022	04/04/2022	20.2	2.6	13.1	15.53
	26/04/2022	07/05/2022	6.65	0.86	13.4	4.96
	20/05/2022	31/05/2022	3.72	0.48	9.86	3.72
	14/06/2022	27/06/2022	5.22	0.68	9.74	5.22
	26/06/2022	16/09/2022	2.57	0.33	10.3	2.50
	04/10/2022	13/10/2022	16.3	2.1	12.2	13.36

Table S4: The Hg isotopic ratios of Hg in APM.

Sample pulled from - to			$\delta^{199}Hg$	$\delta^{200}Hg$	$\delta^{201}Hg$	$\delta^{202}Hg$	$\delta^{204}Hg$	$\Delta^{199}Hg$	$\Delta^{200}Hg$	$\Delta^{201}Hg$	$\Delta^{204}Hg$
			[‰]	[‰]	[‰]	[‰]	[‰]	[‰]	[‰]	[‰]	[‰]
Idrija	18/11/2021	22/11/2021	-0.54	-1.48	-2.11	-2.97	-4.61	0.21	0.02	0.13	-0.17
	14/01/2022	14/01/2022	-0.74	-1.41	-2.32	-3.07	-4.67	0.03	0.13	-0.01	-0.09
RCP	13/10/2021	22/12/2021	-0.12	0.08	0.03	0.19	0.26	-0.16	-0.02	-0.11	-0.01
	10/01/2022	04/03/2022	-0.59	-1.11	-1.86	-2.39	-3.67	0.01	0.09	-0.06	-0.10
	28/03/2022	04/04/2022	-0.16	-0.48	-0.67	-1.00	-1.54	0.10	0.03	0.08	-0.05
	26/04/2022	27/06/2022	0.19	-0.77	-0.70	-1.63	-2.62	0.60	0.05	0.52	-0.19
	26/06/2022	13/10/2022	0.12	-0.12	-0.10	-0.28	-0.46	0.19	0.03	0.11	-0.04

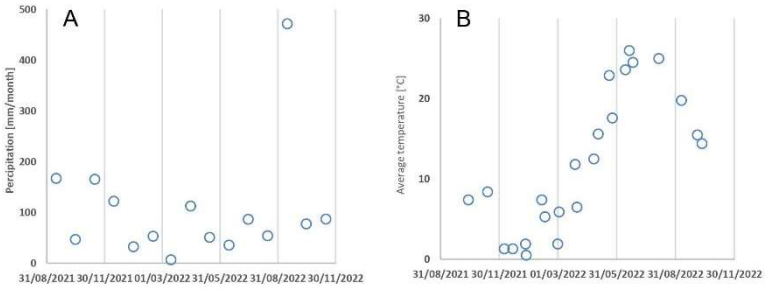

Figure S4: Environmental parameters. Left: the amount of precipitation at the Ljubljana-Bežigrad weather station in mm/month. Right: the average temperature at the RCP measured at of APM sampling location.

samplings were undertaken due to logistical constraints associated with the sampling equipment's transportability and susceptibility to potential damage. No APM samples were obtained from Pokljuka since the equipment required a continuous power source, which was unavailable at the site.

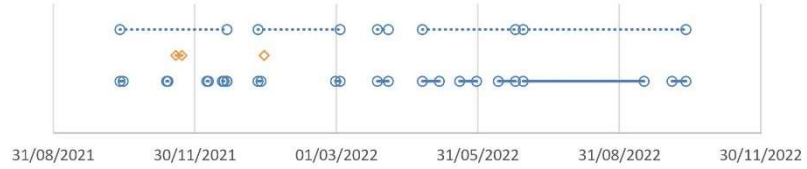

Figure S3: The sampling ranges of the APM collection in blue circles for RCP and in yellow squares for Idrija. The dashed ranges represent the pooled samples for isotopic analysis.

Table S1: Operating conditions of Nu Plasma II MC-ICP-MS.

Sampler cone	Ni, FB9
Skimmer cone	Ni, HS1-7
RF power	1300 W
Ar cooling gas	13.0 L/min
Ar auxiliary gas	0.8 L/min
Ar sweep gas flow	20 mL/min
Ar mix gas flow	70 ml/min
$SnCl_2$ and sample uptake rate	0.9 – 1.1 mL/min
Mass separation	1
Blocks	1
Measurements per block	30
Magnet delay time [s]	2
Transfer time [s]	50
Wash time – 5% HNO_3	10 s
Analytical concentration	1-1.5 ng/mL
Sensitivity	1-5 V
Total analysis time	11min

Table S2: Variability of NIST 8610 reference material, BCR 482 matrix-matched material, and within- and between-bag variability.

Sample name			‰	$\delta^{198}Hg$	$\delta^{199}Hg$	$\delta^{201}Hg$	$\delta^{202}Hg$	$\delta^{204}Hg$	$\Delta^{199}Hg$	$\Delta^{200}Hg$	$\Delta^{201}Hg$	$\Delta^{204}Hg$
NIST 8610	This study	N = 32	Avg.	-0.14	-0.28	-0.46	-0.56	-0.84	0.00	0.00	-0.04	-0.01
			2SD	*0.05*	*0.09*	*0.10*	*0.14*	*0.19*	*0.03*	*0.07*	*0.08*	*0.15*
	NIST	n/a	Avg.	-0.17	-0.27	-0.46	-0.56	-0.82	-0.03	-0,00	-0.04	0.00
			2SD	*0.01*	*0.01*	*0.02*	*0.03*	*0.07*	*0.02*	*0.01*	*0.01*	*0.02*
BCR 482	This study	N = 11	Avg.	-0.98	-0.68	-1.71	-1.50	-2.31	-0.60	0.07	-0.58	-0.07
			2SD	*0.08*	*0.15*	*0.23*	*0.16*	*0.41*	*0.06*	*0.10*	*0.15*	*0.22*
	Estrade et al., 2009	N = 15	Avg.	-0.99	-0.68	-1.71	-1.48	n/a	-0.62	0.06	-0.60	n/a
			2SD	*0.17*	*0.16*	*0.24*	*0.24*	*n/a*	*0.12*	*0.08*	*0.08*	*n/a*
	Bérail et al., 2017	N = 3	Avg.	-1.07	-0.81	-2.00	-1.68	-2.46	-0.64	0.04	-0.73	0.05
			2SD	*0.16*	*0.14*	*0.37*	*0.19*	*0.06*	*0.15*	*0.05*	*0.38*	*0.23*
NIST 1648a	This study	N = 7	Avg.	-0.13	-0.25	-0.46	-0.57	-0.91	0.01	0.03	-0.03	-0.06
			2SD	0.04	0.07	0.11	0.13	0.23	0.02	0.02	0.03	0.06
Within bag	This study	N = 4	Avg.	-0.95	-1.35	-2.25	-2.70	-3.99	-0.27	0.01	-0.23	0.03
			2SD	*0.12*	*0.10*	*0.19*	*0.14*	*0.17*	*0.09*	*0.03*	*0.09*	*0.11*
Between bag	This study	N = 4	Avg.	-0.83	-1.09	-1.87	-2.12	-3.19	-0.30	-0.02	-0.28	-0.02
			2SD	*0.10*	*0.17*	*0.33*	*0.34*	*0.53*	*0.06*	*0.02*	*0.10*	*0.03*

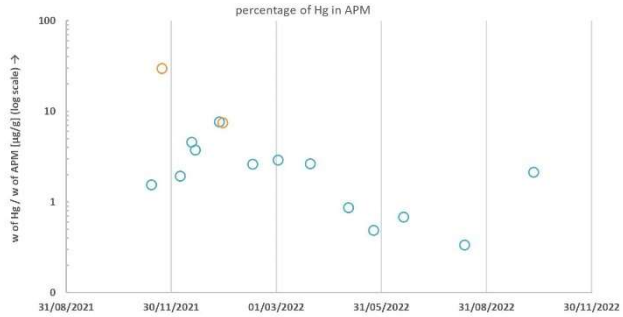

Figure S5: Normalised values of Hg in APM, indicated by orange circles for Idrija and blue circles for RCP.

Table S5: Hg concentrations in lichens. Dates are in dd/mm/yyyy format.

Sample			cHg [µg/g]	±
Idrija	In-situ	18/11/2021	1.164	0.103
		14/01/2022	2.141	0.190
		30/03/2022	1.721	0.153
		11/05/2022	0.908	0.081
		08/06/2022	1.051	0.093
		20/07/2022	1.131	0.100
		17/08/2022	0.928	0.082
		30/08/2022	1.148	0.102
	transplants	14/10/2021	0.212	0.017
		18/11/2021	0.270	0.022
		14/01/2022	0.357	0.029
		30/03/2022	0.606	0.050
		11/05/2022	0.576	0.047
		08/06/2022	0.642	0.053
		20/07/2022	0.916	0.075
		17/08/2022	1.012	0.083
		30/08/2022	1.028	0.084
		10/10/2022	1.481	0.121
Pokljuka	In-situ	02/10/2021	0.087	0.008
		22/11/2021	0.096	0.009
		22/12/2021	0.125	0.011
		02/03/2022	0.109	0.010
		27/04/2022	0.115	0.010
		31/05/2022	0.142	0.013
		15/07/2022	0.164	0.015
		05/08/2022	0.176	0.016
		29/08/2022	0.143	0.013
		10/10/2022	0.159	0.014
	transplants	21/10/2021	0.127	0.010
		22/11/2021	0.200	0.016
		02/03/2022	0.126	0.010
		15/07/2022	0.180	0.015
		05/08/2022	0.162	0.013
		29/08/2022	0.201	0.016
		10/10/2022	0.167	0.014
RCP	In-situ	22/09/2021	0.137	0.012
	transplants	21/10/2021	0.139	0.012
		21/11/2021	0.153	0.014

10/02/2022	0.128	0.011
11/03/2022	0.109	0.010
25/04/2022	0.103	0.009
09/05/2022	0.133	0.012
18/07/2022	0.129	0.011
17/08/2022	0.154	0.014
30/08/2022	0.143	0.013
09/09/2022	0.196	0.017
07/10/2022	0.209	0.018
11/10/2022	0.138	0.012

Table S6: Hg isotopic ratios of Hg in lichens. Dates are in dd/mm/yyyy format.

Sample			$\delta^{199}Hg$	$\delta^{200}Hg$	$\delta^{201}Hg$	$\delta^{202}Hg$	$\delta^{204}Hg$	$\Delta^{199}Hg$	$\Delta^{200}Hg$	$\Delta^{201}Hg$	$\Delta^{204}Hg$
			[‰]	[‰]	[‰]	[‰]	[‰]	[‰]	[‰]	[‰]	[‰]
Idrija	In-situ	18/11/2021	-0.77	-1.36	-2.16	-2.69	-4.00	-0.10	-0.01	-0.13	0.02
		14/01/2022	-0.81	-1.43	-2.31	-2.85	-4.27	-0.09	0.00	-0.16	-0.01
		30/03/2022	-0.52	-0.77	-1.35	-1.56	-2.30	-0.13	0.01	-0.18	0.03
		11/05/2022	-0.66	-0.93	-1.67	-1.92	-2.86	-0.17	0.03	-0.23	0.01
		08/06/2022	-0.68	-1.15	-1.90	-2.30	-3.51	-0.11	0.01	-0.17	-0.08
		20/07/2022	-0.48	-0.88	-1.41	-1.79	-2.69	-0.03	0.02	-0.06	-0.01
		30/08/2022	-0.63	-1.22	-1.92	-2.40	-3.62	-0.03	-0.01	-0.12	-0.04
	transplants	14/10/2021	-0.96	-1.50	-2.48	-3.10	-4.63	-0.18	0.06	-0.15	0.00
		18/11/2021	-0.94	-1.53	-2.49	-3.17	-4.73	-0.14	0.06	-0.10	0.01
		14/01/2022	-0.81	-1.32	-2.11	-2.64	-3.99	-0.14	0.00	-0.12	-0.04
		30/03/2022	-0.70	-1.15	-1.82	-2.24	-3.31	-0.14	-0.02	-0.14	0.03
		11/05/2022	-0.68	-1.16	-1.88	-2.31	-3.50	-0.10	0.00	-0.14	-0.06
		08/06/2022	-0.66	-1.05	-1.70	-2.10	-3.14	-0.13	0.01	-0.12	0.00
		20/07/2022	-0.67	-1.11	-1.81	-2.26	-3.35	-0.10	0.02	-0.11	0.02
		17/08/2022	-0.71	-1.11	-1.81	-2.19	-3.20	-0.15	-0.01	-0.16	0.07
		30/08/2022	-0.65	-1.12	-1.81	-2.22	-3.36	-0.09	0.00	-0.14	-0.04
		10/10/2022	-0.74	-1.36	-2.14	-2.72	-4.12	-0.05	0.01	-0.10	-0.06
Pokljuka	In-situ	02/10/2021	-0.71	-0.92	-1.60	-1.75	-2.60	-0.27	-0.04	-0.29	0.01
		02/03/2022	-0.83	-1.28	-2.12	-2.56	-3.95	-0.18	0.00	-0.20	-0.13
		27/04/2022	-0.82	-1.11	-1.97	-2.29	-3.46	-0.24	0.04	-0.25	-0.04
		31/05/2022	-0.81	-1.09	-1.91	-2.20	-3.27	-0.26	0.01	-0.25	0.03
		05/08/2022	-0.89	-1.23	-2.08	-2.46	-3.69	-0.28	0.01	-0.23	-0.02
		29/08/2022	-0.88	-1.15	-2.01	-2.39	-3.63	-0.28	0.05	-0.21	-0.06
		10/10/2022	-1.01	-1.48	-2.45	-2.83	-4.15	-0.30	-0.06	-0.32	0.07
	transplants	21/10/2021	-0.71	-0.92	-1.60	-1.75	-2.60	-0.27	-0.04	-0.29	0.01
		22/11/2021	-0.80	-1.03	-1.85	-2.09	-3.00	-0.27	0.02	-0.27	0.12
		02/03/2022	-0.95	-1.35	-2.25	-2.70	-3.99	-0.27	0.01	-0.23	0.03
		15/07/2022	-0.75	-1.02	-1.73	-2.06	-3.10	-0.23	0.02	-0.18	-0.03
		05/08/2022	-0.80	-1.00	-1.74	-1.95	-2.95	-0.31	-0.02	-0.27	-0.04
		29/08/2022	-0.84	-1.14	-1.97	-2.27	-3.35	-0.27	0.00	-0.26	0.04
RCP	In-situ	22/09/2021	-0.76	-1.12	-1.91	-2.23	-3.23	-0.19	0.01	-0.23	0.11
	transplants	10/02/2022	-0.60	-0.80	-1.50	-1.59	-2.39	-0.20	0.00	-0.30	-0.01
		11/03/2022	-0.55	-0.67	-1.26	-1.34	-1.94	-0.21	0.00	-0.25	0.07
		25/04/2022	-0.56	-0.54	-1.21	-1.25	-1.74	-0.25	0.09	-0.28	0.12
		09/05/2022	-0.47	-0.49	-1.05	-1.06	-1.55	-0.20	0.04	-0.25	0.03
		18/07/2022	-0.44	-0.43	-0.95	-0.96	-1.40	-0.20	0.05	-0.23	0.03
		30/08/2022	-0.47	-0.37	-0.85	-0.72	-1.02	-0.29	-0.01	-0.31	0.05
		07/10/2022	-0.61	-0.51	-1.16	-1.07	-1.59	-0.34	0.03	-0.35	0.01

References

Bérail, S., Cavalheiro, J., Tessier, E., Barre, J. P. G., Pedrero, Z., Donard, O. F. X., & Amouroux, D. (2017). Determination of total Hg isotopic composition at ultra-trace levels by on line cold vapor generation and dual gold-amalgamation coupled to MC-ICP-MS. *Journal of Analytical Atomic Spectrometry*, *32*(2), 373–384. https://doi.org/10.1039/c6ja00375c

Estrade, N., Carignan, J., Sonke, J. E., & Donard, O. F. X. (2009). Measuring hg isotopes in bio-geo-environmental reference materials. *Geostandards and Geoanalytical Research*, *34*(1), 79–93. https://doi.org/10.1111/j.1751-908X.2009.00040.x

A.6 Optimization of a Pre-Concentration Method for the Analysis of Mercury Isotopes in Low Concentration Foliar Samples

Analytical and Bioanalytical Chemistry
https://doi.org/10.1007/s00216-023-05116-5

RESEARCH PAPER

Optimization of a pre-concentration method for the analysis of mercury isotopes in low-concentration foliar samples

Saeed Waqar Ali[1,2] · Dominik Božič[1,2] · Sreekanth Vijayakumaran Nair[1,2] · Igor Živković[1,2] · Jan Gačnik[1,2] · Teodor-Daniel Andron[1,2] · Marta Jagodic Hudobivnik[1] · David Kocman[1] · Milena Horvat[1,2]

Received: 30 October 2023 / Revised: 12 December 2023 / Accepted: 19 December 2023

Abstract
Hg isotope analysis in samples from background regions is constrained by the presence of low Hg concentration and therefore requires a pre-concentration method. Existing Hg pre-concentration methods are constrained by long sample processing time and limited sample loading capacity. Using foliar samples as a test case, an optimized Hg pre-concentration method is presented that involves the microwave-assisted digestion of samples for Hg isotope analysis with the addition of a pre-digestion step. Microwave-digested foliar samples and CRMs were transferred to an impinger, reduced with $SnCl_2$, and collected in a 2.25 mL concentrated inverse aqua regia (3:1 HNO_3:HCl, v/v). This resulted in an optimal acid concentration in the solution ideal for analysis on MC-ICP-MS. The time for purging with Hg-free N2 was optimized to 30 min and the efficiency of the pre-concentration method was tested using a combination of approaches. Tests performed on pure reagents and matrix of foliar samples spiked with ^{197}Hg radiotracer showed recoveries averaging 99 ± 1.7% and 100 ± 3.0%, respectively. Mercury at concentrations as low as 1.83 ng g^{-1} was pre-concentrated by digesting aliquots of foliage samples in individual digestion vessels. Recoveries following their pre-concentration averaged 99 ± 6.0%, whereas recoveries of 95 ± 4.7% and 95 ± 2.5% were achieved for NIST SRM 1575a (pine needle) and reagents spiked with NIST SRM 3133, respectively. Analysis using multicollector-ICP-MS showed low fractionation of δ^{202}Hg during sample pre-concentration with no significant mass-independent fractionation. The proposed method is a relatively simple and robust way to prepare Hg samples for Hg isotopic analysis and is suitable even for complex biological matrices.

Keywords Foliage · Hg isotopes · Pre-concentration · Hg fractionation

Introduction

Recent advancements in inductively coupled plasma mass spectrometry (ICP-MS) enable the utilization of Hg stable isotopes to understand Hg biogeochemical cycling in the environment. Their application in various environmental compartments has allowed monitoring of changes in Hg sources, and their magnitudes. In this regard, an important utility of Hg isotopes is the acquisition of comparable data on the relative importance of Hg sources which is essential for global Hg monitoring programs and effective evaluation of the Minamata convention on mercury [1]. Stable Hg isotope signatures have provided new insights into transport and transformation processes [2], thus improving global Hg models to accurately estimate Hg pool sizes of major reservoirs and the magnitude of their intercompartmental exchanges [3]. In particular, the utilization of Hg isotope signatures has established forest ecosystems as a major sink for atmospheric Hg mainly via foliar Hg uptake and subsequent deposition to the forest floor via litterfall [4, 5].

Measuring Hg isotopes in samples is, however, constrained by the sensitivity of the analytical technique. Generally, the study of Hg isotopes in samples requires at least 0.5 ng g^{-1} of Hg in solution for analysis using a multicollector inductively coupled plasma mass spectrometer (MC-ICP-MS) with a sufficient level of certainty [6]. This is often challenging to achieve due to the low Hg concentration in samples. Foliar samples from sites having low anthropogenic influence tend to be at the lower spectrum

✉ Milena Horvat
milena.horvat@ijs.si

[1] Jožef Stefan Institute, 1000 Ljubljana, Slovenia

[2] Jožef Stefan International Postgraduate School, 1000 Ljubljana, Slovenia

Published online: 09 January 2024

of Hg concentrations [7]. This particularly relates to the foliar samples from the early spring season during which Hg concentrations are found to be the lowest, although Hg concentrations steadily increase across the season [8]. Studying Hg dynamics at background sites is, however, essential to understanding the Hg biogeochemical cycle, by exploring the natural variability of Hg in environmental reservoirs. In addition, background sites enable validation of existing Hg models and improve their accuracy for developing effective strategies to reduce Hg emissions and mitigate their impact on the environment [9]. The current effort is therefore aimed at addressing this by enabling Hg isotope analysis in foliar samples having low Hg concentration.

Several offline Hg pre-concentration methods exist [10–13] and among them is the widely used method that involves sample pyrolysis with dual-stage combustion followed by trapping of released Hg into a variety of oxidizing solutions [13]. The thermal-based reduction of solid samples at high temperatures has been shown to work ideally for a variety of samples with varying Hg concentrations. Solid samples are loaded in a quartz tube, plugged with quartz wool on both ends, and placed in the combustion furnace that reaches a temperature of 900 °C. Mercury-free O_2 gas carries the combusted samples to the decomposition furnace that is held at 1000 °C before being purged into a trapping solution of inverse aqua regia (2:1, v/v) at 25 mL min^{-1} O_2 flow rate. However, it takes 3.5 h to pre-concentrate Hg in one sample for Hg isotope analysis. Although this setup was further optimized for particulate matter (PM) samples collected on a quartz fiber membrane (QFM), the duration for Hg pre-concentration remained the same [11]. Sample loading in the dual-stage combustion method is further constrained by sample mass that may vary from 0.1 to 10g depending on the Hg concentration in the sample. The formation of soot as a result of incomplete combustion is linked with the carbon content which is often higher in samples such as coal or biomass. For instance, the combustion of more than 4 g of coal sample resulted in the formation of black deposits thus affecting the sample oxidation [13].

A similar pre-concentration method for Hg in solid samples involves hot acid digestion of samples before purging the digested solution onto a series of sample and analytical gold traps [10]. The loaded Hg on the gold traps is further desorbed for 40 min and captured in a variety of trapping solutions. The longer sample digestion time therefore does not make it suitable especially when working with a larger number of samples. To address this issue, the utilization of a pyrolysis unit for simultaneous detection of Hg in solid samples and Hg pre-concentration for Hg isotope analysis has also been proposed [12]. Analysis of certified reference materials (CRMs) using this method was statistically comparable to those reported previously with recoveries averaging 90 ± 4.0% based on certified values. This method offers a very short sample preparation time (8 min) although the amount of sample loaded is limited by the sample boat size. Pre-concentration methods involving purge and trap require the presence of Hg in a solution which is often challenging for samples with low Hg concentration as higher sample mass needs to be processed. While the existing offline pre-concentration methods are suitable for a wide range of environmental samples [10, 11, 13], Hg pre-concentration in environmental samples having low Hg concentration remains a challenge.

A few online Hg pre-concentration methods based on purge and trap systems have also been proposed [14–17]. The setup generally involves an online pre-concentration method using cold vapor generation and dual gold amalgamation coupled to MC-ICP-MS for Hg isotopic analysis. However, due to the transient nature of the output signal, precision loss may occur compared to continuous signal techniques. Additionally, the low signal-blank ratio for lower Hg mass introduced could potentially affect the accuracy of the method [15]. The online coupling of automated purge and trap with MC-ICP-MS for rapid and sensitive mercury isotopic analysis has been reported using a modified sample-standard bracketing (SSSSSB) sequence for isotopic measurements at ultra-trace levels without pre-concentration [14]. In such cases, the shorter integration time may lead to minor drift in Hg isotopic measurements. The potential of using chlorine-impregnated activated carbon (CIC) traps as an alternative to gold traps has also been studied [17], although there is a lack of information on the long-term stability and performance of the CIC traps over multiple uses or in varied environmental conditions. Conversely, modification of the arrangement of cones for enhanced signal sensitivity and optimization of instrument gas flows for steady and high Hg signal sensitivity have also been explored to obtain precise measurements of low Hg solutions [16]. In one study, an isotope binary mixing model was applied to calculate Hg isotopic compositions in low Hg concentration samples by mixing with a high-concentration Hg standard solution and using MC-ICP-MS for measurement [18]. The standard addition method was used to validate the precision and accuracy of the isotope data obtained from the binary mixing model. However, the study's reliance on the standard addition method may not fully represent the complexity of different matrices found in natural samples.

Microwave-assisted digestion, on the other hand, involves the use of microwave radiation to facilitate the digestion of samples under analysis and offers application for a wide range of samples [19–23]. In addition to the rapid and efficient sample digestion under high temperatures and pressure, this method of sample digestion offers improved analyte sample recovery through complete decomposition of the sample. Consequently, this minimizes the matrix effect and interferences which is otherwise observed during thermal

decomposition. Besides, the ability to process multiple samples under similar conditions enhances the reproducibility of results. However, samples with low Hg concentration particularly those from remote and low anthropogenically influenced regions require higher sample mass which subsequently restricts the use of a microwave-assisted digestion system. We, therefore, selected foliar samples with varying Hg concentrations to test the suitability of the optimized microwave-assisted digestion for sample preparation.

One of the main challenges of increasing sample mass with this method is the risk of strong reactions in the digestion vessels, leading to pressure build-up from the formation of gaseous NOx. Therefore, this requires the addition of a pre-digestion step where foliar samples react with reagents (HNO_3, HCl, and H_2O_2) while allowing the generated fumes to escape. This enables higher sample mass to be completely digested while maintaining a high sample throughput. The pre-digestion step in addition to the versatility of microwave-assisted digestion therefore enables Hg pre-concentration and subsequently Hg isotope analysis in a wide range of samples. The current study therefore aimed at optimizing Hg pre-concentration in foliar samples as a test case. Furthermore, the aim was to validate the efficiency of the proposed pre-concentration method using ^{197}Hg radiotracer and CRMs and investigate the associated Hg isotope fractionation during sample pre-concentration.

Methodology

Digestion

The proposed Hg pre-concentration method is schematically illustrated in Fig. 1. In the current study, up to 2 g of foliar samples was digested with the addition of 10 mL HNO_3 (65% Suprapur), 1 mL HCl (37% Suprapur), and 1 mL H_2O_2 (37% Suprapur) using a microwave digestion system ETHOS 1 (Milestone Inc., Shelton, CT, USA). CRMs were digested in each batch along with foliar samples ($n=42$) and procedural blanks. CRMs used in this study include NIST SRM 1575a (pine needles) ($n=14$) and NIST SRM 1547 (peach leaves) ($n=2$). Foliar samples were collected as part of the sample collection campaign under the ongoing GMOS-Train project (www.gmos-train.eu) to study Hg dynamics and fractionation in forests under various impacts in terms of Hg sources. The amount of foliar sample needed for digestion was determined by measuring Hg concentrations using a triple-quadrupole inductively coupled plasma mass spectrometer (ICP-QQQ-MS) (Agilent 8800, USA) following the method reported elsewhere [24]. Hg concentrations in foliar samples selected for this study ranged between 1.83 and 43.20 ng g^{-1} ($n=42$) out of which 38% were below 10 ng g^{-1}. The mass of the sample weighed in individual pre-cleaned Teflon vessels varied between 0.5 and 2 g. The concentration of foliar Hg was decisive for how much to weigh in each vessel. For instance, foliar samples that had Hg concentrations close to 2 ng g^{-1} were equally weighed in 8 vessels to have an equivalent of ~ 15 ng in the trapping solution. Samples having sufficient Hg concentration were weighed in 1–2 vessels. Aliquots of reagents were periodically added to the sample following the scheme shown in Fig. 1. Samples were first allowed to react with 10 mL HNO_3 for 30 min before the addition of 1 mL HCl. Following a reaction time of 15 min, 1 mL H_2O_2 was added and allowed to react with the sample for a further 15 min. The generated fumes and pressure as a result of the reaction were frequently released while allowing the sample to react with the reagents.

Samples were subsequently digested in a closed vessel accompanying the microwave-assisted digestion under the following program: ramp-up time of 40 min, digestion at 200 °C for 30 min, and cooling for another 30 min. Following the digestion, the digested samples in the vessel were equilibrated at room temperature and samples were transferred into 50-mL vials and weighed. Before this, the initial weights of sample vials were recorded. Digestion vessels were also rinsed with high-purity MQ water (water with

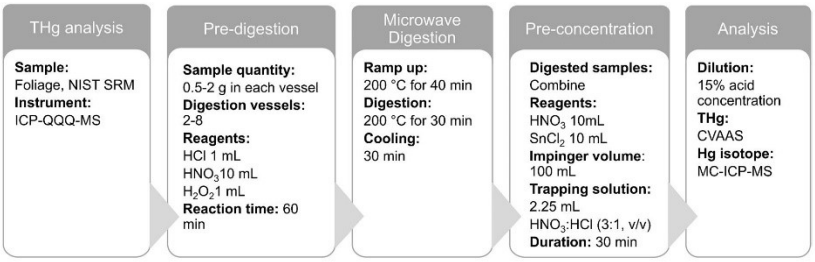

Fig. 1 Schematic diagram of the proposed sample pre-concentration method

a resistivity of 18.2 MΩcm, purified in a Millipore Elix® Essential 5 UV Milli-Q system) and added to the sample vials making the total volume up to 20 mL. In this way, a maximum of 8 samples along with CRM and procedural blank were processed in a single batch of microwave-assisted digestion in less than 3 h.

Pre-concentration

The setup for Hg pre-concentration included a 250-mL impinger connected to a 15-mL conical tube containing an oxidizing solution using a series of FEP (fluorinated ethylene-propylene) tubes of decremental sizes. Though purging Hg from a solution using impinger and pre-concentration in a trapping solution has previously been employed in a variety of schemes [10, 14, 25], the proposed purge and trap setup in this work is relatively simple and offers a robust method for pre-concentration, enabling efficient purging with a lower likelihood of Hg retention on the FEP tube walls. A Teflon adaptor with a press fit bore of 3.175 mm was connected to both openings of the impinger cap using an FEP tube having an inner diameter (ID) of 6 mm and an outer diameter (OD) of 8 mm. One end of the impinger was connected to a Hg-free N2 supply regulated by a mass flow controller (Cole Parmer) and the other end was further connected to a thinner FEP tube (0.8 mm ID × 1.6 mm OD) using an intermediate-sized FEP tubing (1.6 mm ID × 3.175 mm OD). The 15-mL conical tube contained 2.25 mL of a capturing solution prepared using inverse aqua regia (3:1, v/v) and was covered with Parafilm® M Sealing Film (Merck). The thin FEP tube (0.8 mm ID × 1.60 mm OD) was then inserted through the Parafilm and submerged into the capturing solution. The thin FEP tube (0.8 mm ID × 1.60 mm OD) was regularly purged with Hg-free N2 to remove possible droplets accumulated due to rinsing of the impinger. All connections were regularly checked for leakages using a portable gas leak detector (Restek Leak Detector, Restek Corporation, PA, USA).

The robustness of the proposed pre-concentration method along with the trapping efficiency of the inverse aqua regia (3:1, v/v) was evaluated. An acid concentration up to 30% v/v is tolerated for analysis using MC-ICP-MS. We, therefore, tested both diluted and concentrated inverse aqua regia (3:1, v/v) for optimal trapping efficiency at different flow rates and purging duration. This was done by spiking the solution in the impinger with an aliquot of NIST SRM 3133 and capturing it in the trapping solution. Hg in the trapping solution was subsequently measured with a cold vapor-atomic absorption spectrometer (CV-AAS) (Automatic Mercury Analyzer Model Hg-201, Sanso Seisakusho Co., LTD) using the method described previously [26, 27]. The instrument was calibrated using NIST SRM 3133 and peak heights measured for both sample and standard were used to calculate the concentration of Hg in the trapping solution.

Validation of pre-concentration with ^{197}Hg radiotracer

We used a highly sensitive ^{197}Hg radiotracer to validate the efficiency of our proposed pre-concentration method and to check the effect of the sample matrix during this process. The ^{197}Hg radiotracer offers certain advantages for the validation of analytical methods. This is due to its high specific activity, relatively simple detection method, and free of external contamination as ^{197}Hg is not present in nature. The process of ^{197}Hg radiotracer production has been previously well described [28–30]. Following irradiation, the ^{197}Hg stock solution was diluted to the desired concentration to create a working standard for the experiments allowing the evaluation of the efficiency and robustness of the proposed pre-concentration method.

An aliquot of ^{197}Hg radiotracer working standard solution (Hg concentration 300 pg—30 ng in absolute mass) corresponding to 3–300 pg mL^{-1} was added to the impinger containing 100 mL of 10% HNO_3 and 10% $SnCl_2$ (v/v) and capped immediately. Considering the short half-life of the ^{197}Hg tracer (2.671 days), the amount of the used working standard solution had to be increased since the experiments were performed on different days. Otherwise, the measured activity of the same ^{197}Hg spike would be too low for reliable quantification using the gamma detector after several days.

The solution was then purged with N2 for 30 min following the Hg reduction with $SnCl_2$ and ^{197}Hg radiotracer was captured in the 2.25 mL inverse aqua regia (3:1, v/v). To evaluate the effect of the sample solution on pre-concentration efficiency, tests were carried out with digested foliage samples. Similar to the test with pure reagents, around 80 mL of digested samples was transferred to the impinger having 10% HNO_3 and 10% $SnCl_2$ (v/v) making a final acid concentration of 30% (v/v). The sample solution was then spiked with a known concentration of ^{197}Hg radiotracer and captured similar to the test solutions with only pure reagents. As ^{197}Hg is not present in nature, this approach offered a simple test for possible matrix interference during Hg reduction in the solution obtained from the digested sample.

The activity of ^{197}Hg in solution was detected by a well-type HPGe detector (Model GCW6023/S), using the methods described previously [28]. Standards with concentrations corresponding to spikes (ranging from 300 pg to 30 ng) used in each experiment were prepared in triplicate (matching total volumes in the impinger and trapping solution) for the quantification of the ^{197}Hg leftover in impinger and ^{197}Hg recovery in the trapping solution, respectively. The corresponding activities of standards were measured

in the detector and compared with the measured activities of samples (both concentrations in impinger leftover and recovered in trapping solutions). Mass balances are reported as the sum of corresponding leftovers in the bubbler and recoveries in the capture solution. The activity of ^{197}Hg was determined by a peak area comparison of the characteristic doublet peaks of γ-ray and X-ray emissions (67.0 + 68.8 and 77.3 + 78.1 keV) using Genie 2000 Gamma analysis software.

Isotopic analysis

Hg isotopic ratios in samples were measured using Nu Plasma II (Nu Instruments Ltd., Ametek, UK) MC-ICP-MS following the previously reported method [24]. Briefly, the system uses an auto-sampler ASX-520 (Teledyne Cetac, NE, USA) for sample introduction. $SnCl_2$ in a solution (3% m/v in 10% v/v HCl) was used to reduce Hg, and then the mix of solutions was carried to the gas–liquid separator (Phase Separator Assembly, 2600 System, Model 2600-STD Tekran) connected to the torch using Teflon tubes resulting in a recovery as high as 99.6%. The elemental Hg vapor was transported by Ar sweep gas flow to the instrument, allowing for measurements of up to 1 ng mL^{-1}. Intensities at m/z of 202 were between 0.5 and 1.2 V, and outlier rejection of individual measurements within the cycle was done.

To ensure consistency between published data, Hg isotope data obtained in the present study were reported using the sample-standard-sample bracketing technique [31], and outlier rejection of individual measurements within the cycle was done for values above the relative three standard deviations (SD). The results were reported using δ and Δ notations [2]. Δ values were calculated from determined δ^{xxx}Hg values using the expression: $\Delta^{xxx}\text{Hg} \approx \delta^{xxx}\text{Hg} - \delta^{202}\text{Hg} \times f$ (where xxx denotes the mass number of the isotope), and correction factors f of 0.2520 for ^{199}Hg, 0.5024 for ^{200}Hg, 0.7520 for ^{201}Hg, and 1.4930 for ^{204}Hg. The measurement uncertainty is reported as long-term reproducibility of the measurements was evaluated by the NIST SRM 8610 (UM-Almadén) (National Institute of Standards Technology, 2017), and all the uncertainties are expressed at k = 2.

QA/QC

ICP-QQQ-MS was used for the quantification of Hg concentrations in foliage samples. The limit of detection (LOD) reported (0.001 ng g^{-1}) for the measured solutions was calculated as 3 times the standard deviation of procedural blanks divided by the slope of the calibration curve. The limit of quantification (LOQ) was calculated as 3 times the LOD and was 0.003 ng g^{-1}. Hg concentration in all the analyzed samples was above the LOQ. Similarly, the LOD (0.03 ng) for CVAAS used to quantify Hg concentrations in the trapping solution was calculated as three times the standard deviation of the procedural blank (n = 12). The LOQ (0.1 ng) for CVAAS was calculated as 3.33 times the limit of detection. The quality assurance of the analytical method was achieved by analyzing NIST SRM 1575a (pine needle), NIST SRM 1547 (peach leaves), and procedural blanks in each batch of sample digestion step. Hg concentrations in CRMs and procedural blanks, similar to foliage samples, were determined using CVAAS following the pre-concentration step. CVAAS offers several advantages, particularly the ease of operation and shorter analysis time, which allows the instant analysis of Hg concentration in the trapping solution following the pre-concentration step. After each batch of digestion, the vessels were thoroughly rinsed with MQ water and a cleaning cycle was run with the addition of 10 mL HNO_3 and 10 mL MQ. Digestion vessels were cleaned with a clean-up program (15 min ramping up to 200 °C and 30 min of ventilation). Blanks were then checked regularly for each digestion vessel before the next batch of sample digestion. When blanks higher than 0.10 ng corresponding to 5% of Hg in the trapping solution were observed, the contamination of the digestion vessels was checked with an absorbing microwave test. Empty digestion vessels were placed in the microwave digestion system for 1 min at 1000 W and checked for temperature rise. When the temperature of the digestion vessels exceeded 50 °C, an additional cleaning step was performed that involved heating the digestion vessels in a drying oven (SP 55-Easy, Kambic laboratory equipment) at 150 °C for 3 h. This ensured the release of the built-up fumes on the walls of the digestion vessels. This is usually necessary when a change in the color of the digestion vessel is apparent. Impingers used for pre-concentration were rinsed with MQ between each pre-concentration run.

Results and discussion

Mercury pre-concentration efficiency test

Trapping efficiencies of some of the common oxidants have been evaluated elsewhere and tests with 40% v/v inverse aqua regia using thermal desorption of Hg from gold traps have shown recoveries of 92 ± 4.0% and 98 ± 2.0% for 2 mL and 10 mL trapping solutions [10]. In the current work, tests on pure reagents spiked with 15 ng of freshly diluted NIST SRM 3133 (Hg standard solution), corresponding to 1 ng mL^{-1} in the trapping solution, were carried out. Hg trapped in 10 mL of 30% v/v inverse aqua regia solution showed increased recoveries with an increase in purging time thus indicating poor purging efficiency at a lower N2 flow rate (Fig. 2). Additionally, the analyte losses from the 30% inverse aqua regia trapping solution were also observed as the highest recovery achieved with this setup was 83 ± 2.0%

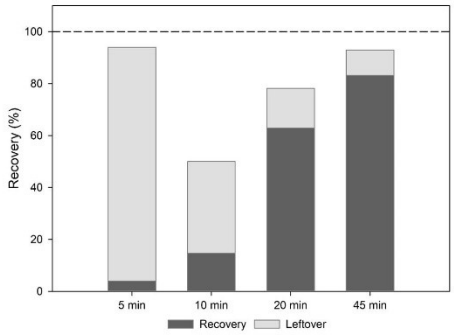

Fig. 2 Hg trapping efficiency in 10 mL of 30% v/v inverse aqua regia (3:1 HNO_3:HCl) at different purging durations

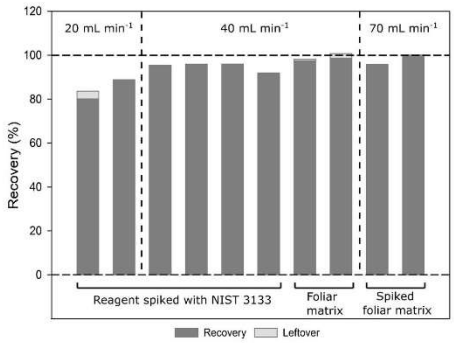

Fig. 3 N2 flow rate influence and Hg recovery of NIST SRM 3133 (Hg solution) and digested sample solution using 4.5 mL of concentrated inverse aqua regia as trapping solution

for 45 min of purge time. Recovery subsequently did not increase with an increase in purging time thus displaying poor trapping efficiency of the 10 mL of 30% v/v inverse aqua regia, and therefore Hg isotope analysis was not performed. Results of poor trapping efficiency even with 40% v/v inverse aqua regia were also noted previously under similar N2 flow rate [12] and are more suited for long purging duration under lower N2 flow rate (5–50 mL min) [11, 13].

Having observed poor trapping efficiency with the 30% v/v inverse aqua regia due to losses, a similar trapping efficiency test was then performed with 4.5 mL concentrated inverse aqua regia. Recovery improved significantly (Fig. 3) for 20- and 40-mL min^{-1} N2 flow rate for 45-min purge time with an average recovery of 84 ± 6.2% and 95 ± 1.9%, respectively. Further tests were carried out for the same purging time to check the effect of the leaf matrix on Hg pre-concentration efficiency. Recoveries of 98 ± 0.91% were observed for tests with microwave-digested sample solution constituting a nominal acid content of 32% (v/v) in the impinger (the acid content refers to the nominal volumes of nitric and hydrochloric acids used for the digestions of two leaf aliquots which were later mixed in the impinger for a single pre-concentration in a trapping solution). Recoveries for the Hg spiked to the sample solution, however, did not significantly improve with an increased N2 flow rate of 70 mL min^{-1}. This indicated a strong trapping efficiency of the concentrated inverse aqua regia (3:1, v/v) even at a lower N2 flow rate. Since the acid content of the trapping solution after dilution with MQ water would amount to 30% of the solution for Hg isotopic analysis, further optimization tests were carried out to reduce the purge time and the acid content.

Subsequent tests involved pre-concentration of Hg into 2.25 mL of the concentrated inverse aqua regia (3:1, v/v) which would represent 15% acid content of the capturing solution when diluted to 15 mL. Having achieved more than 98 ± 0.91% recovery at 45 min of purging time during previous attempts, the aim was to lower the purging time which would significantly impact sample throughput. Therefore, the flow rate of Hg-free N2 was increased to 180 mL min^{-1} and Hg was captured in 2.25 mL of concentrated inverse aqua regia (3:1, v/v). With a purging time of 30 min, recoveries ranged from 91 to 100% with an average recovery of 95 ± 2.5% ($n = 13$) as shown in Table S4. The subsequent decrease in purging time resulted in lower recoveries and optimization of purging time was therefore not further pursued.

One study reported that recoveries as low as 50% did not cause significant mass-dependent fractionation [27], whereas recoveries between 81 and 102% have also been reported to show no systematic variation in Hg isotope signature for selected sample types [13]. However, recoveries close to 100% for Hg isotope analysis are warranted due to the possible loss of light or heavy Hg isotopes during Hg pre-concentration involving different steps [32]. We also tested trapping Hg from two impingers in a single trapping solution and recoveries with this setup averaged 93 ± 2.0% suggesting a significantly strong trapping efficiency of the concentrated inverse aqua regia even at a higher purging rate.

Pre-concentration validation with ^{197}Hg radiotracer

Before Hg pre-concentration in solutions of digested foliar samples and CRMs, a validation test for the proposed Hg pre-concentration method was performed. This was required since working with low Hg concentration increases errors

due to Hg contamination and Hg carryover between samples. Hg^{2+} is a highly reactive Hg species and may be retained on surfaces of sample containers, in this case, the impinger [33] which can be augmented by improper cleaning of the purging unit between samples. For this purpose, the highly sensitive ^{197}Hg radiotracer is an ideal tool to validate our proposed pre-concentration method. Results from the ^{197}Hg radiotracer experiment validated the pre-concentration efficiency of the pre-concentration method with an average 99 ± 1.7% recovery (Fig. 4). With recoveries ranging between 96 and 102% (Table S2), this indicated that Hg carryover between samples was minimal and did not interfere with the pre-concentration efficiency. The effect of the sample matrix on pre-concentration efficiency was also negligible though Hg pre-concentration in the presence of a sample matrix resulted in relatively higher recoveries compared to those performed without the addition of a sample matrix, they remain in the acceptable range of 94–105% recovery (Table S3).

Pre-concentration of CRMs and foliar samples

Having validated the pre-concentration efficiency, Hg in solutions from foliar samples and CRMs was pre-concentrated and determined. With a pre-digestion step, up to 2 g of foliar samples having Hg concentration in the range of 7–8 ng g^{-1} could be digested in a single digestion vessel and thus did not require the merging of digested samples from multiple vessels into individual impingers but was needed for foliar samples with lower Hg concentration. For instance, foliar samples having Hg concentration in the range of 2 ng g^{-1} digested in 8 vessels were transferred equally into 2 bubblers and Hg pre-concentrated into a single trapping solution. This was done to maintain a sufficient acid concentration of solution in the impinger so that the Hg reduction efficiency by $SnCl_2$ would not be affected. Procedural blanks in this case accounted for less than 5% of the lowest Hg concentration and 0.04% in the case of the highest Hg concentration in foliar samples used for the optimization of the pre-concentration method.

Figure 5 summarizes the percent recoveries for foliar samples and CRMs. Recoveries for foliar samples were reported as the Hg concentration measured in the trapping solution relative to the original concentration determined in the samples using ICP-QQQ-MS. Recovery for foliar samples (n = 42) showed a relatively larger variation (99 ± 6.0%), although they were well within the acceptable range of 90–108%. The relatively wider variation in recoveries could also be due to the differences in homogeneity of studied foliar sample used in this study. We calculated the pre-concentration factors by dividing the absolute mass of pre-concentrated Hg (in ng) in the trapping solution with the Hg content in foliage samples (in ng/g). This factor (ranging from 0.77 to 10.70 g) is equal to the sample mass normalized to the procedural recovery. This factor could potentially be useful for comparison with other pre-concentration methods and for the estimation of the required sample weight when applying this method to other sample matrices in future studies. Recoveries for CRMs were on average 95 ± 4.7% for NIST SRM 1575a (pine needle) (n = 14) and 96 ± 5.6% for NIST SRM 1547 (peach leaves) (n = 2). These results therefore validated the robustness and efficiency of the proposed pre-concentration method.

Isotopic fractionation during pre-concentration

Mercury isotopes in the analyzed CRM samples were measured using MC-ICP-MS and the results are summarized in Table S1. Long-term uncertainty was investigated through analysis of the secondary standard NIST SRM 8610 and all uncertainties associated with Hg isotopic data were reported as k = 2. Negligible δ^{202}Hg (0.03 ± 0.15‰), Δ^{199}Hg (− 0.02 ± 0.06‰), and Δ^{200}Hg (0.00 ± 0.03‰) fractionation during Hg pre-concentration were observed for NIST SRM 3133 (Hg standard solution). The δ^{202}Hg for NIST SRM 1575a (pine needle) was − 1.69 ± 0.33‰ whereas Δ^{199}Hg and Δ^{200}Hg were − 0.31 ± 0.08‰ and 0.02 ± 0.03‰, respectively. These results are comparable to previously reported values for this CRM [12, 18, 34–37] as shown in Fig. 6. Meanwhile, to our knowledge, Hg isotopic ratios have not been previously reported for NIST SRM 1547 (peach leaves). This study therefore reports − 1.72 ± 0.02‰, − 0.13 ± 0.01‰, and 0.01 ± 0.01‰ for δ^{202}Hg, Δ^{199}Hg, and Δ^{200}Hg respectively for NIST SRM 1547 (peach leaves). Since the reference materials are not certified for Hg isotope

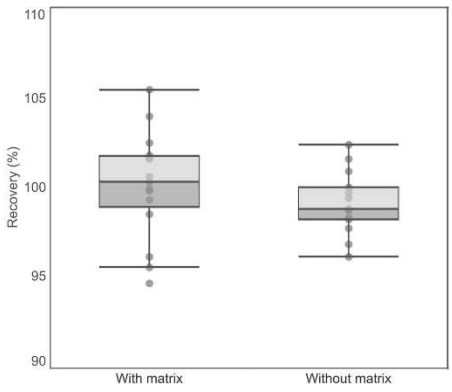

Fig. 4 ^{197}Hg radiotracer recoveries for the effect of sample matrix on pre-concentration efficiency

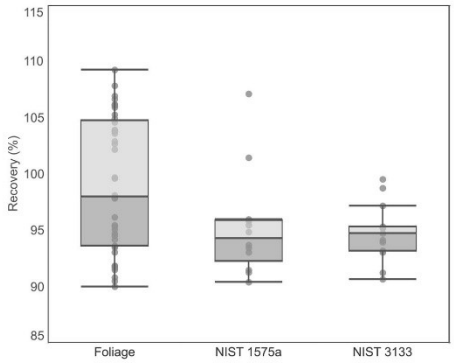

Fig. 5 Recovery of Hg in foliar samples, pine needle (NIST SRM 1575a), and Hg standard solution (NIST SRM 3133)

signatures, our results demonstrate good agreement with values reported in the literature and validate the robustness of the proposed pre-concentration method.

Conclusion

Analyzing Hg isotope signatures is challenging in foliar samples having low Hg concentration due to higher sample mass requirements. This work therefore proposes an optimized Hg pre-concentration method using the lowest foliar sample mass needed. Currently, no existing method is suitable for such low Hg concentration foliar samples. The method enables Hg isotope measurements in low Hg concentration foliar samples to facilitate the study of Hg biogeochemical processes at background sites with low anthropogenic influence. The setup utilizes the microwave-assisted digestion system for the digestion of a higher quantity of samples with the addition of a pre-digestion step. Results from analyzing foliar samples and CRMs showed that the proposed pre-concentration method is a robust and efficient way of preparing low Hg concentration samples for Hg isotopic analysis. Results from experiments with NIST SRM 3133, ^{197}Hg radiotracer, and analysis on MC-ICP-MS validated the efficiency of pre-concentration by showing low Hg fractionation. In addition to its applicability for samples with biological origin having Hg low concentrations, this pre-concentration method can also be suitable for a variety of liquid samples with complex matrices as we observed an insignificant effect of the sample matrix on pre-concentration efficiency. Since the use of a microwave-assisted digestion system is a common practice for sample preparation, the optimized method proposed

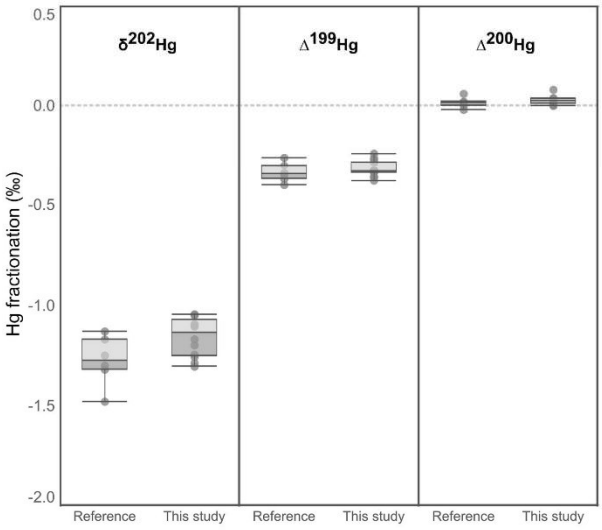

Fig. 6 Hg fractionation in NIST 1575a (pine needle) compared with previously reported data. Data of reference values were acquired from reference [12, 18, 34–37]

in this work would enable Hg pre-concentration for Hg isotope analysis in samples of different origins especially those having low Hg concentration.

Supplementary information The online version contains supplementary material available at https://doi.org/10.1007/s00216-023-05116-5.

Acknowledgements The authors would like to thank Radojko Jaćimović and the crew of the TRIGA Mark II reactor (JSI) for help during the radiotracer experiment.

Funding This project is funded by the European Union's Horizon 2020 research and innovation program under the Marie Sklodowska-Curie grant agreement [860497]. The authors would also like to thank the Slovenian Research Agency (ARRS) for the funding received under Program [P1-0143] and Project IsoCont [J1-3033].

Declarations

Conflict of interest The authors declare no competing interests.

References

1. Kwon SY, Blum JD, Yin R, Tsui MTK, Yang YH, Choi JW. Mercury stable isotopes for monitoring the effectiveness of the Minamata Convention on Mercury. Earth Sci Rev. 2020;203:103111–103111. https://doi.org/10.1016/j.earscirev.2020.103111.
2. Blum JD, Sherman LS, Johnson MW. Mercury isotopes in earth and environmental sciences. Annu Rev Earth Planet Sci. 2014;42:249–69. https://doi.org/10.1146/annurev-earth-050212-124107.
3. Obrist D, Kirk JL, Zhang L, Sunderland EM, Jiskra M, Selin NE. A review of global environmental mercury processes in response to human and natural perturbations: changes of emissions, climate, and land use. Ambio. 2018;47(2):116–40. https://doi.org/10.1007/s13280-017-1004-9.
4. Wang X, Bao Z, Lin CJ, Yuan W, Feng X. Assessment of global mercury deposition through litterfall. Environ Sci Technol. 2016;50:8548–57. https://doi.org/10.1021/acs.est.5b06351.
5. Zhou J, Wang Z, Zhang X. Deposition and fate of mercury in litterfall, litter, and soil in coniferous and broad-leaved forests. J Geophys Res Biogeosci. 2018;123:2590–603. https://doi.org/10.1029/2018JG004415.
6. Yin R, Krabbenhoft DP, Bergquist BA, Zheng W, Lepak RF, Hurley JP. Effects of mercury and thallium concentrations on high precision determination of mercury isotopic composition by Neptune Plus multiple collector inductively coupled plasma mass spectrometry. J Anal At Spectrom. 2016;31:2060–8. https://doi.org/10.1039/C6JA00107F.
7. Zhou J, Obrist D, Dastoor A, Jiskra M, Ryjkov A. Vegetation uptake of mercury and impacts on global cycling. Nat Rev Earth Environ. 2021;2(4):269–84. https://doi.org/10.1038/s43017-021-00146-y.
8. Laacouri A, Nater EA, Kolka RK. Distribution and uptake dynamics of mercury in leaves of common deciduous tree species in Minnesota, U.S.A. Environ Sci Technol. 2013;47:10462–70. https://doi.org/10.1021/es401357z.
9. Feinberg A, Dlamini T, Jiskra M, Shah V. Selin NE Evaluating atmospheric mercury (Hg) uptake by vegetation in a chemistry-transport model. Environ Sci Process Impacts. 2022;24(9):1303–18. https://doi.org/10.1039/d2em00032f.
10. Janssen SE, Lepak RF, Tate MT, Ogorek JM, Dewild JF, Babiarz CL, Hurley JP, Krabbenhoft DP. Rapid pre-concentration of mercury in solids and water for isotopic analysis. Anal Chim Acta. 2019;1054:95–103. https://doi.org/10.1016/j.aca.2018.12.026.
11. Huang Q, Liu Y, Chen J, Feng X, Huang W, Yuan S, Cai H, Fu X. An improved dual-stage protocol to pre-concentrate mercury from airborne particles for precise isotopic measurement. J Anal At Spectrom. 2015;30:957–66. https://doi.org/10.1039/C4JA00438H.
12. Enrico M, Balcom P, Johnston DT, Foriel J, Sunderland EM. Simultaneous combustion preparation for mercury isotope analysis and detection of total mercury using a direct mercury analyzer. Anal Chim Acta. 2021;1154: 338327. https://doi.org/10.1016/j.aca.2021.338327.
13. Sun R, Enrico M, Heimbürger LE, Scott C, Sonke JE. A double-stage tube furnace - acid-trapping protocol for the pre-concentration of mercury from solid samples for isotopic analysis. Anal Bioanal Chem. 2013;405:6771–81. https://doi.org/10.1007/s00216-013-7152-2.
14. Yang L, Yu B, Liu H, Ji X, Xiao C, Liang Y, Hu L, Yin Y, Shi J, Jiang G. Online determination of mercury isotopic compositions at ultratrace levels by automated purge and trap coupled with multicollector inductively coupled plasma-mass spectrometry. J Anal At Spectrom. 2022;37:2480–9. https://doi.org/10.1039/d2ja00148a.
15. Bérail S, Cavalheiro J, Tessier E, Barre JPG, Pedrero Z, Donard OFX, Amouroux D. Determination of total Hg isotopic composition at ultra-trace levels by on line cold vapor generation and dual gold-amalgamation coupled to MC-ICP-MS. J Anal At Spectrom. 2017;32:373–84. https://doi.org/10.1039/C6JA00375C.
16. Geng H, Yin R, Li X. An optimized protocol for high precision measurement of Hg isotopic compositions in samples with low concentrations of Hg using MC-ICP-MS. J Anal At Spectrom. 2018;33:1932–40. https://doi.org/10.1039/C8JA00255J.
17. Li K, Lin C-J, Yuan W, Sun G, Fu X, Feng X. An improved method for recovering and preconcentrating mercury in natural water samples for stable isotope analysis. J Anal At Spectrom. 2019;34:2303–13. https://doi.org/10.1039/C9JA00174C.
18. Huang S, Song Q, Zhang Y, Yuan D, Sun L, Chen Y, Jiang R, Lin H. Application of an isotope binary mixing model for determination of precise mercury isotopic composition in samples with low mercury concentration. Anal Chem. 2019;91:7063–9. https://doi.org/10.1021/acs.analchem.8b05940.
19. Jeon B, Cizdziel JV. Determination of metals in tree rings by ICP-MS using ash from a direct mercury analyzer. Molecules. 2020;25(9):2126. https://doi.org/10.3390/molecules25092126.
20. Antoniadis V, Shaheen SM, Boersch J, Frohne T, Du Laing G, Rinklebe J. Bioavailability and risk assessment of potentially toxic elements in garden edible vegetables and soils around a highly contaminated former mining area in Germany. J Environ Manage. 2017;186:192–200. https://doi.org/10.1016/j.jenvman.2016.04.036.
21. Pola L, Collado S, Oulego P, Díaz M. A proposal for the classification of sludge products throughout hydrothermal treatment. Chem Eng J. 2022;430: 132746. https://doi.org/10.1016/j.cej.2021.132746.
22. Morton-Bermea O, Hernández-Álvarez E, Ordoñez-Godínez SL, Montes-Ávila I. Mercury, platinum, antimony and other trace

elements in the atmospheric environment of the urban area of Mexico City: use of Ficus benjamina as biomonitor. Bull Environ Contam Toxicol. 2021;106:665–9. https://doi.org/10.1007/s00128-020-03080-9.
23. Klun K, Falnoga I, Mazej D, Šket P, Faganeli J. Colloidal organic matter and metal (loid) s in coastal waters (Gulf of Trieste, Northern Adriatic Sea). Aquat Geochem. 2019;25:179–94. https://doi.org/10.1007/s10498-019-09359-6.
24. Božič D, Živković I, Hudobivnik MJ, Kotnik J, Amouroux D, Štrok M, Horvat M. Fractionation of mercury stable isotopes in lichens. Chemosphere. 2022;309: 136592. https://doi.org/10.1016/j.chemosphere.2022.136592.
25. Lin H, Yuan D, Lu B, Huang S, Sun L, Zhang F, Gao Y. Isotopic composition analysis of dissolved mercury in seawater with purge and trap preconcentration and a modified Hg introduction device for MC-ICP-MS. J Anal At Spectrom. 2015;30:353–9. https://doi.org/10.1039/C4JA00242C.
26. Horvat M, Lupšina V, Pihlar B. Determination of total mercury in coal fly ash by gold amalgamation cold vapour atomic absorption spectrometry. Anal Chim Acta. 1991;243:71–9. https://doi.org/10.1016/S0003-2670(00)82542-8.
27. Akagi H, Nishimura H. Speciation of mercury in the environment [Internet]. Advances in Mercury Toxicology. Boston, MA: Springer US; 1991. p. 53–76 https://doi.org/10.1007/978-1-4757-9071-9_3.
28. Gačnik J, Živković I, Ribeiro Guevara S, Jaćimović R, Kotnik J, Horvat M. Validating an evaporative calibrator for gaseous oxidized mercury. Sensors. 2021;21:2501. https://doi.org/10.3390/s21072501.
29. Gačnik J, Živković I, Ribeiro Guevara S, Jaćimović R, Kotnik J, De Feo G, Dexter MA, Corns WT, Horvat M. Behavior of KCl sorbent traps and KCl trapping solutions used for atmospheric mercury speciation: stability and specificity. Atmospheric Measurement Techniques. 2021;14:6619–31. https://doi.org/10.5194/amt-14-6619-2021.
30. Gačnik J, Živković I, Ribeiro Guevara S, Kotnik J, Berisha S, Vijayakumaran Nair S, Jurov A, Cvelbar U, Horvat M. Calibration approach for gaseous oxidized mercury based on nonthermal plasma oxidation of elemental mercury. Anal Chem. 2022;94:8234–40. https://doi.org/10.1021/acs.analchem.2c00260.
31. Peel K, Weiss D, Chapman J, Arnold T, Coles B. A simple combined sample–standard bracketing and inter-element correction procedure for accurate mass bias correction and precise Zn and Cu isotope ratio measurements. J Anal At Spectrom. 2008;23:103–10. https://doi.org/10.1039/B710977F.
32. Ghosh S, Schauble EA, Lacrampe Couloume G, Blum JD, Bergquist BA. Estimation of nuclear volume dependent fractionation of mercury isotopes in equilibrium liquid–vapor evaporation experiments. Chem Geol. 2013;336:5–12. https://doi.org/10.1016/j.chemgeo.2012.01.008.
33. Parker JL, Bloom NS. Preservation and storage techniques for low-level aqueous mercury speciation. Sci Total Environ. 2005;337:253–63. https://doi.org/10.1016/j.scitotenv.2004.07.006.
34. Yamakawa A, Amouroux D, Tessier E, Bérail S, Fettig I, Barre JP, Koschorreck J, Rüdel H, Donard OF. Hg isotopic composition of one-year-old spruce shoots: application to long-term Hg atmospheric monitoring in Germany. Chemosphere. 2021;279: 130631. https://doi.org/10.1016/j.chemosphere.2021.130631.
35. Kurz AY, Blum JD, Washburn SJ, Baskaran M. Changes in the mercury isotopic composition of sediments from a remote alpine lake in Wyoming, USA. Sci Total Environ. 2019;669:973–82. https://doi.org/10.1016/j.scitotenv.2019.03.165.
36. Blum JD, Johnson MW. Recent developments in mercury stable isotope analysis. Rev Mineral Geochem. 2017;82:733–57. https://doi.org/10.2138/rmg.2017.82.17.
37. Zheng W, Obrist D, Weis D, Bergquist BA. Mercury isotope compositions across North American forests. Global Biogeochem Cycles. 2016;30:1475–92. https://doi.org/10.1002/2015GB005323.

Appendix B: Information on reproduction permission

Permission for the reproduction of the publications is presented here.

First and third articles presented here were published by Elsevier (*Chemosphere* and *Environmental Pollution* journals). Their copyright (found at: https://www.elsevier.com/about/policies/copyright#Author-rights 9.5.2023) states that the author has the right to use and share their work for scholarly purposes such as inclusion in a thesis or dissertation (provided it is not published commercially).

The second article (Minerals) was published with MDPI in an open access format was published in the open access format the terms under which this content can be reproduced and its fair use for the publishing in the PhD thesis is provided here (https://www.mdpi.com/openaccess 14.10.2023).

References

Acquavita, A., Emili, A., Covelli, S., Faganeli, J., Predonzani, S., Koron, N., & Carrasco, L. (2012). The effects of resuspension on the fate of Hg in contaminated sediments (Marano and Grado Lagoon, Italy): Short-term simulation experiments. *Estuarine, Coastal and Shelf Science*, *113*, 32–40. https://doi.org/10.1016/j.ecss.2011.12.012

Archer, D. E., & Blum, J. D. (2018). A model of mercury cycling and isotopic fractionation in the ocean. *Biogeosciences*, *15*(20), 6297–6313. https://doi.org/10.5194/bg-15-6297-2018

Ariya, P. A., Amyot, M., Dastoor, A., Deeds, D., Feinberg, A., Kos, G., Poulain, A., Ryjkov, A., Semeniuk, K., Subir, M., & Toyota, K. (2015). Mercury Physicochemical and Biogeochemical Transformation in the Atmosphere and at Atmospheric Interfaces: A Review and Future Directions. *Chemical Reviews*, *115*(10), 3760–3802. https://doi.org/10.1021/cr500667e

Audi, G., Kondev, F. G., Wang, M., Huang, W. J., & Naimi, S. (2017). The NUBASE2016 evaluation of nuclear properties. *Chinese Physics C*, *41*(3), 1–138. https://doi.org/10.1088/1674-1137/41/3/030001

Baptista-Salazar, C., & Biester, H. (2019). The role of hydrological conditions for riverine Hg species transport in the Idrija mining area. *Environmental Pollution*, *247*, 716–724. https://doi.org/10.1016/j.envpol.2019.01.109

Baptista-Salazar, C., Hintelmann, H., & Biester, H. (2018). Distribution of mercury species and mercury isotope ratios in soils and river suspended matter of a mercury mining area. *Environmental Science: Processes and Impacts*, *20*(4), 621–631. https://doi.org/10.1039/c7em00443e

Baptista-Salazar, C., Richard, J. H., Horf, M., Rejc, M., Gosar, M., & Biester, H. (2017). Grain-size dependence of mercury speciation in river suspended matter, sediments and soils in a mercury mining area at varying hydrological conditions. *Applied Geochemistry*, *81*, 132–142. https://doi.org/10.1016/j.apgeochem.2017.04.006

Barre, J. P. G., Deletraz, G., Frayret, J., Pinaly, H., Donard, O. F. X., & Amouroux, D. (2015). Approach to spatialize local to long-range atmospheric metal input (Cd, Cu, Hg, Pb) in epiphytic lichens over a meso-scale area (Pyrénées-Atlantiques, southwestern France). *Environmental Science and Pollution Research*, *22*(11), 8536–8548. https://doi.org/10.1007/s11356-014-3990-5

Barre, J. P. G., Deletraz, G., Sola-Larrañaga, C., Santamaria, J. M., Bérail, S., Donard, O. F. X., & Amouroux, D. (2018). Multi-element isotopic signature (C, N, Pb, Hg) in epiphytic lichens to discriminate atmospheric contamination as a function of land-use characteristics (Pyrénées-Atlantiques, SW France). *Environmental Pollution*, *243*, 961–971. https://doi.org/10.1016/j.envpol.2018.09.003

Bavec, & Gosar, M. (2016). Speciation, mobility and bioaccessibility of Hg in the polluted urban soil of Idrija (Slovenia). *Geoderma*, *273*, 115–130. https://doi.org/10.1016/j.geoderma.2016.03.015

Bavec, Š., Biester, H., & Gosar, M. (2014). Urban sediment contamination in a former Hg mining district, Idrija, Slovenia. *Environmental Geochemistry and Health*, *36*(3), 427–439. https://doi.org/10.1007/s10653-013-9571-6

Bavec, Š., Biester, H., & Gosar, M. (2018). A risk assessment of human exposure to mercury-contaminated soil and household dust in the town of Idrija (Slovenia). *Journal of Geochemical Exploration*, *187*, 131–140. https://doi.org/10.1016/j.gexplo.2017.05.005

Bavec, Š., Gosar, M., Biester, H., & Grčman, H. (2015). Geochemical investigation of mercury and other elements in urban soil of Idrija (Slovenia). *Journal of Geochemical Exploration*, *154*, 213–223. https://doi.org/10.1016/j.gexplo.2014.10.011

Becker, J. S. (2002). Applications of inductively coupled plasma mass spectrometry and laser ablation inductively coupled plasma mass spectrometry in materials science. *Spectrochimica Acta - Part B Atomic Spectroscopy*, *57*(12), 1805–1820. https://doi.org/10.1016/S0584-8547(02)00213-6

Becker, J. S. (2005). Inductively coupled plasma mass spectrometry (ICP-MS) and laser ablation ICP-MS for isotope analysis of long-lived radionuclides. *International Journal of Mass Spectrometry*, *242*(2–3), 183–195. https://doi.org/10.1016/j.ijms.2004.11.009

Bérail, S., Cavalheiro, J., Tessier, E., Barre, J. P. G., Pedrero, Z., Donard, O. F. X., & Amouroux, D. (2017). Determination of total Hg isotopic composition at ultra-trace levels by on line cold vapor generation and dual gold-amalgamation coupled to MC-ICP-MS. *Journal of Analytical Atomic Spectrometry*, *32*(2), 373–384. https://doi.org/10.1039/c6ja00375c

Berce, B. (1958). Geologija živosrebrnega rudišča Idrija.pdf. *Geological Transactions and Reports*, *4*, 1–61.

Bergquist, B. A., & Blum, J. D. (2007). Mass-dependent and -independent fractionation of Hg isotopes by photoreduction in aquatic systems. *Science*, *318*(5849), 417–420. https://doi.org/10.1126/science.1148050

Bergquist, B. A., & Blum, J. D. (2009). The odds and evens of mercury isotopes: Applications of mass-dependent and mass-independent isotope fractionation. *Elements*, *5*(6), 353–357. https://doi.org/10.2113/gselements.5.6.353

Biester, H., Gosar, M., & Müller, G. (1999). Mercury speciation in tailings of the Idrija mercury mine. *Journal of Geochemical Exploration*, *65*(3), 195–204. https://doi.org/10.1016/S0375-6742(99)00027-8

Biswas, A., Blum, J. D., Bergquist, B. A., Keeler, G. J., & Xie, Z. (2008). Natural mercury isotope variation in coal deposits and organic soils. *Environmental Science and Technology*, *42*(22), 8303–8309. https://doi.org/10.1021/es801444b

Blum, J. D., & Bergquist, B. A. (2007). Reporting of variations in the natural isotopic composition of mercury. *Analytical and Bioanalytical Chemistry*, *388*(2), 353–359. https://doi.org/10.1007/s00216-007-1236-9

Blum, J. D., & Johnson, M. W. (2017). Recent developments in mercury stable isotope analysis. *Reviews in Mineralogy and Geochemistry*, *82*(July 2013), 733–757. https://doi.org/10.2138/rmg.2017.82.17

Blum, J. D., Johnson, M. W., Gleason, J. D., Demers, J. D., Landis, M. S., & Krupa, S. (2012). Mercury Concentration and Isotopic Composition of Epiphytic Tree Lichens in the Athabasca Oil Sands Region. In *Developments in Environmental Science* (1st ed., Vol. 11, pp. 373–390). Elsevier Ltd. https://doi.org/10.1016/B978-0-08-097760-7.00016-0

Blum, J. D., Sherman, L. S., & Johnson, M. W. (2014). Mercury isotopes in earth and environmental sciences. *Annual Review of Earth and Planetary Sciences*, *42*(February), 249–269. https://doi.org/10.1146/annurev-earth-050212-124107

Bourdineaud, J. P., Durn, G., Režun, B., Manceau, A., & Hrenović, J. (2020). The chemical species of mercury accumulated by Pseudomonas idrijaensis, a bacterium from a rock of the Idrija mercury mine, Slovenia. *Chemosphere*, *248*. https://doi.org/10.1016/j.chemosphere.2020.126002

Božič, D., Živković, I., Hudobivnik, M. J., Kotnik, J., Amouroux, D., Štrok, M., & Horvat, M. (2022). Fractionation of mercury stable isotopes in lichens. *Chemosphere*, *309*(September), 136592. https://doi.org/10.1016/j.chemosphere.2022.136592

Bratkič, A., Koron, N., Ribeiro Guevara, S., Faganeli, J., & Horvat, M. (2017). Seasonal Variation of Mercury Methylation Potential in Pristine Coastal Marine Sediment from the Gulf of Trieste (Northern Adriatic Sea). *Geomicrobiology Journal*, *34*(7), 587–595. https://doi.org/10.1080/01490451.2016.1247482

Bratkič, A., Ogrinc, N., Kotnik, J., Faganeli, J., Žagar, D., Yano, S., Tada, A., & Horvat, M. (2013). Mercury speciation driven by seasonal changes in a contaminated estuarine environment. *Environmental Research*, *125*, 171–178. https://doi.org/10.1016/j.envres.2013.01.004

Bratkič, A., Tinta, T., Koron, N., Guevara, S. R., Begu, E., Barkay, T., Horvat, M., Falnoga, I., & Faganeli, J. (2018). Mercury transformations in a coastal water column (Gulf of Trieste, northern Adriatic Sea). *Marine Chemistry*, *200*, 57–67. https://doi.org/10.1016/j.marchem.2018.01.001

Buchachenko, A. L. (2013). Mass-independent isotope effects. *Journal of Physical Chemistry B*, *117*(8), 2231–2238. https://doi.org/10.1021/jp308727w

Cai, H., & Chen, J. (2016). Mass-independent fractionation of even mercury isotopes. *Science Bulletin*, *61*(2), 116–124. https://doi.org/10.1007/s11434-015-0968-8

Čar, J. (1985). *Razvoj srednjetriasnih sedimentov v idrijskem tektonskem jarku* [Doktroska disertacija]. FNT VTOZD Montanistika.

Čar, J. (1988). Ali je cerkev sv. Trojice zgrajena an "živosrebrnem studencu"? *Idrijski Razgledi*, 41–42.

Čar, J. (1996). Mineralized rocks and ore residues in the Idrija region. *Meeting of Researchers o Idrija as a Natural and Anthoropogenic Laboratory - Mercury as a Major Pollutant*, 10–15.

Čar, J. (2013). Ladinian skonca beds of the Idrija Ore Deposit (W Slovenia). *Geologija*, *56*(2), 151–174. https://doi.org/10.5474/geologija.2013.010

Carignan, J., Estrade, N., Sonke, J. E., & Donard, O. F. X. (2009). Odd isotope deficits in atmospheric Hg measured in lichens. *Environmental Science and Technology*, *43*(15), 5660–5664. https://doi.org/10.1021/es900578v

Čebulj, A. (1974). Geološke raziskave živega srebra v Idriji in okolici. In *Geološki zavod Slovenije* (pp. 520–521).

Cerovac, A., Covelli, S., Emili, A., Pavoni, E., Petranich, E., Gregorič, A., Urbanc, J., Zavagno, E., & Zini, L. (2018). Mercury in the unconfined aquifer of the Isonzo/SoČa River alluvial plain downstream from the Idrija mining area. *Chemosphere*, *195*, 749–761. https://doi.org/10.1016/j.chemosphere.2017.12.105

Chen, J. Bin, Hintelmann, H., Feng, X. Bin, & Dimock, B. (2012). Unusual fractionation of both odd and even mercury isotopes in precipitation from Peterborough, ON, Canada. *Geochimica et Cosmochimica Acta*, *90*, 33–46. https://doi.org/10.1016/j.gca.2012.05.005

Conti, M. E., & Cecchetti, G. (2001). Lichen Monitoring of Air Pollution in South Parts of Ilmen. *Environmental Pollution*, *114*, 471–492. https://doi.org/https://doi.org/10.1016/S0269-7491(00)00224-4

Covelli, S., Fontolan, G., Faganeli, J., & Ogrinc, N. (2006). Anthropogenic markers in the Holocene stratigraphic sequence of the Gulf of Trieste (northern Adriatic Sea). *Marine Geology*, *230*(1–2), 29–51. https://doi.org/10.1016/j.margeo.2006.03.013

De Laeter, J. R., Böhlke, J. K., De Bièvre, P., Hidaka, H., Peiser, H. S., Rosman, K. J. R., & Taylor, P. D. P. (2003). Atomic weights of the elements: Review 2000 (IUPAC Technical Report). *Pure and Applied Chemistry*, *75*(6), 683–800. https://doi.org/10.1351/pac200375060683

Demers, J. D., Blum, J. D., & Zak, D. R. (2013). Mercury isotopes in a forested ecosystem: Implications for air-surface exchange dynamics and the global mercury cycle. *Global Biogeochemical Cycles*, *27*(1), 222–238. https://doi.org/10.1002/gbc.20021

Donovan, P. M., Blum, J. D., Singer, M. B., Marvin-Dipasquale, M., & Tsui, M. T. K. (2016). Isotopic Composition of Inorganic Mercury and Methylmercury Downstream of a Historical Gold Mining Region. *Environmental Science and Technology*, *50*(4), 1691–1702. https://doi.org/10.1021/acs.est.5b04413

Donovan, P. M., Blum, J. D., Yee, D., Gehrke, G. E., & Singer, M. B. (2013). An isotopic record of mercury in San Francisco Bay sediment. *Chemical Geology*, *349–350*, 87–98. https://doi.org/10.1016/j.chemgeo.2013.04.017

Douglas, T. A., & Blum, J. D. (2019). Mercury Isotopes Reveal Atmospheric Gaseous Mercury Deposition Directly to the Arctic Coastal Snowpack. *Environmental Science and Technology Letters*, *6*(4), 235–242. https://doi.org/10.1021/acs.estlett.9b00131

Drovenik, M., Dolenec, T., Režun, B., & Pezdič, J. (1990). On the mercury ore from the Grübler orebody, Idrija. *Geologija*, *33*(1), 397–446. https://doi.org/10.5474/geologija.1990.010

Emili, A., Koron, N., Covelli, S., Faganeli, J., Acquavita, A., Predonzani, S., & Vittor, C. De. (2011). Does anoxia affect mercury cycling at the sediment-water interface in the Gulf of Trieste (northern Adriatic Sea)? Incubation experiments using benthic flux chambers. *Applied Geochemistry*, *26*(2), 194–204. https://doi.org/10.1016/j.apgeochem.2010.11.019

Enrico, M., Roux, G. Le, Marusczak, N., Heimbürger, L. E., Claustres, A., Fu, X., Sun, R., & Sonke, J. E. (2016). Atmospheric Mercury Transfer to Peat Bogs Dominated by Gaseous Elemental Mercury Dry Deposition. *Environmental Science and Technology*, *50*(5), 2405–2412. https://doi.org/10.1021/acs.est.5b06058

Estrade, N., Carignan, J., & Donard, O. F. X. (2010). Isotope tracing of atmospheric mercury sources in an urban area of Northeastern France. *Environmental Science and Technology*, *44*(16), 6062–6067. https://doi.org/10.1021/es100674a

Estrade, N., Carignan, J., Sonke, J. E., & Donard, O. F. X. (2009). Mercury isotope fractionation during liquid-vapor evaporation experiments. *Geochimica et Cosmochimica Acta*, *73*(10), 2693–2711. https://doi.org/10.1016/j.gca.2009.01.024

Faganeli, J., Falnoga, I., Horvat, M., Klun, K., Lipej, L., & Mazej, D. (2018). Selenium and mercury interactions in apex predators from the gulf of Trieste (Northern Adriatic Sea). *Nutrients*, *10*(3). https://doi.org/10.3390/nu10030278

Faganeli, J., Hines, M. E., Horvat, M., Falnoga, I., & Covelli, S. (2014). Methylmercury in the Gulf of Trieste (Northern Adriatic Sea): From Microbial Sources to Seafood Consumers. *Food Technol. Biotechnol.*, *52*(2), 188–197.

Faganeli, J., Horvat, M., Covelli, S., Fajon, V., Logar, M., Lipej, L., & Cermelj, B. (2003). Mercury and methylmercury in the Gulf of Trieste (northern Adriatic Sea). *Science of the Total Environment*, *304*(1–3), 315–326. https://doi.org/10.1016/S0048-9697(02)00578-8

Feng, X., Foucher, D., Hintelmann, H., Yan, H., He, T., & Qiu, G. (2010). Tracing mercury contamination sources in sediments using mercury isotope compositions. *Environmental Science and Technology*, *44*(9), 3363–3368. https://doi.org/10.1021/es9039488

Foucher, D., Ogrinc, N., & Hintelmann, H. (2009). Tracing mercury contamination from the Idrija mining region (Slovenia) to the gulf of trieste using Hg isotope ratio measurements. *Environmental Science and Technology*, *43*(1), 33–39. https://doi.org/10.1021/es801772b

Fu, X., Zhang, H., Liu, C., Zhang, H., Lin, C. J., & Feng, X. (2019). Significant Seasonal Variations in Isotopic Composition of Atmospheric Total Gaseous Mercury at Forest Sites in China Caused by Vegetation and Mercury Sources. *Environmental Science and Technology*, *53*(23), 13748–13756. https://doi.org/10.1021/acs.est.9b05016

Garty, J. (2002). Biomonitoring Heavy Metal Pollution with Lichens. In *Protocols in Lichenology* (pp. 458–482). https://doi.org/10.1007/978-3-642-56359-1_27

Gehrke, G. E., Blum, J. D., & Marvin-DiPasquale, M. (2011). Sources of mercury to San Francisco Bay surface sediment as revealed by mercury stable isotopes. *Geochimica et Cosmochimica Acta*, *75*(3), 691–705. https://doi.org/10.1016/j.gca.2010.11.012

Ghosh, S., Xu, Y., Humayun, M., & Odom, L. (2008). Mass-independent fractionation of mercury isotopes in the environment. *Geochemistry, Geophysics, Geosystems*, *9*(3), 1–10. https://doi.org/10.1029/2007GC001827

Gichuki, S. W., & Mason, R. P. (2014). Wet and dry deposition of mercury in Bermuda. *Atmospheric Environment*, *87*, 249–257. https://doi.org/10.1016/j.atmosenv.2014.01.025

Gnamuš, A. (2002). *Živo srebro v kopenski prehranski verigi: indikatorski organizmi, privtem in kopičenje*. Jožef Stefan institute.

Gnamuš, A., Byrne, A. R., & Horvat, M. (2000). Mercury in the soil-plant-deer-predator food chain of a temperate forest in Slovenia. *Environmental Science and Technology*, *34*(16), 3337–3345. https://doi.org/10.1021/es991419w

Gosar, M. (2004a). *Mechanisms of mercury dispersion in the Idrija mercury mine surroundings through history*. 2–5.

Gosar, M. (2004b). Soil-plant mercury concentrations in the Idrijca river terraces (Slovenia). *Geologija*, *47*(2), 259–271. https://doi.org/10.5474/geologija.2004.021

Gosar, M., & Čar, J. (2006). Influence of mercury ore roasting sites from 16th and 17th century on the mercury dispersion in surroundings of Idrija. *Geologija*, *49*(1), 91–101. https://doi.org/10.5474/geologija.2006.007

Gosar, M., Pirc, S., & Bidovec, M. (1997). Mercury in the Idrijca River sediments as a reflection of mining and smelting activities of the Idrija mercury mine. *Journal of Geochemical Exploration*, *58*(2–3), 125–131. https://doi.org/10.1016/S0375-6742(96)00064-7

Gosar, M., Pirc, S., Šajn, R., Bidovec, M., Mashyanov, N. R., & Sholupov, S. E. (1997). Distribution of mercury in the atmosphere over Idrija, Slovenia. *Environmental Geochemistry and Health*, *19*(3), 101–112. https://doi.org/10.1023/a:1018402605831

Gosar, M., Šajn, R., & Biester, H. (2002). Mercury speciation in soils and attic dust in the Idrija area. *Geologija*, *45*(2), 373–378. https://doi.org/10.5474/geologija.2002.035

Gosar, M., Šajn, R., & Biester, H. (2006). Binding of mercury in soils and attic dust in the Idrija mercury mine area (Slovenia). *Science of the Total Environment*, *369*(1–3), 150–162. https://doi.org/10.1016/j.scitotenv.2006.05.006

Gosar, M., & Teršič, T. (2012a). Environmental geochemistry studies in the area of Idrija mercury mine, Slovenia. *Environmental Geochemistry and Health*, *34*, 27–41. https://doi.org/10.1007/s10653-011-9410-6

Gosar, M., & Teršič, T. (2012b). Mercury enrichments in soils influenced by Idrija mercury mine, Slovenia. *RMZ – Materials and Geoenvironment*, *59*(3), 59.

Gosar, M., & Teršič, T. (2014). Contaminated sediment loads from ancient mercury ore roasting sites, Idrija area, Slovenia. *Journal of Geochemical Exploration*, *149*, 97–105. https://doi.org/10.1016/j.gexplo.2014.11.012

Gosar, M., & Žibret, G. (2011). Mercury contents in the vertical profiles through alluvial sediments as a reflection of mining in Idrija (Slovenia). *Journal of Geochemical Exploration*, *110*(2), 81–91. https://doi.org/10.1016/j.gexplo.2011.03.008

Gratz, L. E., Keeler, G. J., Blum, J. D., & Sherman, L. S. (2010). Isotopic composition and fractionation of mercury in Great Lakes precipitation and ambient air. *Environmental Science and Technology*, *44*(20), 7764–7770. https://doi.org/10.1021/es100383w

Gray, J. E., Pribil, M. J., & Higueras, P. L. (2013). Mercury isotope fractionation during ore retorting in the Almadén mining district, Spain. *Chemical Geology*, *357*, 150–157. https://doi.org/10.1016/j.chemgeo.2013.08.036

Grönlund, R., Edner, H., Svanberg, S., Kotnik, J., & Horvat, M. (2005). Mercury emissions from the Idrija mercury mine measured by differential absorption lidar techniques and a point monitoring absorption spectrometer. *Atmospheric Environment*, *39*(22), 4067–4074. https://doi.org/10.1016/j.atmosenv.2005.03.027

Gustin, M. S., Amos, H. M., Huang, J., Miller, M. B., & Heidecorn, K. (2015). Measuring and modeling mercury in the atmosphere: A critical review. *Atmospheric Chemistry and Physics*, *15*(10), 5697–5713. https://doi.org/10.5194/acp-15-5697-2015

Gustin, M. S., Bank, M. S., Bishop, K., Bowman, K., Bran, B., Chételat, J., Eckley, C. S., Hammerschmidt, C. R., Lamborg, C., Lyman, S., Martínez-cortizas, A., Sommar, J., Tsui, M. T., & Zhang, T. (2020). Science of the Total Environment Mercury biogeochemical cycling : A synthesis of recent scientific advances. *Science of the Total Environment*, *737*. https://doi.org/10.1016/j.scitotenv.2020.139619

Haynes, K. M., Kane, E. S., Potvin, L., Lilleskov, E. A., Kolka, R. K., & Mitchell, C. P. J. (2017). Gaseous mercury fluxes in peatlands and the potential influence of climate change. *Atmospheric Environment*, *154*, 247–259. https://doi.org/10.1016/j.atmosenv.2017.01.049

Hines, M. E., Horvat, M., Faganeli, J., Bonzongo, J. C. J., Barkay, T., Major, E. B., Scott, K. J., Bailey, E. A., Warwick, J. J., & Lyons, W. B. (2000). Mercury biogeochemistry in the Idrija River, Slovenia, from above the mine into the Gulf of Trieste. *Environmental Research*, *83*(2), 129–139. https://doi.org/10.1006/enrs.2000.4052

Hines, M. E., Poitras, E. N., Covelli, S., Faganeli, J., Emili, A., Žižek, S., & Horvat, M. (2012). Mercury methylation and demethylation in Hg-contaminated lagoon sediments (Marano and Grado Lagoon, Italy). *Estuarine, Coastal and Shelf Science*, *113*, 85–95. https://doi.org/10.1016/j.ecss.2011.12.021

Horvat, M., Covelli, S., Faganeli, J., Logar, M., Mandić, V., Rajar, R., Širca, A., & Žagar, D. (1999). Mercury in contaminated coastal environments; a case study: The Gulf of Trieste. *Science of the Total Environment*, *237–238*, 43–56. https://doi.org/10.1016/S0048-9697(99)00123-0

Horvat, M., Jeran, Z., Spiric, Z., Jacimovic, R., & Miklavcic, V. (2000). Mercury and other elements in lichens near the INA Naftaplin gas treatment plant, Molve, Croatia. *Journal of Environmental Monitoring*, *2*(2), 139–144. https://doi.org/10.1039/a906973i

Horvat, M., Jereb, V., Fajon, V., Logar, M., Kotnik, J., Faganeli, J., Hines, M. E., & Bonzongo, J.-C. (2002). Mercury distribution in water, sediment and soil in the Idrijca and Soča river systems. In *Environment, Analysis* (Vol. 2).

Horvat, M., Kontić, B., Kotnik, J., Ogrinc, N., Jereb, V., Fajon, V., Logar, M., Faganeli, J., Rajar, R., Sirca, A., Petkovšek, G., Zagar, D., & Dizdavevič, T. (2003). Remediation of mercury polluted sites due to mining activities. *Critical Reviews in Analytical Chemistry*, *33*(4), 291–296. https://doi.org/10.1080/714037679

Horvat, M., Kotnik, J., Logar, M., Fajon, V., Zvonarić, T., & Pirrone, N. (2003). Speciation of mercury in surface and deep-sea waters in the Mediterranean Sea. *Atmospheric Environment*, *37*(SUPPL. 1), 93–108. https://doi.org/10.1016/S1352-2310(03)00249-8

Irrgeher, J., & Prohaska, T. (2015). Instrumental isotopic fractionation. *New Developments in Mass Spectrometry*, *2015-January* (3), 107–120.

Jakubowski, N., Prohaska, T., Rottmann, L., & Vanhaecke, F. (2011). Inductively coupled plasma- and glow discharge plasma-sector field mass spectrometry: Part I. Tutorial: Fundamentals and instrumentation. *Journal of Analytical Atomic Spectrometry*, *26*(4), 693–726. https://doi.org/10.1039/c0ja00161a

Jiménez-Moreno, M., Barre, J. P. G., Perrot, V., Bérail, S., Rodríguez Martín-Doimeadios, R. C., & Amouroux, D. (2016). Sources and fate of mercury pollution in Almadeen mining district (Spain): Evidences from mercury isotopic compositions in sediments and lichens. *Chemosphere*, *147*, 430–438. https://doi.org/10.1016/j.chemosphere.2015.12.094

Jiskra, M., Sonke, J. E., Obrist, D., Bieser, J., Ebinghaus, R., Myhre, C. L., Pfaffhuber, K. A., Wängberg, I., Kyllönen, K., Worthy, D., Martin, L. G., Labuschagne, C., Mkololo, T., Ramonet, M., Magand, O., & Dommergue, A. (2018). A vegetation control on seasonal variations in global atmospheric mercury concentrations. *Nature Geoscience*, *11*(4), 244–250. https://doi.org/10.1038/s41561-018-0078-8

Jiskra, M., Wiederhold, J. G., Bourdon, B., & Kretzschmar, R. (2012). Solution speciation controls mercury isotope fractionation of Hg(II) sorption to goethite. *Environmental Science and Technology*, *46*(12), 6654–6662. https://doi.org/10.1021/es3008112

Jiskra, M., Wiederhold, J. G., Skyllberg, U., Kronberg, R. M., Hajdas, I., & Kretzschmar, R. (2015). Mercury Deposition and Re-emission Pathways in Boreal Forest Soils Investigated with Hg Isotope Signatures. *Environmental Science and Technology*, *49*(12), 7188–7196. https://doi.org/10.1021/acs.est.5b00742

Johansson, K., & Tyler, G. (2001). Impact of atmospheric long range transport of lead, mercury and cadmium on the Swedish forest environment. *Water, Air and Soil Pollution*, 279–297.

Kavčič, I. (2008). *Živo srebro: Zgodovina idrijskega žgalništva* (1st ed.).

Kavčič, I. (2020). *Reflections of a Silver Era*. Idrija Mercury Mine.

Kobal, A. B., Snoj Tratnik, J., Mazej, D., Fajon, V., Gibičar, D., Miklavčič, A., Kocman, D., Kotnik, J., Sešek Briški, A., Osredkar, J., Krsnik, M., Prezelj, M., Knap, Križaj, B., Liang, L., & Horvat, M. (2017). Exposure to mercury in susceptible population groups living in the former mercury mining town of Idrija, Slovenia. *Environmental Research*, *152*, 434–445. https://doi.org/10.1016/j.envres.2016.06.037

Kocman, D., & Horvat, M. (2011a). Non-point source mercury emission from the Idrija Hg-mine region: GIS mercury emission model. *Journal of Environmental Management*, *92*(8), 2038–2046. https://doi.org/10.1016/j.jenvman.2011.03.034

Kocman, D., Kanduč, T., Ogrinc, N., & Horvat, M. (2011). Distribution and partitioning of mercury in a river catchment impacted by former mercury mining activity. *Biogeochemistry*, *104*(1–3), 183–201. https://doi.org/10.1007/s10533-010-9495-5

Kocman, D., Vreča, P., Fajon, V., & Horvat, M. (2011). Atmospheric distribution and deposition of mercury in the Idrija Hg mine region, Slovenia. *Environmental Research*, *111*(1), 1–9. https://doi.org/10.1016/j.envres.2010.10.012

Koron, N., Faganeli, J., Falnoga, I., & Kovac, N. (2011). Interaction of macroaggregates and Hg in coastal waters (gulf of Trieste, northern Adriatic Sea). *Geomicrobiology Journal*, *28*(7), 615–624. https://doi.org/10.1080/01490451.2011.576165

Kossmat Franz. (1910). *Erläuterungen zur geologischen Karte Bischoflack und Idria*.

Kotnik, J., Horvat, M., Begu, E., Shlyapnikov, Y., Sprovieri, F., & Pirrone, N. (2017). Dissolved gaseous mercury (DGM) in the Mediterranean Sea: Spatial and temporal trends. *Marine Chemistry*, *193*, 8–19. https://doi.org/10.1016/j.marchem.2017.03.002

Kotnik, J., Horvat, M., & Dizdarevič, T. (2005). Current and past mercury distribution in air over the Idrija Hg mine region, Slovenia. *Atmospheric Environment*, *39*(39 SPEC. ISS.), 7570–7579. https://doi.org/10.1016/j.atmosenv.2005.06.061

Kotnik, J., Horvat, M., Liang, L., & Levanič, T. (2015). *Mercury in tree rings from Idrija Hg mine area*.

Kotnik, J., Horvat, M., Ogrinc, N., Fajon, V., Žagar, D., Cossa, D., Sprovieri, F., & Pirrone, N. (2015). Mercury speciation in the Adriatic Sea. *Marine Pollution Bulletin*, *96*(1–2), 136–148. https://doi.org/10.1016/j.marpolbul.2015.05.037

Kozin, L., Hansen, S., Zakharchenko Nikolai, & Gray Jason. (2013). Environmental Aspects of the Industrial Application of Mercury. In *Mercury Handbook* (pp. 209–227).

Kritee, K., Barkay, T., & Blum, J. D. (2009). Mass dependent stable isotope fractionation of mercury during mer mediated microbial degradation of monomethylmercury. *Geochimica et Cosmochimica Acta*, *73*(5), 1285–1296. https://doi.org/10.1016/j.gca.2008.11.038

Kritee, K., Blum, J. D., & Barkay, T. (2008). Mercury stable isotope fractionation during reduction of Hg(II) by different microbial pathways. *Environmental Science and Technology*, *42*(24), 9171–9177. https://doi.org/10.1021/es801591k

Kritee, K., Blum, J. D., Johnson, M. W., Bergquist, B. A., & Barkay, T. (2007). Mercury stable isotope fractionation during microbial reduction of Hg(II) to Hg(0). *Environmental Science & Technology*, *41*, 1889–1895. https://doi.org/10.1021/es062019t

Križman, M., Stegnar, P., & Miklavčič, V. (1996). Mercury ore processing - A new source of technologically enhanced natural radioactivity. *Environment International*, *22*(SUPPL. 1). https://doi.org/10.1016/S0160-4120(96)00115-8

Krupp, E. M., & Donard, O. F. X. (2005). Isotope ratios on transient signals with GC-MC-ICP-MS. *International Journal of Mass Spectrometry*, *242*(2–3), 233–242. https://doi.org/10.1016/j.ijms.2004.11.026

Kwon, S. Y., Blum, J. D., Carvan, M. J., Basu, N., Head, J. A., Madenjian, C. P., & David, S. R. (2012). Absence of fractionation of mercury isotopes during trophic transfer of methylmercury to freshwater fish in captivity. *Environmental Science and Technology*, *46*(14), 7527–7534. https://doi.org/10.1021/es300794q

Lavrič, J. V., & Spangenberg, J. E. (2003). Stable isotope (C, O, S) systematics of the mercury mineralization at Idrija, Slovenia: Constraints on fluid source and alteration processes. *Mineralium Deposita*, *38*(7), 886–899. https://doi.org/10.1007/s00126-003-0377-9

Lavrič, J. V., Spangenberg, J. E., & Režun, B. (2003). Organic geochemical records of hydrotermal alteration at Idrija mercury deposit, Slovenia. *Geologija*, *46*(1), 129–134. https://doi.org/10.5474/geologija.2003.013

Li, C., Chen, J., Angot, H., Zheng, W., Shi, G., Ding, M., Du, Z., Zhang, Q., Ma, X., Kang, S., Xiao, C., Ren, J., & Qin, D. (2020). Seasonal Variation of Mercury and Its Isotopes in Atmospheric Particles at the Coastal Zhongshan Station, Eastern Antarctica. *Environmental Science and Technology*, *54*(18), 11344–11355. https://doi.org/10.1021/acs.est.0c04462

Liu, Y., Liu, G., Wang, Z., Guo, Y., Yin, Y., Zhang, X., Cai, Y., & Jiang, G. (2022). Understanding foliar accumulation of atmospheric Hg in terrestrial vegetation: Progress and challenges. *Critical Reviews in Environmental Science and Technology*, *52*(24), 4331–4352. https://doi.org/10.1080/10643389.2021.1989235

Lodenius, M. (1998). Dry and wet deposition of mercury near a chlor-alkali plant. *Science of the Total Environment*, *213*(1–3), 53–56. https://doi.org/10.1016/S0048-9697(98)00073-4

Lupsina, V., Horvat, M., Jeran, Z., & Stegnar, P. (1992). Investigation of Mercury Speciation in Lichens*. In *ANALYST* (Vol. 117).

Lyman, S. N., Cheng, I., Gratz, L. E., Weiss-Penzias, P., & Zhang, L. (2020). An updated review of atmospheric mercury. *Science of the Total Environment*, *707*, 135575. https://doi.org/10.1016/j.scitotenv.2019.135575

Madigan, D. J., Li, M., Yin, R., Baumann, H., Snodgrass, O. E., Dewar, H., Krabbenhoft, D. P., Baumann, Z., Fisher, N. S., Balcom, P., & Sunderland, E. M. (2018). Mercury Stable Isotopes Reveal Influence of Foraging Depth on Mercury Concentrations and Growth in Pacific Bluefin Tuna. *Environmental Science and Technology*, *52*(11), 6256–6264. https://doi.org/10.1021/acs.est.7b06429

Manish, T., Ashutosh, K. S., & Devesh, K. S. (2015). Isotopic Fractionation. In *Chemostratigraphy* (pp. 65–92). https://doi.org/10.1016/B978-0-12-419968-2.00003-0

McLagan, D. S., Mitchell, C. P. J., Huang, H., Lei, Y. D., Cole, A. S., Steffen, A., Hung, H., & Wania, F. (2016). A High-Precision Passive Air Sampler for Gaseous Mercury. *Environmental Science and Technology Letters*, *3*(1), 24–29. https://doi.org/10.1021/acs.estlett.5b00319

McLagan, D. S., Schwab, L., Wiederhold, J. G., Chen, L., Pietrucha, J., Kraemer, S. M., & Biester, H. (2022). Demystifying mercury geochemistry in contaminated soil–groundwater systems with complementary mercury stable isotope, concentration, and speciation analyses. *Environmental Science: Processes & Impacts*. https://doi.org/10.1039/d1em00368b

Mead, C., Lyons, J. R., Johnson, T. M., & Anbar, A. D. (2013). Unique Hg stable isotope signatures of compact fluorescent lamp-sourced Hg. *Environmental Science and Technology*, *47*(6), 2542–2547. https://doi.org/10.1021/es303940p

Miklavčič, A., Mazej, D., Jaćimović, R., Dizdarevič, T., & Horvat, M. (2013). Mercury in food items from the Idrija Mercury Mine area. *Environmental Research*, *125*, 61–68. https://doi.org/10.1016/j.envres.2013.02.008

Mlakar, I. (1974). Osnovni parametri proizvodnje rudnika Idrija skozi stoletja do danes. *Irdijski Razgledi*, *21*, 1–40.

Mlakar, I., & Čar, J. (2009). *Geološka karta idrijsko - cerkljanskega hribovja med stopnikom in rovtami 1:25.000*. Geological Survey of Slovenija.

Mlakar, I., & Drovenik, M. (1971). Strukturne in generske posebnosti idrijskega rudišča. *Geologija*, *14*, 67–126. https://www.geologija-revija.si/index.php/geologija/article/view/290

Mlakar, T. L., Horvat, M., Kotnik, J., Jeran, Z., Vuk, T., Mrak, T., & Fajon, V. (2011). Biomonitoring with epiphytic lichens as a complementary method for the study of mercury contamination near a cement plant. *Environmental Monitoring and Assessment*, *181*(1–4), 225–241. https://doi.org/10.1007/s10661-010-1825-5

Monna, F., Bouchaou, L., Rambeau, C., Losno, R., Bruguier, O., Dongarrà, G., Black, S., & Chateau, C. (2012). Lichens used as monitors of atmospheric pollution around Agadir (Southwestern Morocco) - A case study predating lead-free gasoline. *Water, Air, and Soil Pollution*, *223*(3), 1263–1274. https://doi.org/10.1007/s11270-011-0942-2

Morel, F. M. M., Kraepiel, A. M. L., & Amyot, M. (1998). The chemical cycle and bioaccumulation of mercury. *Annual Review of Ecology and Systematics*, *29*, 543–566. https://doi.org/10.1146/annurev.ecolsys.29.1.543

Mughabghab, S. (2003). Thermal neutron capture cross sections. *International Atomic Energy Agency INDC(NDS)-440*. https://doi.org/10.1103/PhysRev.88.412

Naccarato, A., Tassone, A., Martino, M., Moretti, S., MacAgnano, A., Zampetti, E., Papa, P., Avossa, J., Pirrone, N., Nerentorp, M., Munthe, J., Wängberg, I., Stupple, G. W., Mitchell, C. P. J., Martin, A. R., Steffen, A., Babi, D., Prestbo, E. M., Sprovieri, F., & Wania, F. (2021). A field intercomparison of three passive air samplers for gaseous mercury in ambient air. *Atmospheric Measurement Techniques*, *14*(5), 3657–3672. https://doi.org/10.5194/amt-14-3657-2021

National Institute of Standards & Technology. (2016). *Certificate of Analysis Standard Reference Material 3133 Mercury (Hg) Standard Solution*. Department of Commerce - USA.

Nickel, S., Schröder, W., Schmalfuss, R., Saathoff, M., Harmens, H., Mills, G., Frontasyeva, M. V., Barandovski, L., Blum, O., Carballeira, A., de Temmerman, L., Dunaev, A. M., Ene, A., Fagerli, H., Godzik, B., Ilyin, I., Jonkers, S., Jeran, Z., Lazo, P., … Zechmeister, H. G. (2018). Modelling spatial patterns of correlations between concentrations of heavy metals in mosses and atmospheric deposition in 2010 across Europe. *Environmental Sciences Europe*, *30*(1), 1–17. https://doi.org/10.1186/s12302-018-0183-8

Obrist, D., Kirk, J. L., Zhang, L., Sunderland, E. M., Jiskra, M., & Selin, N. E. (2018). A review of global environmental mercury processes in response to human and natural perturbations: Changes of emissions, climate, and land use. *Ambio*, *47*(2), 116–140. https://doi.org/10.1007/s13280-017-1004-9

Obrist, D., Pokharel, A. K., & Moore, C. (2014). Vertical profile measurements of soil air suggest immobilization of gaseous elemental mercury in mineral soil. *Environmental Science and Technology*, *48*(4), 2242–2252. https://doi.org/10.1021/es4048297

O'Connor, D., Hou, D., Ok, Y. S., Mulder, J., Duan, L., Wu, Q., Wang, S., Tack, F. M. G., & Rinklebe, J. (2019). Mercury speciation, transformation, and transportation in soils, atmospheric flux, and implications for risk management: A critical review. *Environment International*, *126*(March), 747–761. https://doi.org/10.1016/j.envint.2019.03.019

Placer, L. (1982). *Tektonski razvoj idrijskega rudišča Structural history of the Idrija mercury deposit. 94*.

Placer, L., & Čar, J. (1977). Srednjetriadna zgradba idrijskega ozemlja. *Geologija*, *20*, 1411–166.

Pribil, M. J., Rimondi, V., Costagliola, P., Lattanzi, P., & Rutherford, D. L. (2020). Assessing mercury distribution using isotopic fractionation of mercury processes and sources adjacent and downstream of a legacy mine district in Tuscany, Italy. *Applied Geochemistry*, *117*(January). https://doi.org/10.1016/j.apgeochem.2020.104600

Ramšak, A., Ščančar, J., Jožef, M. H., & Institute, S. (2012). *Evaluation of Metallothioneins in Blue Mussels (Mytilus galloprovincialis) as a Biomarker of Mercury and Cadmium Exposure in the Slovenian waters (Gulf of Trieste): A Long-term Fie... Data in Acta Adriatica · Matrix Reference Materials for Environmental Analysis and Research View project MIRACLE (Mercury Interdisciplinary Research for Appropriate Clam farming in Lagoon Environment) View project*. https://www.researchgate.net/publication/235322194

Reinfelder, J. R., & Janssen, S. E. (2019). Tracking legacy mercury in the Hackensack River estuary using mercury stable isotopes. *Journal of Hazardous Materials*, *375*(April), 121–129. https://doi.org/10.1016/j.jhazmat.2019.04.074

Rodŕiguez-Gonźalez, P., Epov, V. N., Bridou, R., Tessier, E., Guyoneaud, R., Monperrus, M., & Amouroux, D. (2009). Species-specific stable isotope fractionation of mercury during Hg(II) methylation by an anaerobic bacteria (Desulfobulbus propionicus) under dark conditions. *Environmental Science and Technology*, *43*(24), 9183–9188. https://doi.org/10.1021/es902206j

Rua-Ibarz, A., Bolea-Fernandez, E. & Vanhaecke, F. (2016) An in-depth evaluation of accuracy and precision in Hg isotopic analysis via pneumatic nebulization and cold vapor generation multi-collector ICP-mass spectrometry. *Anal Bioanal Chem*, 408, 417–429. https://doi.org/10.1007/s00216-015-9131-2

Schauble, E. A. (2004). Applying stable isotope fractionation theory to new systems. *Reviews in Mineralogy and Geochemistry*, *55*, 65–111. https://doi.org/10.2138/gsrmg.55.1.65

Schauble, E. A., Méheut, M., & Hill, P. S. (2009). Combining metal stable isotope fractionation theory with experiments. *Elements*, *5*(6), 369–374. https://doi.org/10.2113/gselements.5.6.369

Schroeder, W. H., & Munthe, J. (1998). Atmospheric mercury - An overview. *Atmospheric Environment*, *32*(5), 809–822. https://doi.org/10.1016/S1352-2310(97)00293-8

Sherman, L. S., Blum, J. D., Johnson, K. P., Keeler, G. J., Barres, J. A., & Douglas, T. A. (2010). Mass-independent fractionation of mercury isotopes in Arctic snow driven by sunlight. *Nature Geoscience*, *3*(3), 173–177. https://doi.org/10.1038/ngeo758

Sherman, L. S., Blum, J. D., Keeler, G. J., Demers, J. D., & Dvonch, J. T. (2012). Investigation of local mercury deposition from a coal-fired power plant using mercury isotopes. *Environmental Science and Technology*, *46*(1), 382–390. https://doi.org/10.1021/es202793c

Shlyapnikov, Y., Kocman, D., Štrok, M., Dizdarevič, T., Čar, J., & Horvat, M. (2018). Mercury isotope fractionation during the ore formation in the Idrija mercury mine. *Unpublished*, 1–24.

Si, L., & Ariya, P. A. (2018). Recent advances in atmospheric chemistry of mercury. *Atmosphere*, *9*(2), 1–18. https://doi.org/10.3390/atmos9020076

Širca, A., Rajar, R., Harris, R. C., & Horvat, M. (1999). Mercury transport and fate in the Gulf of Trieste (Northern Adriatic) - A two-dimensional modelling approach. *Environmental Modelling and Software*, *14*(6), 645–655. https://doi.org/10.1016/S1364-8152(99)00006-7

Smith, C. N., Kesler, S. E., Blum, J. D., & Rytuba, J. J. (2008). Isotope geochemistry of mercury in source rocks, mineral deposits and spring deposits of the California Coast Ranges, USA. *Earth and Planetary Science Letters*, *269*(3–4), 399–407. https://doi.org/10.1016/j.epsl.2008.02.029

Smith, R. S., Wiederhold, J. G., Jew, A. D., Brown, G. E., Bourdon, B., & Kretzschmar, R. (2014). Small-scale studies of roasted ore waste reveal extreme ranges of stable mercury isotope signatures. *Geochimica et Cosmochimica Acta*, *137*, 1–17. https://doi.org/10.1016/j.gca.2014.03.037

Smith, R. S., Wiederhold, J. G., Jew, A. D., Brown, G. E., Bourdon, B., & Kretzschmar, R. (2015). Stable Hg isotope signatures in creek sediments impacted by a former Hg mine. *Environmental Science and Technology*, *49*(2), 767–776. https://doi.org/10.1021/es503442p

Smith, R. S., Wiederhold, J. G., & Kretzschmar, R. (2015). Mercury isotope fractionation during precipitation of metacinnabar (β-HgS) and montroydite (HgO). *Environmental Science and Technology*, *49*(7), 4325–4334. https://doi.org/10.1021/acs.est.5b00409

Sommerer, T. J. (1993). A Monte Carlo simulation of resonance radiation transport in the rare-gas-mercury positive column. *Journal of Applied Physics*, *74*(3), 1579–1589. https://doi.org/10.1063/1.354831

Sonke, J. E., Shevchenko, V. P., Prunier, J., Sun, R., Prokushkin, A. S., & Pokrovsky, O. S. (2022). Mercury Stable Isotope Composition of Lichens and Mosses from Northern Eurasia Reveals Hg Deposition Pathways and Sources. *ACS Earth and Space Chemistry*. https://doi.org/10.1021/acsearthspacechem.2c00297

Stanko Buser. (1989). Development of the Dinaric and the Julian Carbonate Platforms and of the intermediate Slovenian Basin (NW Yugoslavia). *Memor. Soc. Geol. Italiana*, *40*, 313–320.

Stetson, S. J., Gray, J. E., Wanty, R. B., & Macalady, D. L. (2009). Isotopic variability of mercury in ore, mine-waste calcine, and leachates of mine-waste calcine from areas mined for mercury. *Environmental Science and Technology*, *43*(19), 7331–7336. https://doi.org/10.1021/es9006993

Štrok, M., Hintelmann, H., & Dimock, B. (2014). Development of pre-concentration procedure for the determination of Hg isotope ratios in seawater samples. *Analytica Chimica Acta*, *851*(C), 57–63. https://doi.org/10.1016/j.aca.2014.09.005

Sun, R., Sonke, J. E., Heimbürger, L. E., Belkin, H. E., Liu, G., Shome, D., Cukrowska, E., Liousse, C., Pokrovsky, O. S. & Streets D. G. (2014) *Environmental Science & Technology, 48* (13), 7660-7668 DOI: 10.1021/es501208a

Sun, R., Jiskra, M., Amos, H. M., Zhang, Y., Sunderland, E. M., & Sonke, J. E. (2019). Modelling the mercury stable isotope distribution of Earth surface reservoirs: Implications for global Hg cycling. *Geochimica et Cosmochimica Acta*, *246*, 156–173. https://doi.org/10.1016/j.gca.2018.11.036

Szczepaniak, K., & Biziuk, M. (2003). Aspects of the biomonitoring studies using mosses and lichens as indicators of metal pollution. *Environmental Research*, *93*(3), 221–230. https://doi.org/10.1016/S0013-9351(03)00141-5

Szponar, N., McLagan, D. S., Kaplan, R. J., Mitchell, C. P. J., Wania, F., Steffen, A., Stupple, G. W., Monaci, F., & Bergquist, B. A. (2020). Isotopic Characterization of Atmospheric Gaseous Elemental Mercury by Passive Air Sampling. *Environmental Science and Technology*, *54*(17), 10533–10543. https://doi.org/10.1021/acs.est.0c02251

Teršič, T. (2010). Contents and spatial distributions of chemical elements in soil at the ancient roasting site Pšnk (Idrija area, Slovenia). *Geologija*, *53*(2), 121–128. https://doi.org/10.5474/geologija.2010.009

Teršič, T., Gosar, M., & Biester, H. (2011). Distribution and speciation of mercury in soil in the area of an ancient mercury ore roasting site, Frbejžene trate (Idrija area, Slovenia). *Journal of Geochemical Exploration*, *110*(2), 136–145. https://doi.org/10.1016/j.gexplo.2011.05.002

Thomas, R. (2013). *Practical Guide to ICP-MS Tutorial for beginners* (3rd ed.). Taylor & Francis Group.

Tomiyasu, T., Kodamatani, H., Imura, R., Matsuyama, A., Miyamoto, J., Akagi, H., Kocman, D., Kotnik, J., Fajon, V., & Horvat, M. (2017). The dynamics of mercury near Idrija mercury mine, Slovenia: Horizontal and vertical distributions of total, methyl, and ethyl mercury concentrations in soils. *Chemosphere*, *184*, 244–252. https://doi.org/10.1016/j.chemosphere.2017.05.123

Tomiyasu, T., Matsuyama, A., Imura, R., Kodamatani, H., Miyamoto, J., Kono, Y., Kocman, D., Kotnik, J., Fajon, V., & Horvat, M. (2012). The distribution of total and methylmercury concentrations in soils near the Idrija mercury mine, Slovenia, and the dependence of the mercury concentrations on the chemical composition and organic carbon levels of the soil. *Environmental Earth Sciences*, *65*(4), 1309–1322. https://doi.org/10.1007/s12665-011-1379-z

Tsui, M. T. K., Blum, J. D., Finlay, J. C., Balogh, S. J., Kwon, S. Y., & Nollet, Y. H. (2013). Photodegradation of methylmercury in stream ecosystems. *Limnology and Oceanography*, *58*(1), 13–22. https://doi.org/10.4319/lo.2013.58.1.0013

Tsui, M. T. K., Blum, J. D., & Kwon, S. Y. (2020). Review of stable mercury isotopes in ecology and biogeochemistry. *Science of the Total Environment*, *716*, 135386. https://doi.org/10.1016/j.scitotenv.2019.135386

UNEP. (2018). *Technical Background Report to the Global Mercury Assessment 2018*. United Nations Environment Programme/Arctic Monitoring and Assessment Programme, 2019.

UNEP. (2019). *Global Mercury assessment 2018*.

UNEP. (2022). *Guidance on monitoring of mercury and mercury compounds to support evaluation of the effectiveness of the Minamata Convention*.

United Nations Environment Programme. (2019). *Minamata Convention on Mercury*. United Nations.

United Nations Environmental Programme. (2023). *The Intergovernmental Panel on Climate Change*. Https://Www.Ipcc.Ch/.

U.S. EPA. (1997). Mercury Study Report to Congress Volume I: Executive Summary. *Officer of Air Quality Planning & Standards and Officer of Research and Development*, *1*, 1–95. papers2://publication/uuid/708EE337-C5BA-4F4E-8A9A-2577724D6FFE

Vanhaecke, F., & Degryse, P. (Eds.). (2012). *Isotopic Analysis, Fundamentals and Applications Using ICP-MS*. Wiley-VCH.

Verbič, M. (1966). *Idrijski rudnik do konca 16. stoletja*.

Wang, X., Bao, Z., Lin, C. J., Yuan, W., & Feng, X. (2016). Assessment of Global Mercury Deposition through Litterfall. *Environmental Science and Technology*, *50*(16), 8548–8557. https://doi.org/10.1021/acs.est.5b06351

Wang, X., Yuan, W., Lin, C. J., & Feng, X. (2021). Mercury cycling and isotopic fractionation in global forests. *Critical Reviews in Environmental Science and Technology*, *0*(0), 1–24. https://doi.org/10.1080/10643389.2021.1961505

Wang, X., Yuan, W., Lin, C. J., Luo, J., Wang, F., Feng, X., Fu, X., & Liu, C. (2020). Underestimated Sink of Atmospheric Mercury in a Deglaciated Forest Chronosequence. *Environmental Science and Technology*, *54*(13), 8083–8093. https://doi.org/10.1021/acs.est.0c01667

Wang, X., Yuan, W., Lin, C. J., Zhang, L., Zhang, H., & Feng, X. (2019). Climate and Vegetation As Primary Drivers for Global Mercury Storage in Surface Soil. *Environmental Science and Technology*, *53*(18), 10665–10675. https://doi.org/10.1021/acs.est.9b02386

Wiederhold, J. G. (2015). Metal stable isotope signatures as tracers in environmental geochemistry. *Environmental Science and Technology*, *49*(5), 2606–2624. https://doi.org/10.1021/es504683e

Wiederhold, J. G., Cramer, C. J., Daniel, K., Infante, I., Bourdon, B., & Kretzschmar, R. (2010). Equilibrium mercury isotope fractionation between dissolved Hg(II) species and thiol-bound Hg. *Environmental Science and Technology*, *44*(11), 4191–4197. https://doi.org/10.1021/es100205t

Wiederhold, J. G., Smith, R. S., Siebner, H., Jew, A. D., Brown, G. E., Bourdon, B., & Kretzschmar, R. (2013). Mercury isotope signatures as tracers for Hg cycling at the new idria Hg mine. *Environmental Science and Technology*, *47*(12), 6137–6145. https://doi.org/10.1021/es305245z

Wien, W. (1898). Untersuchungen über die electrische Entladung in verdünnten Gasen. *Annalen Der Physik*, *301*(6), 440–452. https://doi.org/10.1002/andp.18983010618

Yamakawa, A., Bérail, S., Amouroux, D., Tessier, E., Barre, J., Sano, T., Nagano, K., Kanwal, S., Yoshinaga, J., & Donard, O. F. X. (2020). Hg isotopic composition and total Hg mass fraction in NIES Certified Reference Material No. 28 Urban Aerosols. *Analytical and Bioanalytical Chemistry*, *412*(19), 4483–4493. https://doi.org/10.1007/s00216-020-02691-9

Yang, L., & Sturgeon, R. E. (2009). Isotopic fractionation of mercury induced by reduction and ethylation. *Analytical and Bioanalytical Chemistry*, *393*(1), 377–385. https://doi.org/10.1007/s00216-008-2348-6

Yin, R., Feng, X., & Shi, W. (2010). Application of the stable-isotope system to the study of sources and fate of Hg in the environment: A review. *Applied Geochemistry*, *25*(10), 1467–1477. https://doi.org/10.1016/j.apgeochem.2010.07.007

Yu, B., Fu, X., Yin, R., Zhang, H., Wang, X., Lin, C. J., Wu, C., Zhang, Y., He, N., Fu, P., Wang, Z., Shang, L., Sommar, J., Sonke, J. E., Maurice, L., Guinot, B., & Feng, X. (2016). Isotopic composition of atmospheric mercury in China: New evidence for sources and transformation processes in air and in vegetation. *Environmental Science and Technology*, *50*(17), 9362–9369. https://doi.org/10.1021/acs.est.6b01782

Yuan, W., Sommar, J., Lin, C. J., Wang, X., Li, K., Liu, Y., Zhang, H., Lu, Z., Wu, C., & Feng, X. (2019). Stable Isotope Evidence Shows Re-emission of Elemental Mercury Vapor Occurring after Reductive Loss from Foliage. *Environmental Science and Technology*, *53*(2), 651–660. https://doi.org/10.1021/acs.est.8b04865

Žagar, D., Knap, A., Warwick, J. J., Rajar, R., Horvat, M., & Četina, M. (2006). Modelling of mercury transport and transformation processes in the Idrijca and Soča river system. *Science of the Total Environment*, *368*(1), 149–163. https://doi.org/10.1016/j.scitotenv.2005.09.068

Zambardi, T., Sonke, J. E., Toutain, J. P., Sortino, F., & Shinohara, H. (2009). Mercury emissions and stable isotopic compositions at Vulcano Island (Italy). *Earth and Planetary Science Letters*, *277*(1–2), 236–243. https://doi.org/10.1016/j.epsl.2008.10.023

Zheng, W., Foucher, D., & Hintelmann, H. (2007). Mercury isotope fractionation during volatilization of Hg(0) from solution into the gas phase. *Journal of Analytical Atomic Spectrometry*, *22*(9), 1097–1104. https://doi.org/10.1039/b705677j

Zheng, W., Obrist, D., Weis, D., & Bergquist, B. A. (2016). Mercury isotope compositions across North American forests. *Global Biogeochemical Cycles*, 1475–1492. https://doi.org/10.1111/1462-2920.13280

Zhou, J., & Obrist, D. (2021). Global Mercury Assimilation by Vegetation. *Environmental Science & Technology*. https://doi.org/10.1021/acs.est.1c03530

Zhou, J., Obrist, D., Dastoor, A., Jiskra, M., & Ryjkov, A. (2021). Vegetation uptake of mercury and impacts on global cycling. *Nature Reviews Earth and Environment*, *2*(4), 269–284. https://doi.org/10.1038/s43017-021-00146-y

Zhu, W., Li, Z., Li, P., Yu, B., Lin, C. J., Sommar, J., & Feng, X. (2018). Re-emission of legacy mercury from soil adjacent to closed point sources of Hg emission. *Environmental Pollution*, *242*, 718–727. https://doi.org/10.1016/j.envpol.2018.07.002

Žibret, G., & Gosar, M. (2006). Calculation of the mercury accumulation in the Idrijca River alluvial plain sediments. *Science of the Total Environment*, *368*(1), 291–297. https://doi.org/10.1016/j.scitotenv.2005.09.086

Žižek, S., Horvat, M., Gibičar, D., Fajon, V., & Toman, M. J. (2007). Bioaccumulation of mercury in benthic communities of a river ecosystem affected by mercury mining. *Science of the Total Environment*, *377*(2–3), 407–415. https://doi.org/10.1016/j.scitotenv.2007.02.010

Bibliography

Here, personal bibliography of Dominik Božič is presented for his scientific publications in the years 2020 to 2024. Bibliography is arranged by typology.

Original scientific articles

Božič, D., Živković, I., Jagodic Hudibivnik, M., Kotnik, J., Amouroux, D., Štrok, M., Horvat, M. (2022) Fractionation of mercury stable isotopes in lichens. *Chemosphere*, vol. 309, part 1, pages: 136592-1-136592-9. DOI: 10.1016/j.chemosphere.2022.136592

Božič, D., Živković, I., Dizdarjevič, T., Peljhan, M., Štrok, M., Horvat, M. (2023) Insights into the heterogeneity of the mercury isotopic fingerprint of the Idrija mine (Slovenia). *Minerals*, vol. 13, no. 9, 1-11, DOI: doi.org/10.3390/min13091227

Božič, D., Horvat, M. (2024) Insights into seasonal variations in mercury isotope composition of lichens. *Environmental Pollution*, vol. 340, part 1, no. 122740, DOI: doi.org/10.1016/j.envpol.2023.122740

Ali, S. W., Božič, D., Vijayakumaran Nair, S., Živković, I., Gačnik, J., Andron, T. D., Jagodic Hudobivnik, M., Kocman, D., Horvat, M. (2024) Optimization of a pre-concentration method for the analysis of mercury isotopes in low-concentration foliar samples. *Analytical and bioanalytical chemistry,* [Online ed.]. [in press] DOI:10.1007/s00216-023-05116-5

Published scientific conference contribution abstracts

Božič, D., Ali, S. W., Jagodic Hudobivnik, M., Kocman, D., Horvat, M. (2022) Investigating seasonal patterns of mercury uptake across forest sites in Slovenia. In: Reducing mercury emissions to achieve a greener world: 15th International Conference on Mercury as a Global Pollutant (ICMGP), 24th - 29th July 2022, virtual event. [S. l.]: ILM Exhibitions. [1] str. https://app.swapcard.com/widget/event/icmgp-2022/planning/UGxhbm5pbmdfOTUyODE3

Božič, D., Kotnik, J., Jagodic Hudobivnik, M., Živković, I., Dizdarevič, T., Ali, S. W., Štrok, M., Horvat, M. (2022) Mercury tracking via isotopic signature at Idrija contaminated site. In: Novak, R. (ed.), et al. 14th Jožef Stefan International Postgraduate School Students' Conference: book of abstracts: 1st - 3rd June, 2022, 14th Jožef Stefan International Postgraduate School Students' Conference, 1st - 3rd June, 2022, Kamnik, Slovenia. Ljubljana: Jožef Stefan Institute: Jožef Stefan International Postgraduate School, Str. 30. http://ipssc.mps.si/Book_of_Abstracts.pdf

Božič, D., Horvat, M. (2023) "Mercury isotopes reveal the link between soils and ores in Idrija", V: 15th Jožef Stefan International Postgraduate School Students' Conference, 31st May - 2nd June 2023, Kamnik, Slovenia: Book of abstracts, Kuzmić, N. (editor), et al., Ljubljana: Jožef Stefan Institute: Jožef Stefan International Postgraduate School, str. 12, http://ipssc.mps.si/auxiliary_material/BoA%20IPSSC%202023.pdf

Božič, D., Shlyapnikov, Y., Jagodic Hudobivnik, M., Kotnik, J., Dizdarevič, T., Štrok, M., Horvat, M. (2022) Mercury isotopes in soils and ores at the site of a former mercury mine. In: Reducing mercury emissions to achieve a greener world: 15th International Conference on Mercury as a Global Pollutant (ICMGP), 24th - 29th July 2022, virtual event. [S. l.]: ILM Exhibitions. [1] str. https://app.swapcard.com/widget/event/icmgp-022/planning/UGxhbm5pbmdfOTU2NzQw

Božič, D., Wakar, S. A., Vijayakumaran Nair, S., Horvat, M. (2023) Mercury isotope measurement method in samples with low mercury concentration using MC-ICP-MS. In: ŠELIH, Vid Simon (ed.), ŠALA, Martin (ed.). European Winter Conference on Plasma Spectrochemistry: book of abstracts: Ljubljana, Slovenia, January 29th - February 3rd, 2023. Ljubljana: National Institute of Chemistry, Str. 376. ISBN 978-961-6104-85-2

Božič, D., Živković, I., Kotnik, J., Jagodic Hudobivnik, M., Mazej, D., Štrok, M., Horvat, M. (2022) Fractionation of mercury stable isotopes in lichens over a period of one year. In: EGU General Assembly 2022: Vienna, Austria & Online: 23–27 May 2022. [S. l.]: European Geosciences Union, 1 spletni vir. https://meetingorganizer.copernicus.org/EGU22/EGU22-1108.html, DOI: 10.5194/egusphere-egu22-1108

Božič, D., Živković, I., Jagodic Hudobivnik, M., Andron, T.-D., Štrok, M., Horvat, M. (2021) Optimization of sample preparation procedures for Hg isotopic measurements. In: ŽAGAR, Klara (ed.), et al. Throughout knowledge towards a green new world: 13th Jožef Stefan International Postgraduate School Students' Conference and 15th Young Researchers' Day of Chemistry, material science, biochemistry and environment, (CMBE day), 27th-28th May 2021, online: book of abstracts. 13th Jožef Stefan International Postgraduate School Students' Conference and 15th Young Researchers' Day, 27th-28th May 2021. Ljubljana: Jožef Stefan International Postgraduate School: Jožef Stefan Institute, Str. 36. http://ipssc.mps.si/bookOfAbstracts/Book_of_abstracts_v04.pdf

Ali, S. W., Božič, D., Jagodic Hudobivnik, M., Kocman, D., Horvat, M. (2022) Understanding the role of forest ecosystems in atmospheric mercury inputs to terrestrial compartment. In: Novak, R. (ed.), et al. 14th Jožef Stefan International Postgraduate School Students' Conference: book of abstracts: 1st - 3rd June, 2022, Kamnik, Slovenia. 14th Jožef Stefan International Postgraduate School Students' Conference, 1st - 3rd June, 2022, Kamnik, Slovenia. Ljubljana: Jožef Stefan Institute: Jožef Stefan International Postgraduate School, Str. 42. http://ipssc.mps.si/Book_of_Abstracts.pdf

Ali, S. W., Kocman, D., Božič, D., Jagodic Hudobivnik, M., Horvat, M. (2022) Methodological assessment of mercury measurements in foliar samples from contaminated sites. In: Reducing mercury emissions to achieve a greener world: 15th International Conference on Mercury as a Global Pollutant (ICMGP), 24th - 29th July 2022, virtual event. [S. l.]: ILM Exhibitions

Gačnik, J., Živković, I., Kotnik, J., Božič, D., Maaire Gyengne, F., Berisha, S., Tassone, A., Naccarato, A., P., Nicola, Sprovieri, F., Horvat, M. (2022) Comparison of yearly atmospheric mercury monitoring with passive sampling, biomonitoring and active measurements. In: Reducing mercury emissions to achieve a greener world: 15th International Conference on Mercury as a Global Pollutant (ICMGP), 24th - 29th July, virtual event. [S. l.]: ILM Exhibitions. 2022, [1] str. https://app.swapcard.com/widget/event/icmgp-2022/planning/UGxhbm5pbmdfOTUxNjIw

Saniewska, D., Božič, D., Živković, I., Bełdowska, M., Horvat, M. (2023) Mercury cycling in the Antarctic coastal zone (Admiralty Bay). V: SETAC North America 44th Annual Meeting : 12-16 November 2023, Louisville : "One environment. One health" : abstract book. Washington: Society of Environmental Toxicology and Chemistry (SETAC), cop. 2023. Str. 405-406. Annual meeting - SETAC (Society), Meeting. ISSN 1087-8939

Treatises, preliminary studys, studys

Božič, D., Jagodic Hudobivnik, M., Kotnik, J., Mazej, D., Horvat, M. (2022) Multi-elemental analysis of soils at Pokljuka reference location, Anhovo cement plant and Idrija mining area. IJS delovno poročilo, 13767

Božič, D., Jagodic Hudobivnik, M., Mazej, D., Štrok, M., Horvat, M. (2021) Comparison between hot-plate and microwave digestion recoveries of soil samples. IJS delovno poročilo, 13685

Božič, D., Živković, I., Jagodic Hudobivnik, M., Mazej, D., Štrok, M., Horvat, M. (2021) Evaluation of select procedures for analysis: Multi-elemental and isotopic composition of hg in lichens. IJS delovno poročilo, 13492

Božič, D., Živković, I., Jagodic Hudobivnik, M., Potočnik, D., Krajnc, B., Kotnik, J., Mazej, D., Ogrinc, N., Štrok, M., Horvat, M. (2021) Lichen biomonitoring in Western Slovenia: results of multi-elemental concentration and isotopic composition analysis. IJS delovno poročilo, 13610

Amouroux, D., Horvat, M., Živković, I., Kotnik, J., Jaćimović, R., Berisha, S., Božič, D., et al. (2020) Report on bulk species-specific isotope ratio measurements to determine Hg migration pathways, its origin and species interconversion including the use of biomonitors as passive monitors for Hg speciation and isotopic signatures representing the origin and fate of atmospheric Hg: MercOx deliverable D3. [S. l.]: EMPIR, 59 str., ilustr. Hg-ox, 16ENV01

Tassone, A., Živković, I., Kotnik, J., Božič, D., Berisha, S., Gačnik, J., Begu, E., Horvat, M., et al. (2020) Validation report on the field testing of new existing methods for on-line and sorbent-based Hg measurements in the atmosphere: MercOx deliverable D8. [S. l.]: EMPIR, 110 str., ilustr. Hg-ox, 16ENV01

Editor

Kuzmić, N. (editor), Čontala, A. (editor), Lobato, A. C. B. (editor), Oberlintner, A. (editor), Pavlovič, A. (editor), Hrepić, A. (editor), Repič, B. (editor), Gec, B. (editor), Božič, D. (editor), Noveski, G. (editor), Caf, M. (editor), Zver, M. (editor), Borštnar, P. (editor), Novak, R. (editor), Mežnar, S. (editor), Salmanov, S. (editor), Černič, T. (editor), Hribar, U. (editor), Gostenčnik, Ž. (editor), Šadl, M. (editor), (2023) 15th Jožef Stefan International Postgraduate School Students' Conference, 31st May - 2nd June 2023, Kamnik, Slovenia: Book of abstracts. Ljubljana: Jožef Stefan Institute: Jožef Stefan International Postgraduate School, http://ipssc.mps.si/auxiliary_material/BoA%20IPSSC%202023.pdf

Novak, R. (editor), Čontala, A. (editor), Lobato, A. C. B. (editor), Evkoski, B. (editor), Terro, C. (editor), Andreasidou, E. (editor), Božič, D. (editor), Noveski, G. (editor), Žagar, K. (editor), Zver, M. (editor), Novak, M. (editor), Šadl, M. (editor), Rehman, N. (editor), Kuzmić, N. (editor), Gostenčnik, Ž. (editor), (2022). 14th Jožef Stefan International Postgraduate School Students' Conference, 1st - 3rd June, 2022, 14th Jožef Stefan International Postgraduate School Students' Conference: book of abstracts: 1st - 3rd June, 2022, Kamnik, Slovenia. Ljubljana: Jožef Stefan Institute: Jožef Stefan International Postgraduate School, http://ipssc.mps.si/Book_of_Abstracts.pdf

Žagar, K. (editor), Jovanovska, L. (editor), Zver, M. (editor), Kraš, A. (editor), Dlouhy, M. (editor), Novak, R. (editor), Evkoski, B. (editor), Kogej Zwitter, Z. (editor), Jovičević Klug, P. (editor), Božič, D. (editor), Maksimović, O. (editor), Lončarević, Z. (editor), Dežman, M. (editor), (2021). 13th Jožef Stefan International Postgraduate School Students' Conference and 15th Young Researchers' Day, 27th-28th May 2021. Throughout knowledge towards a green new world: 13th Jožef Stefan International Postgraduate School Students' Conference and 15th Young Researchers' Day of Chemistry, material science, biochemistry and environment, (CMBE day), 27th-28th May 2021, online: book of abstracts. Ljubljana: Jožef Stefan International Postgraduate School: Jožef Stefan Institute, 2021. 1 spletni vir, http://ipssc.mps.si/bookOfAbstracts/Book_of_abstracts_v04.pdf

Biography

The author of this Ph.D. thesis was born on 17 August 1996 in Postojna (Slovenia). His primary schooling started at Božidar Jakac school and was completed at Miran Jarc school. Afterwards, he enrolled in Gimnazija Vič, where he graduated with the matura exam in 2015.

In 2015, he enrolled at the Faculty of Natural Sciences and Engineering at the University of Ljubljana, where he studied at the Department of Geology, earning his Bachelor's degree in 2018 with a thesis entitled: Petrological, mineralogical, geochemical characteristics and radiometric dating of an igneous rock from Puerto Angelo in Mexico. In 2018, he continued with his master's degree studies at the Department of Geology. He attended the courses of the Geo-environment and Geo-materials module. In 2019, he transferred to the Jožef Stefan International Postgraduate School, where he was a regular full-time student of the 2nd year of the Ecotechnologies program. In his M.Sc. degree, he focused on strontium measurements in sedimentary rocks with a focus on strontium isotope stratigraphy. He graduated in 2020 with a thesis titled: Mass spectrometry & strontium isotope stratigraphy: $^{87}Sr/^{86}Sr$ measurements in fossils from Trnovski Gozd with multi-collector inductively coupled plasma mass spectrometer.

In 2020, he commenced employment at the Department of Environmental Sciences, Jožef Stefan Institute, where he contributed to the Inorganic Biogeochemistry Group headed by Dr. Milena Horvat. The research conducted within this group laid the foundation for his Ph.D. thesis.

In 2023, he joined the Slovenian Armed Forces, serving in the mobile response laboratories of the chemical, nuclear, and biological defense unit.